Biological Mechanisms of Response and Resistance to CDK4/6 Inhibitors in Hormone Receptor-Positive HER2-Negative Breast Cancer

Doctoral thesis presented by Natàlia Lorman Carbó to obtain the degree of Doctor of Philosophy (PhD) in Medicine and Translational Research at the University of Barcelona

Author: Natàlia Lorman Carbó

Tutor and Co-director: Dr. Aleix Prat Aparicio

Co-director: Dr. Fara Brasó Maristany

School of Medicine and Health Sciences, University of Barcelona

Barcelona, 2025

AUTORIZATION FOR THE PRESENTATION OF THE THESIS

Dr. Aleix Prat Aparicio, Professor at the University of Barcelona, Director of the Institute of Cancer & Blood Disorders at Hospital Clínic Barcelona, and Head of the Translational genomics and targeted therapies in solid tumors group at FCRB-IDIBAPS, with identity card 47713204A, and Dr. Fara Brasó Maristany, Investigator at the Institute of Cancer & Blood Disorders at Hospital Clínic Barcelona and Investigator and Scientific Coordinator of the Translational genomics and targeted therapies in solid tumors group at FCRB-IDIBAPS, with identity card 38860975Z,

DECLARE THAT:

The thesis manuscript presented by Ms. Natàlia Lorman Carbó entitled "Biological mechanisms of response and resistance to CDK4/6 inhibitors in hormone receptor-positive HER2-negative breast cancer" has been developed under their supervision, and they authorize its deposit for defense and evaluation by a tribunal.

Signed on: October 23rd, 2025

Aleix Prat Aparicio - DNI 47713204A (TCAT)
Signat digitalment per Aleix Prat Aparicio - DNI 47713204A (TCAT)
Data: 2025.10.23 16:25:24 +02'00'

Director

Fara Brasó Maristany 38860975Z
Firmado digitalmente por Fara Brasó Maristany 38860975Z
Fecha: 2025.10.23 14:18:23 +02'00'

Director

STATEMENT OF THE DOCTORAL CANDIDATE AND DIRECTORS ON THE ORIGINALITY AND GOOD PRACTICES OF THE THESIS

Dr. Aleix Prat Aparicio, Professor at the University of Barcelona, Director of the Institute of Cancer & Blood Disorders at Hospital Clínic Barcelona, and Head of the Translational genomics and targeted therapies in solid tumors group at FCRB-IDIBAPS, with identity card 47713204A; Dr. Fara Brasó Maristany, Investigator at the Institute of Cancer & Blood Disorders at Hospital Clínic Barcelona and Investigator and Scientific Coordinator of the Translational genomics and targeted therapies in solid tumors group at FCRB-IDIBAPS, with identity card 38860975Z; and the doctoral candidate Natàlia Lorman Carbó, with identity card 41632412C,

DECLARE THAT:

The doctoral thesis entitled "Biological mechanisms of response and resistance to CDK4/6 inhibitors in hormone receptor-positive HER2-negative breast cancer" is original, containing own results and information, without plagiarism from other theses, publications, or research from other authors. They also confirm that ethical codes and good practices have been followed in its preparation. They declare that they consent to the thesis being submitted to procedures to verify its originality.

Signed on: October 23rd, 2025

Aleix Prat Aparicio - DNI 47713204A (TCAT)
Signat digitalment per Aleix Prat Aparicio - DNI 47713204A (TCAT)
Data: 2025.10.23 16:25:55 +02'00'

Director

Fara Brasó Maristany 38860975Z
Firmado digitalmente por Fara Brasó Maristany 38860975Z
Fecha: 2025.10.23 14:18:48 +02'00'

Director

NATALIA LORMAN I CARBO - DNI 41632412C
Digitally signed by NATALIA LORMAN I CARBO - DNI 41632412C
Date: 2025.10.23 14:55:42 +02'00'

Candidate

DECLARATION OF AUTHORSHIP OF THE THESIS

The doctoral candidate Ms. Natàlia Lorman Carbó, with identity card 41632412C,

DECLARES THAT:

She is the author of the doctoral thesis entitled “Biological mechanisms of response and resistance to CDK4/6 inhibitors in hormone receptor-positive HER2-negative breast cancer”.

Signed on: October 23rd, 2025

NATALIA LORMAN I CARBO - DNI 41632412C

Digitally signed by NATALIA LORMAN I CARBO - DNI 41632412C
Date: 2025.10.23 14:56:00 +02'00'

Candidate

ACKNOWLEDGEMENTS

M’agradaria aprofitar aquest espai per donar les gràcies a totes les persones que m’han acompanyat i ajudat durant aquests últims tres anys de tesi, tant dins com fora del laboratori. Ha sigut un camí intens, enriquidor i ple d’aprenentatges, que no hauria estat possible sense tots vosaltres.

En primer lloc, vull expressar el meu agraïment més profund a totes les pacients amb càncer de mama que participen en estudis i assaigs clínics. Gràcies per la vostra generositat, valentia i compromís amb l’avenç científic i mèdic.

Fara, gràcies per obrir-me la porta del lab fa gairebé cinc anys després d’una curta entrevista per zoom. De tu he après moltíssim. Gràcies per oferir-me fer la tesi sota la teva tutela i per acompanyar-me al llarg de tot aquest procés. Gràcies per la confiança i la llibertat que m’has donat. Ets una gran científica i una inspiració per a mi.

Aleix, gràcies per acollir-me al teu grup de recerca i fer-me sentir sempre benvinguda. Gràcies pel teu coneixement, els teus consells i la teva predisposició a ajudar sempre.

Als nostres col·laboradors de projecte de l’IRB: Roger, Teresa, Sara, Marc... Ha sigut un plaer treballar amb vosaltres. Gràcies pel vostre coneixement i ajuda des dels meus inicis en el projecte. Ha estat una sort poder comptar amb vosaltres!

To the team at ONA therapeutics: Valerie, Haijun, Bea, Diana, Salva, Lucía, Elisa… Working with you has been truly enriching. I have learned a lot from your expertise. Thank you for the trust and kindness you have shown me throughout this journey.

A tots els membres del Translational Genomics and Targeted Therapies in Solid Tumors Lab i de l’equip de càncer de mama de l’Hospital Clínic de Barcelona: ha estat un privilegi compartir aquest camí amb vosaltres. La passió que poseu en la vostra feina és realment inspiradora.

Patri, Julia, Sergio, Sonia i Maite, gràcies per la vostra amabilitat, ajuda i predisposició en tot moment! Als membres de les diferents plataformes de l’IDIBAPS, especialment la de citometria (Sara, Cristina, Isabel, Selma, Joel...), gràcies pel vostre suport tècnic.

Un gràcies immens a tots els integrants de l'OncoLab. Vam començar que érem literalment quatre i ara no cabem al menjador. Vosaltres heu fet que sigui tot molt més divertit. A l'Elba i al Diouldé, els primers a qui vaig conèixer i a qui trobem moltíssim a faltar al lab, gràcies per l'acollida i per ser tan macus. A la Paula i l'Oleguer (el meu matrimoni preferit), i també a la Valeria i l'Ángela: gràcies per la vostra ajuda sempre. Sou uns grans professionals però, sobretot, molt bons amics. A l'Ángela, que m'ha fet la (preciosa) portada de la tesi, vull fer-li un agraïment especial! A la Nat J, per escoltar-me i aconsellar-me sempre tan bé. A l'Anabel i la Sandra, les meves compis de despatx: gràcies per escoltar-me i sempre estar disposades a fer xerrapeta, heu sigut una súper incorporació al grup. Anabel, gràcies per tots els consells i ajuda amb la tesi. A la Sandra i al Gerard, gràcies per l'ajuda i la paciència que heu tingut fent-me classes d'estadística i R. A en Martí, una altra gran incorporació al grup (encara que alguns ho van posar en dubte al principi jaja), gràcies per sempre oferir la teva ajuda i per l'energia tan positiva que aportes. Sam, Julia, Maria, Leire, Víctor, Fede, Mario, David, Julieth, Tolu, Sabrina, Giulio, Giuseppe i tothom qui ha passat pel lab en un moment o altre: que guai ha sigut compartir tantes estones amb vosaltres :)

To the Duncnestos: we started this journey together and it warms my heart every time someone shares their latest achievement so we can celebrate together. You are a bunch of science-lovers and I have no doubt you'll do amazing with your theses. I miss you all xx.

A les meves amigues i amics de sempre: la vida al vostre costat és fantàstica! Us estimo moltíssim i em fa feliç veure com anem creixent i assolint metes junts. Gràcies per ser-hi sempre i per fer-ho tot tan millor!

I, sobretot, a la meva xarxa de suport incondicional:

Manu, com m'agrada compartir la vida amb tu. Gràcies per cuidar-me, per fer-me el sopar cada dia i per fer-me riure sempre. A la Blanca i la Sara, les meves germanes, el millor regal que la vida em podia fer i la meva font d'inspiració des de sempre. Als meus pares, per l'amor, el carinyo, la paciència i el suport infinit. Crec que no hi ha paraules d'agraïment suficients per vosaltres 5. Us estimo molt.

To Nanna and Grandpa, for being the sweetest and most loving grandparents. Thank you for giving me all the opportunities I could have asked for. I miss you deeply.

Iaia, gràcies per tot el carinyo que em dones, per sempre fer samfaina quan vinc a dinar i per regalar-me la millor família del món. Que afortunats som de tenir-te!

I a tu, avi, et vull dedicar aquesta tesi. Et recordo i enyoro cada dia, i sovint et (re)llegeixo:

"Ara que la vida t'esclata per tot els porus de la pell.
Ara que, amb les teves 18 primaveres, contagies a tothom qui et tracta l'alegria de viure.
Ara que els somnis t'embolcallen amb la suavitat de les il·lusions...
Desperta! EL MÓN ET NECESSITA!
No és envà que has arribat aquí, recorda-ho sempre.
No són teus els talents de què disposes ni els tens per guardar-los avariciosament. Mira al teu voltant i descobriràs les mancances a cobrir. Sigues generosa, sembra amor, regala simpatia, acull a qui cerca, dona't i estima a tothom com t'estimes a tu mateixa.
La felicitat, la veritable felicitat, la trobaràs solament reflexionant seriosament i actuant en conseqüència.
Avui i sempre el teu avi et desitja i et desitjarà MOLTES FELICITATS!, Tatiana estimada."

Gràcies pels teus consells i pel teu humor que ens acompanyen sempre!

FUNDING

The research conducted in this thesis has been supported by:

CRIS Excelencia grant (1,250,000€). In 2022, Prof. Aleix Prat was awarded this 5-year grant to carry out the project entitled “Dissecting and overcoming mechanisms of resistance to CDK4/6 inhibition in advanced hormone receptor-positive/HER2-negative HER2-enriched breast cancer” (PR_EX_2021-14). This grant supported the work conducted for Objective 1, partially supported the research carried out for Objectives 2 and 3 of this thesis, and has funded the work contract I hold with FCRB-IDIBAPS.

RETOS grant (427,220€). In 2023, the Agencia Estatal de Investigación (AEI) awarded this 3-year public-private collaboration grant to support de project entitled “Desarrollo preclínico y clínico de un nuevo fármaco biológico para el tratamiento del cancer de mama HR+/HER2-negativo” (CPP2022-009755). This funding has partially supported the research carried out for Objectives 2 and 3 of this thesis.

TABLE OF CONTENTS

ABBREVIATIONS AND ACRONYMS

ABC	Antibody binding capacity
ADC	Antibody drug conjugate
AI	Aromatase inhibitors
AJCC	American Joint Committee on Cancer
AKT	Protein kinase B
APC	Allophycocyanin
ATM	Ataxia telangiectasia mutated
ATCC	American Type Culture Collection
BM	Basal membrane
BRCA1	Breast cancer 1
BRCA2	Breast cancer 2
C1D15	Cycle 1 day 15
CAR-T	Chimeric antigen receptor T-cell
CCND1	Cyclin D1
CDK4/6	Cyclin-dependent kinase 4/6
CDR	Complementarity-determining region
CDX	Cell-derived xenograft
CHEK2	Checkpoint kinase 2
CMC	Chemistry, manufacturing and controls
CI	Confidence interval
CTC	Circulating tumor cell
ctDNA	Circulating tumor DNA
Cys552	Cysteine 552
D-PBS	Dulbecco's Phosphatase Buffered Saline
DAB	3,3'-Diaminobenzidine
DAR	Drug-antibody ratio
Dato-DXd	Datopotamab deruxtecan
DAG	Diacylglycerol
DCIS	Ductal carcinoma in situ
DMEM	Dulbecco's Modified Eagle Medium
DTC	Disseminated tumor cell
DXd	Deruxtecan
E2	Estradiol
ECM	Extracellular matrix
EC50	Half-maximal effective concentration
EGFR	Epidermal growth factor receptor
EMA	European Medicines Agency
EMP	Epithelial-mesenchymal plasticity

EMT	Epithelial-mesenchymal transition
ER	Estrogen receptor
ESMO	European Society for Medical Oncology
ESR1	Estrogen receptor 1
FBS	Fetal bovine serum
FDA	Food and Drug Administration
FDR	False discovery rate
FGFR4	Fibroblast growth receptor factor 4
FRS2	FGFR substrate 2
FSH	Follicle-stimulating hormone
FFPE	Formalin-fixed, paraffin-embedded
GnRH	Gonadotropin-releasing hormone
GnRHa	Gonadotropin-releasing hormone agonists
GRB2	Growth factor receptor-bound 2
GRB7	Growth factor receptor-bound 7
gBRCA1	Germline Breast Cancer 1
gBRCA2	Germline Breast Cancer 2
H&E	Hematoxylin & Eosin
HCC	Hepatocellular carcinoma
HER2	Human epidermal growth factor receptor 2
HER3-DXd	Patritumab deruxtecan
HIER	Heat-induced epitope retrieval
HPSGs	Heparan sulphate proteoglycans
h	Hour
HR	Hormone receptor
IC50	Half maximal inhibitory concentrations
ICI	Immune checkpoint inhibitors
IHC	Immunohistochemistry
ISH	In situ hybridization
IV	Intravenously
JNK	c-Jun N-terminal kinase
LCIS	Lobular carcinomas in situ
LH	Luteinizing hormone
LTR	Lapatinib trastuzumab resistant
MAPK	Mitogen-activated protein kinase
MFI	Mean Fluorescence Intensity
MET	Mesenchymal-epithelial transition
MKI67	Marker of proliferation Ki-67
MKP1	MAPK phosphatase 1
MKP3	MAPK phosphatase 3
ADC-2-R	ADC-2-resistant

MMAE	Monomethyl auristatin E
MMAF	Monomethyl auristatin F
MRI	Magnetic resonance imaging
MMP	Matrix metalloproteinase
mTOR	Mammalian target of rapamycin
MST1/2	Mammalian sterile 20-like kinase 1/2
NGS	Nottingham Grading System
ORR	Overall response rate
OS	Overall survival
PALB2	Partner and localizer of *BRCA2*
PARP	Poly (ADP-ribose) polymerase
PD	Progressive disease
PD-1	Programmed cell death protein 1
PD-L1	Programmed cell death protein 1 ligand
PFS	Progression-free survival
PIK3CA	Phosphoinositide-3-kinase catalytic subunit alpha
PI3K	Phosphatidylinositol 3-kinases
PIP2	Phosphatidylinositol-4,5-biphosphate
PIP3	Phosphatidylinositol-3,4,5-triphosphate
PK	Pharmacokinetics
PKC	Protein kinase C
PLCγ	Phospholipase Cγ
PR	Palbociclib-resistant
PTB	Phosphotyrosine-binding
PTEN	Phosphatase and tensin homolog
p-Rb	Phosphorylation of RB1
RB1	Retinoblastoma 1
RIPA	Radioimmunoprecipitation
RSK2	Ribosomal S6 kinase 2
RT	Room temperature
RTK	Receptor tyrosine kinase
SA-β-gal	Senescence-associated β galactosidase
SABC	Specific antibody binding capacity
SAM	Significant analysis of microarray
SASP	Senescence-associated secretory phenotype
Sac-TMT	Sacituzumab tirumotecan
SEOM	Spanish Society of Medical Oncology
SERD	Selective ER degraders
SERM	Selective ER modulators
SG	Sacituzumab govitecan
SNP	Single nucleotide polymorphism

SOS	Son of sevenless
Spry	Sprouty
STAT	Signal transducer and activator of transcription
SYD985	Trastuzumab duocarmazine
Tagg	Thermal aggregation propensity
TAA	Tumor-associated antigen
TCGA	The cancer genome atlas
T-DM1	Trastuzumab emtansine
T-DXd	Trastuzumab deruxtecan
TIL	Tumor infiltrating lymphocyte
TK	Tyrosine kinase
TKI	Tyrosine kinase inhibitor
TMDD	Target-mediated drug disposition
Tm	Thermal stability
TME	Tumor microenvironment
TNBC	Triple-negative breast cancer
TOP1	Topoisomerase I
TP53	Tumor protein p53
TROP2	Trophoblast cell-surface antigen 2
TSA	Tumor-specific antigen
TTR	Tucatinib trastuzumab resistant
WGS	Whole genome sequencing

LIST OF ARTICLES INCLUDED IN THE THESIS

Thesis in classic format with 1 published article annexed. The thesis consists of 3 objectives and 1 article:

Natàlia Lorman-Carbó, Olga Martínez-Sáez, Aranzazu Fernandez-Martinez, Patricia Galván, Nuria Chic, Isabel Garcia-Fructuoso, Adela Rodríguez, Raquel Gómez-Bravo, Francesco Schettini, Paula Blasco, Oleguer Castillo, Blanca González-Farré, Barbara Adamo, Maria Vidal, Montserrat Muñoz, Charles M. Perou, Marcos Malumbres, Joaquín Gavilá, Tomás Pascual, Aleix Prat & Fara Brasó-Maristany, Comparative biological activity of palbociclib and ribociclib in hormone receptor-positive breast cancer, Scientific Reports, 2024, 14.

Journal Impact Factor and Quartile (SJR): 3.9, Q1.

SUMMARY

Breast cancer is a heterogeneous disease, with hormone receptor-positive and HER2-negative (HR+/HER2-) tumors accounting for approximately 70% of cases. The addition of CDK4/6 inhibitors such as palbociclib and ribociclib to endocrine therapy has marked a significant advancement in the treatment of these tumors, leading to improved patient outcomes. However, despite these advances, the distinct effects of different CDK4/6 inhibitors and the development of resistance to these drugs remain major clinical challenges that warrant further investigation. In this thesis, we examined the molecular changes induced by palbociclib and ribociclib in HR+ breast cancer, explored treatment-associated shifts in intrinsic molecular subtypes, and identified FGFR4 as a key driver of resistance to CDK4/6 inhibitors in HR+/HER2- and HER2-enriched breast cancer. Furthermore, we evaluated therapeutic strategies targeting FGFR4, including the development of FGFR4-directed antibody-drug conjugates (ADCs) as a promising treatment option in this resistant context.

In the first part of the thesis, we examined the biological effects of palbociclib and ribociclib in hormone receptor-positive breast cancer. We investigated the downstream effects of CDK4/6 inhibitors in HR+ breast cancer using breast cancer cell lines, at different doses, alone and in combination with endocrine therapy, and across various time points. Both inhibitors induced equal cytotoxic effects and a similar dose-dependent inhibition of cell cycle progression and induction of cellular senescence. Analysis of PAM50 gene expression revealed that both drugs elicited comparable shifts in intrinsic subtypes. These findings were validated in tumor samples of patients with early-stage HR+/HER2- breast cancer from the CORALLEEN and NeoPalAna phase II clinical trials. Notably, in surgical samples from these trials, these molecular changes were more consistently maintained in ribociclib-treated patients, particularly the changes observed in the HER2-enriched subtype.

In the second part of the thesis, we studied FGFR4 as a potential driver of resistance to CDK4/6 inhibitors and as a novel therapeutic target. Tumor samples from patients with HR+/HER2- metastatic breast cancer treated with CDK4/6 inhibitors and endocrine therapy were analyzed.

Consistent with previously described findings, the HER2-enriched subtype and high FGFR4 expression were associated with worse outcomes and were increased in samples of progressive disease to CDK4/6 inhibitors. FGFR4 protein levels correlated with transcript abundance and were low or absent in normal tissues, indicating that FGFR4 could be a promising therapeutic target in this resistant setting. In breast cancer cell lines, treatment with the selective FGFR4 kinase inhibitor INCB062079 demonstrated limited efficacy, underscoring the need for alternative therapeutic strategies. To address this, three FGFR4-specific monoclonal antibodies were characterized for binding affinity and internalization in breast cancer cell lines with variable FGFR4 expression; and three FGFR4-directed ADCs were developed, all using monomethyl auristatin E (MMAE), a potent tubulin inhibitor, as the payload, but employing different conjugation chemistries and drug-to-antibody ratios (DARs). The three ADCs demonstrated potent and selective cytotoxicity in FGFR4-high breast cancer cell lines, and the lysine-conjugated ADC with a DAR of 4, named ADC-2, was selected for further study. Treatment with ADC-2 induced a shift in PAM50 subtypes toward less aggressive and proliferative phenotypes *in vitro*. Moreover, ADC-2 exhibited a bystander killing effect, which could potentially enhance its efficacy in tumors with heterogeneous FGFR4 expression. *In vivo*, treatment with ADC-2 led to dose-dependent tumor growth inhibition in an FGFR4-high xenograft model with complete tumor regressions at the higher doses, whilst eliciting minimal effect in an FGFR4-low xenograft model, which confirmed its target-dependent activity. Resistance models generated by continuous ADC-2 exposure displayed loss of FGFR4 expression and subtype shifts to more aggressive and proliferative profiles.

Our findings indicate that while both CDK4/6 inhibitors similarly impact key pathways in HR+/HER2- breast cancer, their differential effects, particularly on the HER2-enriched signature, are dose- and context-dependent, shaped by fulvestrant co-treatment and deserving of further study. Moreover, we confirmed that tumors progressing on CDK4/6 inhibitors and endocrine therapy shift toward increased HER2-enriched phenotypes with elevated *FGFR4* expression, which are associated with poorer outcomes. While a tyrosine kinase inhibitor and naked anti-FGFR4 antibody failed to yield activity, an ADC targeting FGFR4 demonstrated rapid internalization, high potency, selective cytotoxicity against FGFR4-high cells, a bystander effect in co-culture, and marked tumor growth inhibition in xenografts.

These findings position FGFR4 as a novel, clinically actionable mediator of resistance to CDK4/6i inhibidors combined with endocrine therapy in HR+/HER2– breast cancer and highlight an ADC strategy to overcome this barrier. Overall, this thesis contributes to the understanding of CDK4/6 inhibitor biology, elucidates a new mechanism of resistance, and provides preclinical validation for a novel FGFR4-directed ADC aimed at improving clinical outcomes in resistant HR+/HER2-/HER2-enriched breast cancer.

Key words: Breast cancer, CDK4/6 inhibitor, ADC, HER2-enriched, FGFR4.

RESUM

El càncer de mama és una malaltia heterogènia, on els tumors receptors hormonals positius i HER2 negatius (HR+/HER2-) representen aproximadament el 70% dels casos. La incorporació d'inhibidors de CDK4/6, com el palbociclib i el ribociclib, a la teràpia endocrina ha suposat un avenç significatiu en el tractament d'aquests tumors. Tot i això, els diferents efectes entre inhibidors de CDK4/6 i el desenvolupament de resistències continuen sent desafiaments clínics rellevants que requereixen una investigació més profunda. En aquesta tesi, hem estudiat els canvis moleculars induïts pel palbociclib i pel ribociclib en el càncer de mama HR+, hem explorat les alteracions en els subtipus moleculars intrínsecs associades al tractament i hem identificat FGFR4 com un factor clau implicat en la resistència als inhibidors de CDK4/6 en tumors HR+/HER2- i HER2-enriquits. A més, hem avaluat estratègies terapèutiques dirigides contra FGFR4, incloent-hi el desenvolupament de conjunts anticòs-fàrmac (ADCs, per les seves sigles en anglès) com a opció prometedora en aquest context de resistència.

A la primera part de la tesi, vam analitzar els efectes biològics del palbociclib i del ribociclib en el càncer de mama HR+. Utilitzant línies cel·lulars de càncer de mama, vam examinar els efectes d'aquests inhibidors a diferents dosis, sols i en combinació amb teràpia endocrina i en diversos intervals de temps. Ambdós fàrmacs van induir efectes citotòxics iguals i una inhibició dependent de la dosi del cicle cel·lular i una inducció de la senescència cel·lular similars. L'anàlisi de l'expressió gènica mitjançant PAM50 va revelar canvis comparables en els subtipus moleculars entre els diferents tractaments. Aquests resultats es van validar en mostres tumorals de pacients amb càncer de mama HR+/HER2- en estadi inicial, inclosos en els assaigs clínics de fase II CORALLEEN i NeoPalAna. Tot i així, en les mostres quirúrgiques d'aquests estudis, els canvis moleculars es van mantenir de manera més estable en pacients tractats amb ribociclib, especialment pel que fa al subtipus HER2-enriquit.

A la segona part, vam estudiar FGFR4 com a possible mediador de resistència als inhibidors de CDK4/6 i com a nova diana terapèutica. Es van analitzar mostres tumorals de pacients amb càncer de mama metastàtic HR+/HER2- tractats amb inhibidors de CDK4/6 i teràpia endocrina. D'acord amb estudis previs, el subtipus HER2-enriquit i l'elevada expressió de FGFR4 es van associar amb pitjors resultats clínics, i es va observar un augment de FGFR4 en

les mostres obtingudes després de la progressió a aquests inhibidors. Els nivells de proteïna de FGFR4 es van correlacionar amb l'abundància de transcrits i es van detectar a nivells molt baixos o absents en teixits normals, fet que suggereix que FGFR4 podria ser una diana terapèutica atractiva en aquest context de resistència. En línies cel·lulars, el tractament amb l'inhibidor selectiu de FGFR4 INCB062079 va mostrar una eficàcia limitada, posant de manifest la necessitat de noves estratègies terapèutiques. Arran d'això, es van caracteritzar tres anticossos monoclonals específics per FGFR4, valorant la seva afinitat i capacitat d'internalització en línies cel·lulars amb diferents nivells d'expressió de FGFR4, i es van desenvolupar tres ADCs dirigits contra FGFR4. Tots ells contenien monometil auristatina E (MMAE) com a càrrega citotòxica, però es diferenciaven en les tècniques de conjugació i els ràtios fàrmac/anticòs (DAR, per les seves sigles en anglès). Els tres ADCs van demostrar una citotoxicitat potent i selectiva en línies amb alta expressió de FGFR4, i es va seleccionar el conjugat ADC-2 (DAR 4, conjugació per lisina) per a estudis posteriors. El tractament amb ADC-2 va induir canvis en els subtipus PAM50 cap a perfils menys agressius i proliferatius. A més, ADC-2 va mostrar un efecte citotòxic en cèl·lules veïnes sense expressió de FGFR4 (concepte conegut com a "bystander effect" en anglès), fet que podria afavorir-ne l'eficàcia en tumors amb expressió heterogènia de FGFR4. En models animals, ADC-2 va induir una inhibició dependent de la dosi del creixement tumoral en xenotransplants amb alta expressió de FGFR4, amb regressions completes a dosis elevades, i un efecte mínim en models amb baixa expressió, confirmant la seva activitat específica. Els models de resistència generats per exposició contínua a ADC-2 van mostrar una pèrdua d'expressió de FGFR4 i canvis de subtipus cap a perfils més agressius i proliferatius.

En conclusió, els nostres resultats indiquen que, tot i que el palbociclib i el ribociclib actuen de manera similar en tumors HR+/HER2-, els seus efectes diferencials, especialment sobre la signatura HER2-enriquida, depenen de la dosi i del context, i estan modulats pel co-administrament de fulvestrant. Addicionalment, hem demostrat que els tumors que progressen després del tractament amb inhibidors de CDK4/6 i teràpia endocrina tendeixen a evolucionar cap a fenotips HER2-enriquits amb una expressió elevada de FGFR4, associats a un pronòstic més desfavorable. Tot i que l'inhibidor de FGFR4 INCB062079 i tres anticossos dirigits al mateix receptor no van mostrar cap efecte citotòxic en línies cel·lulars, un ADC dirigit contra FGFR4 va demostrar una ràpida internalització, alta potència, citotoxicitat

selectiva contra cèl·lules amb alta expressió, un “bystander effect” en cultius mixtos i una marcada inhibició del creixement tumoral en models de xenotransplant. Aquestes dades posicionen FGFR4 com un nou mediador de resistència clínicament abordable als inhibidors de CDK4/6 combinats amb teràpia endocrina en càncer de mama HR+/HER2-, i posen en relleu l’estratègia dels ADCs per superar aquesta resistència. En conjunt, aquesta tesi aporta coneixement sobre la biologia dels inhibidors de CDK4/6, revela un nou mecanisme de resistència i valida preclínicament un ADC dirigit a FGFR4 amb l’objectiu de millorar els resultats clínics en tumors resistents HR+/HER2-/HER2-enriquits.

Paraules clau: Càncer de mama, Inhibidors de CDK4/6, ADC, HER2-enriquit, FGFR4.

INTRODUCTION

1. An overview of breast cancer

1.1 Breast cancer epidemiology and risk factors

Cancer remains a leading cause of death worldwide, with rising incidence rates due to an aging population, lifestyle factors, and advancements in diagnostic techniques. In 2022, nearly 20 million new cancer cases were diagnosed globally, a number projected to reach 32.6 million by 2050. The most frequently diagnosed cancers included lung (12.4%), female breast (11.6%), colorectal (9.6%), and prostate (7.3%) **(Figure 1)**, with breast, colorectal, and prostate cancers also having the highest prevalence due to their relatively high survival rates (1). Despite advancements in cancer treatment, mortality remains high, with approximately 9.7 million cancer-related deaths reported in 2022. Although early detection and improved therapies have enhanced outcomes for many patients, cancer-related mortality is expected to rise, surpassing 18.3 million deaths by 2050 (1).

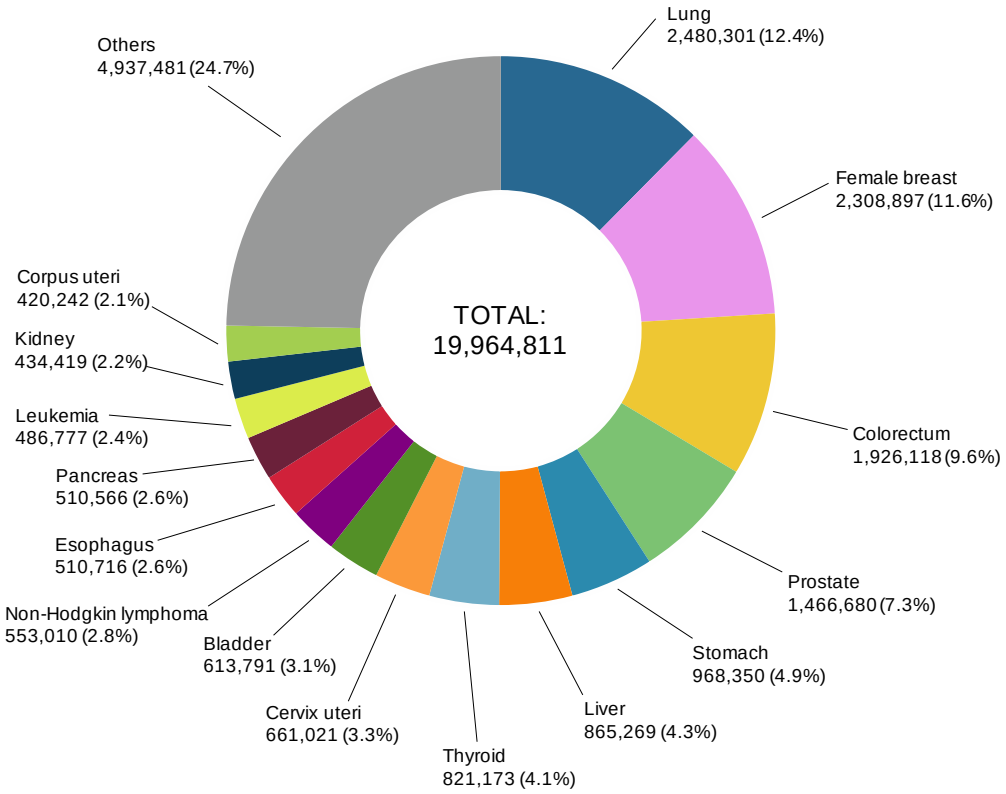

Figure 1. Cancer incidence worldwide. Most frequently diagnosed tumors according to GLOBLOCAN's global cancer statistics 2022. Both genders are included and non-melanoma skin tumors excluded. Adapted from references (1,2).

According to the Spanish Society of Medical Oncology (SEOM), approximately one in eight women will develop breast cancer in their lifetime (2). Advances in surgery, radiotherapy, and systemic treatments have significantly improved survival and quality of life of patients with breast cancer. However, despite initial successful treatment, about one in three patients will experience disease recurrence, which can lead to metastatic breast cancer. While early-stage breast cancer has a five-year survival rate of approximately 90%, this drops significantly to approximately 30% in distant metastatic disease (3), highlighting the urgent need for better therapeutic strategies for metastatic breast cancer.

Breast cancer risk is influenced by a combination of genetic, hormonal, and lifestyle factors. Age is the most significant risk factor, as the likelihood of developing breast cancer increases over time (4,5). A family history of breast cancer further elevates risk, particularly when associated with hereditary mutations in the breast cancer 1 and breast cancer 2 (*BRCA1* and *BRCA2*) genes, or other susceptibility genes such as partner and localizer of *BRCA2* (*PALB2*), tumor protein p53 (*TP53*), checkpoint kinase 2 (*CHEK2*) or ataxia telangiectasia mutated (*ATM*) (6). It is estimated that 5%-10% of women with breast cancer carry a germline mutation in *BRCA1* or *BRCA2 (gBRCA1 or gBRCA2)* (5,7,8).

Hormonal factors also play a key role. Elevated endogenous estrogen levels due to early menarche or late menopause prolongs lifetime estrogen exposure, increasing risk (5,9,10). Similarly, nulliparity and older age at first childbirth are linked to a higher likelihood of developing breast cancer (5). Hormone replacement therapy has also been associated with increased risk (5,11).

Lifestyle and environmental factors contribute as well. Alcohol consumption has a dose-dependent effect on risk (5), while postmenopausal obesity increases breast cancer likelihood due to greater estrogen production in adipose tissue (5,12). Dense breast tissue, which can make detection more difficult, is also a risk factor (5,13). Additionally, a personal history of breast cancer or benign breast disease suggests a predisposition to malignancy (5,14–17). Radiation exposure to the chest, especially at a young age, further elevates risk (18).

Understanding these factors is crucial for early detection, risk assessment, and developing preventive strategies.

1.2 Breast cancer tumorigenesis and progression

Cancer arises due to the uncontrolled proliferation of abnormal cells, which fail to respond to standard regulatory signals. In addition to sustaining proliferative signaling, cancer cells acquire a range of biological capabilities that drive tumor progression. These include evading growth suppressors, resisting cell death, enabling replicative immortality, inducing angiogenesis, activating invasion and metastasis, reprogramming cellular metabolism, avoiding immune destruction, and presence of senescent cells, among others (19–21).

Cancers are classified based on their tissue of origin: carcinomas, which account for around 90% of cases, arise from epithelial cells, sarcomas develop from connective tissues, and leukemias/lymphomas originate from blood-forming or immune cells (22). Breast carcinomas can also be divided into two major histological subtypes: ductal carcinomas, which account for over 75% of all breast carcinomas, and lobular carcinomas, which comprise 10%-15% of all cases. Less common special subtypes include mucinous, cribriform, micropapillary, papillary, tubular, medullary, metaplastic, and inflammatory carcinomas (4,23).

Breast tumors are believed to develop through a stepwise progression from atypical hyperplasia (benign abnormal cell growth) to ductal carcinomas in situ (DCIS) due to genetic and/or epigenetic alterations. DCIS can evolve from their preinvasive state to an invasive state due to further alterations, becoming invasive ductal carcinomas, which may eventually progress to metastatic disease if tumor cells disseminate through the bloodstream or the lymphatic system to distant organs (23,24) (Invasion-metastasis cascade described in Section 2.1). Even though they are less frequent, lobular carcinomas in situ (LCIS) can also be considered a precursor lesion for invasive lobular carcinoma (25).

1.3 Breast cancer classification

Staging classifications were introduced in the early 20th century to help clinicians better understand cancer progression, categorize patients into subgroups, and compare clinical outcomes within these groups. In 1977, the American Joint Committee on Cancer (AJCC) published the first staging system based on the TNM concept, which classifies patients with

breast cancer according to tumor size, lymph node involvement, and metastasis (26). Over the years, this system has evolved to incorporate new research findings, leading to the implementation of the 8th edition in 2018. This latest edition expands the traditional TNM classification by incorporating advancements in tumor biology and prognostic biological markers, such as histological grade, hormone receptor (HR) status, human epidermal growth factor receptor 2 (HER2) status, proliferation marker Ki-67, and gene expression profiling (when available). These guidelines enable clinicians to classify patients into prognostic groups and treat breast cancer as the heterogeneous disease that it is (27,28).

1.3.1 The TNM classification

The TNM classification for breast cancer consists of three main components:

- Tumor size (T): Describes the size of the primary tumor. Ranges from Tis (in situ) to T4 (invasive tumor with chest wall or skin involvement).
- Lymph node involvement (N): Indicates whether the cancer has spread to nearby lymph nodes, ranging from no lymph node involvement (N0) to extensive nodal involvement (N3).
- Metastasis (M): Identifies whether the cancer has spread to distant organs and is classified as no distant metastasis (M0) or presence of distant metastasis (M1).

According to the AJCC staging manual, each category is assigned a number or letter, which helps determine the overall cancer stage, ranging from 0 to IV **(Table 1)** (27).

Table 1. Breast cancer staging following the AJCC's TNM classification (27)**.**

Stage	Description	Tumor	Lymph nodes	Metastasis
0	Non-invasive carcinoma in situ	Tis	N0	M0
I	Small tumor, no lymph node involvement	T1 (≤ 2 cm)	N0	M0
II	Minimal lymph node spread or larger tumor	T0 to T2	N1 (1-3 nodes)	M0
		T2 (> 2, ≤ 5 cm)	N0	M0
III	Locally advanced cancer with significant lymph node involvement	T3 (> 5 cm) to T4 (chest wall or skin involvement)	N2 (4-9 nodes) to N3 (≥ 10 nodes)	M0
IV	Metastatic cancer	Any T	Any N	M1

1.3.2 The Nottingham Grading System

The Nottingham (Elston-Ellis) modification of the Scarff-Bloom-Richardson grading system, also known as the Nottingham Grading System (NGS), grades breast tumors based on the degree of tubule/duct formation, nuclear size, nuclear pleomorphism, and mitotic rate, ranging from 1 (well differentiated) to 3 (poorly differentiated). This system helps predict breast cancer aggressiveness and, along with other clinicohistological information, helps guide treatment decisions and prognosis (29).

1.3.3 Immunohistochemical classification

Breast cancer is classified based on the expression of estrogen receptor (ER), progesterone receptor (PR), and HER2. HR status, defined by ER and PR expression, is assessed using immunohistochemistry (IHC), with $\geq$ 1% staining considered positive (30). HER2 status is also evaluated by IHC, where staining intensity is graded as follows: negative (0 or 1+), equivocal (2+), or positive (3+). A score of 0 indicates no staining, 1+ represents weak and incomplete membrane staining in less than 10% of tumor cells, and 3+ indicates strong and complete membrane staining in more than 30% of tumor cells. A score of 2+ indicates moderate and incomplete membrane staining in more than 10% of tumor cells, which is considered equivocal. For these cases, in situ hybridization (ISH) is performed to determine *ERBB2*/HER2 gene amplification. Tumors with a HER2/CEP17 ratio < 2.0 (non-amplified) are classified as HER2-negative, while those with a ratio $\geq$ 2.0 (amplified) are considered HER2-positive (31).

This classification results in four major clinical subgroups **(Figure 2)**:

1. HR-positive/HER2-negative (HR+/HER2-)
2. HR-positive/HER2-positive (HR+/HER2+)
3. HR-negative/HER2-positive (HR-/HER2+)
4. HR-negative/HER2-negative (HR-/HER2-) or triple-negative breast cancer (TNBC)

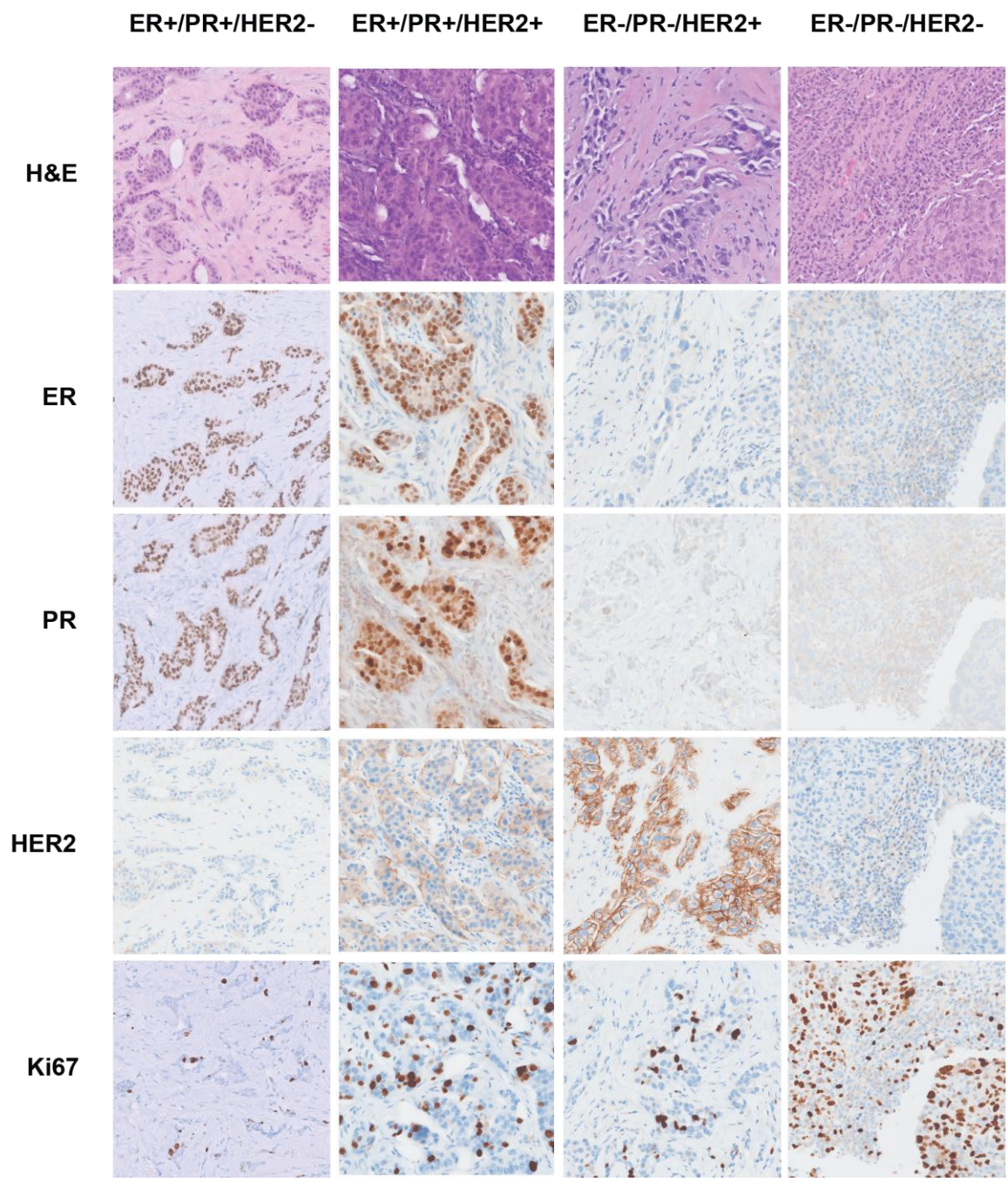

Figure 2. Representative IHC images of breast cancer subtypes based on HR and HER2 status. Representative IHC images showing the expression patterns of ER, PR, HER2, and Ki-67 in each clinical subgroup: HR+/HER2-, HR+/HER2+, HR-/HER2+, and HR-/HER2-. Cancer histology is illustrated using hematoxylin and eosin (H&E) staining. Original magnification, x20. Image courtesy of Dr. Sanfeliu.

The traditional IHC classification of breast cancer has historically divided tumors into HER2-positive and HER2-negative. However, emerging research has revealed a spectrum of HER2 expression, which has led to the identification of two additional groups. While HER2-negative, null, or 0 tumors are completely free of staining, HER2-ultralow tumors have an IHC staining

of 0 but show faint membrane staining, and HER2-low tumors are IHC 1+ or IHC 2+/ISH-negative (32,33). HER2-low tumors represent 59.7% of all HER2-negative cases, 67.6% are classified as IHC 1+, and are more common in HR+ breast cancer than in TNBC (65.4% vs. 36.6%) (34). Further research is ongoing to better understand the clinicopathological and molecular characteristics of these groups in order to optimize treatment strategies.

Together with the disease burden, the histopathological classification is of great importance for the choice of therapy in the clinical setting, as it is a key determinant of the treatment each patient will receive (23).

HR+/HER2- tumors account for approximately 70% of all breast cancers (3,35). The standard treatment includes hormone or endocrine therapy, such as tamoxifen or aromatase inhibitors (AIs), with chemotherapy reserved for aggressive or high-risk cases (5,36). In patients at high risk of relapse, the addition of adjuvant cyclin-dependent kinase 4/6 (CDK4/6) inhibitors to standard endocrine therapy significantly improves invasive disease-free survival (37).

HER2+ breast cancers are characterized by the overexpression or amplification of the HER2 receptor (31). These tumors tend to be more aggressive than HER2-negative tumors but have significantly benefited from the development of HER2-targeted therapies, such as trastuzumab, pertuzumab, tyrosine kinase (TK) inhibitors (TKIs) such as lapatinib, tucatinib or neratinib, and antibody-drug conjugates (ADCs) such as trastuzumab emtansine (T-DM1) or trastuzumab deruxtecan (T-DXd) (38). Standard regimens often include a combination of agents, sometimes starting with neoadjuvant chemotherapy to shrink the tumor and allow for more conservative surgery (5,36). Additionally, patients with HR+/HER2+ tumors, which express both HER2 and HRs, are also typically treated with endocrine therapy (5,36).

Lastly, TNBCs, which lack both HRs and HER2, represent 15%-20% of all breast cancer cases. These tumors are often high-grade and associated with a poor prognosis (39). Patients with TNBC heavily rely on chemotherapy (e.g., anthracycline, taxanes, platinum), although newer treatments, such as Poly (ADP-ribose) polymerase (PARP) inhibitors for gBRCA1/2 mutation carriers (See Section 2.2.4) (40,41) or immunotherapy, are available (5,36). Immune checkpoint inhibitors (ICIs), such as pembrolizumab and atezolizumab (programmed cell

death protein 1 (PD-1) and its ligand (PD-L1) inhibitors), have shown clinical benefit in PD-L1+ TNBC patients (42,43).

Tumor-infiltrating lymphocytes (TILs) have emerged as a valuable biomarker in breast cancer, with their presence and density offering insights into the tumor microenvironment (TME) and potential treatment responses. TNBCs typically have higher levels of TILs compared to other subtypes. Studies have demonstrated that higher TIL levels in TNBC are associated with improved overall prognosis and better response to chemotherapy (44–48). A high TIL presence suggests an active immune microenvironment, making TNBC a prime candidate for immunotherapy. Similar to TNBC, HER2+ tumors can exhibit varying levels of TILs. Increased TILs in these tumors have been linked with a favorable prognosis and enhanced response to anti-HER2-based chemotherapies (49,50). While TILs contribute to a better prognosis and treatment response in HER2+ tumors (46–52), HER2-targeted therapies remain the cornerstone of treatment. Finally, HR+/HER2- tumors generally have lower TIL counts compared to TNBC and HER2-positive tumors. While high TILs in these tumors are less common, emerging data suggest that a high-risk subset of HR+/HER2- cancers with increased TILs might exhibit different clinical behavior or potentially benefit from immunomodulatory treatments (47,53).

1.3.4 PAM50 intrinsic subtypes

Over the past two decades, advancements in gene expression profiling have greatly improved our understanding of the molecular heterogeneity of breast cancer. These advances provide valuable prognostic information that complements traditional clinical and histopathological assessments. Four main molecular subtypes of breast cancer have been identified: Luminal A, Luminal B, HER2-enriched, and Basal-like, along with a Normal-like group (54–57). This has led to the development of Prosigna, a clinically applicable gene expression-based test that uses the PAM50 algorithm to classify tumors into these intrinsic subtypes (58). These subgroups have revealed key differences in incidence (59), survival (55,58), and response to treatment (60–62) among patients with breast cancer, enabling more personalized treatment options.

Luminal breast cancers exhibit the greatest heterogeneity in gene expression, mutation spectrum, copy number alterations, and patient outcomes (63–65). Both Luminal A and Luminal B subtypes show similarly high mRNA and protein levels of the luminal expression signature, along with a high mutation frequency of phosphoinositide-3-kinase catalytic subunit alpha (*PIK3CA*) (49% and 32%, respectively) and cyclin D1 (*CCND1*) amplification (29% and 58%, respectively) (64). Luminal A tumors are less aggressive and are associated with the most favorable prognosis. Although ER levels are similar in both subtypes, Luminal A tumors express higher levels of PR (63,65,66) and lower Ki-67. These tumors are also considered the most likely to preserve retinoblastoma 1 (*RB1*) and *TP53* function, as indicated by high *RB1* expression and elevated markers of functional *TP53*, along with intact *TP53* activity (63,64). In contrast, Luminal B tumors exhibit a higher frequency of *TP53* mutations (32% compared to 12% in Luminal A), contributing to their more proliferative and aggressive phenotype (64,66).

The HER2-enriched intrinsic subtype is characterized by elevated expression of HER2-related and proliferation-related genes, such as *ERBB2* and growth factor receptor-bound protein 7 (*GRB7*), and their corresponding proteins. At a DNA level, these tumours exhibit the highest mutation burden, with notable mutations in *TP53* (75%) and *PIK3CA* (42%). Beyond HER2 signaling, HER2-enriched tumors also demonstrate increased expression of other receptor TKs (RTKs), including fibroblast growth factor receptor 4 (*FGFR4*) and epidermal growth factor receptor (*EGFR*) (64). Additionally, HER2-enriched tumors frequently harbor *APOBEC3B*-associated mutations, which are a result of DNA replicative stress (67).

Basal-like tumors are considered the most aggressive form of breast cancer and are associated with the worst prognosis. These tumors are characterized by high proliferation rates, evidenced by elevated levels of marker of proliferation Ki-67 (*MKI67*) and other proliferation-related genes. They also express basal cytokeratins (such as 5, 6, and 17) and generally lack expression of estrogen and HER2-related genes. *TP53* loss is observed in up to 75% of all cases, and loss of *RB1* and *BRCA1* are also common features of Basal-like tumors (63,64,68).

A group resembling normal tissue, exhibiting gene expression patterns typically associated with adipose tissue and clustering with fibroadenoma and normal breast tissue, has also been

identified and labeled as “Normal-like” (69). Its clinical significance remains unclear, and many, including our group, consider it an artifact, likely resulting from contamination of the specimen by normal tissue (55,56,58,70,71).

Each of the PAM50 subtypes is represented across all histological groups **(Figure 3)** (57). Luminal A and Luminal B subtypes are predominantly found in HR+ breast cancers (90%), while the HER2-enriched subtype is typically associated with HER2+ breast cancers (54.6%), and the Basal-like subtype is most commonly observed in TNBC (78.8%). However, other intrinsic subtypes are also present within each IHC group (63–65,72). Understanding the distribution of PAM50 subtypes within IHC groups is crucial, since this intraheterogeneity adds significant complexity to treatment decision-making, underscoring the importance of personalized treatment strategies as patients with apparently similar subtypes can respond differently to the same therapies.

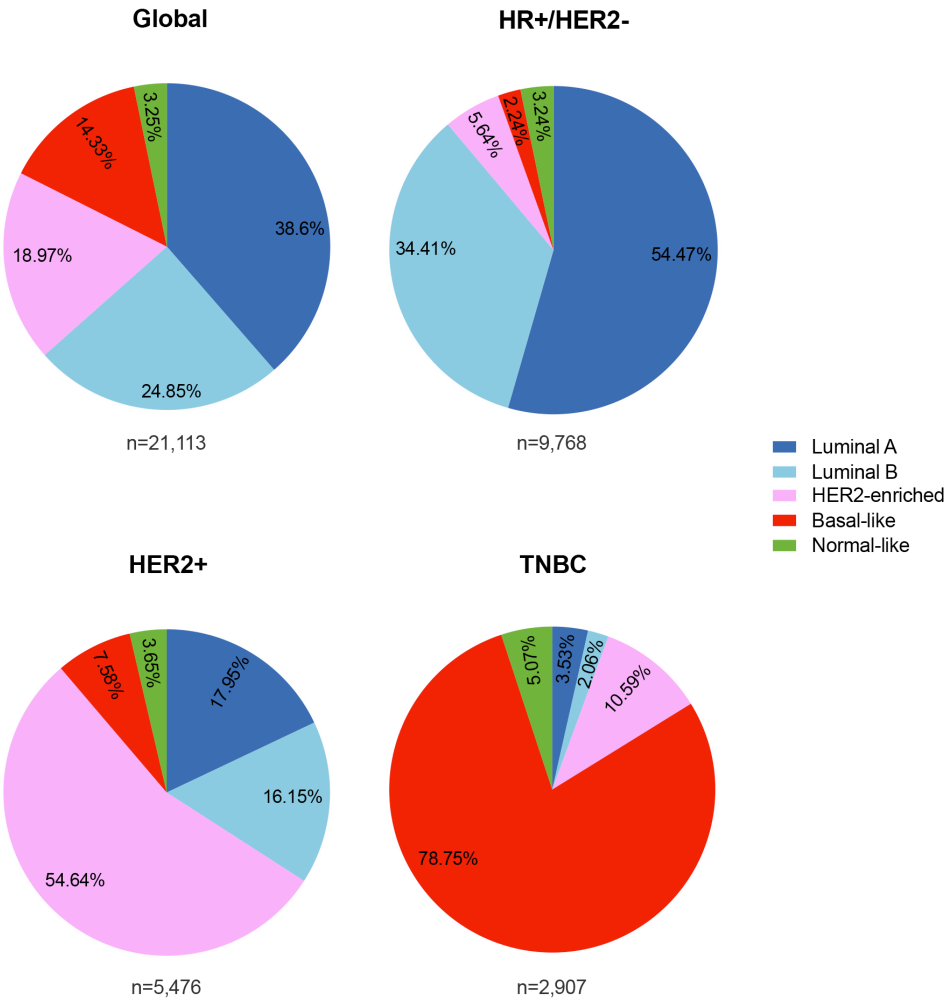

Figure 3. Molecular heterogeneity of early breast cancer. Intrinsic subtype distribution in the global cohort, HR+/HER2-, HER2+, and TNBC by IHC. Adapted from reference (72).

2. Metastatic breast cancer

Following recent progress in classifying and understanding primary breast cancer, more focus has been put on the importance of metastasis, which accounts for 90% of solid tumor-related deaths and is considered an uncurable disease (73,74).

Metastasis continues to be the most elusive aspect of cancer progression. It arises from a complex evolutionary process where interactions between cancer cells and their surrounding environment trigger changes that enable them to spread, adapt, and survive in different tissues, ultimately resulting in organ failure and death (75). De novo metastatic breast cancer, which accounts for approximately 5% of all breast cancer presentations, is diagnosed when metastases are already present at the time of initial diagnosis, indicating that the cancer has spread before detection. In contrast, recurrent metastatic breast cancer occurs when metastases develop after a period of remission following primary treatment (76).

Breast cancer commonly spreads to the bones, lungs, liver, and brain, as well as to distant lymph nodes, and the pattern of metastasis varies depending on the molecular subtype (77). For HR+ breast tumors, the bones are the most frequent site of metastasis (77). These tumors have the best prognosis and a low incidence rate within the first five years, which gradually increases beyond five years (78). In contrast, HER2+ breast tumors, which tend to be more aggressive, have a higher propensity to metastasize to the brain (77,78). While HER2+ breast cancer has numerous targeted treatment options, the development of brain metastases significantly complicates prognosis (79,80). Meanwhile, TNBC is known for its highly aggressive nature and increased likelihood of spreading to visceral organs, as well as the brain. TNBC metastases often occur earlier in the disease course, within the first two years, and are associated with a poorer prognosis due to the limited availability of targeted therapies (77,78,81).

2.1 The invasion-metastasis cascade

The invasion-metastasis cascade is a complex multistep process by which cancer cells escape the primary tumor and spread to distant organs **(Figure 4)** (73,74,82–84). It is rare for individual cancer cells to successfully complete all steps due to several mechanical and

molecular bottlenecks. In animal models, fewer than 0.01% of the cancer cells entering circulation ultimately develop into metastases (85).

Most cancers originate in epithelial tissues, separated from the stroma by the extracellular matrix (ECM) (22). Carcinomas remain non-invasive as long as they are confined to the epithelial side of the ECM. They become invasive once they breach the basement membrane (BM) of the ECM, allowing them to detach from the primary tumor and invade the surrounding stroma as disseminated tumor cells (DTCs) **(Figure 4.1)**. Matrix metalloproteinases (MMPs) have a proteolytic activity and are primarily responsible for the degradation of the BM (86). After breaching the BM, DTCs enter the stromal compartment, where they gain access to blood and lymphatic vessels (87).

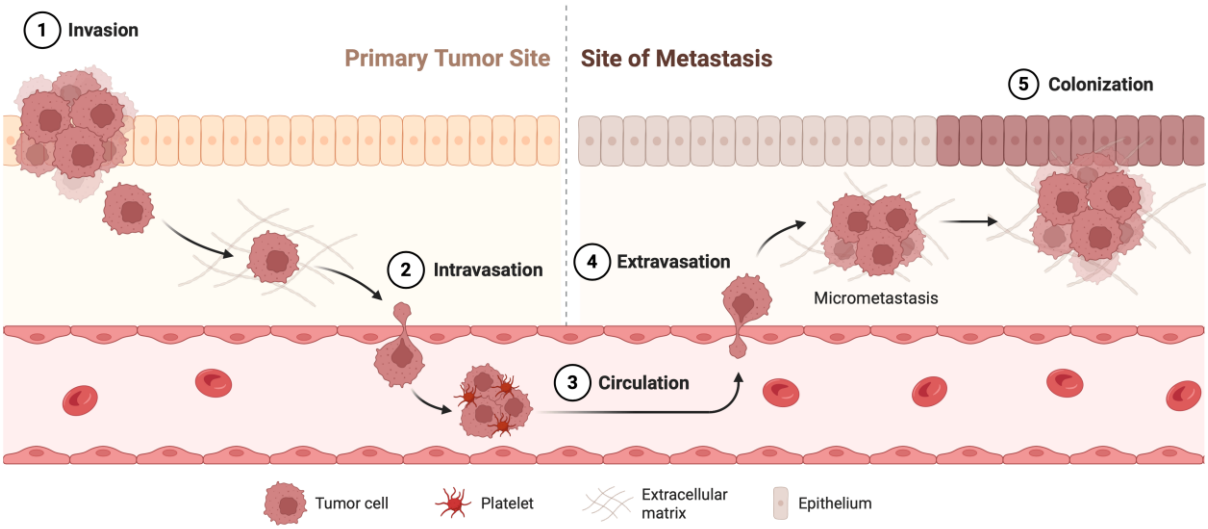

Figure 4. Tumor cell dissemination via the invasion-metastasis cascade. Schematic overview of the multistep process by which cancer cells spread from the primary tumor to distant organs. The sequence includes: (1) invasion of surrounding tissue, (2) intravasation into the blood or lymphatic vessels, (3) survival and transport through the circulatory system, (4) extravasation into distant tissues, leading to the formation of micrometastases, and (5) colonization, where micrometastases grow into clinically detectable macrometastases. Illustration created using a template in BioRender.com

A key driver of this first step of the metastatic cascade is the epithelial-mesenchymal transition (EMT), where epithelial cells can undergo a phenotypic shift to acquire mesenchymal characteristics, such as enhanced motility and invasiveness (88,89). This transition is regulated by a network of signaling pathways and transcription factors that drive cellular changes, including the disruption of cell-cell adhesion by loss of E-cadherin (88,90–93), loss of cell polarity, and reorganization of the cytoskeleton (88). In the reverse process, the mesenchymal-epithelial transition (MET), cells regain epithelial characteristics after

undergoing EMT (88,89). It has been suggested that EMT and MET are not strict, linear processes but instead represent a continuum of dynamic and reversible transitions, contributing to epithelial-mesenchymal plasticity (EMP) (94)**.** This plasticity leads to a spectrum of phenotypic states that contribute to the heterogeneous nature of tumors. Alternative metastatic mechanisms beyond EMT have also been proposed, such as collective or amoeboid migration, which allow cancer cells to disseminate and invade surrounding tissues without undergoing a full EMT (95).

Individual or small clusters of DTCs that detach from the primary tumor can enter the vessel lumina through a process called intravasation **(Figure 4.2)**. Upon entering the circulatory system, DTCs become circulating tumor cells (CTCs). These migrating cells must overcome many challenges during the circulation stage **(Figure 4.3)**, including cell death from anoikis due to the lack of anchorage to substrates (96), cell damage due to hydrodynamic shear forces in the circulation, and attacks from the immune system. Some have shown that CTCs enhance survival by forming clusters or interacting with blood platelets (97,98).

The physical lodging of CTCs in small vessels represents the first step of extravasation **(Figure 4.4)** (99). Once trapped, CTCs exit the bloodstream either by attaching to the vessel walls and penetrating the endothelium of the surrounding tissue (parenchyma) (84) or by proliferating within the vessel's lumen until causing vessel disruption (100). Once in the tissue's parenchyma, DTCs can form micrometastases, which may eventually grow into macrometastases through a process called colonization **(Figure 4.5)**. Colonization is considered a rate-limiting step in the metastatic cascade (84,99). Other DTCs may remain dormant for months or years, forming micrometastases that are too small to detect with conventional imaging techniques. Over time, these quiescent cells can reactivate, leading to the formation of macrometastases that are usually accompanied by a second wave of dissemination, typically responsible for most metastasis-associated deaths.

Once established in a secondary site, metastatic tumors can stimulate the formation of new blood vessels, a process known as angiogenesis, considered a hallmark of metastatic cancer (19–21). This new vasculature is essential for supplying the growing tumor with nutrients and oxygen, supporting continued tumor expansion and the formation of macrometastases.

2.2 Targeted therapeutic strategies for metastatic HR+/HER2- breast cancer

Metastatic breast cancer is considered an incurable disease, and although advancements in therapy have improved patients' quality of life and extended survival rates, most patients eventually experience disease progression and do not survive.

HR+/HER2- tumors represent approximately 70% of all breast cancers (35), therefore, this thesis will focus exclusively on this subgroup of patients moving forward. The European Society for Medical Oncology (ESMO) 2024 guidelines recommend a stepwise treatment strategy for advanced HR+/HER2- patients, incorporating endocrine therapy, targeted agents, and chemotherapy, depending on disease progression and molecular profiling (5). Since the identification of ER as a predictive biomarker for endocrine therapy response, hormone-based treatments have significantly contributed to reducing breast cancer-related mortality (101). The current international consensus guidelines for treatment of advanced HR+ breast cancer recommend endocrine therapy in combination with CDK4/6 inhibitors as part of the initial first-line treatment unless there is evidence of a visceral crisis (5). The addition of CDK4/6 inhibitors to endocrine therapy in patients with advanced HR+/HER2- breast cancer has led to substantial improvements in progression-free survival (PFS) and overall survival (OS) (102–116). Second-line treatment options and beyond depend on factors such as prior treatments, disease burden, mutational status, and patient preferences.

2.2.1 Endocrine therapy

ERs are nuclear HRs that mediate the effects of estrogen within cells. In breast cancer, ERα is the predominant form and plays a critical role in disease progression. Estradiol (E2), mainly produced in the ovaries, is the primary and most biologically active form of estrogen in premenopausal women (117). In HR+ breast cancer, E2 stimulates tumor growth by selectively binding to ERα, which leads to the activation of pathways that promote cell proliferation. As a result, hormone therapies are used to block estrogen signaling and prevent cancer progression in hormone-dependent tumors. Various endocrine therapy agents are available for HR+ breast cancer treatment, each acting through distinct mechanisms (118).

Selective ER modulators (SERMs) compete with E2 for binding to ER in breast tissues, acting as ER antagonists that inhibit estrogen-driven tumor growth. However, SERMs also exert

agonistic effects in other tissues, such as bone, liver, and uterus. Tamoxifen, the first hormone-based treatment option for HR+ patients, remains a standard therapy for premenopausal women with HR+ breast cancer (117,119).

Selective ER degraders (SERDs) such as fulvestrant inhibit ER dimerization, DNA binding, and nuclear translocation, thereby accelerating ER degradation and blocking estrogen signaling. Unlike SERMs, SERDs do not exert agonistic effects in other tissues (117,120). Of note, another SERD, elacestrant, was recently approved by the Food and Drug Administration (FDA) for the treatment of patients with HR+/HER2- and estrogen receptor 1 (*ESR1*)-mutated metastatic breast cancer who have progressed after at least one line of endocrine therapy. *ESR1* mutations, typically acquired following treatment with AIs, are considered a mechanism of resistance to endocrine therapy. The EMERALD phase III trial demonstrated that elacestrant significantly improves PFS in these patients compared to standard endocrine therapies such as AIs or tamoxifen (5,121).

AIs inhibit the enzyme aromatase, which is responsible for converting androgens into estrogen, thereby reducing overall E2 levels. Nonsteroidal AIs, such as anastrazole and letrozole, as well as the steroidal AI exemestane (5,122–124), are commonly used in postmenopausal women. Meta-analyses have shown that AIs are the preferred first-line treatment for postmenopausal HR+ patients, offering better efficacy than tamoxifen (123,124).

For premenopausal women, ovarian function suppression should also be considered as part of endocrine therapy. This can be achieved using gonadotropin-releasing hormone (GnRH) agonists (GnRHa) such as goserelin and leuprolide. These GnRHa work by initially stimulating the release of luteinizing hormone (LH) and follicle-stimulating hormone (FSH), resulting in a temporary increase in estrogen levels. However, with continuous use, they cause downregulation of GnRH receptors in the pituitary gland, ultimately suppressing ovarian function and reducing estrogen levels, thereby enhancing the efficacy of endocrine therapy in premenopausal patients (5,125,126).

For patients who progress on first-line endocrine therapy but remain endocrine-sensitive, a switch in endocrine therapy is typically recommended. This may involve changing from one

AI to another, or from an AI to tamoxifen or fulvestrant, helping to delay the need for intravenous (IV) chemotherapy (5).

2.2.2 CDK4/6 inhibitors

2.2.2.1 Clinical evidence

Three CDK4/6 inhibitors (i.e., palbociclib, ribociclib, and abemaciclib) are approved by the FDA and the European Medicines Agency (EMA) for first-line treatment of HR+/HER2- metastatic breast cancer. These inhibitors are administered in combination with endocrine therapy agents such as AIs, fulvestrant, or tamoxifen (5,127).

Several clinical trials have demonstrated the significant benefit of adding CDK4/6 inhibitors to endocrine therapy, showing improved PFS in patients with HR+/HER2- metastatic breast cancer compared to endocrine therapy alone **(Table 2)** (128). Palbociclib was evaluated in three key randomized clinical trials: PALOMA-1 (102), PALOMA-2 (103), and PALOMA-3 (104). Ribociclib was studied in the MONALEESA trial series, including MONALEESA-2 (106), MONALEESA-3 (107), and MONALEESA-7 (109). Similarly, abemaciclib was evaluated in the MONARCH trials, namely MONARCH 2 (110) and MONARCH 3 (112,113). Additionally, MONARCH 1 assessed abemaciclib as a monotherapy (129), leading to its approval in the later-line setting for HR+/HER2- metastatic breast cancer in patients who had progressed on prior endocrine therapy. In addition to prolonging PFS, OS improvement was reported in the MONALEESA-2 (115), MONALEESA-3 (114), and MONALEESA-7 (108) trials for ribociclib and in MONARCH 2 (111) for abemaciclib **(Table 2)**. These findings reinforce the role of CDK4/6 inhibitors in improving clinical outcomes for patients with HR+/HER2- metastatic breast cancer.

Table 2. Characteristics of pivotal clinical trials investigating CDK4/6 inhibitors in breast cancer.

Trial	Phase	Menopausal status	Combination	Median PFS (months)	Median OS (months)
PALOMA-1	II	Postmenopausal	Palbociclib + letrozole vs letrozole	20.2 vs 10.2 (h.r. 0.488; 95% CI, 0.319-0.748; p=0.0004)	NS: 37.5 vs 33.3 (h.r. 0.81; 95% CI 0.49-1.35; p=0.42)
PALOMA-2	III	Postmenopausal	Palbociclib + letrozole vs letrozole	24.8 vs 14.5 (h.r. 0.58; 95% CI, 0.46-0.72; p<0.001)	NS: 51.6 vs 44.6 (h.r. 0.869; 95% CI, 0.706-1.069)
PALOMA-3	III	Pre-, peri- and postmenopausal	Palbociclib + fulvestrant vs fulvestrant	9.5 vs 4.6 (h.r. 0.46; 95% CI, 0.36-0.59; p<0.0001)	NS: 34.9 vs 28.0* (h.r. 0.81; 95% CI, 0.64-1.03; p=0.09)
MONALEESA-2	III	Postmenopausal	Ribociclib + letrozole vs letrozole	25.3 vs 16.0 (h.r. 0.57; 95% CI, 0.46-0.70; p<0.0001)	63.9 vs 51.4 (h.r. 0.76; 95% CI, 0.63-0.93; p=0.008)
MONALEESA-3	III	Postmenopausal	Ribociclib + fulvestrant vs fulvestrant	20.5 vs 12.8 (h.r. 0.59; 95% CI, 0.48-0.73; p<0.001)	NR vs 40.0 (h.r. 0.72; 95% CI, 0.57-0.92; p=0.004)
MONALEESA-7	III	Pre- and perimenopausal	Ribociclib + tamoxifen or AI + GnRHa vs tamoxifen or AI + GnRHa	23.8 vs 13.0 (h.r. 0.553; 95% CI, 0.441-0.694; p<0001)	NR vs 40.9 (h.r. 0.71; 95% CI, 0.54-0.95; p=0.01)
MONARCH-1	II	Postmenopausal	Abemaciclib	6.0 (95% CI, 4.2-7.5)	17.7 (95% CI, 16.0-NR)
MONARCH-2	III	Pre- and perimenopausal	Abemaciclib + fulvestrant vs fulvestrant	16.4 vs 9.3 (h.r. 0.55; 95% CI, 0.45-0.68; p<0.001)	46.7 vs 37.3 (h.r. 0.76; 95% CI, 0.61-0.95; p=0.014)
MONARCH-3	III	Postmenopausal	Abemaciclib + non-steroidal AI vs non-steroidal AI	28.18 vs 14.76 (h.r. 0.54; 95% CI, 0.42-0.79; p<0.0001)	NS: 66.8 vs 53.7 (h.r. 0.80; 95% CI, 0.64-1.02; p=0.066)

Data from references (102–114,129). NR: Not Reached. NS: Not Significant. CI: Confidence Interval. h.r.: Hazard Ratio. *In patients with HR+/HER2- advanced breast cancer who had sensitivity to previous endocrine therapy, treatment with palbociclib-fulvestrant resulted in longer OS than treatment with placebo-fulvestrant (39.7 vs 29.7 (h.r. 0.71; 95% CI, 0.55-0.94).

2.2.2.2 Biology and mechanism of action

Cyclins and CDKs are key regulators of cell cycle progression, controlling transitions through the G1, S, G2, and M phases **(Figure 5)**. CDKs are serine/threonine kinases that require activation by specific cyclins and are regulated by CDK inhibitors. In human cells, 20 CDKs and 29 cyclins have been identified (130). Among these, CDK1, CDK2, CDK4, and CDK6 directly regulate cell cycle transitions, while CDK7 functions as a CDK-activating kinase and also

participates in transcriptional regulation. CDKs 8–11 primarily regulate transcription of genes associated with the cell cycle (131,132).

CDK4/6 inhibitors are designed to selectively block CDK4 and CDK6, which are crucial for the transition from the G1 to S phase. These kinases interact with D-type cyclins (cyclin D1-3) to drive cell cycle progression **(Figure 5)** (133,134). In HR+ breast cancer, estrogen signaling increases cyclin D1 expression, leading to CDK4/6 activation (135,136). This, in turn, phosphorylates and inactivates the tumor suppressor RB1, releasing E2F transcription factors that drive cell cycle progression and may lead to uncontrolled cell proliferation (134). Under normal physiological conditions, CDK4/6 activity is tightly regulated by INK4 family inhibitors, such as $p16^{INK4A}$, which suppress their function **(Figure 5)** (137). However, in cancerous cells, these regulatory mechanisms are often disrupted, allowing for uncontrolled growth (137).

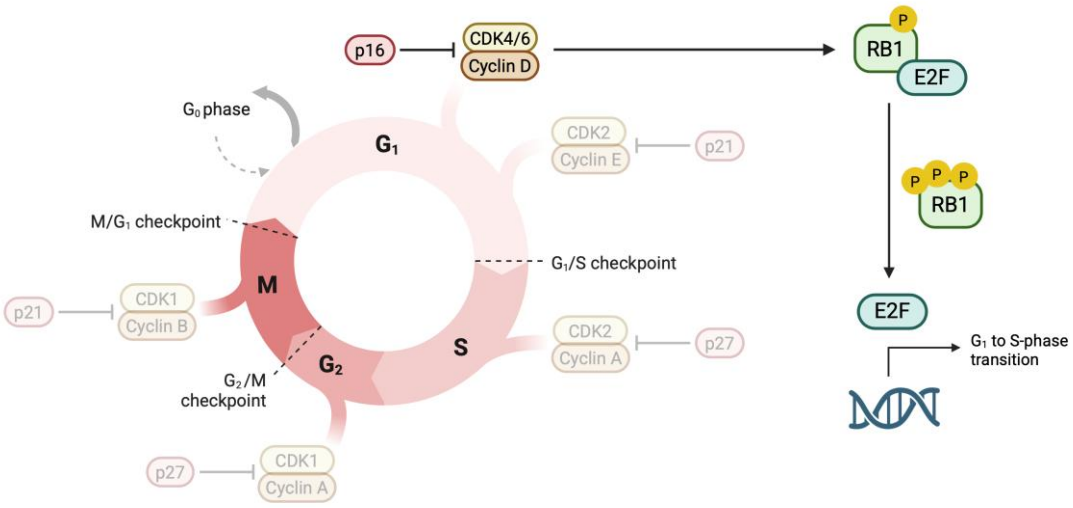

Figure 5. Regulation of cell cycle progression by CDKs. Mitogenic signals activate CDK4 and CDK6, promoting cell cycle entry through phosphorylation of RB1, which enables E2F-mediated transcription of genes required for DNA replication. This activation also induces expression of cyclins E and A, leading to CDK2 activation and further RB1 phosphorylation. Antiproliferative signals can inhibit CDK4/6 directly or via induction of the CDK inhibitor p16. Additional checkpoints regulate CDK2 through inhibitory proteins such as p21 and p27. As DNA replication completes, CDK1-cyclin A and CDK1-cyclin B complexes control G2/M transition. In the absence of DNA damage, CDK1-cyclin B drives mitotic entry, with checkpoints able to halt progression if errors are detected. Degradation of cyclin B is essential for anaphase progression and completion of mitosis. During this transition from M phase back into G1 phase, RB is dephosphorylated, and the cycle is once more responsive to mitogenic and antiproliferative signaling. The central role of the CDK4/6-Cyclin D-RB1-E2F pathway in regulating G1/S transition is highlighted in this illustration. Adapted from reference (137). Illustration created using a template in BioRender.com

Palbociclib, ribociclib, and abemaciclib bind to the ATP-binding pocket of CDK4 and CDK6, blocking their kinase activity. This prevents RB1 phosphorylation, enforces G1 phase arrest,

and effectively halts tumor progression (137–139). Prolonged CDK4/6 inhibition can drive cellular senescence, leading to irreversible growth arrest and phenotypic changes in breast cancer cell lines (140).

While all three CDK4/6 inhibitors share a common mechanism of action, they differ in their pharmacology, selectivity, pharmacokinetics (PK), and toxicity profiles. A summary of their key characteristics is provided in **Table 3**.

Table 3. Pharmacological characteristics of CDK4/6 inhibitors

	Palbociclib (PD-0332991)	**Ribociclib (LEE011)**	**Abemaciclib (LY-2835219)**
Chemical structure	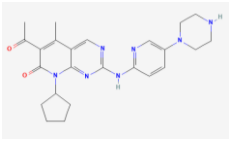	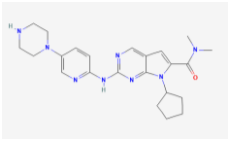	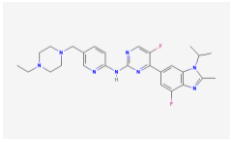
First FDA approval in combination with ET	2015	2017	2017
CDK4 (IC_{50})	11 nM	10 nM	2 nM
CDK6 (IC_{50})	15 nM	39 nM	10 nM
Other targets	No	No	CDK1, CDK2, CDK5, CDK9, CDK14, CDK16-18
Cell cycle arrest	G1 phase	G1 phase	G1, G2 phase
Recommended dose	125 mg/day on a 21-on-28-days schedule	600 mg/day on a 21-on-28-days schedule	150 mg twice daily
Administration	Oral	Oral	Oral
Half-life	29 (+/- 5) hours	32 hours	18.3 hours

Adapted from references (5,138,139,141,142). Chemical structures from: https://pubchem.ncbi.nlm.nih.gov

In brief, among the three, abemaciclib stands out due to its broader kinase inhibition profile. While palbociclib and ribociclib are highly selective for CDK4 and CDK6, abemaciclib also inhibits CDK1, CDK2, CDK5, CDK9, CDK14, and CDK16-18 (143). Despite its wider range of targets, abemaciclib is the most potent CDK4/6 inhibitor and has demonstrated the ability to cross the blood-brain barrier (144). Pharmacokinetically, abemaciclib has a shorter half-life and is administered twice daily. In contrast, palbociclib and ribociclib have longer half-lives and are administered once daily for 21 days, followed by a 7-day break to manage potential myelosuppressive effects (5,127). All three inhibitors can cause myelosuppression; however, abemaciclib is associated with a lower incidence of bone marrow suppression compared to

palbociclib and ribociclib (138,141). In contrast, it has a higher incidence of gastrointestinal toxicities, particularly diarrhea, nausea, and fatigue (110,141). Additionally, abemaciclib has been linked to elevated creatinine levels (110,129), whereas palbociclib and ribociclib are more frequently associated with neutropenia and other hematologic toxicities (104,107,141).

2.2.3 PI3K/AKT/mTOR inhibitors

Increased activation of the phosphatidylinositol 3-kinases/protein kinase B/mammalian target of rapamycin (PI3K/AKT/mTOR) pathway is a common mechanism of resistance to endocrine therapy and CDK4/6 inhibitors, and several targeted treatment options address this pathway (5,118).

For *PIK3CA*-mutated tumors, the combination of PI3K inhibitor alpelisib with fulvestrant is an approved treatment following progression to endocrine therapy and CDK4/6 inhibitors. The SOLAR-1 trial demonstrated that this combination significantly improves PFS in patients with HR+/HER2-/*PIK3CA*-mutated advanced breast cancer who have previously received endocrine therapy. However, this treatment is associated with adverse events such as hyperglycemia, gastrointestinal issues, and rash, which require careful patient selection and close monitoring (5,145).

For tumors harboring *AKT1* or phosphatase and tensin homolog (*PTEN*) mutations, AKT inhibitor capivasertib combined with fulvestrant provides an effective strategy to overcome endocrine therapy resistance by targeting the PI3K/AKT pathway. The CAPItello-291 phase III trial demonstrated that adding capivasertib to fulvestrant therapy provides a significant clinical benefit, prolonging PFS in patients with HR+/HER2- advanced breast cancer, especially those with *PIK3CA*/*AKT1*/*PTEN* mutations (5,146).

mTOR activation is also known to contribute to endocrine therapy resistance. The BOLERO-2 phase III clinical trial evaluated the efficacy and safety of combining mTOR inhibitor everolimus with exemestane in patients with HR+/HER2- advanced breast cancer who had developed resistance to prior nonsteroidal AI therapy. The combination treatment resulted in a significant increase in the median PFS, with common adverse events including stomatitis, anemia, hyperglycemia, dyspnea, and fatigue (5,147).

2.2.4 PARP inhibitors

PARP inhibitors, like olaparib or talazoparib, target the DNA repair mechanism and are promising options for patients with *gBRCA1/2* mutations**.** The OlympiAD and the EMBRACA phase III trials compared the efficacy of olaparib and talazoparib to chemotherapy in HR+/HER2-/*gBRCA1/2*-mutated patients. Both PARP inhibitors significantly improved PFS and overall response rates (ORR), while also providing patients with a better quality of life compared to chemotherapy. The main side effects observed were anemia, fatigue, and nausea (5,40,41).

2.2.5 ADCs

Over the past decade, ADCs have emerged as one of the most promising therapeutic strategies in the fight against cancer. ADCs are designed to deliver cytotoxic drugs directly to cancer cells, combining the specificity of monoclonal antibodies with the potency of chemotherapy agents. This targeted approach allows for the selective killing of tumor cells while minimizing off-target toxicity, a significant limitation of traditional chemotherapy. The structure of an ADC typically consists of a monoclonal antibody, which recognizes and binds to a cell surface tumor-specific antigen (TSA) or a tumor-associated antigen (TAA), linked to a potent cytotoxic agent through a linker that releases the drug once the ADC is internalized into the tumor cell. Depending on their design, linkers may be cleavable, responding to tumor-specific conditions such as acidic pH or lysosomal enzymes, or non-cleavable, releasing the active payload only after the antibody is fully degraded within the lysosome. The cytotoxic agent is often a highly potent chemotherapy drug or a toxin, designed to induce cell death upon its release inside the cancer cell (148).

To date, 13 ADCs have received clinical approval by the FDA (149). In the context of HR+/HER2- metastatic breast cancer, three have demonstrated significant clinical efficacy: sacituzumab govitecan (SG), datopotamab deruxtecan (Dato-DXd), and T-DXd.

SG is a first-in-class ADC targeting trophoblast cell-surface antigen 2 (TROP2) (150). It consists of a humanized anti-TROP2 monoclonal antibody conjugated through a hydrolysable CL2A linker to SN-38, the active metabolite of irinotecan (151), with a drug-antibody ratio (DAR) of 8. TROP2, a transmembrane calcium signal transducer, is highly expressed in solid tumors,

especially in HR+/HER2- and TNBC, and is associated with tumor progression and poor prognosis (152–154). In the TROPiCS-02 phase III study, SG demonstrated a benefit in PFS and OS in heavily pretreated, endocrine-resistant HR+/HER2- tumors (155). Since 2023, SG has been approved for the treatment of patients with metastatic HR+/HER2- breast cancer who have previously received at least one line of endocrine therapy, a CDK4/6 inhibitor, and two to four prior lines of chemotherapy (5).

Dato-DXd is an ADC targeting TROP2, composed of a humanized anti-TROP2 monoclonal antibody conjugated to topoisomerase I (TOP1) inhibitor deruxtecan (DXd) through a cleavable tetrapeptide linker, with a DAR of 4. This novel ADC has demonstrated promising efficacy in clinical trials, including in patients with pretreated HR+/HER2- metastatic breast cancer (156). The TROPION-Breast 01 phase III trial is currently evaluating Dato-DXd in comparison to chemotherapy in this patient population, with preliminary results indicating improved PFS (157). This has led to its recent FDA approval for the treatment of patients with HR+/HER2- metastatic breast cancer who have previously undergone endocrine-based therapy and chemotherapy.

T-DXd is an ADC targeting HER2, which consists of a humanized anti-HER2 monoclonal antibody conjugated to DXd through a cleavable tetrapeptide linker, with a DAR of 8 (158,159). The efficacy of T-DXd in HER2-low tumors was first evaluated in the DESTINY-Breast04 phase III trial, in which a significant improvement in PFS and OS compared to standard chemotherapy was demonstrated (160). The ongoing DESTINY-Breast06 phase III trial is further assessing T-DXd in both HER2-low and HER2-ultralow tumors. Primary results confirmed prolonged PFS in patients with HER2-low tumors and, for the first time, demonstrated improved PFS in the exploratory HER2-ultralow population (161). This led to the FDA approval of T-DXd for HER2-low and HER2-ultralow tumors, which, until recently, were deemed unlikely to benefit from HER2-targeted therapies (5).

In addition to these ADCs, others are under investigation for HR+/HER2- metastatic breast cancer. Patritumab deruxtecan (HER3-DXd), which targets HER3, is being tested for its potential to treat both HR+/HER2- and HR+/HER2-low tumors (162). Sacituzumab tirumotecan (Sac-TMT, also known as SKB264/MK-2870), a TROP2-directed ADC, is in early-phase trials and shows promise for HR+/HER2- patients (163,164). Several HER2-directed

ADCs are also being tested in HR+/HER2-low breast cancer patients, which may include HR+/HER2- patients with low HER2 expression. These are trastuzumab duocarmazine (SYD985) (165), MRG002 (166), and RC48-ADC (167).

These studies highlight the growing role of ADCs in HR+/HER2- breast cancer, offering new therapeutic opportunities for patients with limited options. However, treatment resistance and disease progression remain inevitable for some patients, underscoring the need for new targets, payloads, and combination strategies. Most ADCs in this setting currently use TOP1 inhibitor payloads due to their potent cytotoxicity and favorable therapeutic window (168). Yet, emerging studies show that tumor cells can acquire TOP1 mutations following treatment. These mutations can cause resistance not only to the given ADC but also cross-resistance to others using the same payload (169). This underscores the importance of developing ADCs with alternative payloads, such as microtubule inhibitors like monomethyl auristatin E (MMAE), which may remain effective despite TOP1-based resisistance and broaden therapeutic options for patients.

2.3 Molecular intrinsic subtype evolution

Breast cancer is a heterogeneous disease and its molecular classification plays a crucial role in guiding treatment decisions and predicting patient outcomes. However, accumulating evidence suggests that intrinsic subtypes are not static and may evolve as the disease progresses from primary to metastatic stages (65,170–173). These shifts can have significant clinical implications, potentially influencing treatment resistance and overall prognosis.

In 2017, Cejalvo et al. analyzed 123 paired primary and metastatic breast tumor samples, 70% of which were HR+/HER2- (170). While no significant differences were observed in the distribution of histological subtypes (HR+, HER2+, and TNBC), notable shifts in intrinsic subtypes were identified. Luminal A and Normal-like subtypes were significantly more prevalent in primary tumors, whereas Luminal B, HER2-enriched, and the Proliferation signature were more frequently expressed in metastatic tumors. During disease progression, approximately 40% of tumors underwent intrinsic subtype changes. Specifically, 55% of Luminal A tumors transitioned to Luminal B (40.4%) or HER2-enriched (14.9%). When Luminal A and B tumors were grouped, they found that 14.3% of luminal tumors evolved into HER2-

enriched, despite mostly being clinically HER2- (81% of the cases). Notably, the prevalence of the HER2-enriched subtype doubled following tumor progression (11.4% vs. 22%).

A subsequent study analyzed the distribution of intrinsic subtypes within HR+ breast cancer using publicly available data from 13,264 breast cancer samples across 39 studies (65). Among these tumors, 81.1% were classified as HR+/HER2-, while 18.9% were HR+/HER2+. Within the HR+/HER2- primary tumors, the intrinsic subtype distribution was: 54.5% Luminal A, 34.9% Luminal B, 5.8% HER2-enriched, 2.2% Basal-like, and 2.6% Normal-like. In the metastatic setting, these proportions shifted to 49.7% Luminal A, 28.7% Luminal B, 11.6% HER2-enriched, 2.0% Basal-like, and 8.1% Normal-like. Consistent with their previous study (170), the proportion of HER2-enriched tumors doubled after progression (5.8% to 11.6%).

Similar results were observed in another study that analyzed intrinsic subtype conversion in paired samples from 152 patients enrolled in the AURORA study (171). Subtype switching was detected in 36% of cases. Notably, 90% of Luminal A tumors switched to more aggressive subtypes in metastatic samples, and the proportion of HER2-enriched metastatic tumors was nearly twice that of primary tumors, having converted from Luminal A, Luminal B, Basal-like, and Normal-like tumors.

In a study led by Denkert et al., the proportion of HER2-enriched tumors was 17.2% before treatment, 13.8% after treatment, and 27.6% at metastasis. Notably, tumors that adopted the HER2-enriched phenotype at the metastatic stage were originally classified as luminal, with the majority being Luminal A (174).

In a recent study, 10,458 primary tumor samples and 763 metastatic samples from 27 different studies were collected and analyzed for changes in intrinsic subtype distribution (172). The proportions of the Luminal B and Basal-like subtypes remained relatively stable throughout tumor progression. However, the proportion of HER2-enriched tumors was significantly higher in metastatic samples compared to primary tumors (18% vs. 6%), while Luminal A tumors were observed at a significantly lower proportion in metastases than in primary tumors (34% vs. 54%) **(Figure 6)**.

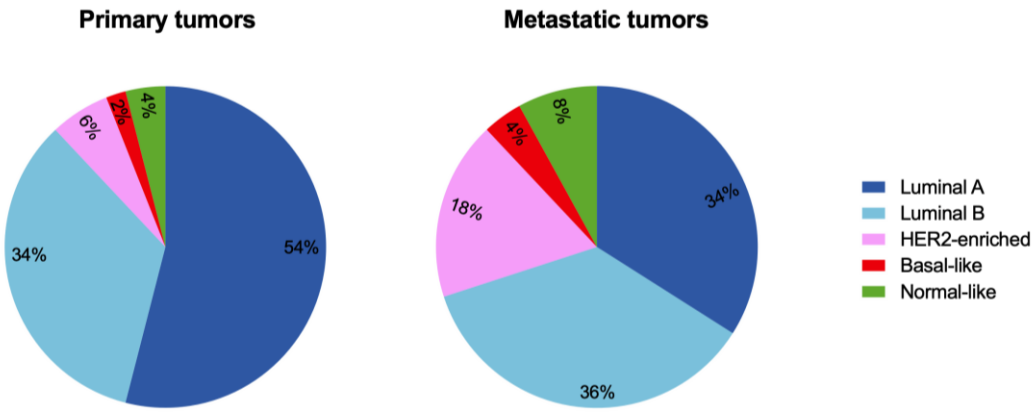

Figure 6. PAM50 subtype distribution in HR+/HER2- breast cancer. The distribution of the five intrinsic subtypes Luminal A, Luminal B, HER2-enriched, Basal-like, and Normal-like in Primary (n = 10,458) and Metastatic (n = 763) tumors are shown. Adapted from reference (172).

The dynamic nature of intrinsic subtype evolution underscores the need to reassess tumor classification throughout disease progression. Given that these subtypes are associated with distinct clinical outcomes, understanding their role in prognosis is crucial.

2.4 Prognostic value of intrinsic subtypes

Intrinsic molecular subtypes not only define the biological characteristics of breast cancer but also serve as key predictors of patient prognosis. Each subtype is associated with distinct survival outcomes, treatment responses, and risks of recurrence or metastasis. This section explores the prognostic value of intrinsic subtypes in metastatic HR+/HER2- breast cancer, highlighting their impact on disease progression and patient outcomes.

According to Falato et al., the distribution of intrinsic subtypes of HR+/HER2- breast cancer in metastatic sites is as follows: 34% of tumors are Luminal A, 36% are Luminal B, 18% are HER2-enriched, 4% are Basal-like, and 8% are Normal-like **(Figure 6)** (172). Hence, 22% of all tumors fall into the “non-luminal” intrinsic subtype group (i.e., HER2-enriched and Basal-like). The predictive value of intrinsic subtypes in response to endocrine therapy with or without targeted therapy has been explored in several studies.

In the EGF30008 phase III clinical trial, patients with HR+ metastatic breast cancer were randomized to letrozole with or without lapatinib (175). Among the 644 HR+/HER2- samples,

Luminal A tumors showed the longest median PFS and OS. The risk of progression was 1.46-fold higher in Luminal B, 2.88-fold higher in HER2-enriched, and 2.26-fold higher in Basal-like tumors. In HR+/HER2-/HER2-enriched tumors a benefit from lapatinib therapy was observed (median PFS, 6.49 vs 2.60 months, hazard ratio 0.238; 95% CI, 0.066-0.863; p=0.02) (62). Based on these findings, the NEREA phase II trial was designed to evaluate neratinib and endocrine therapy in patients with HR+/HER2-/HER2-enriched metastatic breast cancer that had progressed to prior endocrine therapy and a maximum of one line of chemotherapy (176).

The BOLERO-2 trial further elucidated the predictive value of intrinsic subtypes in response to targeted therapy. This phase III study enrolled postmenopausal patients with HR+/HER2- advanced breast cancer who had previously received endocrine therapy and randomized them to receive either the mTOR inhibitor everolimus or placebo, in combination with exemestane (147). While everolimus with exemestane significantly improved median PFS in all intrinsic subtypes compared to exemestane alone, a statistically significant PFS benefit from everolimus compared to placebo was only reported in Luminal A (8.3 vs 4.1 months, hazard ratio 0.39; 95% CI, 0.25-0.61; p<0.0001) and HER2-enriched tumors (5.8 vs. 4.1 months; hazard ratio 0.49; 95% CI, 0.26-0.90; p=0.034). Of note, a higher proportion of HER2-enriched samples were observed in metastatic tumors compared to primary tumors (32% vs. 19%) (177).

The ability of the molecular subtypes to predict benefit from CDK4/6 inhibitors in breast cancer was evaluated in samples from the PALOMA-2 (178), the NeoPalAna (179), and the MONALEESA-2, -3, and -7 (180) studies. A retrospective analysis of the PALOMA-2 trial, which randomized patients with HR+/HER2- advanced breast cancer to letrozole with or without palbociclib, analyzed the molecular subtype of 455 tumors. Whilst Luminal A (50%) and Luminal B (30%) subtypes benefited from the addition of palbociclib to letrozole, the HER2-enriched (18.7%) and Basal-like (0.5%) subtypes were associated with worse PFS in both treatment arms compared to the Luminal A group (178). In the NeoPalAna study, which evaluated the effects of palbociclib combined with anastrozole in patients with primary breast cancer, the PAM50 subtype was determined in 32 tumors at baseline. Of note, two tumors with non-luminal subtypes were identified, and were both resistant to palbociclib (179). Additionally, the SOLTI-1303 PATRICIA study of palbociclib and trastuzumab in HR+/HER2+

advanced breast cancer showed that the Luminal A and B subtypes benefited substantially from palbociclib, while the HER2-enriched group had a very small absolute benefit (181).

In contrast, a retrospective pooled analysis of the MONALEESA-2, -3, and -7 pivotal trials with ribociclib and endocrine therapy evaluated the PAM50 subtype of 1,160 tumor samples. Except for Basal-like tumors (2.6%), all other intrinsic subtypes showed a consistent PFS and OS benefit from the combination of endocrine therapy and ribociclib over endocrine therapy alone, with the HER2-enriched subtype (12.7%) exhibiting the highest relative and absolute benefit (180,182).

One could argue that despite both being CDK4/6 inhibitors, palbociclib and ribociclib differ in their chemical structures, mechanisms of action, and PKs **(Table 3)**, which might lead to dissimilarities in efficacy. In clinical practice, palbociclib is given at a lower dose than ribociclib (125 mg daily vs. 600 mg daily, respectively (5,127)), which could indicate a dose-dependent efficacy of CDK4/6 inhibitors in the biologically aggressive subtype HER2-enriched. These differences may have relevant clinical implications as ribociclib, but not palbociclib, has shown clinical benefit in other clinical scenarios, such as high-risk early breast cancer (183–186). The SOLTI-2101 HARMONIA phase III trial (187), which was designed to compare ribociclib plus endocrine therapy versus palbociclib plus endocrine threapy in HR+/HER2-/HER2-enriched advanced breast cancer, has now closed to recruitment. Although the study will not be able to formally assess its primary endpoint, analyses of collected samples are expected to provide valuable biological insights.

Finally, in a meta-analysis conducted by Schettini et al. (188), which included multiple prospective trials, it was observed that all non-Luminal A subtypes were significantly associated with worse PFS compared to Luminal A, independent of HER2 status, systemic treatment, and menopausal status. Notably, Luminal B tumors showed better prognostic outcomes than HER2-enriched and Basal-like subtypes.

Understanding the distribution and behavior of intrinsic subtypes in advanced disease stages is crucial for optimizing treatment strategies. Ongoing clinical trials aim to validate the prognostic and predictive value of intrinsic subtyping, with the goal of eventually integrating these insights into routine clinical practice. In particular, aggressive subtypes, such as HER2-

enriched (which accounts for 18% of all metastatic HR+/HER2- tumors **(Figure 6)**) (172), present unique therapeutic challenges and underscore the need for further research on targeted therapies to improve patient outcomes.

For instance, the TATEN phase II trial evaluated the combination of pembrolizumab and paclitaxel in patients with metastatic HR+/HER2- breast cancer and non-luminal PAM50 subtypes who had progressed on prior CDK4/6 inhibitor. The study was designed particularly for non-luminal subtypes (i.e., HER2-enriched and Basal-like), which are highly proliferative, have higher expression of immune-related genes and TILs, and may be more sensitive to chemotherapy in combination with immunotherapy. Indeed, the trial met its pre-specified primary endpoint with an ORR of 53.3% and a clinical benefit rate of 86.6% (189). These promising results suggest that combining pembrolizumab with paclitaxel could be a viable treatment strategy for patients with aggressive non-luminal subtypes. The ongoing correlative studies aim to identify predictive biomarkers of response, which could further refine personalized treatment approaches for this patient group.

3. Overcoming resistance to CDK4/6 inhibitors

3.1 Mechanisms of resistance to CDK4/6 inhibitors

The emergence of resistance to CDK4/6 inhibitors represents a significant clinical challenge, limiting the long-term efficacy of these therapies in HR+ breast cancer. Although many patients initially exhibit favorable responses to endocrine therapy combined with CDK4/6 inhibitors, resistance inevitably develops, leading to disease progression. Understanding the molecular mechanisms underlying this resistance is crucial for the development of new therapeutic strategies. This section provides an overview of the most well-established resistance mechanisms to CDK4/6 inhibitors to date **(Figure 7)**.

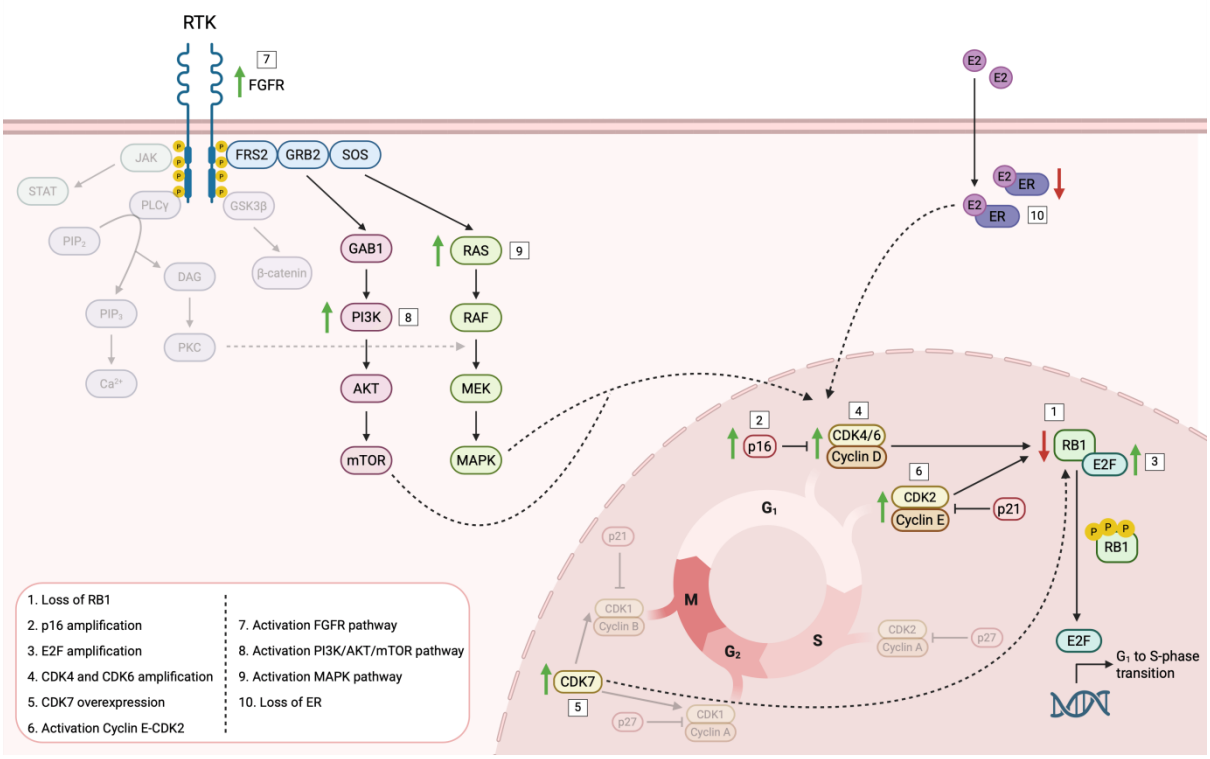

Figure 7. Mechanisms of resistance to CDK4/6 inhibitors. Schematic representation of key resistance mechanisms to CDK4/6 inhibitors. Cell cycle-dependent mechanisms include: (1) loss of RB1, (2) p16 amplification, (3) E2F amplification, (4) CDK4 and CDK6 amplification, (5) CDK7 overexpression, and (6) Cyclin E-CDK2 activation. Non-cell cycle-dependent mechanisms include: (7) FGFR pathway activation, (8) PI3K/AKT/mTOR pathway activation, (9) MAPK pathway activation, and (10) loss of ER. Adapted from reference (190). Illustration created using a template in BioRender.com

3.1.1 Cell cycle-dependent mechanisms

Cell cycle-dependent resistance mechanisms involve alterations that directly impact cell cycle regulation. Loss of RB1 is a well-established resistance mechanism, as RB1 is essential for

CDK4/6 inhibitors to effectively halt cell cycle progression **(Figure 7.1)**. Multiple studies have described the correlation between *RB1* mutations and resistance to CDK4/6 inhibitors (140,191,192), and a gene expression signature indicative of RB1-loss-of-function has been developed to predict palbociclib resistance (193,194). The absence of RB1 can lead to compensatory p16 tumor suppressor amplification **(Figure 7.2)**, which inhibits CDK4 function, thereby decreasing available CDK4 target proteins (195). An ex vivo breast tumor tissue model confirmed that tumors with high p16 levels or RB1 loss failed to respond to palbociclib (196).

Overexpression of E2F transcription factors has been linked to resistance by allowing cells to bypass CDK4/6 inhibition and proliferate uncontrollably **(Figure 7.3)** (140). Similarly, direct amplification of CDK4 and CDK6 also plays a role in resistance **(Figure 7.4)** (197,198). In a model of abemaciclib-resistant MCF7 cells, elevated CDK6 mRNA and protein levels were detected, with some cells exhibiting *CDK6* copy number gains. Overexpression of CDK6 reduced sensitivity to abemaciclib, whereas its inhibition restored sensitivity (198). Additionally, CDK7 overexpression, which is involved in the G2 to M transition, can also promote resistance by bypassing CDK4/6 dependency and sustaining tumor growth **(Figure 7.5)** (199).

Cyclin E-CDK2 activation is another key driver of resistance **(Figure 7.6)**. Overexpression or amplification of CCNE1 has been observed in acquired resistance models (194). In MCF7 cells with acquired resistance to palbociclib, CCNE1 amplification was identified, and silencing of either CCNE1 or CDK2 led to enhanced cell cycle arrest and suppressed growth (192). Prolonged CDK4/6 inhibition in RB1-deficient tumors results in the upregulation of E2F target genes, such as cyclins A and E, which promote a CDK2-driven proliferative state (140). In the PALOMA-3 clinical trial, high *CCNE1* mRNA expression was associated with relative resistance to palbociclib (200,201). These findings suggest that CCNE1-CDK2 activation serves as an alternative mechanism to RB1 phosphorylation, promoting cell cycle progression and contributing to resistance to CDK4/6 inhibitors.

3.1.2 Non-cell cycle-dependent mechanisms

Non-cell cycle-dependent mechanisms involve signaling pathways and transcriptional changes that enable tumor survival and proliferation independent of CDK4/6 regulation.

The activation of the FGFR pathway provides an alternative proliferative signal **(Figure 7.7)**. FGFR1-4 play a role in cancer progression and FGFR1 and FGFR2 have been associated with resistance to endocrine therapy and CDK4/6 inhibitors (202–205). In *in vitro* breast cancer cell models overexpressing FGFR1 or FGFR2, Mao et al. observed that resistance to fulvestrant and palbociclib was conferred and linked to increased p-Rb and CCND1 levels. The authors also reported clinical evidence supporting these findings. Specifically, two patients with mutated *FGFR2* (M538I and N550K) did not respond to the combination of endocrine therapy and palbociclib (203). In a separate study, resistance to fulvestrant and palbociclib was also observed in an *in vitro* breast cancer cell model overexpressing FGFR1 (204). When analyzing NGS data from circulating tumor DNA (ctDNA) samples of 34 patients who had progressed after treatment with CDK4/6 inhibitors, Formisano et al. found *FGFR1* or *FGFR2* amplification or activating mutations in 41% of patients. Notably, ctDNA from patients enrolled in MONALEESA-2 revealed that those with *FGFR1* amplification exhibited a shorter PFS compared to patients with wild type *FGFR1* (204).

The role of the PI3K/AKT/mTOR pathway in resistance to CDK4/6 inhibitors has also been extensively studied **(Figure 7.8)** (192,206–208). Approximately 40% of ER+ breast cancers harbor a *PIK3CA* mutations (64), and breast cancer cell lines resistant to CDK4/6 inhibitors exhibit an increased dependency on PI3K/AKT/mTOR signaling over ER signaling (209). Inhibition of CDK4/6 has been shown to activate the PI3K/AKT/mTOR pathway via AKT phosphorylation by PDK1 in ribociclib-resistant breast cancer cell lines. Specifically, AKT phosphorylation at S477/T479, a CDK2-dependent site, was observed (206). Furthermore, Michaloglou et al. demonstrated that mTORC1/2 inhibition suppressed the p-Rb and E2F activation induced by CDK2, thereby restoring sensitivity to CDK4/6 inhibitors (210). Additionally, PI3K inhibitors have been identified as synergistic partners of CDK4/6 inhibitors in both *in vitro* and *in vivo* studies (192,211). Current treatment strategies targeting this pathway in breast cancer are discussed in Section 2.2.3.

The mitogen-activated protein kinase (MAPK) pathway, a central signaling cascade involved in cell growth and differentiation, can also contribute to resistance to CDK4/6 inhibitors in ER+ breast cancer **(Figure 7.9)**. Studies suggest that activation of the RAS/RAF/MEK/ERK cascade reduces sensitivity to these inhibitors by promoting compensatory signaling that drives cell cycle progression, such as Cyclin D1 upregulation. Combinatorial therapy with

CDK4/6 inhibitors and MAPK inhibitors is currently under clinical investigation across multiple cancers (212).

Loss of ER and PR expression is another key resistance mechanism **(Figure 7.10)**. Treatment with endocrine therapy and CDK4/6 inhibitors can reduce tumors' dependence on hormonal signaling, increasing reliance on alternative growth pathways. In the abemaciclib-resistant breast cancer cell model generated by Yang et al., where elevated CDK6 levels were detected, researchers found that CDK6 overexpression not only mediated resistance to CDK4/6 inhibitors but also led to reduced ER and PR expression, decreasing responsiveness to ER antagonists. A similar reduction was observed in tumor biopsy specimens from patients treated with CDK4/6 inhibitors (198).

Senescent cells can also contribute to treatment resistance by adopting transient, reversible states of dormancy, allowing them to evade the cytotoxic effects of therapies targeting proliferating cancer cells (21,213). These cells often exhibit a senescence-associated secretory phenotype (SASP). While therapy-induced senescence can initially act as a protective mechanism against tumor growth, the SASP secreted by these cells can drive tumor progression and survival by modulating the TME and immune response, increasing survival signals, and enhancing angiogenesis, among others (214–216). Therefore, the presence of senescent cells with a pro-tumorigenic SASP represents a unique mechanism by which cancers can develop resistance to treatment and ultimately progress.

Other non-cell cycle-related resistance mechanisms include increased AP-1 activity, which regulates Cyclin D1 transcription; Smad suppression, disrupting tumor suppressor signaling; autophagy activation, serving as a survival mechanism; and immune-related mechanisms, enabling tumor evasion of therapeutic targets (190).

Understanding the diverse mechanisms of resistance to CDK4/6 inhibitors is essential for optimizing subsequent treatment strategies. By identifying specific alterations in resistant tumors, clinicians can tailor therapies to target alternative pathways, ultimately improving patient outcomes. Continued research into these mechanisms may uncover novel therapeutic targets, paving the way for more effective treatment approaches in the future.

3.2 HER2-enriched tumors and FGFR4

HR+/HER2- breast cancer is a heterogeneous disease with diverse biological behaviors and treatment responses. While endocrine therapy combined with CDK4/6 inhibitors has transformed its management, resistance remains a major challenge, particularly in aggressive tumors with poor prognosis, such as HER2-enriched tumors. Increasing evidence suggests that FGFR4, an RTK involved in cell survival and proliferation, plays a critical role in HER2-enriched tumors and that its expression is increased in HER2-enriched and metastatic tumors.

In 2012, Koboldt et al. studied the differences in gene expression between HER2+/HER2-enriched and HER2+/Luminal primary tumours (70). Compared to HER2+/Luminal, HER2+/HER2-enriched primary tumors exhibited decreased expression of ER-related genes, but significantly higher *FGFR4* expression, suggesting a role for FGFR4 in this aggressive subtype. Since in HER2-enriched tumors no major differences are observed between HER2+ and HER2- status beyond *ERBB2* levels (217), we decided to include these findings here.

In 2017, Cejalvo et al. identified *FGFR4* as the most upregulated gene in metastatic HR+/HER2- breast cancer (170). Notably, tumors that switched from a Luminal A or B subtype in the primary tumor to HER2-enriched in metastases exhibited increased *FGFR4* expression, but not *ERBB2* amplification. This suggests that *FGFR4* may drive the HER2-enriched phenotype in metastatic lesions independently of HER2 amplification.

Further supporting these findings, Garcia-Recio et al. demonstrated that *FGFR4* expression is significantly higher in HER2-enriched tumors and in tumors that acquire a HER2-enriched phenotype at metastasis (218). Their analysis revealed that 15% of Luminal A tumors transitioned to HER2-enriched at metastasis, and 60% of metastatic HER2-enriched tumors exhibited high *FGFR4* expression. Importantly, the cancer genome atlas (TCGA) dataset analysis confirmed that *FGFR4* mRNA levels were higher in HER2-enriched tumors compared to other breast cancer subtypes and normal tissue, while expression of other FGFR family members was not. Moreover, *FGFR4* overexpression was not driven by DNA copy-number alterations or mutations, indicating a non-genomic mechanism of regulation. To further investigate FGFR4's functional role, the authors developed a patient-derived xenograft (PDX) model from a tumor sample from an HR+/HER2-/HER2-enriched/FGFR4+ patient. Treatment

with BLU9931, a selective FGFR4 inhibitor, significantly reduced tumor volume and weight. Gene expression analysis showed that FGFR4 inhibition led to the upregulation of luminal-related genes and downregulation of proliferation, survival, EMT, and HER2-enriched differentiation-associated genes (218).

A recent study further elucidated the molecular characteristics and clinical implications of HER2-enriched tumors. Hohmann et al. conducted a comprehensive genomic analysis of HR+/HER2- breast cancers across two large cohorts: SCAN-B and METABRIC (219). Their findings revealed that HER2-enriched tumors exhibit aggressive clinical features and poorer outcomes compared to Luminal A and Luminal B subtypes. Notably, *FGFR4* expression was significantly elevated in HER2-enriched tumors within these cohorts, reinforcing its association with this aggressive phenotype. Similar findings were reported by Ding et al. (220). Building on their initial findings, Hohmann et al. analyzed HR+/HER2-/HER2-enriched tumors from two databases (SCAN-B and TCGA) and breast cancer cell lines using Whole Genome Sequencing (WGS) and found no *FGFR4* gene amplifications or mutations. The authors suggest that these increased levels of *FGFR4* expression are likely controlled by an epigenetic mechanism, specifically a DNA hypomethylation in the promoter region of the *FGFR4* gene, which could be driving higher levels of *FGFR4* gene activity and protein production (219).

Clinical data also support the poor prognosis of the HER2-enriched subtype in the context of CDK4/6 inhibition. Retrospective PAM50 analyses of the MONALEESA trials demonstrated that patients with HR+/HER2-/HER2-enriched breast cancer benefited from ribociclib; however, their PFS and OS remained worse compared to Luminal A or B tumors (180,182). In the PALOMA-2 trial, while Luminal A and Luminal B tumors benefited from the addition of palbociclib to letrozole, the HER2-enriched subtype was associated with inferior PFS (178). These observations highlight HER2-enriched tumors as a poor-outcome group despite responsiveness to CDK4/6 inhibitors.

Overall, preclinical and clinical evidence strongly suggest that *FGFR4* activation contributes to tumor progression, resistance, and subtype switching, making it a promising therapeutic target in HER2-enriched tumors. *FGFR4* expression is not only a characteristic feature of the HER2-enriched intrinsic subtype but is also enriched in metastatic lesions that acquire this phenotype, further supporting its role in disease progression and resistance mechanisms.

These insights underscore the potential of FGFR4 as a therapeutic target in HER2-enriched breast cancers, particularly in the metastatic setting, and highlight the urgent need for alternative therapeutic strategies for patients with CDK4/6 inhibitor resistant breast cancer by targeting this pathway.

3.3 FGFR4 as a therapeutic target

3.3.1 FGFR signaling pathway

FGFs interact with FGFRs to regulate various biological processes, from early embryonic development (such as mesoderm patterning and organ formation (221,222)) to essential functions in adulthood, including angiogenesis and wound healing (223).

The FGF family consists of 23 glycoproteins, 18 of which act as FGFR ligands. Most FGFs operate through autocrine or paracrine signaling, while a subset of FGFs, namely FGF19, FGF21, and FGF23, function as endocrine ligands (224,225). There are four main FGFRs, which are highly conserved transmembrane RTKs composed of three extracellular immunoglobulin domains (with an acid box), a single-pass transmembrane domain, and a cytoplasmic TK domain **(Figure 8)** (224,226). The specificity of FGF-FGFR interactions varies and depends on factors such as the FGFRs' binding capacities, alternative splicing, and their expression along with the expression of other related proteins (e.g., Klotho family) in different tissues (224,225,227). FGFRs are expressed in various cell types and regulate processes such as cell proliferation, differentiation, and survival. Consequently, aberrant FGFR signaling can be exploited by cancer cells (224).

Upon secretion, FGFs are sequestered in the ECM and on the cell surface by heparan sulphate proteoglycans (HPSGs). When signaling is initiated, FGFs are liberated and bind to HPSGs, which stabilize ligand-receptor interactions and facilitate the formation of a tertiary complex with FGFR. Ligand binding induces FGFR dimerization, triggering a conformational change that activates the intracellular kinase domain through intermolecular transphosphorylation (224,226). The phosphorylated TK domains serve as docking sites for adaptor proteins, which may themselves be phosphorylated, ultimately activating multiple downstream signal transduction pathways **(Figure 8)** (224,228).

A key adaptor protein in this cascade is FGFR substrate 2 (FRS2), which binds to the juxtamembrane region of FGFRs through its phosphotyrosine-binding (PTB) domains. Upon phosphorylation, FRS2 recruits and activates additional adaptor proteins, including growth factor receptor-bound 2 (GRB2) and son of sevenless (SOS). These interactions subsequently activate major signaling cascades, including the PI3K/AKT and the RAS/RAF/MEK/ERK pathways, both of which regulate cell proliferation and survival **(Figure 8)** (224,228).

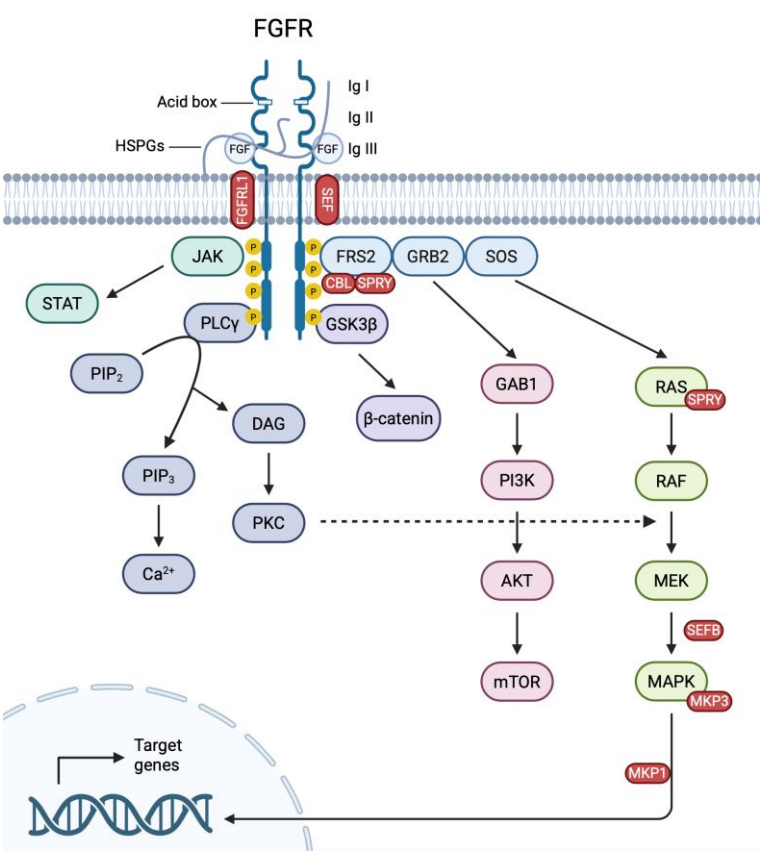

Figure 8. FGFR downstream signaling pathway. Activation of signaling pathways following the binding of FGFs to FGFRs. Ligand binding induces FGFR dimerization, activating the intracellular kinase domain, which recruits adaptor proteins like FRS2. This activates key pathways PI3K/AKT and RAS/RAF/MEK/ERK, promoting cell proliferation and survival. Other pathways such as the JAK/STAT and PLCγ are also activated. Negative feedback mechanisms (proteins in red) help control FGFR signaling and maintain cellular homeostasis. Adapted from reference (224). Created in BioRender.com

Beyond FRS2-dependent signaling, phospholipase Cγ (PLCγ) can be directly recruited and activated by phosphotyrosine residues in the carboxyl terminus of FGFRs. PLCγ hydrolyzes phosphatidylinositol-4,5-biphosphate (PIP_2) to phosphatidylinositol-3,4,5-triphosphate (PIP_3) and diacylglycerol (DAG), activating protein kinase C (PKC), which in turn reinforces the RAS/RAF/MEK/ERK pathway **(Figure 8)** (228). Additional FRS2-independent mechanisms also

contribute to FGFR-mediated cellular responses, including activation of the signal transducer and activator of transcription (STAT) pathway, ribosomal S6 kinase 2 (RSK2), p38 mitogen-activated protein kinase (p38 MAPK), and c-Jun N-terminal kinase (JNK) (224).

To maintain cellular homeostasis and prevent aberrant signaling, FGFR activation is tightly regulated by multiple negative feedback mechanisms. These include receptor internalization and the induction of negative regulators that either modulate ligand binding (FGFRL1 and SEF) or interfere with intracellular signaling (SEF, CBL, Sprouty (SPRY), SEFB, MAPK phosphatase 1 (MKP1) and 3 (MKP3)) **(Figure 8)** (229–232).

3.3.2 FGFR4 as a distinct target

FGFR4 is distinct from other FGFRs due to its lower overall homology (233), possessing only one isoform of loop III (loop IIIc) and a unique cysteine residue in its kinase domain, cysteine 552 (Cys552), which allows for the design of specific inhibitors (224,234). FGFR4 is involved in tissue differentiation and organogenesis during the embryonic stage (235). After birth, FGFR4 plays a role in bile acid regulation, where binding with FGF19 activates the mammalian sterile 20-like kinase 1/2 (MST1/2) pathway, downregulating bile acid synthesis, a function not shared by other FGFRs (236). In mice, FGFR4 has also been implicated in metabolic regulation (237), muscle differentiation, and tissue repair (238).

These structural and functional differences make FGFR4 an attractive therapeutic target in cancer treatment. Although it has been less extensively studied than other FGFRs, likely due to its lower frequency of somatic mutations (239), specific alternations, particularly hotspot mutations such as the N535, are significantly enriched in metastatic invasive lobular carcinoma (3.5%) compared to invasive ductal carcinoma (0.5%), where they enhance FGFR4 activity and contribute to therapeutic resistance (240). Additionally, FGFR4 single nucleotide polymorphism (SNP) rs351855 has been associated with increased protein expression, lymph node metastasis, and poor survival in breast cancer (241). While *FGFR4* somatic DNA alterations are relatively rare, its overexpression is frequently observed in breast cancer, especially in HR+ metastatic tumors (170,218,219,240). Recent functional studies have expanded the mutational landscape of FGFR4 in solid tumors by identifying novel activating non-kinase domain variants, including K503R, Y367C, G388R, and T179A, that promote

oncogenic behaviour through altered growth factor dependency and increased colony formation *in vitro* and broaden the spectrum of clinically relevant FGFR4 alterations (242).

Garcia-Recio et al. showed that *FGFR4* mRNA expression is lower in normal breast tissues compared to breast cancer tissues, highlighting not only its potential role in tumor progression but also its viability as a therapeutic target (218). This differential expression makes FGFR4 an attractive candidate for targeted therapy, as inhibiting FGFR4 signaling in cancers where it is upregulated could provide an effective and well-tolerated treatment strategy with high specificity and minimal off-target effects.

3.3.3 Drugs targeting FGFR4

Several highly selective FGFR4-directed agents have been developed to specifically target FGFR4 signaling through distinct mechanisms: TKIs, monoclonal antibodies, and ADCs.

Unlike pan-FGFR inhibitors, which affect multiple FGFR family members and may cause off-target toxicity, FGFR4-targeted inhibitors offer greater precision with potentially fewer side effects. BLU9931 is an irreversible inhibitor that covalently binds to Cys552 near the ATP-binding site of FGFR4 and has demonstrated strong anticancer activity in hepatocellular carcinoma (HCC) xenograft tumors with elevated FGF19-FGFR4 signaling (243). BLU554, developed as a successor with improved pharmacokinetic properties, is currently being evaluated in a Phase I clinical trial for advanced HCC (244).

INCB062079 is another selective and potent FGFR4 inhibitor designed to block aberrant FGF19-FGFR4 signaling, a pathway frequently upregulated in HCC. Preclinical studies showed that INCB062079 effectively suppressed tumor growth in FGF19-driven HCC models (245,246). A Phase I clinical trial assessed its safety, tolerability, and preliminary efficacy in patients with advanced solid tumors harboring FGF19-FGFR4 pathway alterations. While the treatment showed manageable toxicity and some clinical activity, the study was terminated before a maximum tolerated dose could be established, primarily due to slow patient accrual (247). Other FGFR4 inhibitors such as H3B-6527 (248,249) and FGF401 (250,251) have also shown promising preclinical efficacy and have been or are currently under clinical investigation for HCC treatment.

High *FGFR4* expression and mutations have also been identified as drivers of metastasis in rhabdomyosarcomas, making FGFR4 a potential target for chimeric antigen receptor T-cell (CAR-T) therapy (252,253). Additionally, an ADC against FGFR4 is also under development for rhabdomyosarcoma and HCC (254).

In breast tumors, an *in silico* analysis identified FGFR4 as one of 36 potential subtype-specific cell surface targets suitable for CAR-T cell therapy and ADCs (255). Furthermore, FGFR4 has been recognized as a potential therapeutic target in HR+/HER2-/HER2-enriched tumors (170,218–220), which could represent a significant advancement in personalizing treatment strategies for this aggressive subtype after progression to endocrine therapy and CDK4/6 inhibitors.

HYPOTHESES

In this thesis, we hypothesize that:

1. Ribociclib but not palbociclib induces a luminal state in HER2-enriched tumors, increasing sensitivity to endocrine therapy.
2. FGFR4 is a driver of resistance to CDK4/6 inhibition and a potential therapeutic target.

OBJECTIVES

Our ultimate goal is to enhance the clinical management of patients with hard-to-treat HR+/HER2- metastatic breast cancer by developing novel therapeutic strategies that boost treatment response and extend survival.

Objective 1: To compare the biological activity of palbociclib and ribociclib in HR+ breast cancer.

Objective 2: To study the association of FGFR4 expression with the HER2-enriched subtype and with clinical outcomes in patients with metastatic HR+/HER2- breast cancer treated with CDK4/6 inhibitors.

Objective 3: To evaluate the effects of pharmacologically targeting FGFR4 in breast cancer preclinical models of resistance to CDK4/6 inhibitors.

Objective 1 corresponds to the published article.

In this thesis, Objective 1 corresponds to “Chapter 1”, Objective 2 corresponds to “Chapter 2”, and Objective 3 corresponds to “Chapter 3”.

MATERIAL AND METHODS

1. Methods for comparative analysis of palbociclib and ribociclib activity in HR+ breast cancer cell lines

1.1 Cell lines and drugs

MCF7, T47D, BT474, and MDA-MB-468 were obtained from the American Type Culture Collection (ATCC, Manassas, VA, USA) and cultured in Dulbecco's Modified Eagle Medium (DMEM)/nutrient mixture F-12 supplemented with 10% v/v heat-inactivated fetal bovine serum (FBS) (*Gibco*; Thermo Fisher Scientific Inc., Waltham, MA, USA), 1% GlutaMAX (*Gibco*; Thermo Fisher Scientific Inc.), and 1% Penicillin/Streptomycin (Sigma-Aldrich, Saint Louis, MO, USA) in a 37 ºC, 5% CO_2 humidified incubator. Cells were detached from flasks by incubation with 0.25% Trypsin-EDTA (1X) (*Gibco*; Thermo Fisher Scientific Inc.), washed with Dulbecco's Phosphate Buffered Saline (D-PBS) (*Gibco*; Thermo Fisher Scientific Inc.), and routinely tested for mycoplasma using Mycoplasma Gel Detection Kit (Biotools B&M Labs S.A., Madrid, Spain). Palbociclib, ribociclib, and fulvestrant were purchased from Selleckchem (Houston, TX, USA).

1.2 Clinical samples

The SOLTI-1402 CORALLEEN phase II study (NCT03248427) randomized 106 postmenopausal women with stage I–IIIA HR+/HER2- breast cancer and Luminal B by PAM50 with histologically confirmed, operable primary tumour size of at least 2 cm in diameter as measured by magnetic resonance imaging (MRI). Patients were randomly assigned (1:1) to receive either six 28-days cycles of ribociclib (oral 600 mg once daily for 3 weeks on, 1 week off) plus daily letrozole (oral 2.5 mg/day) or four cycles of doxorubicin (60 mg/m², IV) and cyclophosphamide (600 mg/m², IV) every 21 days followed by weekly paclitaxel (80 mg/m², IV) for 12 weeks (256). Here, we analyzed formalin-fixed, paraffin-embedded (FFPE) tumor samples of the ribociclib plus letrozole arm, including 49 paired baseline versus cycle 1 day 15 (C1D15) samples and 49 paired baseline versus surgery samples.

Additionally, gene expression data of the NeoPalAna phase II trial (NCT01723774), which treated 50 patients with HR+/HER2- early breast cancer with anastrazole (1 mg daily) for 4

weeks, followed by four 28-day cycles of palbociclib (125 mg daily) plus anastrazole (1 mg daily) (179), was downloaded from the Gene Expression Omnibus (GSE93204). We analyzed 23 paired baseline versus C1D15 samples and 16 paired baseline versus surgery samples.

1.3 Ethics approval and consent to participate

This study was approved by the Ethics Committee at Hospital Clinic of Barcelona (HCB/2022/0086) and all methods were carried out in accordance with relevant guidelines and regulations. This study involves the use of tissue samples of patients that have received treatment with CDK4/6 inhibitors within the context of the CORALLEEN trial. These samples are stored in the biorepository of the Translational genomics and targeted therapies in solid tumors group at IDIBAPS as long as patients sign the specific informed consent of the collection.

1.4 RNA extraction

RNA of the internal cohort of patients treated with CDK4/6 inhibitors and of the CORALLEEN study was extracted using the High Pure FFPET RNA isolation kit (Roche, Indianapolis, IN, USA) following manufacturer's protocol. At least 1-5 10 µm FFPE slides were used for each tumor specimen and macrodissection was performed to avoid contamination with normal breast tissue if needed. For *in vitro* studies, cells were seeded in a 6-well plate at a density of 150,000 cells per well and after overnight incubation medium was replaced with two different dose levels of palbociclib or ribociclib (i.e., 100 nM and 500 nM) +/- fulvestrant (1 nM) for 72 hours (h). mRNA was extracted using QIAGEN's RNeasy extraction kit (QIAGEN, Hilden, Germany) following manufacturer's instructions. NanoDrop One (Thermo Fisher Scientific Inc.) was used to quantify extracted mRNA samples.

1.5 Gene expression analysis

The nCounter platform (NanoString Technologies, Seattle, WA, USA) analyzed RNA samples from tumor samples and cell lines. A minimum of 100 ng of total RNA was used to measure the expression of 50 genes of the PAM50 intrinsic subtype predictor assay and 5 housekeeping genes (*ACTB, MRPL19, PSADC-1, RPLP0* and *SF3A1*). Expression counts were then normalized and the PAM50 signature scores (Basal-like, HER2-enriched, Luminal A and

B, Normal-like) and the proliferation signature score were calculated using customized R scripts (58). PAM50 molecular subtypes were calculated in the publicly available gene expression data from the NeoPalAna including 23 baseline samples, 23 week-2 samples, and 16 surgery samples.

1.6 *In vitro* cell growth assay

Cells were seeded in triplicate at a density of 5,000 cells per well in 96-well plates. Following overnight incubation, cells were treated with increasing doses of palbociclib or ribociclib. Cell viability was assessed after 72 h with Hoechst 33342 staining solution (*Invitrogen*, Thermo Fisher Scientific Inc.) and quantified using SynergyHT microplate reader and Windows based Gen5 software.

1.7 Protein extraction and Western blotting

Cells were seeded in 6-well plates at a density of 150,000 cells per well and after overnight incubation medium was replaced with palbociclib or ribociclib (100 or 500 nM). After 24, 72, or 144 h cell lysates were obtained using radioimmunoprecipitation (RIPA) lysis and extraction buffer (Thermo Fisher Scientific Inc.) supplemented with protease inhibitors: 5 mM sodium fluoride, 1 mg/ml aprotinin, 1 mM phenylmethylsulfonyl fluoride, 1 mM sodium orthovanadate, 1 mM benzamidine, 1 mM leupeptin, and 1 mM dithiothreitol. Total protein extracts were quantified using the DC Protein Assay (BioRad Laboratories, Hercules, CA, USA) and 50 µg of proteins were separated in reducing conditions (2.5% β-mercaptoethanol [Sigma-Aldrich]) by SDS-PAGE and transferred to nitrocellulose membranes (BioRad Laboratories) for further processing, following standard western blotting procedures.

The primary antibodies used in this study were phospho-RB1 (Ser807/811) (D20B12) and Lamin-B1 (D9V6H) from Cell Signaling Technology (Danvers, MA, USA), and anti-actin (A2066) from Sigma-Aldrich. The secondary fluorescent antibody used was the IRDye 800CW Donkey anti-Rabbit IgG (LI-COR Biosciences, Lincoln, NE, USA). Fluorescent signal was acquired by the Odyssey Imaging System (LI-COR Biosciences).

1.8 Senescence-associated β-galactosidase activity

Cells were seeded in 24-well plates at a density of 35,000 cells per well and after overnight incubation medium was replaced with palbociclib or ribociclib (100 or 500 nM). Following 24, 72, or 144 h treatments, senescence dye from the Senescence Assay Kit (Abcam, Cambridge, UK) was added to wells. Cells were incubated for 1-2 h in a 37 ºC, 5% CO_2 humidified incubator and the mean fluorescence was analysed by flow cytometry for the detection of β-galactosidase activity. Propidium iodide (PI; *Invitrogen*, Thermo Fisher Scientific Inc.) was used as a viability marker. Untreated controls were added, as well as unstained controls for the evaluation of potential auto-fluorescence.

1.9 Statistical analysis

Changes in gene expression and PAM50 signatures upon CDK4/6 inhibition were determined by paired t-tests and paired and multiclass significant analysis of microarray (SAM) with a false discovery rate (FDR) < 5%. These analyses were performed using R software. All statistical tests were two sided and the statistical significance level was set to $p < 0.05$. For *in vitro* cell growth, determination of half maximal inhibitory concentrations (IC50s), and senescence assays, GraphPad Prism was used for statistics.

2. Methods for evaluating FGFR4 as a driver of resistance to CDK4/6 inhibitors in clinical samples

2.1 Clinical samples

The CDK clinical cohort included 312 tumor samples from 275 patients over the age of 18 years with a histologic diagnosis of HR+/HER2-negative metastatic breast cancer treated with CDK4/6 inhibitors, including palbociclib, ribociclib and abemaciclib at Hospital Clínic of Barcelona between years 2014 and 2021. For the validation of FGFR4 as a driver of resistance we used all 253 baseline samples (130 primary and 123 metastasis) and 59 progressive disease (PD) samples were available for molecular characterization. This included 37 paired baseline-PD samples.

2.2 Ethics approval and consent to participate

This study involves the use of tissue samples of patients who have received treatment with CDK4/6 inhibitors. These samples are part of the collection “Biospecimens of patients with solid tumors at Hospital Clinic of Barcelona” (Reference C.0004038), overseen by Prof. Aleix Prat. These samples are stored in the collection as long as patients have signed the specific informed consent. This project has been approved by the Ethics Committee of Hospital Clínic de Barcelona (HCB/2022/0086).

2.3 Immunohistochemistry

FGFR4 IHC staining was performed in accordance with the methodology described by Tian et al. (257). Assessment of FGFR4 was performed on tumor cells by pathologists at Hospital Clínic de Barcelona using the H-Score method, which combines staining intensity with the percentage of stained cells to provide a semi-quantitative measure of protein expression (258). Intensity was categorized as follows: 0 = no staining, 1 = weak staining, 2 = moderate staining, and 3 = strong staining. The H-Score was calculated using the formula: H-Score = (0 * % no-staining) + (1 * % weak staining) + (2 * % moderate staining) + (3 * % strong staining).

2.4 Statistical analysis

PFS was defined as the period between start of the treatment with endocrine therapy and CDK4/6 inhibitor and the time of progression. OS was defined as the period between start of the treatment with endocrine therapy and CDK4/6 inhibitor treatment and death or last follow-up. Estimates of survival were derived from the Kaplan-Meier curves, and differences were assessed using the log-rank test. Univariate and multivariable Cox models were used to test the prognostic significance of each variable. Gene expression differences across groups were assessed using one-way ANOVA. Paired and multiclass SAM analyses with an FDR > 5 were used to identify differential gene expressions. All statistical analyses were performed using R software. A p-value < 0.05 was considered statisticaly significant.

3. Methods for preclinical targeting of FGFR4 in HR+/HER2- breast cancer

3.1 Cell lines

T47D, MCF7, ZR751, BT474, SKBR3, MDA-MB-231, and MDA-MB-453 cell lines were obtained from the ATCC. BT474 cells with acquired resistance to anti-HER2 dual therapy (lapatinib or tucatinib plus trastuzumab; BT474 LTR and BT474 TTR) were generated in our lab as described in Brasó-Maristany et al., 2020 (259). T47D and MCF7 cells with acquired resistance to 500 nM palbociclib (T47D PR and MCF7 PR) were generated in our lab by sustained treatment with increasing doses of palbociclib over 6 months. T47D PR cells with acquired resistance to ADC-2 (0.007 μg/ml) were also generated in our lab following the same methodology.

DNA from plasmid pLOCTurbo-RFP (#OHS5833) (named empty vector or control) was purchased from Dharmacon (Horizon Discovery, Cambridge, UK). A plasmid containing the constitutively active *FGFR4* (Y367C) mutation was provided by Dr. Gomis' group at Institut de Recerca Biomèdica (Barcelona, Spain). This plasmid was produced by site-directed mutagenesis using the Precision LentiORF Human *FGFR4* plasmid (#OHS5897-202616292; Horizon Discovery) and the QuikChange Lightning Multi Site-Directed Mutagenesis Kit (#210515-5 (Agilent, Santa Clara, CA, USA). Lentiviral particles were produced in HEK293T cells and T47D cells were infected. MDA-MB-231-RFP+ cells were obtained by transducing parental MDA-MB-231 cells with a pLL-CMV-RFP-T2A-Blast Lenti-Labeler Plasmid (System Biosciences, Palo Alto, CA, USA). MDA-MB-231-RFP+ cells were sorted with BD FACSAria II Cell Sorter (BD Biosciences, San Jose, CA, USA).

All cell lines were cultured and manipulated as described in Methods section 1.1 (Cell lines and drugs). Additionally, T47D PR and MCF7 PR cells were cultured in complete medium with 500 nM palbociclib and the *FGFR4*-mutated cell line, as well as the MDA-MB-231-RFP+ cell line, were cultured in complete medium with Blasticidine S hydrochloride (10 μg/ml, Sigma-Aldrich) for continuous antibiotic selection of genetically modified cells.

3.2 Antibodies and antibody-drug conjugate

Unless otherwise stated, all experimental procedures described in this section were conducted by a team at ONA Therapeutics (Barcelona, Spain).

3.2.1 Selection and production of FGFR4-targeting monoclonal antibodies

Two humanized monoclonal antibodies and one human monoclonal antibody targeting FGFR4 were selected: Eixiris clone 3B6 (WO 2019/034427 A1 (260), Given name: Ab-1), Genentech clone hLD1.v22 (WO 2012/138975 A1 (261), Given name: Ab-2), and Daichi clone U4-3 (WO 2016/023894 A1 (262), Given name: Ab-3), respectively. The sequences of the selected antibodies were obtained from the corresponding patents, and antibody recombinant production was performed by transient transfection in CHO-K1 mammalian cells (Biointron Biological, Shanghai, China) in two formats: with a human IgG1 backbone and as antibodies that featured Fc-silencing STR mutations (mAbsolve Limited, Oxford, UK) (263). No functional differences were observed between Fc variants *in vitro* and the Fc-silent format was used for all *in vivo* applications.

3.2.2 Binding and stability of naked antibodies

Binding affinities were evaluated using ELISA against recombinant His-tagged FGFR4 ectodomain (Sino Biological, #10538-H08H). Half-maximal effective concentrations (EC50) were as follows: Ab-1: 0.26 nM, Ab-2: 0.32 nM, Ab-3: 0.30 nM. Stability was assessed by incubating antibodies in mouse plasma at 37 ºC for 7 days or in PBS at 4 ºC. Comparable binding activity was observed across all samples, as determined by ELISA.

3.2.3 Computational and biophysical characterization

In silico assessments of complementarity-determining region (CDR) liabilities, hydrophobicity, and overall molecular properties were performed following the methods described by Raybould et al., 2019 (264). Biophysical characterization, as part of the Chemistry, Manufacturing, and Controls (CMC) evaluation, included thermal stability and aggregation propensity assessment (Tm and Tagg). Among the selected antibodies, Ab-3 exhibited slightly higher hydrophobicity and was more aggregation-prone.

3.2.4 ADC design and production

Ab-2 was selected for ADC generation. The Fc-silent IgG1 format was used for conjugation with the cytotoxic payload MMAE, linked via VC-PAB-MMAE (patent US7829531B2). Two average DARs were evaluated: DAR4 and DAR8. ADC conjugation strategies included random

lysine conjugation (ADC-2) and cysteine conjugation (ADC-1 and ADC-3) **(Table 4)**. The production of ADCs was outsourced to Intellective Bio (Suzhou, China).

Table 4. Characteristics of the ADCs used in this study.

ID	Amount (mg)	Conc (mg/ml)	MW (kDa)	Reaction scale (mg)	DAR0	DAR2	DAR4	DAR6	DAR8	Average DAR	Monomer % (SEC)	Tm (ºC)
ADC-1[a]	9.59	0.88	153.83	40	3.9%	23.6%	40.8%	22.1%	9.7%	4.20	96.8%	72
ADC-2[b]	10.11	1.52	153.54	40.8	NA	NA	NA	NA	NA	4.30	98.4%	76
ADC-3[c]	20.30	1.40	158.47	38	0.0%	0.0%	2.0%	9.3%	88.7%	7.73	97.4%	67
Isotype-ADC-1[d]	12.26	1.19	154.84	35	7.9%	25.5%	35.2%	22.9%	8.6%	3.98	97.5%	nd

[a]ADC-1 (maleimide-Cys DAR 4), [b]ADC-2 (OSu-Lys DAR4), [c]ADC-3 (maleimide-Cys DAR8), [d]anti-fluorescein isotype control (maleimide-Cys DAR4)

3.2.5 ADC binding and stability assessment

The binding properties of the ADCs were evaluated by ELISA, demonstrating retention of FGFR4 affinity: Ab-2 (EC50: 0.74 nM), FC-silent Ab-2 (EC50: 0.93 nM), ADC-1 (EC50: 0.63 nM), ADC-2 (EC50: 0.88 nM), ADC-3 (EC50: 1.88 nM). Mouse plasma stability of naked antibodies and ADCs was assessed by ELISA after incubation at 37 ºC for 7 days, confirming stability across all constructs. To evaluate potential non-specific interactions, constructs were incubated at 500 nM with sticky polymers (DNA, heparin, insulin). Cysteine-conjugated ADCs exhibited higher non-specific binding, which correlated with DAR.

3.2.6 Pharmacokinetic studies

The PK profile of all constructs was assessed in BALB/c mice (10 mg/kg, IV). Serum samples were collected at selected time points and analyzed by ELISA. Among the tested molecules, ADC-2 maintained detectable levels 2 weeks post-injection.

3.3 RNA extraction

Cells were seeded in 6-well plates at a density of 150,000 cells per well. After overnight incubation, the medium was replaced with one of the following treatments: FGFR4 inhibitor INCB062079 (100 nM; provided by Incyte Corporation, Wilmington, DE, USA), naked anti-FGFR4 Ab-2 (10 μg/ml), anti-FGFR4 ADC-2 (0.1 μg/ml), or free MMAE payload (0.01 μg/ml). After 72 h of treatment, mRNA was extracted and quantified as described in Methods section 1.4 (RNA extraction).

3.4 Gene expression analysis

The nCounter platform (NanoString Technologies) analyzed RNA samples from tumor samples and cell lines. The expression of 50 genes of the PAM50 intrinsic subtype predictor assay and 5 housekeeping genes (*ACTB, MRPL19, PSADC-1, RPLP0* and *SF3A1*) was analyzed using a customized nCounter panel, as described in Methods section 1.5 (Gene expression analysis).

3.5 Histological preparation and staining of cellular pellets

Cell pellets for paraffin embedding were prepared as follows. Cells were pelleted by centrifugation at 1,200 rpm for 4 min and washed with 1X PBS. To preserve cellular structure, samples were fixed in Cytolyt (Hologic, Marlborough, MA, USA) for 5-10 min at room temperature (RT). Concurrently, a tube of HistoGel (*Epredia*, Thermo Fisher Scientific Inc.) was pre-warmed in an incubator at 65 ºC until liquified. The fixed samples were then centrifuged at 2800 rpm for 5 min, and the supernatant was discarded. Depending on pellet size, 4-10 drops of Histogel were added, and the pellet was gently mixed with a pipette to ensure homogeneity. The mixture was allowed to solidify by refrigeration for 5-10 min or at RT until fully set. Once solidified, the pellet block was carefully detached using a pipette, transferred to a cassette, and placed in formalin for further processing. All steps were carried out under a biosafety cabinet to maintain sterile conditions. IHC staining for FGFR4 on these cell pellet-derived FFPE blocks, as well as determination of FGFR4 H-Scores, followed the same protocol described for tissue sections in Methods section 2.3 (Immunohistochemistry).

3.6 *In vitro* cell growth assay

Cells were seeded in triplicate at a density of 2,500 cells per well in 96-well plates. Following overnight incubation, cells were treated with increasing doses of INCB062079. Cell viability was assessed after 144 h with Hoechst 33342 staining solution and quantified using SynergyHT microplate reader and Windows based Gen5 software.

Cells were seeded in triplicate at a density of 2,500 or 5,000 cells per well in 96-well plates. Following overnight incubation, cells were treated with increasing doses of anti-FGFR4 antibodies (Ab-1, Ab-2, Ab-3). Cell viability was assessed after 72 h or 144 h with Hoechst 33342 staining solution. Cells were also treated with increasing doses of anti-FGFR4 ADCs

(ADC-1, ADC-2, ADC-3, and Ab-2-DXd-ADC), MMAE, and DXd. Cell viability was assessed after 72 h or 144 h with Cell Titer 96® AQ_{ueous} One Solution Cell Proliferation Assay (Promega, Madison, WI, USA) and quantified using SynergyHT microplate reader and Windows based Gen5 software.

For experiments with Moradec's secondary antibody-drug constructs (Moradec, San Diego, CA, USA), T47D PR and MDA-MB-453 cells were seeded in triplicate at a density of 2,500 cells per well (100 μl per well) in 96-well plates. Following overnight incubation, anti-FGFR4 primary antibodies (Ab-1, Ab-2, Ab-3) or an unspecific isotype antibody (Isotype Ab-1) were added to corresponding wells at increasing doses (50 μl per well) and cells were incubated at RT for 10 min. Next, Fab Anti-Human IgG Fc-MMAE Antibody with Cleavable Linker (Fab-αHFc-CL-MMAE; Average DAR of 1.3 per Fab), Fab Anti-Human IgG Fc-Duocarmycin Antibody with Cleavable Linker (Fab-αHFc-CL-DMDM; Average DAR of 1.3-1.5 per Fab), or Fab Anti-Human IgG Fc-Monomethyl auristatin F (MMAF) Antibody with Non-Cleavable Linker (Fab-αHFc-NC-MMAF; Average DAR of 1.3-1.5 per Fab) were added to wells at increasing doses (50 μl per well) following a 1:6 primary-secondary antibody ratio. Cell viability was assessed after 144 h with Cell Titer 96® AQ_{ueous} One Solution Cell Proliferation Assay and quantified using SynergyHT microplate reader and Windows based Gen5 software.

3.7 Colony formation assay

Cells were seeded in triplicate at a density of 2,000 cells per well in 6-well plates. After overnight incubation, cells were treated with increasing doses of ADC-2. Medium and ADC-2 were replenished every 3 days until untreated cells reached confluency. Next, cells were fixed with cold methanol (VWR, Avantor, Radnor, PA, USA) and incubated at -20 ºC for 15 min. Cells were then stained with 20% methanol/80% water/0.5% crystal violet (Sigma-Aldrich) for 20 min, washed with water and left to air-dry. Finally, crystal violet was solubilized with 20% acetic acid (Merck Group, Darmstadt, Germany) and quantified by spectrophotometric detection at 490 nm using SynergyHT microplate reader and Windows based Gen5 software.

3.8 Protein extraction and Western blotting

Cells were seeded in 6-well plates at a density of 150,000 cells per well and after overnight incubation medium was replaced with ADC-2 (0.1 μg/ml), MMAE (0.001 μg/ml), or medium. After 72 h, cell lysates were obtained, quantified, and processed as described in Methods section 1.7 (Protein extraction and Western blotting).

The primary antibodies used in this study were FGF Receptor 4 (D3B12) XP® Rabbit mAb and phospho-Rb (Ser807/811) (D20B12) mAb from Cell Signaling Technology and anti-actin (A2066) from Sigma-Aldrich. The secondary fluorescent antibody used was the IRDye 800CW Donkey anti-Rabbit. Fluorescent signal was acquired by the Odyssey Imaging System.

3.9 Antibody-receptor binding

Cells were seeded in triplicate at a density of 50,000 cells per well in cold FACS buffer (1X PBS, 0.1% FBS, 0.5 mM EDTA) in V-bottom 96-well plates (Thermo Fisher Scientific Inc.). Cells were treated with increasing doses of anti-FGFR4 antibody (Ab-1, Ab-2, Ab-3) and incubated on ice for 45 min. Plates were centrifuged at 400 x g for 6 min at 4 ºC and supernatant was removed by inverting the plate. Next, cells were washed with cold FACS buffer and cell pellets were resuspended with Allophycocyanin (APC) AffiniPure™ $F(ab')_2$ Goat Anti-Human IgG Fcγ fragment specific secondary antibody (Jackson ImmunoResearch Laboratories, West Grove, PA, USA) diluted in FACS buffer (1/150) and incubated for 12 min at RT and in the dark. Following incubation, plates were centrifuged at 400 x g for 6 min at 4 ºC, supernatant was removed by inverting the plate, and cells were resuspended in cold FACS buffer containing viability marker PI (1 μg/ml) right before being loaded into the cytometer. BD LSRFortessa 4L Cell Analyzer + HTS (BD Biosciences) was used to establish the mean APC intensity in the PI+ population for every condition. The geometric MFI was used to build the curves.

3.10 Antibody cellular internalization

Cells were added to tubes at a density of 1,000,000 cells per tube in cold FACS buffer (1X PBS, 2% FBS, 2 mM EDTA). Cells were centrifuged at 500 x g for 5 min and cell pellets were resuspended with 1 ml of FACS buffer containing 10 μg/ml anti-FGFR4 antibody (Ab-1, Ab-2, Ab-3). Control tubes were resuspended in FACS buffer only. Following a 1-h incubation on ice,

cells were washed twice with cold FACS buffer. Cell pellets were resuspended in 600 μl of cold FACS buffer, distributed in 3 tubes and incubated overnight on ice. Next, cells were incubated at 37 ºC for 0, 2, or 4 h to allow cellular internalization. Following incubations, cells were washed with FACS buffer, resuspended with APC AffiniPure^{TM} F(ab')$_2$ Goat Anti-Human IgG Fcγ fragment specific secondary antibody diluted in FACS buffer (1/200), and incubated for 1 h on ice. Next, cells were washed in cold 1X PBS, resuspended with Zombie Violet dye (Biolegend, San Diego, CA, USA) diluted in 1X PBS (1/1000), and incubated for 20 min at RT and in the dark. Cells were then centrifuged at 500 x g for 5 min at 4 ºC, supernatant was removed, cell pellets were washed with FACS buffer, and fixed at RT with 4% PFA for 15 min. Once fixed, cells were washed, resuspended in FACS buffer, and moved to FACS tubes. BD LSRFortessa 4L Cell Analyzer + HTS was used to establish the median APC intensity in the Zombie Violet+ population for every condition. A viability threshold of 80% was established. Experiments in which cell viability fell below this threshold were discarded.

3.11 Bystander effect

MDA-MB-231-RFP+ and MDA-MB-453 cells were seeded in 12-well plates both as mono- and co-cultures (1:5 or 1:20). Following overnight incubation, cells were treated with ADC-2 (0.3 μg/ml), Isotype-ADC-2 (0.3 μg/ml), or MMAE (0.0036 μg/ml) for 96 or 120 h. Next, cells were collected, washed with FACS buffer (1X PBS, 0.4% FBS, 0.01% EDTA), and stained with DAPI diluted in FACS buffer (1/20,000). Following a 20-min incubation in the dark, cells were washed and transferred to FACS tubs. The Cytek Aurora (Cytek Biosciences, Fremont, CA, USA) cytometer was used to establish the number of RFP events in the alive DAPI- population for every condition in a fixed volume of 200 μl.

3.12 Animal studies

All animal experiments were approved by The Ethical Committee of Animal Experimentation of the Government of Catalonia (protocol 9096_P1) and conducted in collaboration with the Growth Control and Cancer Metastasis Research Group, led by Roger Gomis at the Institut de Recerca Biomèdica (IRB) in Barcelona.

Twelve-week-old female BALB/c nude mice were used. Mice that died of were euthanized for ethical reasons before experimental endpoints were excluded from analysis. To support the

growth of ER+ tumors, 60-day release estrogen pellets (beta-estradiol 0.18 mg per pellet; 320 ng/μl) were implanted subcutaneously. Mice were anesthetized with ketamine (100 mg/kg body weight) and xylazine (10 mg/kg body weight). A total of 1 x 10^6 ZR751 or T47D cells were resuspended in 100 μl of a 1:1 mixture of PBS and Matrigel Basement Membrane Matrix (#354234, Corning Life Sciences, Corning, NY, USA), and injected subcutaneously into the dorsal flanks of the mice. When tumors reached the designated size, mice were randomized into treatment groups: IV vehicle, Isotype-ADC-1 (2 or 5 mg/kg), or ADC-2 (2 or 5 mg/kg), administered weekly. Tumor growth was monitored every 3-5 days using calipers, and tumor volume was calculated using the formula: $V = (\pi/6) \times Length \times Width^2$. Treatment continued until humane endpoints were reached. The duration of each experiment following the start of treatment was 29 days for the ZR751 CDX model and 26 days for the T47D CDX model.

3.13 Statistical analysis

For *in vitro* and *in vivo* experiments, statistical analyses included two-way ANOVA and Mann-Whitney U tests (two-tailed, non-paremetric, unpaired), performed using GraphPad Prism. Changes in gene expression and PAM50 signatures upon treatment were determined by multiclass SAM with an FDR < 5% using R software. All statistical tests were two sided, and the significance level was set to $p < 0.050$.

RESULTS

1. Comparative biological activity of palbociclib and ribociclib in hormone receptor-positive breast cancer

Although CDK4/6 inhibitors have become a cornerstone in the treatment of HR+/HER2- breast cancer, their efficacy across intrinsic molecular subtypes remains variable. Several studies, including the PALOMA-2 (178), NeoPalAna (179), and MONALEESA (180) trials, have highlighted different responses to CDK4/6 inhibitors among PAM50 subtypes, highlighting limited benefit with palbociclib in HER2-enriched and Basal-like tumors, while ribociclib appears to retain clinical activity in a broader range of subtypes, including HER2-enriched. These observations suggest that both subtype-specific and drug-specific properties may influence therapeutic outcomes. To better understand the biological basis of these clinical differences, we conducted a series of *in vitro* and transcriptomic analyses to investigate how two different CDK4/6 inhibitors (i.e., palbociclib and ribociclib) affect proliferation and molecular subtype dynamics in breast cancer cell lines, as well as in tumor samples from patients enrolled in the NeoPalAna and the CORALLEEN studies.

1.1. Phenotypic changes in breast cancer cell lines during CDK4/6 inhibition

The biological changes that occur during CDK4/6 inhibition were assessed in T47D (HR+/HER2-/HER2-enriched), MCF7 (HR+/HER2-/Luminal B), and BT474 (HR+/HER2+/HER2-enriched) breast cancer cell lines. Despite being HER2+, the inclusion of the BT474 cell line to our study is relevant since it belongs to the HER2-enriched subtype by PAM50, and palbociclib has been shown to be less efficient in HR+/HER2+/HER2-enriched breast cancer (181). Moreover, it has been shown that, except for the amplification and RNA/protein overexpression of *ERBB2*/HER2 in HER2+ tumors, very minor biological differences exist at DNA, RNA, and protein levels between HER2+/HER2-enriched and HER2-/HER2-enriched tumors (217).

First, we analyzed the proliferation inhibitory effect of palbociclib and ribociclib +/− fulvestrant against all three cell lines and found that both CDK4/6 inhibitors had very similar effects at 72 h from treatment **(Figure 9)**.

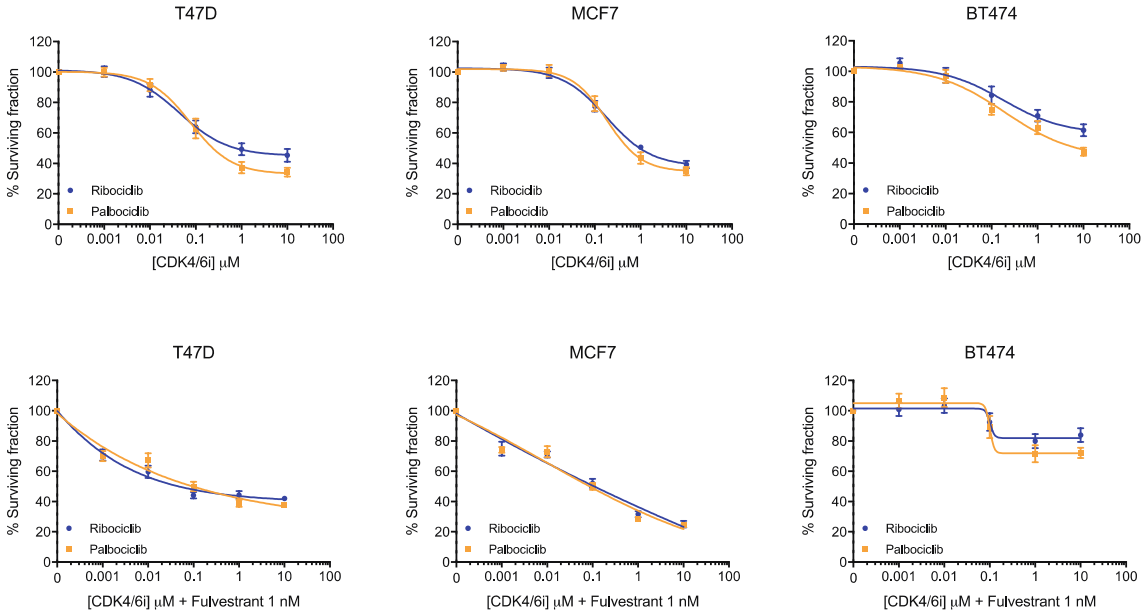

Figure 9. Proliferation inhibitory effect of palbociclib and ribociclib +/- fulvestrant in breast cancer cell lines. T47D, MCF7, BT474 cells were treated with increasing doses of palbociclib or ribociclib +/- fulvestrant (1 nM) for 72 h. Shown are representative graphs of cell viability readouts determined by Hoechst 33342. Data was normalized to untreated cells and three independent experiments were performed. Mean values ± SEM are shown.

In T47D and MCF7 cells, the combination of CDK4/6 inhibitors and fulvestrant was superior than palbociclib or ribociclib alone ($p < 0.001$), while in BT474 no significant differences were observed between the combination of CDK4/6 inhibitors with fulvestrant and palbociclib or ribociclib alone **(Figure 10)**.

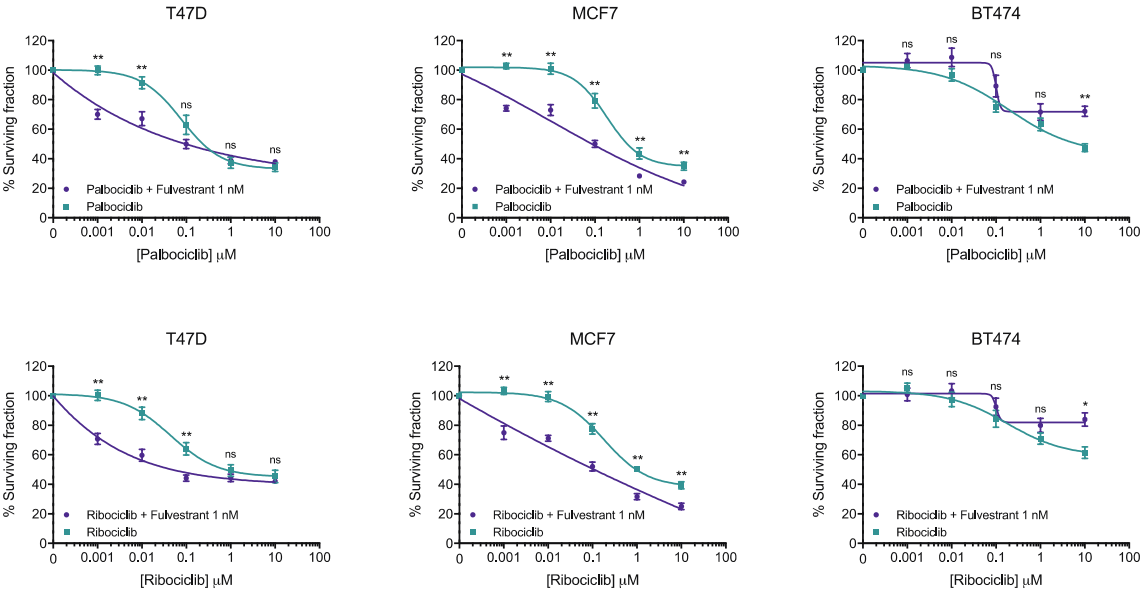

Figure 10. Comparing the proliferation inhibitory effect of CDK4/6 inhibitors with or without fulvestrant in breast cancer cell lines. MCF7, T47D, and BT474 cells were treated with increasing doses of palbociclib or ribociclib +/- fulvestrant (1 nM) for 72 h. Shown are representative graphs of cell viability readouts determined by Hoechst 33342. Data was normalized to untreated cells and three independent experiments were performed. Mean values ± SEM are shown. Statistical analyses were performed using the Mann-Whitney U test. * $p < 0.05$, ** $p < 0.01$.

RB1-competent T47D, MCF7, and BT474 cell lines were treated with two different doses of palbociclib or ribociclib (i.e., 100 or 500 nM) for different periods of time (i.e., 24, 72, or 144 h) in order to assess changes in the phosphorylation of RB1 (p-Rb). To ensure that no off-target effects were given with the chosen doses (i.e., 100 or 500 nM) the cytotoxic effect of palbociclib and ribociclib was also assessed in the *RB1*-mutated MDA-MB-468 cell line, where no effect was observed with after treatment with either CDK4/6 inhibitor **(Figure 11)**.

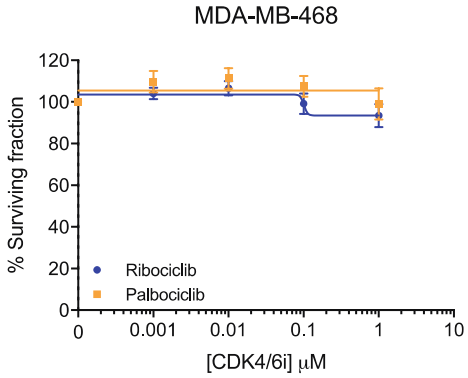

Figure 11. Proliferation inhibitory effect of palbociclib and ribociclib in RB1-mutated breast cancer cell line. MDA-MB-468 cells were treated with increasing doses of palbociclib or ribociclib for 72 h. Shown are representative graphs of cell viability readouts determined by Hoechst 33342. Data was normalized to untreated cells and three independent experiments were performed. Mean values ± SEM are shown.

In T47D and MCF7 cells, treatment with 100 nM CDK4/6 inhibitors partially reduced p-Rb with a further decrease observed in cells treated with 500 nM palbociclib or ribociclib regardless of treatment duration **(Figure 12A)**.

Next, the effect on cellular senescence was assessed upon treatment with CDK4/6 inhibitors by determining protein expression levels of Lamin-B1, a structural component of the nucleus whose loss has been associated with senescence (265,266). In T47D and MCF7 cells, CDK4/6 inhibitors decreased the expression of Lamin-B1 in a time and dose-dependent manner, with the lowest expression levels corresponding to those treated with 500 nM palbociclib or ribociclib for 144 h **(Figure 12A)**.

Additionally, we assessed the senescence-associated β galactosidase (SA-β-gal) activity (267) of cells treated with the same conditions. Both palbociclib and ribociclib (100 or 500 nM) increased β-galactosidase staining in T47D and MCF7 cell lines after 72 or 144 h treatments compared to non-treated controls indicating induction of senescence **(Figure 12B)**. Although

no significant differences were observed between treatment conditions, a dose- and time-related tendency was also noticeable, with the highest β-galactosidase staining levels corresponding to cells treated with 500 nM CDK4/6 inhibitors for 144 h. Of note, similar changes were observed in cells treated with palbociclib or ribociclib for all treatment conditions.

As for the BT474 cell line, a reduction of p-Rb was also observed upon 24 or 72 h treatments with CDK4/6 inhibitors (100 or 500 nM), although p-Rb levels were reestablished at 144 h from treatment. Lower expression of Lamin-B1 was detected, with little to no changes in expression after treatment **(Figure 12A)**. Lower levels of SA-β-gal activity were also detected generally and the highest activity was detected after 72 h treatments with either CDK4/6 inhibitor, followed by a decrease in cellular senescence 144 h from treatments **(Figure 12B)**. These results suggest that the BT474 cell line may possess an intrinsic resistance to CDK4/6 inhibition, with or without fulvestrant, which becomes most apparent at 144 h post-treatment, while earlier time points still show measurable responses.

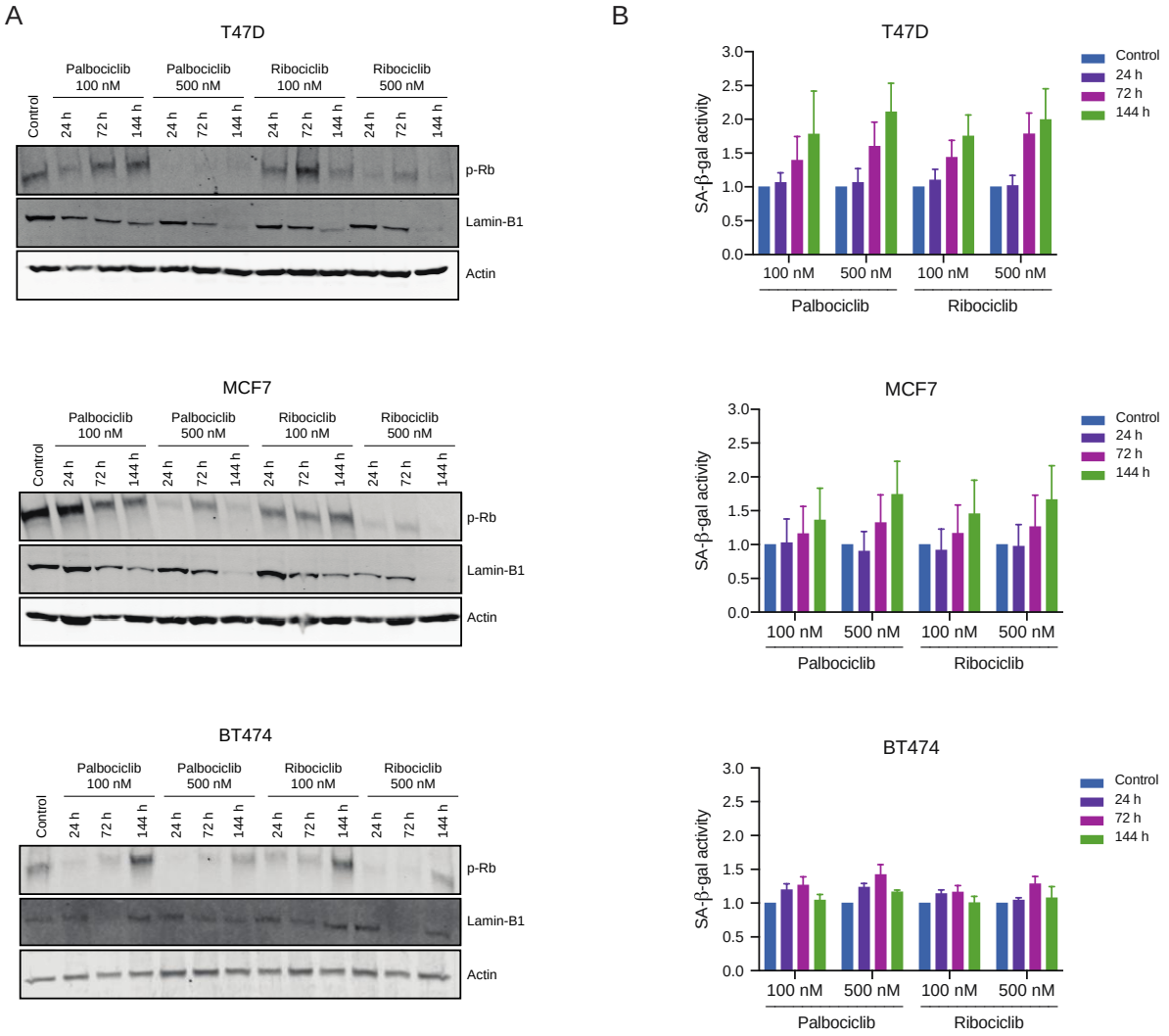

Figure 12. Biological changes during CDK4/6 inhibition *in vitro* in breast cancer cell lines. (A) T47D, MCF7, and BT474 cells were treated with palbociclib or ribociclib (100 or 500 nM) for 24, 72 or 144 h and expression of p-Rb and Lamin-B1 was assessed by western blot. Actin was used as a loading control. (B) T47D, MCF7, and BT474 cells were treated with palbociclib or ribociclib (100 or 500 nM) for 24, 72 or 144 h and SA-β-gal activity was determined by flow cytometry. Data was normalized to untreated cells and three independent experiments were performed. Mean values ± SEM are shown.

1.2. Effects of CDK4/6 inhibition on gene expression in breast cancer cell lines

Gene expression profiling was performed both in untreated cells and upon treatment in order to identify changes in the PAM50 biology induced by CDK4/6 inhibitors in T47D, MCF7, and BT474 cell lines treated with different doses of palbociclib and ribociclib (100 or 500 nM) +/− fulvestrant (1 nM). The expression of the 50 genes of the PAM50 intrinsic subtype predictor and 6 signatures (Basal-like, HER2-enriched, Luminal A, Luminal B, Normal-like, and the 11 gene Proliferation Score) were explored at both treatment conditions. Paired t-tests and

multiclass SAM analysis showed that both CDK4/6 inhibitors (100 or 500 nM) +/− fulvestrant (1 nM) significantly increased (FDR < 5%) the Luminal A and Normal-like signatures and significantly decreased (FDR < 5%) the Luminal B, Basal-like and Proliferation signatures **(Figures 13A and 14)**. Interestingly, the HER2-enriched signature was only significantly reduced when the CDK4/6 inhibitors were given at 500 nM either alone (palbociclib p = 0.045, ribociclib p = 0.041) or in combination with fulvestrant (palbociclib p = 0.002, ribociclib p = 0.012), while no significant changes were observed with 100 nM CDK4/6 inhibitor monotherapy (palbociclib p = 0.275, ribociclib p = 0.596) or in combination with fulvestrant (palbociclib p = 0.466, ribociclib p = 0.613). Treatment with fulvestrant alone significantly increased the HER2-enriched signature (p < 0.001) **(Figures 13A and 13B)**.

Next, we assessed individual gene expression across treatments using multiclass SAM. Forty-three (64.2%) genes were differentially expressed across treatment groups (FDR < 5%) **(Figure 13A)**. Notably, both inhibitors, especially at 500 nM, led to a lower expression of proliferative genes, including *CDC20*, *UBE2C*, *KNTC2*, *MKI67*, *BIRC5*, *CDCA1*, *PTTG1*, *CEP55*, *TYMS*, and *RRM2*. Interestingly, at the lower dose of 100 nM CDK4/6 inhibitors, the combination of fulvestrant and palbociclib had a stronger inhibitory effect on cell proliferation than the combination of fulvestrant and ribociclib. Additionally, cells treated with 500 nM palbociclib exhibited higher expression of the HER2-enriched genes *FGFR4* and *TMEM45B* compared to those treated with 500 nM ribociclib.

We also performed a paired SAM analysis to compare the differences between 500 nM palbociclib and 500 nM ribociclib, both with and without fulvestrant. A proportion of 19.4% and 25.3% of genes were differentially expressed after treatment with 500 nM palbociclib vs 500 nM ribociclib, with or without fulvestrant, respectively **(Table 5)**. Notably, almost 80% of the differentially expressed genes were common between the palbociclib vs ribociclib and palbociclib + fulvestrant vs ribociclib + fulvestrant comparisons **(Table 5)**, suggesting a largely consistent transcriptional response to these CDK4/6 inhibitors regardless of fulvestrant co-treatment. Genes that were not common between groups included *MYBL2*, *MELK*, *EXO1*, *CDC20*, and *KRT14*, which were uniquely differentially expressed after ribociclib treatment; *TMEM45B*, which was only expressed after palbociclib alone; *GRB7,* which was only expressed after treatment with ribociclib + fulvestrant; and *CD8A*, *SLC39A6*, *ORC6L*, *BCL2*, and *CCND1,* which were specifically expressed after palbociclib + fulvestrant treatment **(Table 5)**.

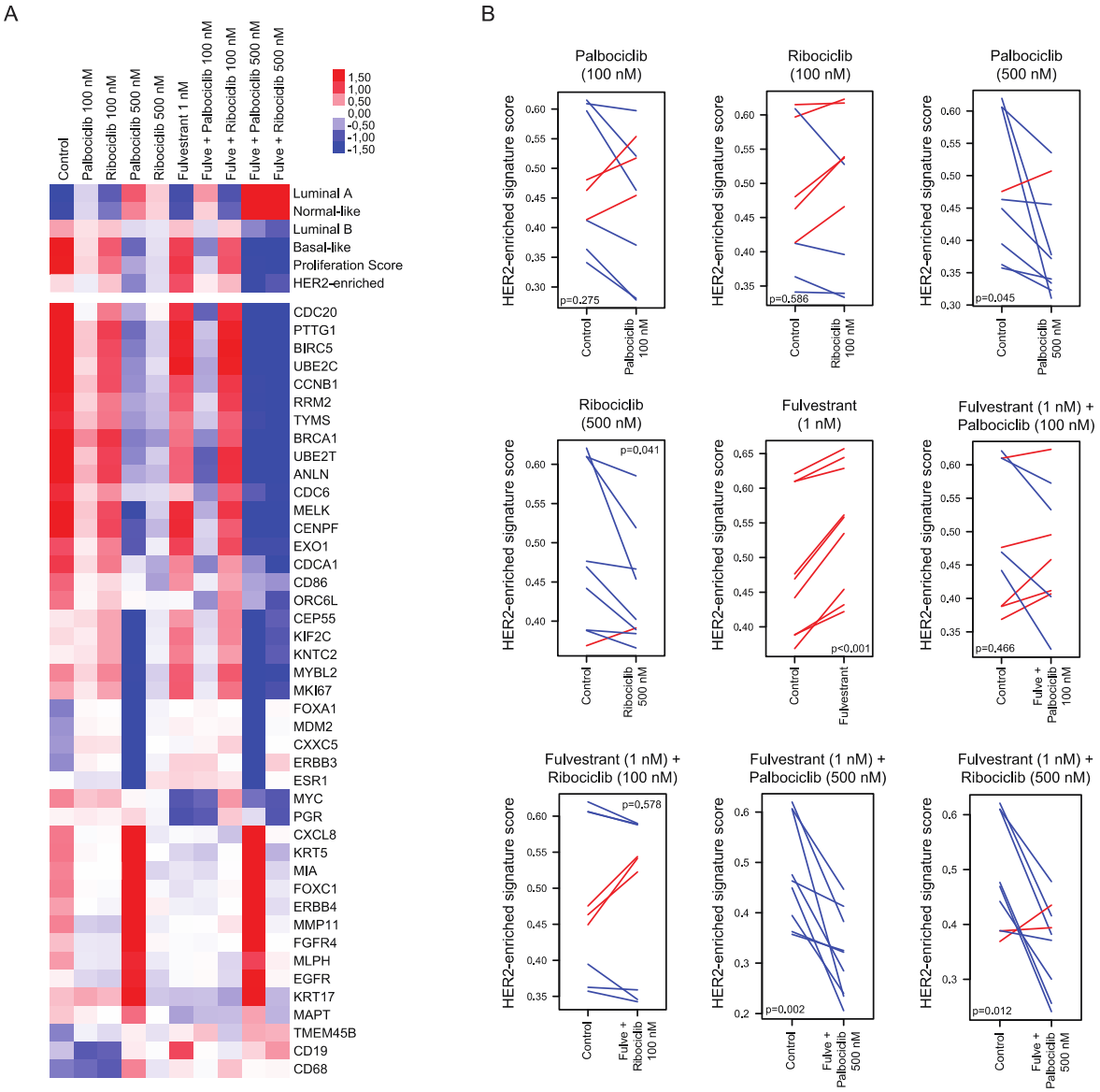

Figure 13. Changes in the HER2-enriched signature upon treatment with CDK4/6 inhibitors +/- fulvestrant in breast cancer cell lines. (A) Heatmap of a multiclass SAM representing the PAM50 molecular subtypes, Proliferation Score and genes that are differentially expressed (FDR < 5%) in T47D, MCF7, and BT474 cells treated with CDK4/6 inhibitors (100 or 500 nM) +/- fulvestrant (1 nM). Three independent mRNA extractions per cell line were performed. (B) Paired samples t-test analyses showing changes in the HER2-enriched signature following treatment of T47D, MCF7, and BT474 cells with CDK4/6 inhibitors (100 or 500 nM) +/- fulvestrant (1 nM). Three independent mRNA extractions and gene expression analyses were performed for each cell line.

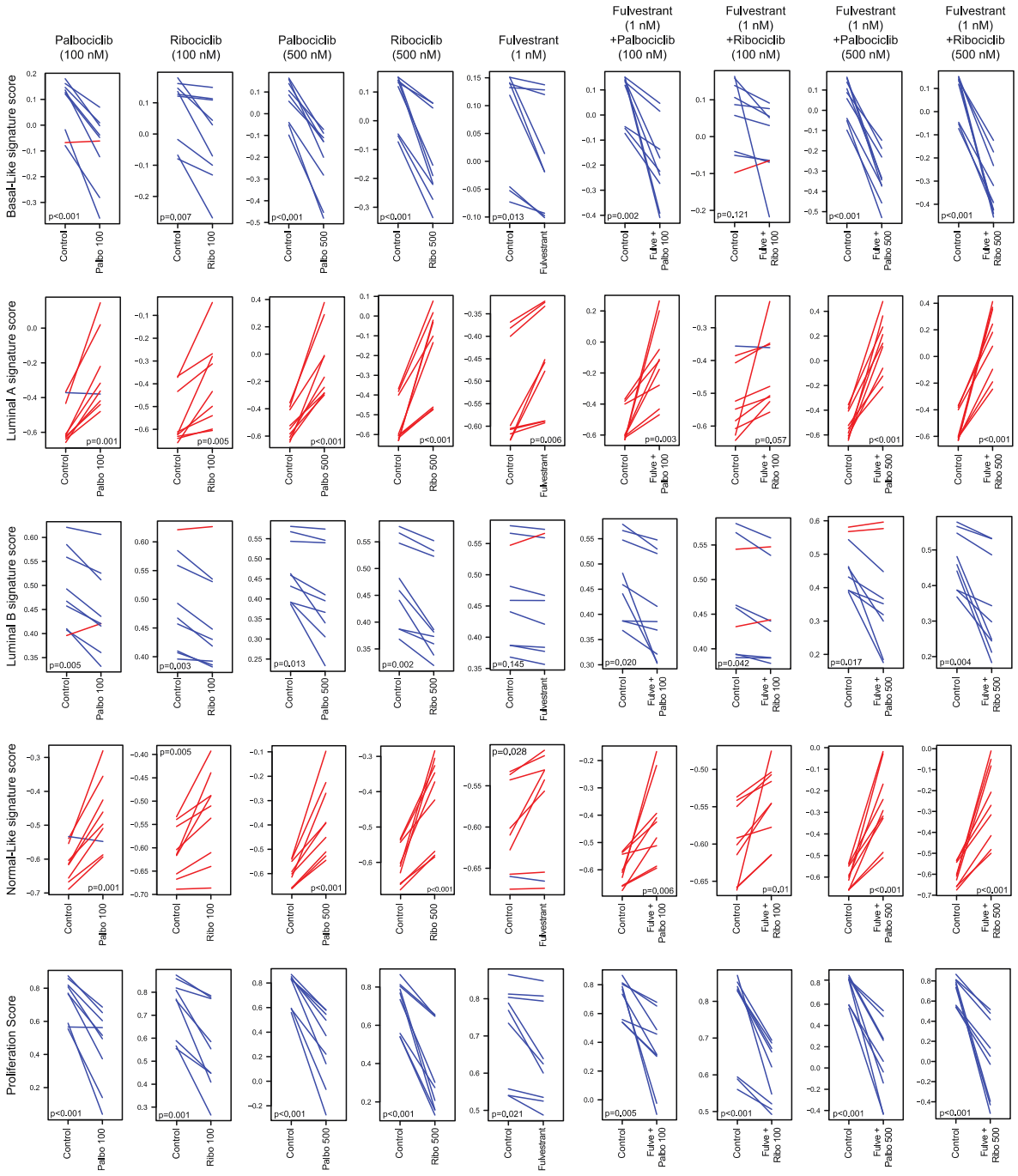

Figure 14. Changes in the PAM50 signatures upon treatment with CDK4/6 inhibitors +/- fulvestrant in breast cancer cell lines. Paired samples t-test analyses showing changes in the Basal-Like, Luminal A, Luminal B and Normal-like signatures as well as the Proliferation Score following treatment with CDK4/6 inhibitors (100 or 500 nM) +/- fulvestrant (1 nM). Three independent mRNA extractions and gene expression analyses were performed for each cell line.

Table 5. Differentially expressed genes after treatments. Paired SAM analysis between samples treated with palbociclib 500 nM (negative Score (d)) vs ribociclib 500 nM (positive Score (d)) and palbociclib 500 nM + fulvestrant 1 nM (negative Score (d)) vs ribociclib 500 nM + fulvestrant 1 nM (positive Score (d)) to show differentially expressed genes after treatment (FDR < 5%)

Palbociclib 500 nM vs Ribociclib 500 nM			
Gene ID	Score (d)	FDR (%)	PAM50 subtype
KIF2C	4.3014	0	Basal-like
CEP55	4.1995	0	Basal-like
MKI67	4.0133	0	Proliferation Score
FOXA1	3.6911	0	Luminal
MYBL2	3.6539	0	Basal-like
KNTC2	3.5728	0	Proliferation Score
MDM2	3.5258	0	Normal-like
CXXC5	3.5096	0	Luminal
ESR1	3.2821	0	Luminal
ERBB3	2.8874	0	NA
MELK	2.4888	0	Basal-like
EXO1	2.3875	0	Basal-like
GPR160	1.5991	4.6677	HER2-enriched
CDC20	1.5942	4.6677	Proliferation Score
ERBB2	1.4374	4.6677	HER2-enriched
KRT14	1.3944	4.6677	Normal-like
CXCL8	-4.9209	0	NA
KRT5	-3.7660	0	Normal-like
MMP11	-3.6778	0	Luminal
KRT17	-3.6773	0	Normal-like
FGFR4	-3.6420	0	HER2-enriched
MIA	-3.6215	0	Normal-like
ERBB4	-3.5005	0	NA
FOXC1	-3.4982	0	Basal-like
EGFR	-3.0385	0	Basal-like
MLPH	-2.8741	0	Luminal
MAPT	-2.5946	0	Luminal
PGR	-2.3712	0	Luminal
TMEM45B	-2.0383	0	HER2-enriched

Fulvestrant + Palbociclib 500 nM vs Fulvestrant + Ribociclib 500 nM			
Gene ID	Score (d)	FDR (%)	PAM50 subtype
CEP55	3.8310	0	Basal-like
FOXA1	3.6475	0	Luminal
KIF2C	3.4859	0	Basal-like
MDM2	3.3436	0	Normal-like
CXXC5	3.2832	0	Luminal
ERBB3	3.0693	0	NA
ESR1	2.6292	0	Luminal
GRB7	2.2987	0	HER2-enriched
MKI67	2.2081	0	Proliferation Score
KNTC2	2.1457	0	Proliferation Score
ERBB2	2.0022	0	HER2-enriched
GPR160	1.6941	3.7789	HER2-enriched
ERBB4	-4.4375	0	NA
CXCL8	-4.2148	0	NA
KRT5	-4.1695	0	Normal-like
MIA	-3.9053	0	Normal-like
PGR	-3.7338	0	Luminal
FOXC1	-3.7221	0	Basal-like
MMP11	-3.5001	0	Luminal
FGFR4	-3.4890	0	HER2-enriched
KRT17	-3.0806	0	Normal-like
CD8A	-2.8615	0	NA
MAPT	-2.8144	0	Luminal
EGFR	-2.6807	0	Basal-like
MLPH	-2.2781	0	Luminal
SLC39A6	-2.0990	0	Luminal
ORC6L	-1.6925	2.0294	Basal-like
BCL2	-1.6640	2.0294	Normal-like
CCND1	-1.6226	2.0294	NA

1.3. Early biological changes during CDK4/6 inhibition in tumor samples from CORALLEEN and NeoPalAna phase II studies

To identify molecular changes induced by CDK4/6 inhibitors, we performed gene expression analyses in baseline, day 15, and surgery tumor samples of patients treated with ribociclib plus letrozole in the CORALLEEN trial **(Figure 15A)**, as well as in baseline, day 15, and surgery samples of patients treated with palbociclib plus anastrazole in the NeoPalAna trial **(Figure 15B)**. First, we assessed early changes in 49 paired baseline and day 15 tumor samples from the CORALLEEN trial **(Figure 15C)** and 23 paired baseline and day 15 tumor samples from the NeoPalAna trial **(Figure 15D)**. Treatment with ribociclib and endocrine therapy led to a significant increase in Luminal A ($p < 0.001$) and Normal-like ($p < 0.001$) signatures and a significant decrease in Basal-like ($p < 0.001$), HER2-enriched ($p < 0.001$), Luminal B ($p < 0.001$), and Proliferation ($p < 0.001$) signatures **(Figure 15C)**. Similarly, treatment with palbociclib plus endocrine therapy led to a significant increase in Luminal A ($p < 0.001$) and Normal-like ($p < 0.001$) signatures and a significant decrease in HER2-enriched ($p < 0.001$), Luminal B ($p < 0.001$), and Proliferation ($p < 0.001$) signatures **(Figure 15D)**.

1.4. Biological changes after CDK4/6 inhibition in tumor samples from CORALLEEN and NeoPalAna phase II studies

Next, we assessed changes in 49 paired baseline and surgery tumor samples from the CORALLEEN **(Figure 15E)** and 16 paired baseline and surgery tumor samples from the NeoPalAna **(Figure 15F)**.

Treatment with ribociclib and endocrine therapy led to a significant increase in Luminal A ($p < 0.001$) and Normal-like ($p < 0.001$) signatures and a significant decrease in HER2-enriched ($p < 0.001$), Luminal B ($p < 0.001$), and Proliferation ($p < 0.001$) signatures **(Figure 15E)**. Treatment with palbociclib and endocrine therapy led to a significant increase in the Normal-like ($p = 0.012$) signature and a significant decrease in the Luminal B ($p = 0.021$) and Proliferation signature ($p = 0.018$) **(Figure 15F)**. Importantly, the HER2-enriched signature did not significantly decrease in surgical samples of patients treated with palbociclib ($p = 0.194$), although a difference in sample size could explain this result **(Figure 15F)**.

In CORALLEEN, the median number of days between the last dose of ribociclib and surgery was 13.1 days (range: 1–78) (256), whereas in NeoPalAna the median number of days

between the last dose of palbociclib and surgery was 29 days (range: 8–49), except for 8 patients who received additional 10–12 days of palbociclib immediately before surgery (179). In patients from CORALLEEN, the HER2-enriched signature was significantly decreased in those who underwent surgery at 8 days from the last dose of ribociclib or before ($p < 0.001$), as well as in those who underwent surgery after more than 8 days from the last dose of ribociclib ($p < 0.001$) **(Figure 15G)**. In 4 patients from NeoPalAna who underwent surgery at 8 days from the last dose of palbociclib or before, a tendency of reduction in the HER2-enriched signature was also observed. However, in patients who underwent surgery after more than 8 days from the last dose of palbociclib, the HER2-enriched signature increased in 50% of the cases **(Figure 15H)**.

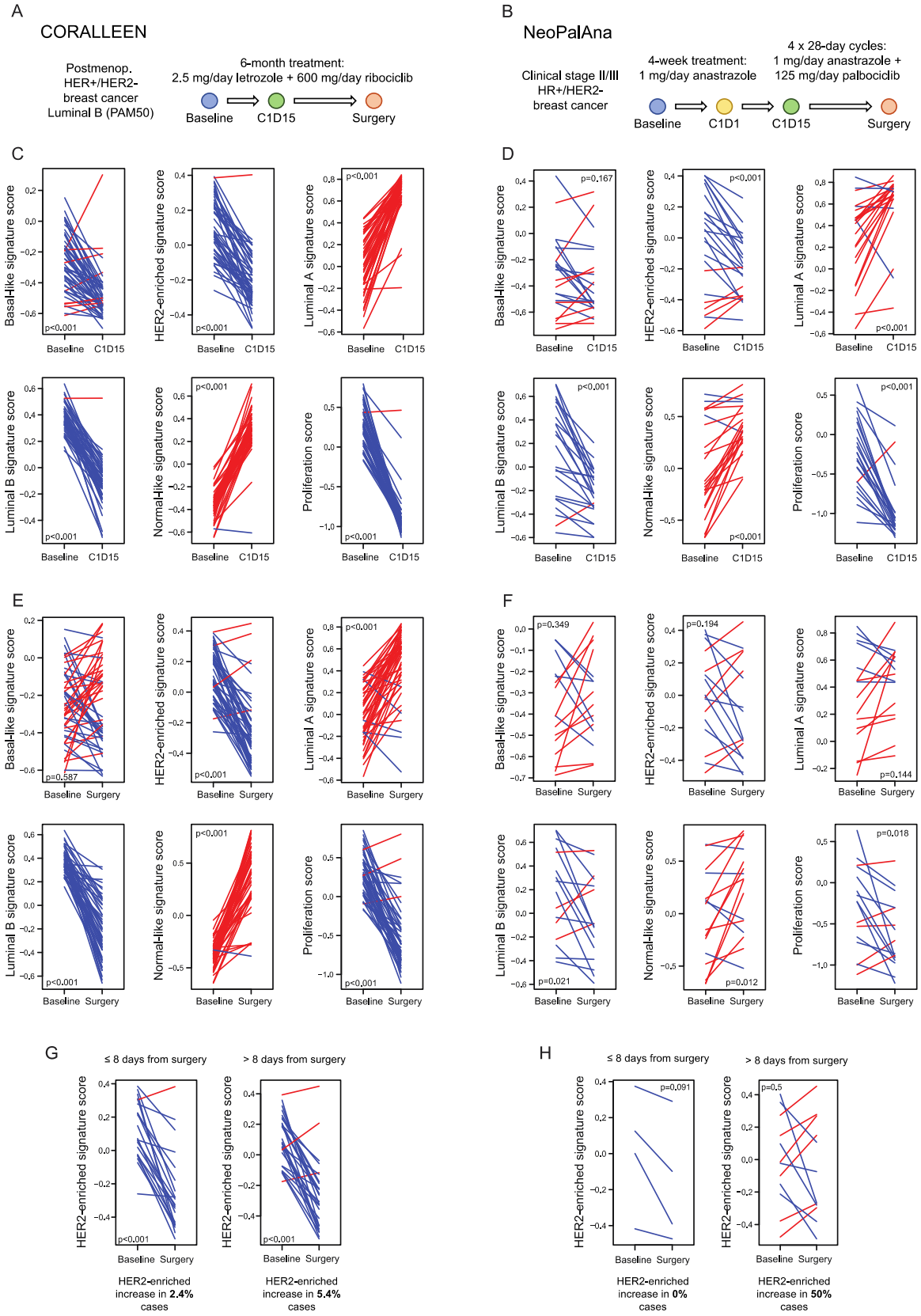

Figure 15. Changes in the PAM50 signatures in the CORALLEEN and NeoPalAna studies. Schematic summaries of the samples analyzed from (A) the CORALLEEN and (B) the NeoPalAna trial design. (C) Paired samples t-test analyses showing changes in the PAM50 signatures at cycle 1 day 15 (C1D15) in samples from CORALLEEN and (D) NeoPalAna phase II studies. (E) Changes in the PAM50 signatures at surgery in samples from CORALLEEN and (F) NeoPalAna. (G) Changes in the HER2-enriched signature in samples from CORALLEEN and (H) NeoPalAna from patients who underwent surgery ≤ 8 or > 8 days from the last dose of CDK4/6i and endocrine therapy.

In this first part of the thesis, we have demonstrated that while palbociclib and ribociclib effectively modulate key biological pathways in HR+/HER2- breast cancer, nuances in their impact, particularly on the HER2-enriched signature, are dose-dependent, influenced by the addition of fulvestrant, and warrant further investigation. The results from this chapter of the thesis were published in Scientific Reports in 2024 (268).

2. FGFR4 as a driver of resistance to CDK4/6 inhibitors in HR+/HER2- breast cancer

The development of resistance to CDK4/6 inhibitors in HR+/HER2- breast cancer represents a major clinical challenge, limiting the long-term efficacy of current standard of care treatments. In this chapter, we build upon existing evidence linking the HER2-enriched intrinsic subtype and aberrant FGFR4 signaling to poor clinical outcomes and therapeutic resistance in HR+ breast cancer (70,170,218,219), by analyzing real-world data from a clinical cohort of patients treated with endocrine therapy and CDK4/6 inhibitors. Furthermore, we explore the role of FGFR4 as a potential driver of resistance.

2.1. PAM50 determination in baseline and progressive disease samples of patients treated with CDK4/6 inhibitors

To study the PAM50 distribution before and after treatment with CDK4/6 inhibitors and endocrine therapy, we analyzed samples of the CDK clinical cohort. This is a real-world dataset of 375 patients with a histologic diagnosis of HR+/HER2-negative metastatic breast cancer treated with CDK4/6 inhibitors, including palbociclib, ribociclib and abemaciclib at Hospital Clínic of Barcelona between years 2014 and 2024, and it includes 253 baseline tumor samples (130 primary tumors and 123 metastasis) and 59 progressive disease (PD) samples collected after treatment with endocrine therapy and CDK4/6 inhibitors. This cohort also included 37 paired baseline-PD samples **(Figure 16A)**.

At baseline, the median age of patients was 62.7 years, 99.2% were female, 76.1% postmenopausal, 33.3% had de novo metastasis, 22.1% bone only disease, 58.1% visceral disease, 1.6% brain metastasis, 64.4% less than 3 metastatic sites, and most patients had

ECOG 0 or 1 (41.8% and 49.8%, respectively). Regarding treatment, 36.8% received palbociclib, 58.3% ribociclib, and 5.1% abemaciclib. CDK4/6 inhibitors were administered as first-line therapy in 66.0% patients, second-line in 19.8%, and successive lines in 14.2% **(Table 6)**.

Table 6. Clinical characteristics of patients in the CDK cohort

	n	%
Median age (range) (years)	62.7 (24.6-88.4)	
Sex		
Female	251	99.2
Male	2	0.8
Menopausal status		
Premenopausal	60	23.9
Postmenopausal	191	76.1
Type of metastasis		
Recurrent	168	66.7
De novo	84	33.3
Bone only	56	22.1
Visceral disease	147	58.1
Brain disease	4	1.6
Number of metastatic sites		
<3	163	64.4
> or = 3	90	35.6
Performance status		
ECOG 0	106	41.8
ECOG 1	126	49.8
ECOG 2	18	7.1
ECOG 3	3	1.2
CDK4/6 inhibitor		
Palbociclib	93	36.8
Ribociclib	147	58.1
Abemaciclib	13	5.1
Setting in advanced disease		
1st line	167	66
2nd line	50	19.8
3rd line	36	14.2

At baseline, PAM50 distribution was 39.5% Luminal A, 32.4% Luminal B, 14.6% HER2-enriched, 6.7% Basal-like, 6.7% Normal-like. PAM50 subtypes at PD were 45.8% HER2-enriched, 25.4% Luminal B, 16.9% Luminal A, 10.2% Basal-like, and 1.7% Normal-like, significantly differing from the baseline distribution ($p < 0.001$) **(Figure 16B)**.

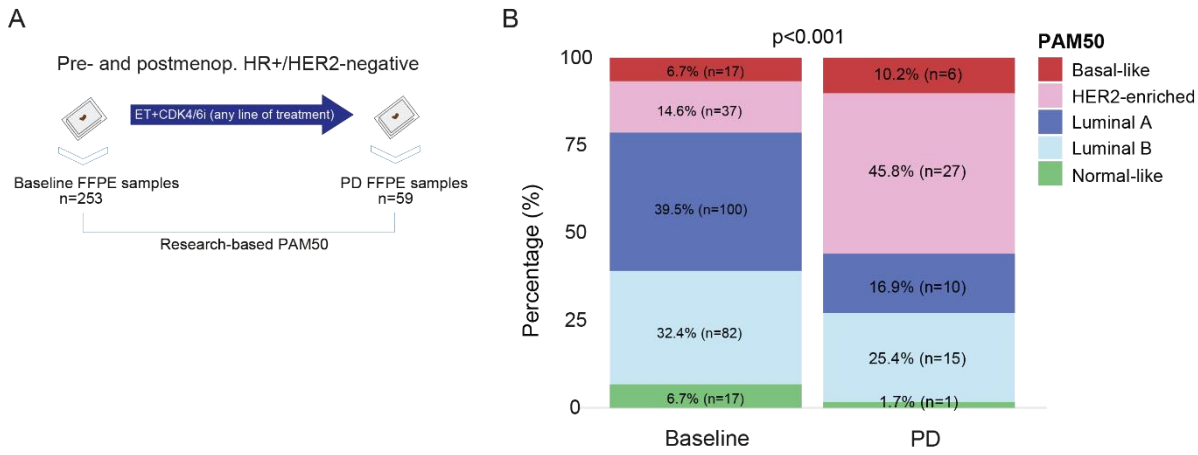

Figure 16. Baseline and PD samples from the CDK patient cohort (A) Schematic overview of the samples analyzed from the CDK patient cohort. (B) PAM50 subtype distribution in 253 baseline and 59 PD samples of the CDK patient cohort.

Notably, a subtype shift was observed in 64.9% of the 37 paired baseline-PD, most frequently toward the HER2-enriched subtype. Nine out of 12 HER2-enriched tumors remained unchanged at PD **(Figure 17A)**. Consistently, all PAM50 scores significantly changed from baseline to PD: HER2-enriched, Luminal B and Proliferation scores increased, while the Luminal A and Normal-like scores decreased **(Figure 17B)**.

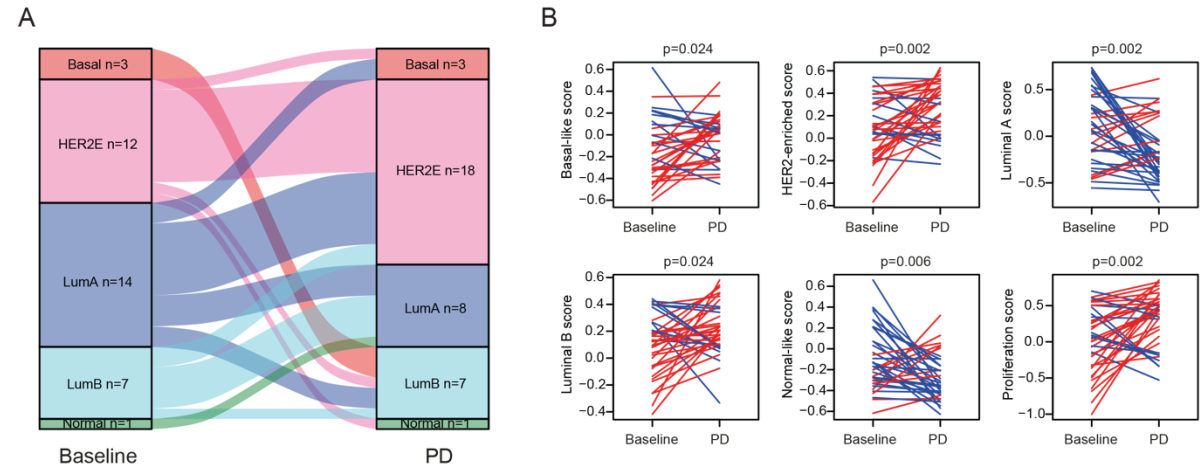

Figure 17. PAM50 subtype dynamics and score changes from baseline to progression in the CDK cohort. (A) Subtype shifts between 37 paired baseline and progression samples from the CDK cohort. (B) Changes in the PAM50 signature scores and the Proliferation Score in 37 paired baseline and progression samples from the CDK cohort. Statistical significance was assessed with paired t-tests.

2.2. Association of the HER2-enriched subtype with survival outcomes

Next, we studied the association of baseline PAM50 subtypes with survival outcomes using Cox regression models in the CDK cohort. In the CDK cohort, the HER2-enriched subtype was significantly associated with poor PFS (hazard ratio=3.7 [95% CI=2.3-5.9], p < 0.001) and OS (hazard ratio=4.3 [95% CI=2.3-7.7], p < 0.001) after adjusting for clinical variables **(Figure 18)**.

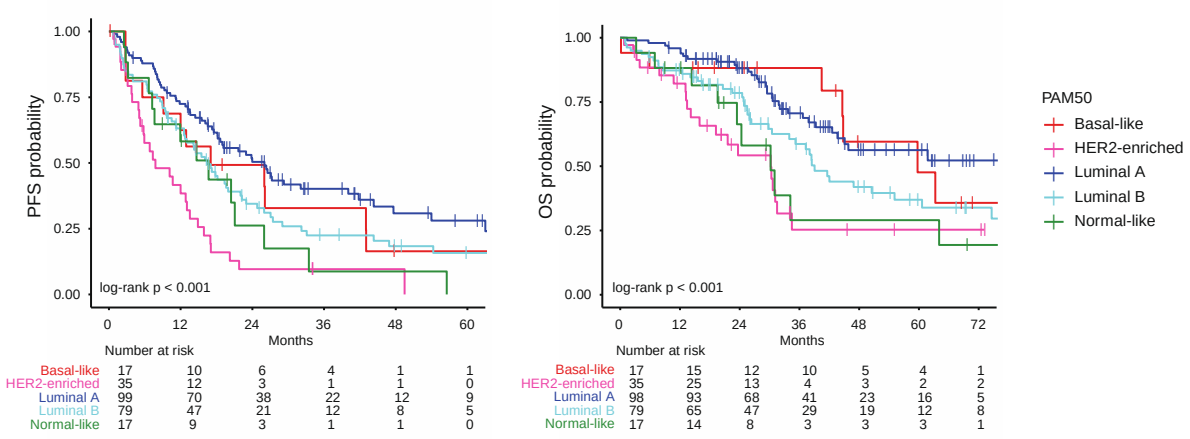

Figure 18. Association of PAM50 with PFS and OS. Kaplan-Meier of the association of PAM50 subtype with PFS and OS in 253 baseline tumor samples of the CDK patient cohort.

2.3. Association of *FGFR4* with the HER2-enriched subtype and survival outcomes

To date, our group and others have pointed to high *FGFR4* expression as a driver of the HER2-enriched subtype within HR+/HER2- BC (218,219). Here, we analyzed the association of *FGFR4* across PAM50 groups using the samples of the CDK cohort and confirmed that *FGFR4* was significantly associated with HER2-enriched **(Figure 19)**.

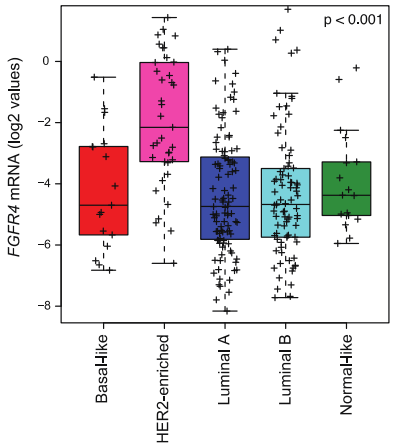

Figure 19. Association between *FGFR4* mRNA expression and PAM50 subtypes. *FGFR4* expression was assessed in 253 baseline samples from the CDK cohort. Statistical analyses were performed using one-way ANOVA to compare FGFR4 expression across groups.

Next, we analyzed the association of *FGFR4* with survival outcomes. High *FGFR4* in baseline samples was significantly associated with worse PFS (hazard ratio 1.14, 95% CI=1.06-1.22, p < 0.001) and OS (hazard ratio 1.18, 95% CI=1.08-1.28, p < 0.001) in univariate analysis **(Figure 20, Table 7)**. When adjusting for PAM50 subtype, CDK4/6 inhibitor type, and line of therapy in a multivariable analysis, *FGFR4* remained significantly associated with PFS (hazard ratio 1.18, 95% CI=1.10-1.28, p < 0.001) and OS (hazard ratio 1.23, 95% CI=1.11-1.37, p < 0.001) **(Table 7)**.

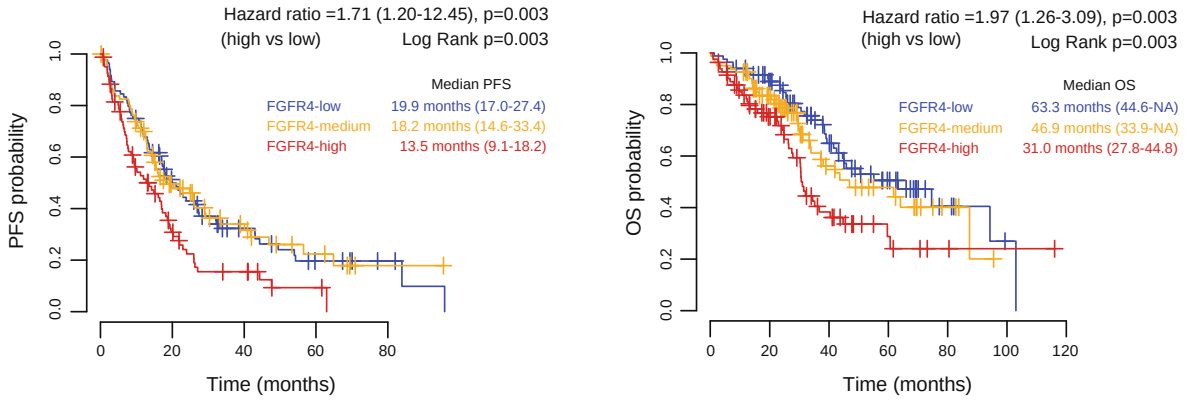

Figure 20. Association of *FGFR4* mRNA expression with PFS and OS. Kaplan-Meier curves showing the association of *FGFR4* mRNA expression (divided into tertiles: Low, Medium, High) with PFS and OS in 253 baseline tumor samples from patients in the CDK cohort. Hazard ratio and p-values comparing *FGFR4* High vs Low expression groups are indicated on each graph.

Table 7. Cox regression models of the association of PAM50 and *FGFR4* expression with PFS

Variable		PFS						OS					
		Univariable			Multivariable			Univariable			Multivariable		
		HR	95% CI	p	HR	95% CI	p	HR	95% CI	p	HR	95% CI	p
FGFR4		1.14	1.06-1.22	**<0.001**	1.18	1.10-1.28	**<0.001**	1.18	1.08-1.28	**<0.001**	1.23	1.11-1.37	**<0.001**
PAM50 subtype	**Luminal A**	Ref.			Ref.			Ref.			Ref.		
	Luminal B	1.51	1.05-2.16	**0.025**	1.70	1.15-2.71	**0.007**	1.73	1.08-2.75	**0.021**	1.89	1.15-3.11	**0.012**
	Basal-like	1.34	0.72-2.49	0.363	1.90	0.99-3.61	0.052	1.08	0.48-2.46	0.851	1.18	0.50-2.77	0.709
	Her2-enriched	3.04	1.95-4.75	**<0.001**	2.97	1.83-4.83	**<0.001**	3.09	1.76-5.43	**<0.001**	2.54	1.33-4.89	**0.005**
	Normal-like	1.95	1.09-3.50	**0.025**	1.66	0.91-3.02	0.097	2.71	1.36-5.39	**0.005**	2.49	1.22-5.09	**0.013**
Age		0.99	0.98-0.99	**0.029**	0.99	0.98-1.00	0.071	1.01	0.99-1.02	0.240	-	-	-
Menopausal status	**Premenopausal**	Ref.			-	-	-	Ref.			-	-	-
	Postmenopausal	0.94	0.66-1.34	0.723	-	-	-	1.24	0.77-1.98	0.376	-	-	-
CDK4/6i	**Palbociclib**	Ref.			Ref.			Ref.			-	-	-
	Ribociclib	0.69	0.51-0.93	**0.015**	0.67	0.48-0.95	**0.022**	0.79	0.54-1.16	0.229	-	-	-
	Abemaciclib	1.10	0.50-2.39	0.818	1.31	0.58-2.96	0.511	1.45	0.58-3.27	0.433	-	-	-
Line of treatment	**First**	Ref.			Ref.			Ref.			Ref.		
	Second	1.16	0.79-1.71	0.443	1.09	0.72-1.66	0.680	1.20	0.74-1.95	0.455	1.23	0.73-2.07	0.443
	Successive	2.18	1.48-3.21	**<0.001**	1.75	1.13-2.71	**0.012**	2.31	1.45-3.67	**<0.001**	2.40	1.42-4.06	**0.001**
Type of metastasis	**Relapsed**	Ref.			Ref.			Ref.			Ref.		
	De novo	0.65	0.47-0.90	**0.010**	0.60	0.43-0.85	**0.004**	0.52	0.33-0.81	**0.004**	0.53	1.87-0.33	**0.011**
Bone only disease	**No**	Ref.			-	-	-	Ref.			Ref.		
	Yes	0.74	0.52-1.07	0.107	-	-	-	0.50	0.29-0.85	**0.010**	0.55	0.28-1.08	0.083
Visceral disease	**No**	Ref.			-	-	-	Ref.			Ref.		
	Yes	1.19	0.88-1.62	0.255	-	-	-	1.59	1.06-2.37	**0.024**	0.87	0.48-1.56	0.636
Number of metastatic sites	**<3**	Ref.			-	-	-	Ref.			Ref.		
	≥3	1.12	0.83-1.52	0.456	-	-	-	1.57	1.08-2.28	**0.019**	1.02	0.62-1.67	0.941
Performance status	**ECOG 0**	Ref.			Ref.			Ref.			Ref.		
	ECOG 1	1.21	0.88-1.67	0.236	1.29	0.93-1.80	0.127	1.60	1.04-2.44	**0.031**	1.70	1.08-2.67	**0.023**
	ECOG 2	3.01	1.75-5.15	**<0.001**	6.87	3.76-12.55	**<0.001**	3.99	2.00-7.94	**<0.001**	7.38	3.52-15.47	**<0.001**
	ECOG 3	0.53	0.07-3.80	0.524	1.11	0.15-8.56	0.918	3.52	0.84-14.76	0.085	12.35	2.55-59.90	**0.002**

Additionally, *FGFR4* expression was assessed in both baseline and PD samples from the CDK clinical cohort. As anticipated, *FGFR4* levels were significantly elevated in PD samples compared to baseline samples ($p < 0.001$), further reinforcing its role in treatment resistance **(Figure 21)**.

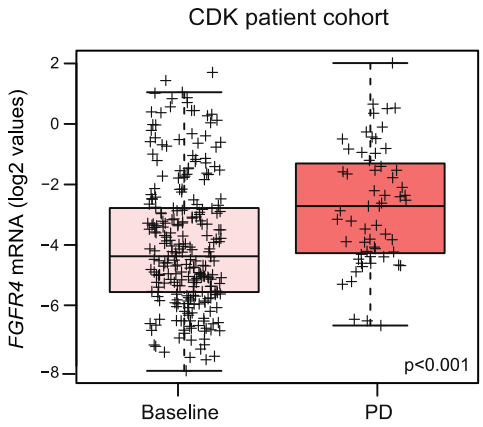

Figure 21. Expression of *FGFR4* in baseline and PD samples. *FGFR4* mRNA expression was assessed in 253 baseline and 59 PD samples from patients of the CDK cohort. Statistical analyses were performed using one-way ANOVA to compare FGFR4 expression across groups.

2.4. Characterization of FGFR4 protein expression levels in tumor samples from patients with breast cancer

Building on the observed association between *FGFR4* gene expression and poor clinical outcomes, we next sought to characterize FGFR4 at the protein level in tumor samples to better understand its role in resistance mechanisms and to evaluate its potential as a therapeutic target.

To this end, we analyzed FGFR4 protein expression using IHC in 47 baseline and 36 progressive disease samples from the CDK cohort and observed that FGFR4 H-Scores were higher in PD samples compared to baseline samples (average H-Score 120 vs 60) **(Figure 22A)**. Importantly, the FGFR4 H-Score significantly correlated with its mRNA expression (Pearson correlation = 0.66, $p < 0.001$) **(Figure 22B)** and PD samples had a higher proportion of tumors with an FGFR4 H-Score above 50 compared to baseline samples **(Figure 22C)**.

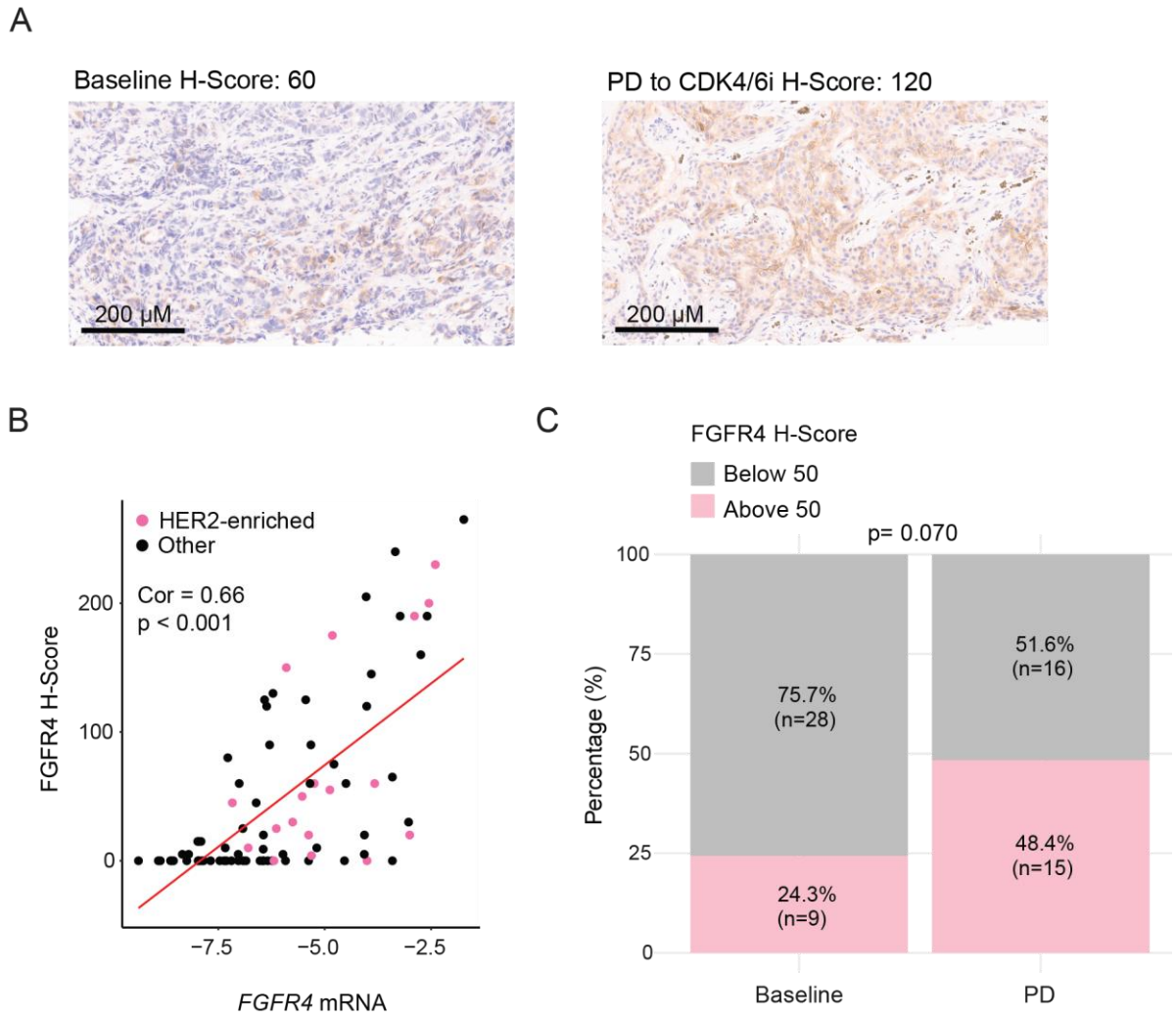

Figure 22. FGFR4 expression in breast cancer tumor samples by IHC. (A) Example of FGFR4 IHC staining in a baseline and a PD sample from patients of the CDK cohort. (B) Pearson correlation between *FGFR4* mRNA expression and FGFR4 protein expression in 37 baseline and 31 PD samples of the CDK cohort. (C) Distribution of FGFR4 protein expression above and below an H-Score of 50 in 37 baseline and 31 PD samples of the CDK cohort.

In parallel, we evaluated FGFR4 protein expression by IHC in 39 healthy tissue samples **(Figure 23)**. FGFR4 expression was undetectable in healthy tissue, suggesting that targeting FGFR4 may result in low toxicity.

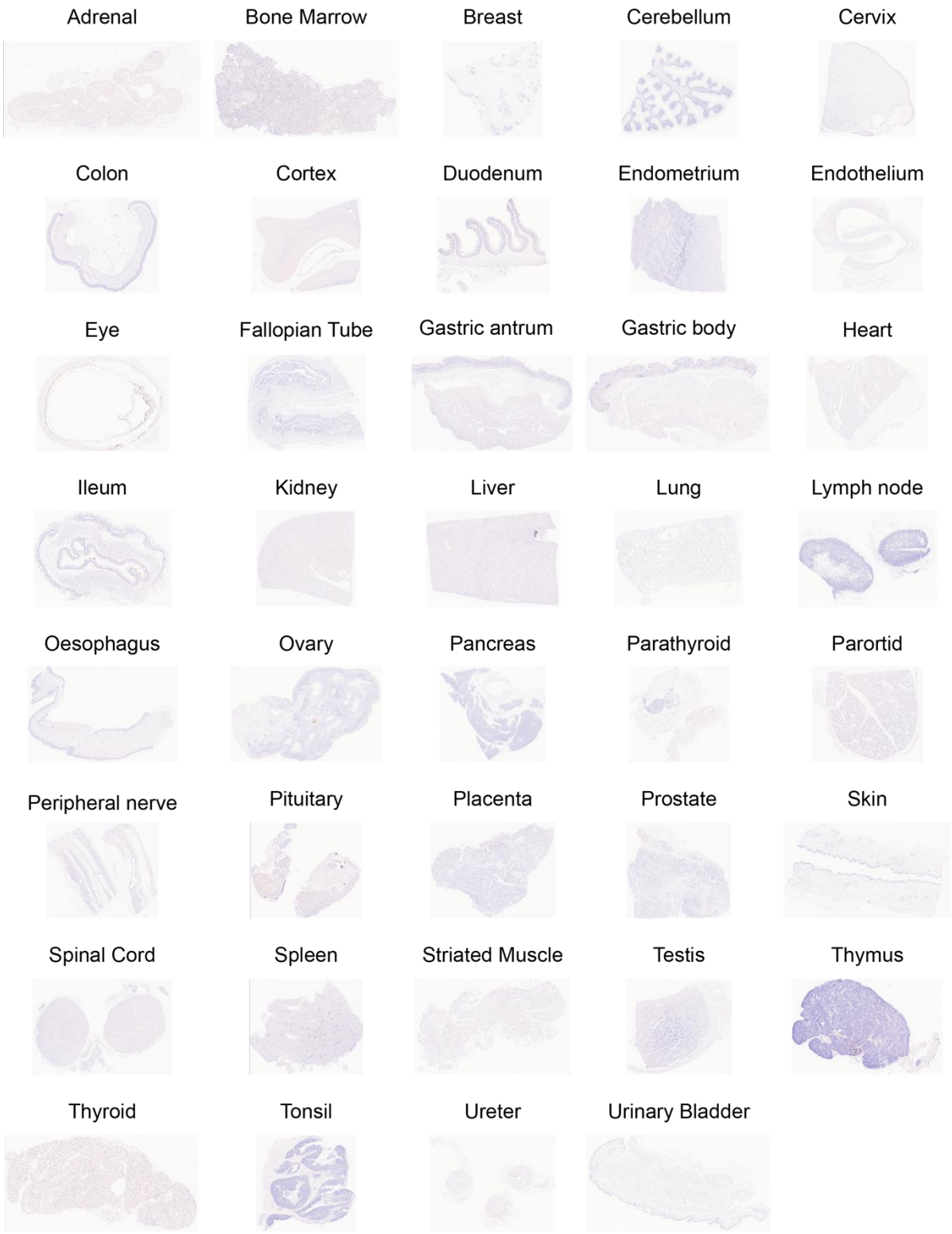

Figure 23. FGFR4 expression across healthy tissues. FGFR4 IHC staining in 39 healthy tissues. Original magnification, x0.7.

3. Targeting FGFR4 in HR+/HER2- breast cancer

3.1. Characterization of FGFR4 in cell line models

FGFR4 is an RTK implicated in tumor progression and therapeutic resistance, making it an attractive target for treatment with TKIs or monoclonal antibodies. To evaluate the therapeutic potential of targeting FGFR4, we assembled a panel of 6 breast cancer cell lines with varying levels of FGFR4 expression: MDA-MB-231, T47D, ZR751, T47D palbociclib-resistant (PR), T47D Y367C, and MDA-MB-453.

The T47D PR cell line was generated in our laboratory through prolonged exposure to increasing doses of palbociclib over 6 months. This process led to the acquisition of resistance to 500 nM palbociclib and a phenotypic shift toward a HER2-enriched subtype. Similarly, the T47D Y367C cell line was generated by introducing a constitutively activating *FGFR4* Y367C mutation, which is intrinsically found in the MDA-MB-453 cell line (269), into parental T47D cells. Like the PR variant, this engineered line also exhibited a HER2-enriched phenotype based on PAM50 subtyping.

The expression of ER, PR, HER2, and molecular intrinsic subtypes were validated using IHC and PAM50 gene expression profiling, respectively. ZR751, T47D PR, T47D Y367C, and MDA-MB-453 cell lines were classified as HER2-enriched, while T47D showed a borderline Luminal B/HER2-enriched profile, and MDA-MB-231 was categorized as Basal-like **(Figure 24A).**

Although our primary focus was on HR+/HER2- breast cancer, we included the TNBC MDA-MB-231 and MDA-MB-453 cell lines since they represent relevant models for FGFR4 expression and mutational status. Notably, MDA-MB-453 cells harbor the *FGFR4* Y367C mutation, which made them a valuable model for studying FGFR4-targeted therapies. In contrast, MDA-MB-231 cells lack FGFR4 expression and served as a negative control for the assessment of target specificity.

FGFR4 expression was evaluated across the cell line panel using multiple techniques, allowing classification into three categories: FGFR4-negative, FGFR4-low, and FGFR4-high. Quantification of total FGFR4 mRNA **(Figure 24B)** and protein levels **(Figure 24C)** identified four cell lines (i.e., ZR751, T47D PR, T47D Y367C, and MDA-MB-453) with high FGFR4

expression. Notably, all four were also classified as HER2-enriched by PAM50 **(Figure 24A)**. T47D displayed low FGFR4 expression, while MDA-MB-231 lacked detectable FGFR4, supporting its role as a negative control. IHC staining of FFPE cell pellets confirmed both membranous and cytoplasmic FGFR4 localization in the high-expressing lines, with membrane H-scores ranging from 165 to 230. In contrast, MDA-MB-231 cells showed no membrane staining (H-Score = 0) **(Figure 24D)**.

Together, these findings validated the selected cell line panel as a robust platform for evaluating FGFR4-targeted drugs.

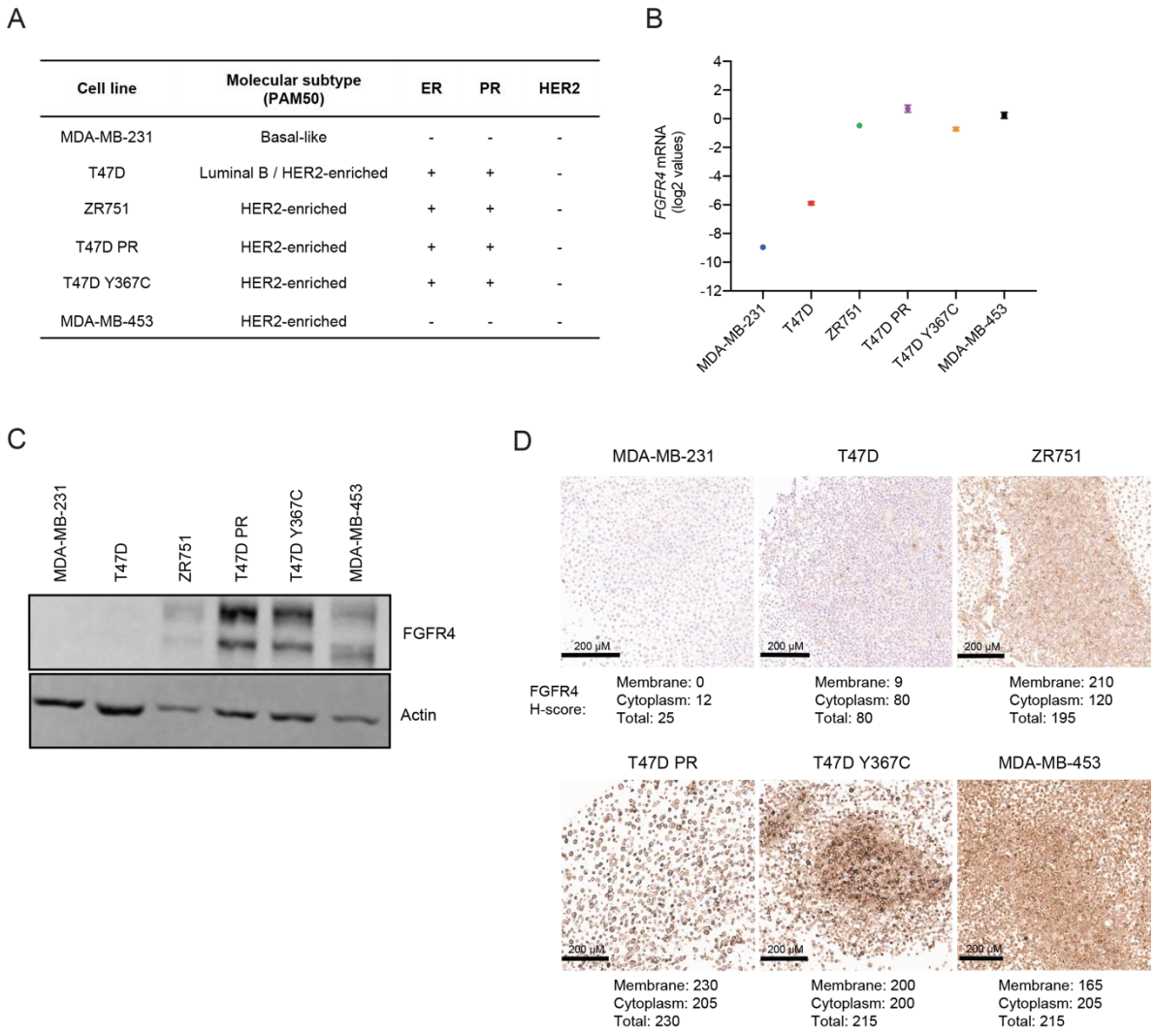

Cell line	Molecular subtype (PAM50)	ER	PR	HER2
MDA-MB-231	Basal-like	-	-	-
T47D	Luminal B / HER2-enriched	+	+	-
ZR751	HER2-enriched	+	+	-
T47D PR	HER2-enriched	+	+	-
T47D Y367C	HER2-enriched	+	+	-
MDA-MB-453	HER2-enriched	-	-	-

Figure 24. Selection of a panel of six breast cancer cell lines for ADC optimization. Cell lines with different levels of expression of FGFR4 were selected for the optimization of an anti-FGFR4 ADC. (A) Molecular subtype of each cell line by PAM50 and ER, PR, and HER2 status determined by IHC. (B) *FGFR4* mRNA expression. At least three independent mRNA extractions per cell line were performed. Mean values ± SEM are shown. (C) FGFR4 protein expression. Actin was used as a loading control. (D) FGFR4 IHC staining from cellular pellets. Shown are the H-Scores for membrane, cytoplasm, and total stainings.

3.2. Targeting FGFR4 with a selective FGFR4 tyrosine kinase inhibitor in breast cancer cell line models

Given the association of FGFR4 expression with poor clinical outcomes and resistance to therapy, we investigated the therapeutic potential of INCB062079, a potent, selective, and irreversible FGFR4 inhibitor. INCB062079 covalently binds to Cys552, a unique cysteine residue within the ATP-binding pocket of FGFR4 that is not conserved in FGF1-3, and effectively blocks FGFR4 autophosphorylation and downstream signaling (246). This structural specificity provides a significant advantage over pan-FGFR inhibitors by minimizing off-target activity and reducing the risk of systemic toxicity, thereby enabling more precise targeting of FGFR4-driven oncogenic pathways. The compound has demonstrated promising preclinical activity in cancers with aberrant FGFR4 signaling, such as HCC, where it suppressed tumor growth and proliferation both *in vitro* and *in vivo* (245,246). A phase I clinical trial (NCT03144661) was initiated; however, the study was terminated early due to slow patient accrual (247).

To evaluate the potential of INCB062079 in breast cancer, we assessed its efficacy across our panel of breast cancer cell lines exhibiting varying levels of FGFR4 expression. Cells were treated with increasing concentrations of the inhibitor (0, 0.001, 0.01, 0.1, 1, 2.5, 5, and 10 µM) for 72 h. A cytotoxic effect was observed exclusively in the *FGFR4*-mutant MDA-MB-453 cell line. However, no cytotoxicity was detected in other cell lines with similarly high FGFR4 levels, such as ZR751 and the T47D PR cells, except at the highest drug concentrations. Notably, the T47D Y367C mutant cell line, which harbors the same activating mutation as MDA-MB-453 (269), also failed to respond to treatment **(Figure 25)**.

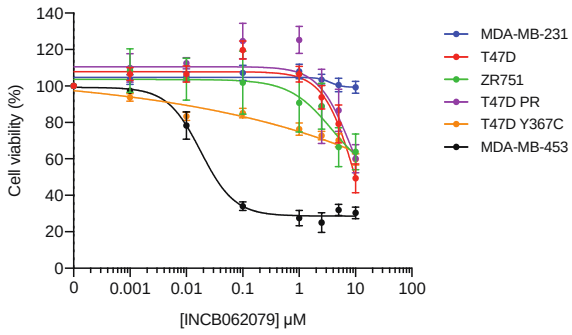

Figure 25. Cytotoxic effect of INCB062079 in FGFR4-expressing breast cancer cell lines. MDA-MB-231, T47D, ZR751, T47D PR, T47D Y367C, and MDA-MB-453 cells were treated with increasing doses of INCB062079 for 72h. Shown are representative graphs of cell viability readouts determined by Hoechst 33342 staining. Data were normalized to untreated controls, and three independent experiments were performed. Mean values ± SEM are shown.

To further assess this selective sensitivity, we expanded the analysis to include additional breast cancer cell lines with a range of FGFR4 expression levels **(Figure 26A).** In this second panel, INCB062079 treatment did not reduce cell viability across any of the tested cell lines, regardless of FGFR4 levels **(Figure 26B)**. These results indicate that the cytotoxic activity of INCB062079 is restricted to the MDA-MB-453 cell line, with no broader efficacy observed *in vitro* within the tested breast cancer models.

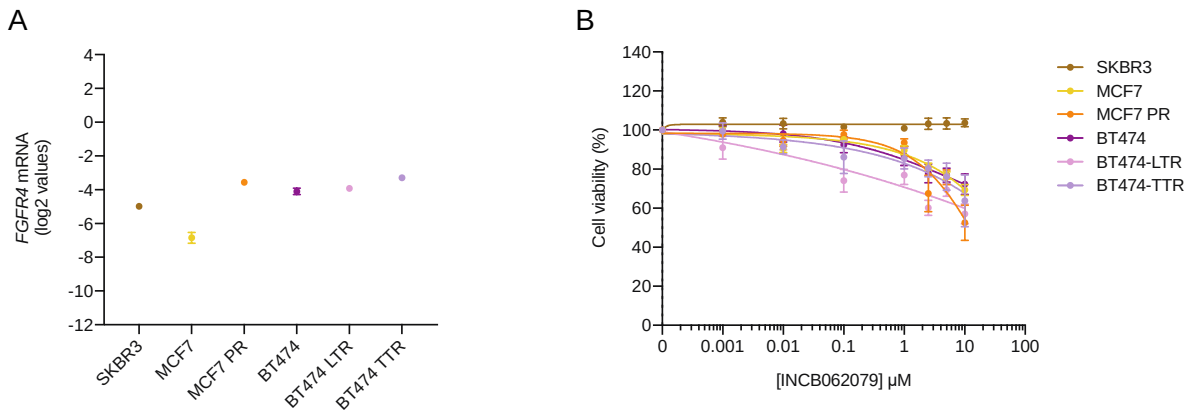

Figure 26. *FGFR4* expression and cytotoxic effect of INCB062079 in an extended panel of breast cancer cell lines. (A) *FGFR4* mRNA expression. At least three independent mRNA extractions per cell line were performed. Mean values ± SEM are shown. (B) SKBR3, MCF7, MCF7 PR, BT474, BT474 LTR, and BT474 TTR cells were treated with increasing doses of INCB062079 for 72h. Shown are representative graphs of cell viability readouts determined by Hoechst 33342 staining. Data were normalized to untreated controls, and three independent experiments were performed. Mean values ± SEM are shown.

Gene expression profiling was conducted 72 h after treatment with 100 nM INCB062079 in all cell lines. In MDA-MB-453 cells, treatment resulted in a marked reduction in genes associated to the Basal-like signature and the Proliferation Score, along with an increase in genes related to the Luminal A and Normal-like signatures **(Figure 27)**. In contrast, minimal or no transcriptional changes were observed in the remaining eleven cell lines, consistent with their lack of sensitivity to the inhibitor.

Taken together these findings highlight the limited activity of INCB062079 in breast cancer cell lines, with efficacy restricted to the MDA-MB-453 cell line. Consequently, we concluded that INCB062079 is not a viable broadly applicable therapeutic agent for breast cancer and we shifted our focus toward exploring alternative strategies to target FGFR4.

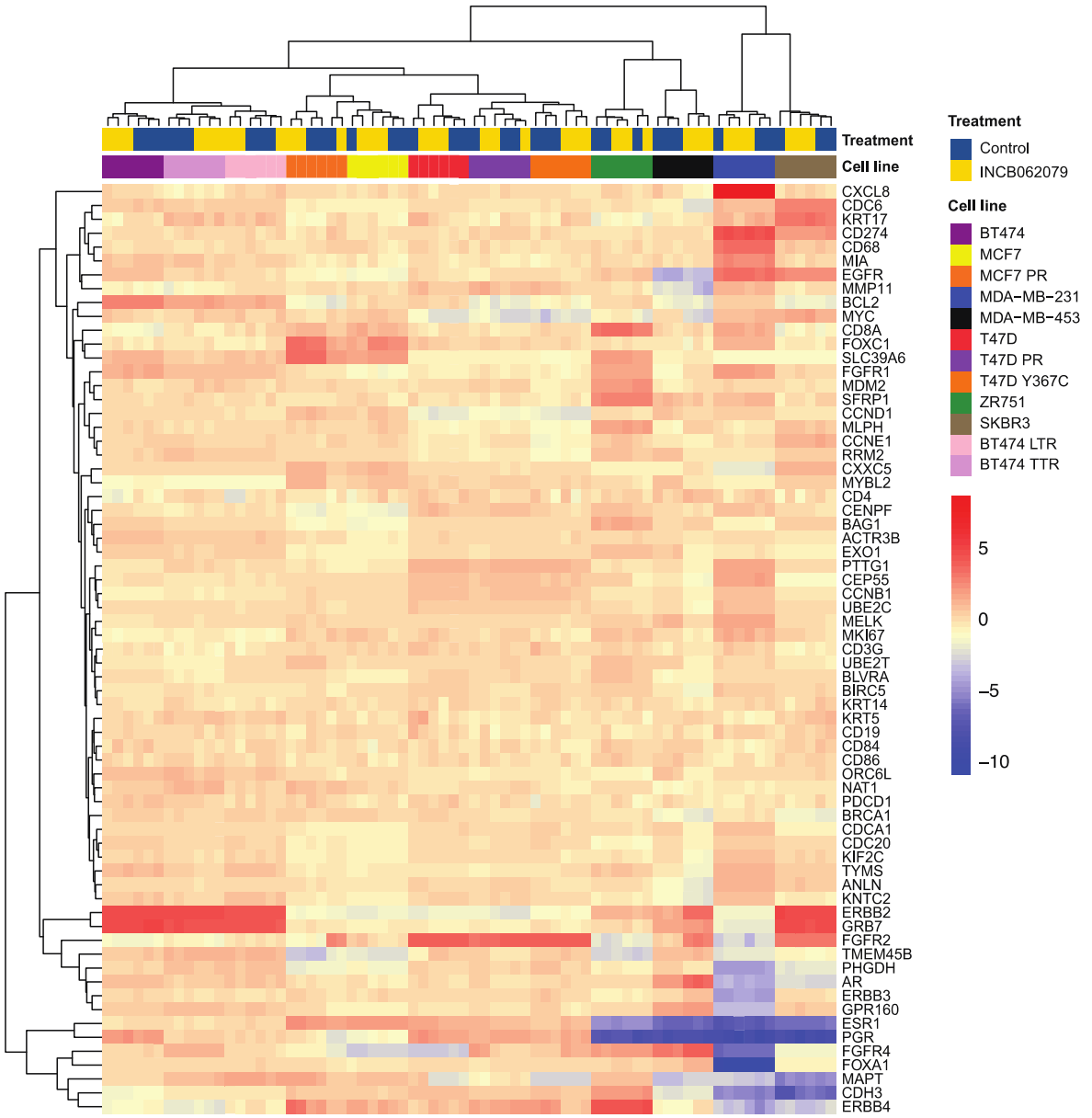

Figure 27. Transcriptomic changes after treatment with INCB062070 in breast cancer cell lines. Gene expression of 12 cell lines before and after treatment with 100 nM INCB062079 for 72 h. Three independent mRNA extractions per condition were performed.

3.3 Selection and validation of FGFR4-directed monoclonal antibodies in breast cancer cell lines

The emergence of ADCs has transformed breast cancer therapy, offering a targeted approach to deliver cytotoxic agents to tumor cells while minimizing off-target toxicity (148). In this thesis, we sought to explore the potential of targeting FGFR4 with ADCs. The identification of monoclonal antibodies with high specificity and affinity for FGFR4 is a critical step in the

development of such therapeutics. Here, we selected three previously reported humanized monoclonal antibodies (named here as Ab-1 (260), Ab-2 (261), Ab-3 (262)) for evaluation in our panel of breast cancer cell lines. All three antibodies target the extracellular domain of FGFR4, binding either to the acid box region or domain 2 **(Figure 28)**. Detailed descriptions of the chosen antibodies, including their origin and characteristics, are provided in the Methods section 3.2 (Antibodies and antibody-drug conjugates).

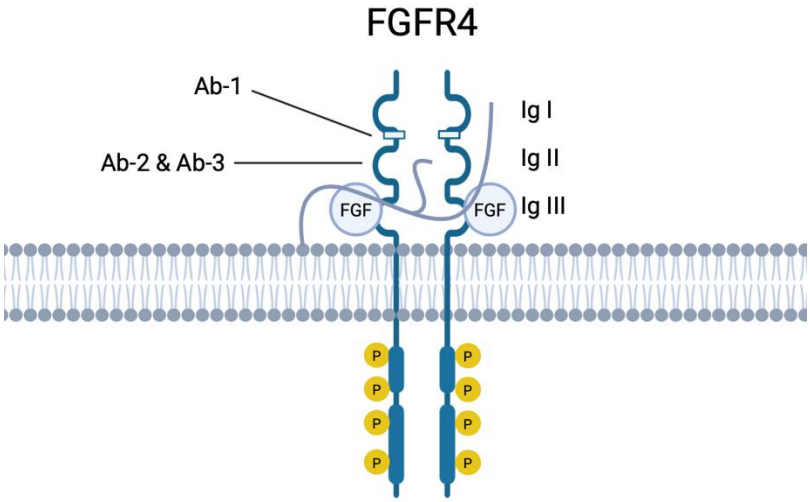

Figure 28. Binding sites of monoclonal antibodies Ab-1, Ab-2, and Ab-3 on the extracellular domain of FGFR4. Schematic representation created in BioRender.com

We first evaluated the antigen-binding capacity of the antibodies using flow cytometry. Breast cancer cell lines were incubated with the primary antibodies Ab-1, Ab-2, and Ab-3, followed by an APC-conjugated anti-human secondary antibody. No detectable binding was observed in FGFR4-negative and FGFR4-low cell lines, consistent with their low receptor expression. In contrast, all FGFR4-high cell lines exhibited robust, dose-dependent binding to each of the three antibodies **(Figure 29)**, confirming their specificity for cell surface FGFR4.

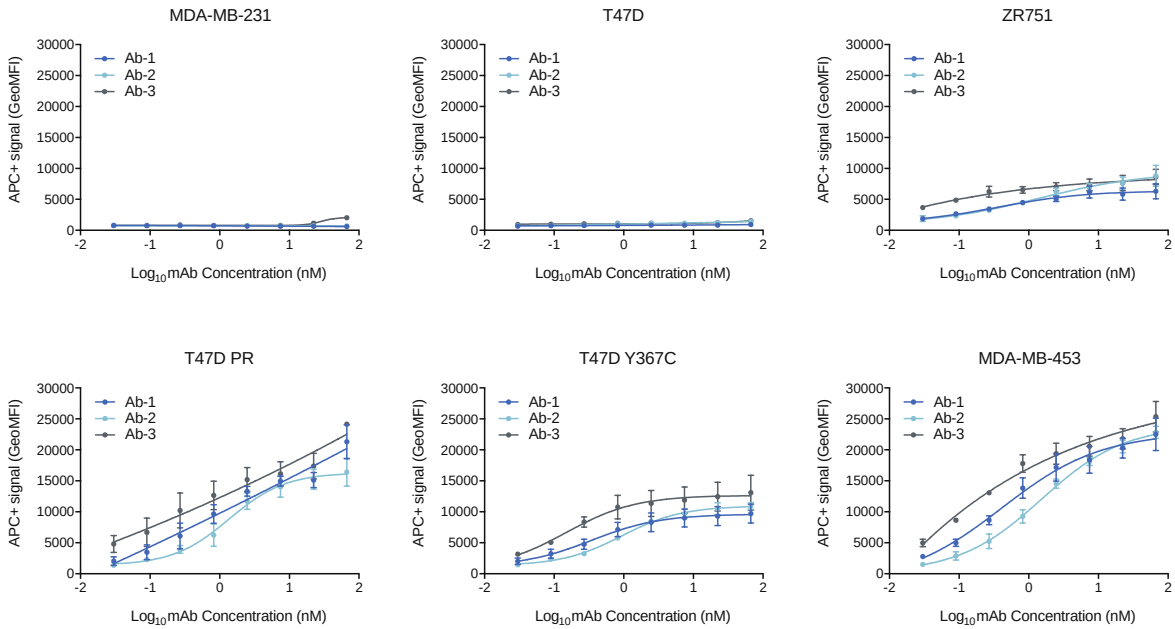

Figure 29. Assessment of the antigen-binding capacity of Ab-1, Ab-2, and Ab-3. Binding capacity of cell lines to increasing doses of the three antibodies against FGFR4. Assessed by cytometry using an APC-conjugated anti-human secondary antibody. Three independent experiments were performed. Mean values of the geometric MFI ± SEM are shown.

To assess antibody internalization, cells were incubated with the antibodies Ab-1, Ab-2, or Ab-3 at 37 ºC for 0, 2, or 4 h. Internalization was monitored by measuring the reduction in cell surface-associated APC fluorescence, reflecting the loss of membrane-bound antibody-antigen complexes over time. At the 0-hour timepoint, all three FGFR4-specific antibodies showed consistent and comparable binding profiles across FGFR4-high cell lines, confirming similar affinities for cell surface FGFR4. In contrast, little to no signal was observed in the FGFR4-low and FGFR4-negative cell lines. A non-specific primary antibody was included as a negative control, which showed no detectable binding with any of the cell lines, regardless of FGFR4 expression **(Figure 30)**.

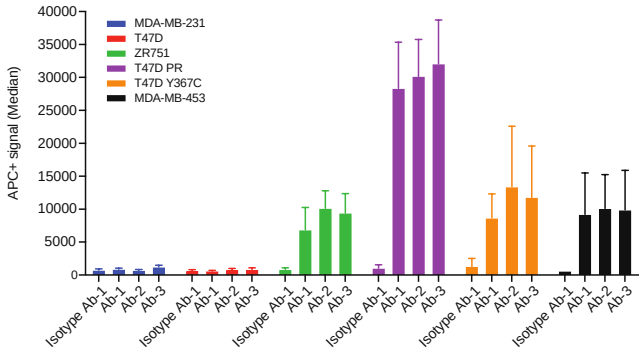

Figure 30. APC signal across cell lines at 0-h timepoint. Cells were treated with an isotype control, Ab-1, Ab-2, or Ab-3 antibodies and an APC-conjugated anti-human secondary antibody. Three independent experiments were performed. Mean values of the median fluorescence signal ± SEM are shown.

In FGFR4-high cell lines, a significant reduction of up to a 60% in surface APC signal was observed after 4 h, indicating efficient and FGFR4-specific internalization of the antibody-antigen complex **(Figure 31)**. In contrast, FGFR4-negative and FGFR4-low cell lines showed minimal APC signal **(Figure 30)** and no statistically significant internalization **(Figure 31)**, consistent with limited or absent antibody binding at the tested dose **(Figure 29)**.

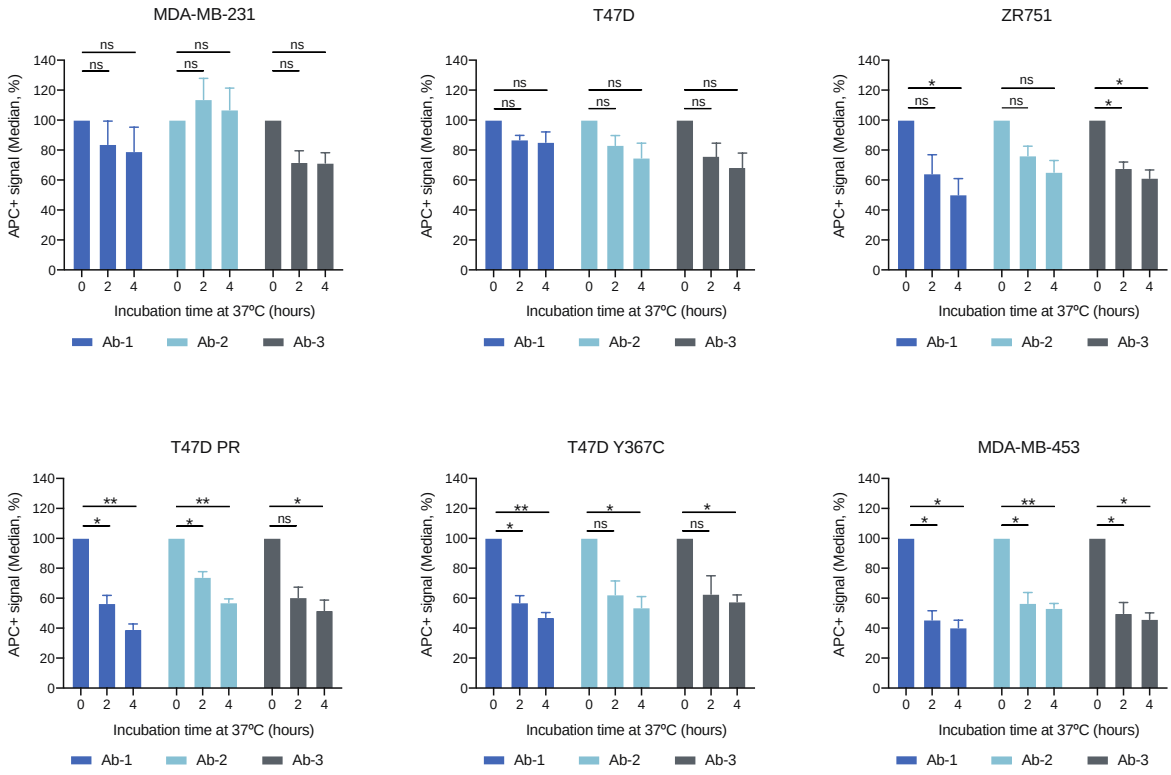

Figure 31. Assessment of the internalization capacity of Ab-1, Ab-2, and Ab-3. Internalization of the antibody-antigen complexes in cell lines. Assessed by cytometry using an APC-conjugated anti-human secondary antibody. Data was normalized to 0 h control and three independent experiments were performed. Mean values of the median fluorescence signal ± SEM are shown. Statistical analyses were performed using two-way ANOVA. ns > 0.05, * p < 0.05, ** p < 0.01.

Given that monoclonal antibodies can exert therapeutic effects without the need for conjugation, we first sought to determine whether these anti-FGFR4 antibodies possess intrinsic *in vitro* anti-tumor activity prior to their development as ADCs. To this end, we evaluated cell viability following treatment with increasing antibody concentrations, up to 3 µg/ml. No cytotoxic effect was observed at either 72 h **(Figure 32A)** or 144 h **(Figure 32B)**, regardless of FGFR4 expression levels. Given that these antibodies lack inherent cytotoxic activity, the absence of a response may be attributed to the lack of immune effector cells in the *in vitro* culture system.

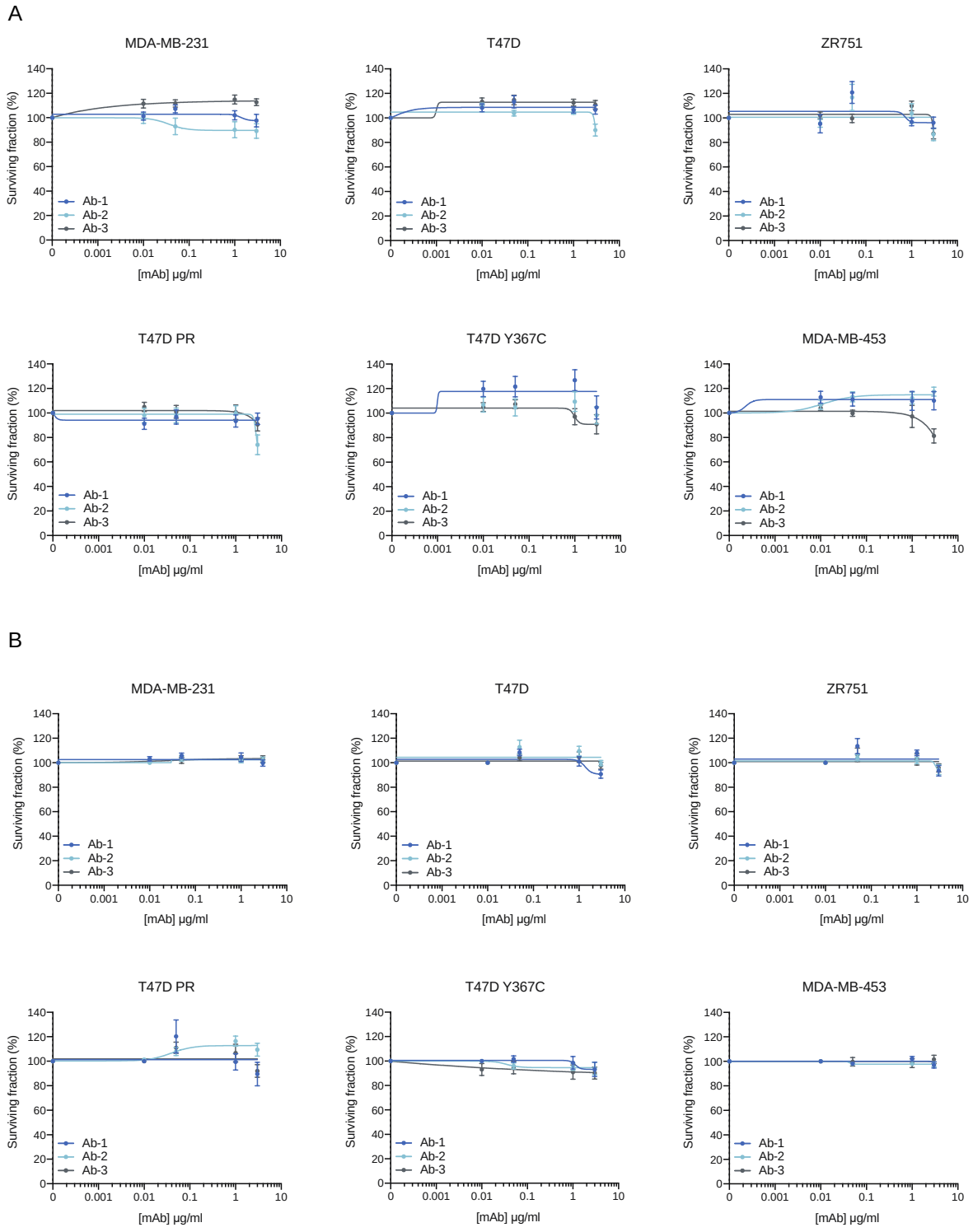

Figure 32. Assessment of the cytotoxic properties of Ab-1, Ab-2, and Ab-3. Cells were treated with increasing doses of Ab-1, Ab-2 or Ab-3 for (A) 72 h or (B) 144 h. Shown are representative graphs of cell viability readouts determined by Hoechst 33342. Data was normalized to untreated cells and three independent experiments were performed. Mean values ± SEM are shown.

3.4 Exploring payload conjugates for FGFR4-targeted therapy

Based on the observation that the three antibodies bind to and are internalized by FGFR4-high cell lines but do not exert a cytotoxic effect on their own, we next explored their potential as delivery vehicles for cytotoxic payloads. To this end, we evaluated antibody-payload conjugates using anti-human secondary antibodies linked to cytotoxic agents. From this point forward, FC tail-silenced versions of the primary antibodies were employed to prevent Fc receptor-mediated immune activation in future *in vivo* applications and potential clinical translation.

Cytotoxicity was observed in T47D PR cells treated with each of the three primary antibodies (Ab-1, Ab-2, Ab-3) in combination with a secondary Fab-cleavable linker-MMAE antibody, with corresponding IC50 values of 0.874, 0.686, and 0.278 µg/ml, respectively. No cytotoxic effect was detected in cells treated with a non-specific isotype control antibody (Isotype Ab-1) in combination with secondary Fab-cleavable linker-MMAE antibody, confirming the specificity of the antibody-antigen interaction, successful conjugation, and absence of premature payload release **(Figure 33)**.

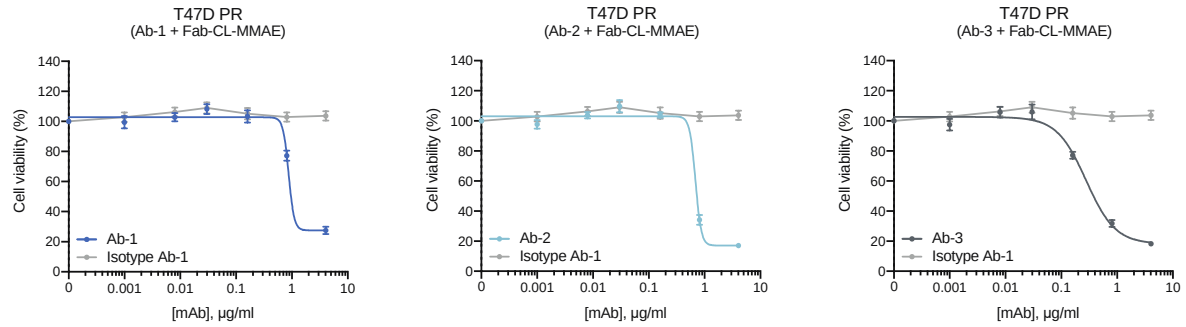

Figure 33. Cytotoxicity of Ab-1, Ab-2, and Ab-3 antibodies in combination with MMAE-conjugated secondary antibody. Cells were treated for 144 h with increasing doses of primary and secondary antibodies (1:6). Cell viability was assessed using Cell Titer Aqueous and normalized to untreated controls. T47D PR cells treated with FGFR4-specific antibodies Ab-1, Ab-2, Ab-3 in combination with secondary Fab-cleavable linker-MMAE. Three independent experiments were performed. Mean values ± SEM are shown.

We next investigated the cytotoxic potential of different payloads by treating MDA-MB-453 and T47D PR cells with Ab-2 in combination with secondary antibodies conjugated to Fab-cleavable linker-MMAE, Fab-cleavable linker-Duocarmycin, or Fab-non-cleavable linker-MMAF. In MDA-MB-453 cells, the IC50 values for these combinations were 0.227, 0.148, and

0.137 µg/ml, respectively, while in T47D PR cells, they were 0.686, 0.029, and 0.667 µg/ml, respectively. The non-specific primary Isotype Ab-1 was again used as a negative control. While no cytotoxic effect was observed when pairing Isotype Ab-1 with MMAE and MMAF-based secondary antibodies, the combination with the Fab-cleavable linker-Duocarmycin secondary antibody resulted in cytotoxicity at higher concentrations, particularly in T47D PR cells (IC50: 0.866 µg/ml), suggesting some degree of off-target toxicity or premature release associated with the Ab-2-Duocarmycin combination **(Figure 34)**.

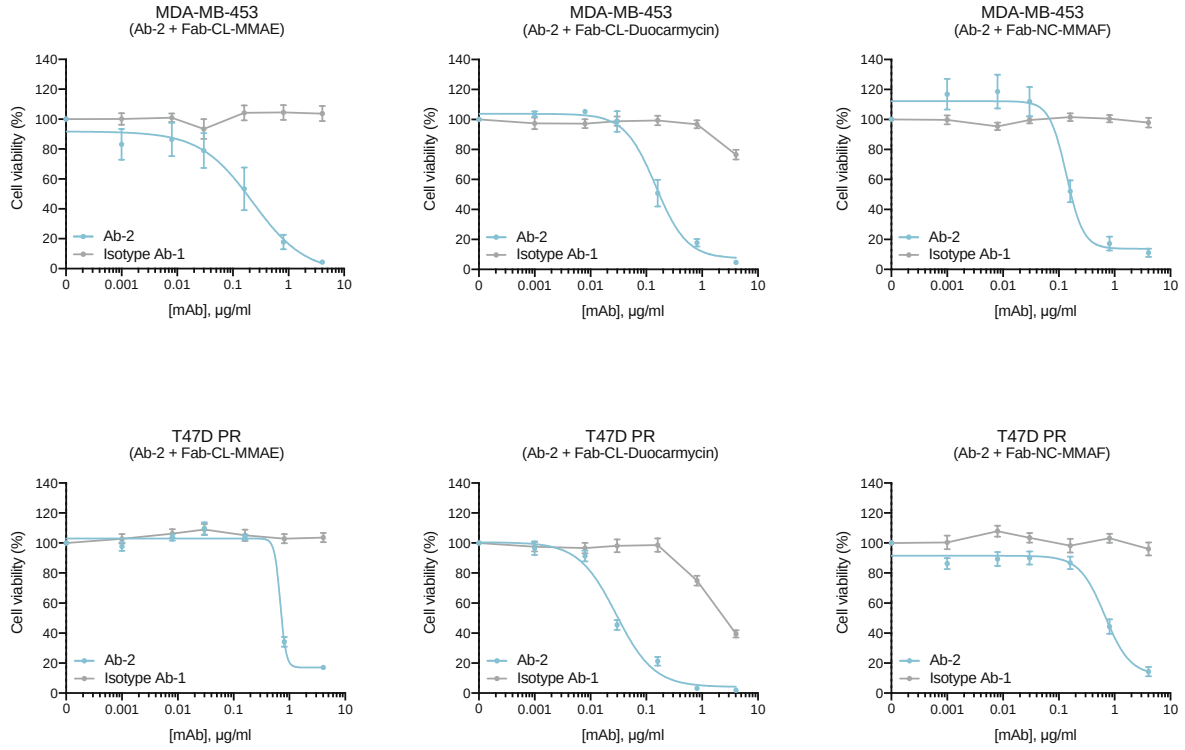

Figure 34. Cytotoxicity of different Ab-2-payload combinations in T47D PR and MDA-MB-453 cells. Cells were treated for 144 h with increasing doses of primary and secondary antibodies (1:6). Cell viability was assessed using Cell Titer Aqueous and normalized to untreated controls. MDA-MB-453 and T47D PR cells treated with Ab-2 primary antibody in combination with CL-MMAE, CL-Duocarmycin, or NC-MMAF conjugates. Three independent experiments were performed. Mean values ± SEM are shown.

These findings highlighted the potential of all three FGFR4-targeting antibodies in the development of an ADC. Each demonstrated specific binding to FGFR4-expressing breast cancer cells and induced cytotoxicity when paired with a cytotoxic payload, supporting their suitability for FGFR4-targeted ADC applications **(Figures 33 and 34)**. Ab-2 showed consistent and potent cytotoxic activity across both cell lines and with multiple payload types, underscoring its versatility. Notably, the MMAE payload emerged as the most promising

candidate, as it is delivered via a cleavable linker and showed no cytotoxic effect when co-administered with the isotype control antibody, reinforcing its specificity and therapeutic potential **(Figure 34)**. Moreover, most approved ADCs for HR+/HER2- breast cancer rely on TOP1 inhibitors as payloads (168), which can be limited by resistance mechanisms, highlighting the need for novel ADCs with alternative targets and diverse cytotoxic payloads.

3.5 Targeting FGFR4 with an ADC in breast cancer cell line models

Building on the promising cytotoxic results observed with the secondary antibody-payload conjugates, we next sought to develop fully assembled anti-FGFR4 ADCs. Based on its consistent target binding and potent activity across multiple payload types, Ab-2 was selected for ADC production and optimization. MMAE, a potent microtubule inhibitor, was chosen as the cytotoxic payload. MMAE is typically conjugated to antibodies via a cleavable valine-citrulline-p-aminobenzyloxycarbonyl (VC-PAB) linker, which ensures targeted intracellular drug release while minimizing off-target effects (270). Notably, MMAE's membrane permeability allows it to exert a bystander effect, killing adjacent tumor cells independent of target expression (271–273).

To assess the impact of conjugation chemistry and DAR, we generated three ADC constructs using either cysteine or lysine conjugation sites and DARs of 4 or 8 **(Figure 35)**.

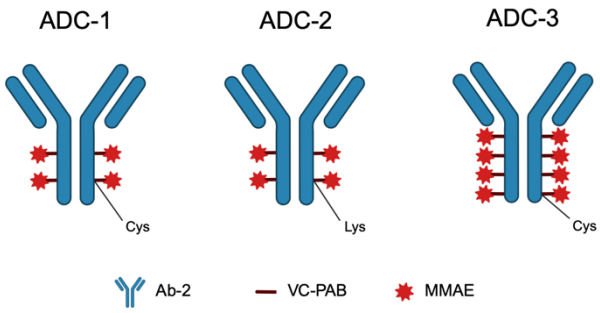

Figure 35. Schematic representation of the three anti-FGFR4 ADC candidates: ADC-1, ADC-3, and ADC-2. Each ADC consists of the Fc-silent anti-FGFR4 antibody conjugated to the cytotoxic payload (MMAE) via a cleavable VC-PAB linker at a DAR of 4 or 8. ADC conjugation strategies include cysteine and lysine conjugation sites. ADC-1: cysteine conjugation site and DAR 4. ADC-2: lysine conjugation site and DAR 4. ADC-3: cysteine conjugation site and DAR 8. Illustration created in BioRender.com

The design and production of these ADCs were carried out in collaboration with ONA Therapeutics. Additional details on the generation and characterization of the ADCs are provided in the Methods section 3.2 (Antibodies and antibody-drug conjugates).

The cytotoxic effects of the 3 anti-FGFR4 ADCs were evaluated *in vitro* in our panel of breast cancer cell lines with varying levels of FGFR4 expression. All 3 ADCs induced significant cell death in FGFR4-high but had no impact on FGFR4-negative or FGFR4-low cells following both 72 h **(Figure 36A)** and 144 h treatments **(Figure 36B)**.

The cytotoxic response in FGFR4-high cell lines was more pronounced after 144 h, reaching 70%-100% cell mortality **(Figure 36B)**, highlighting the time-dependent efficacy of the ADCs. While all constructs were effective, ADC-3 showed lower potency than ADC-1 and ADC-2 at the longer time point **(Figure 36B)**.

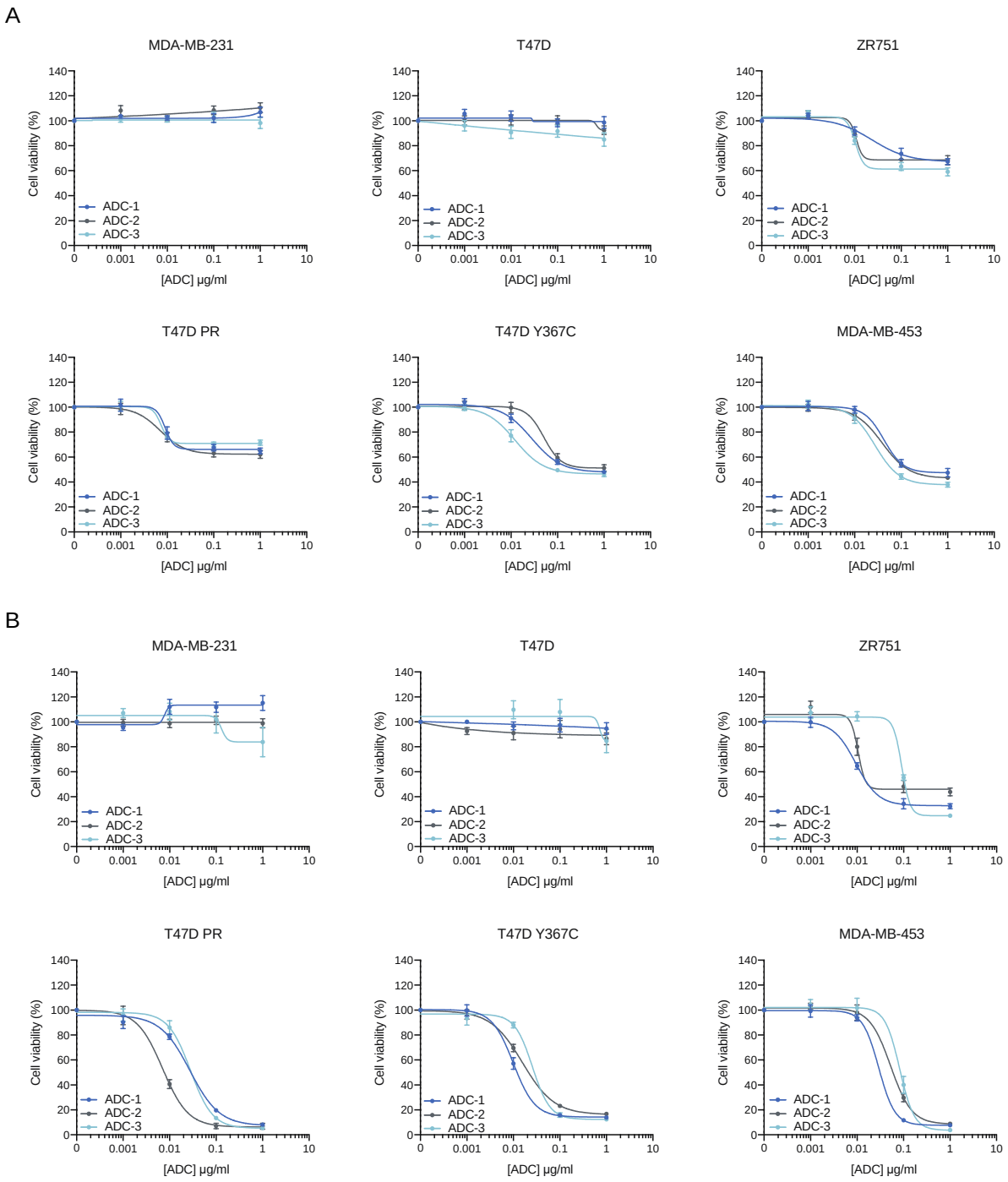

Figure 36. Assessment of the cytotoxic properties of ADC-1, ADC-2 and ADC-3. Cells were treated with increasing doses of ADC-1, ADC-2 or ADC-3 for (A) 72 h or (B) 144 h. Shown are representative graphs of cell viability readouts determined by Cell Titer AQueous. Data was normalized to untreated cells and three independent experiments were performed. Mean values ± SEM are shown.

Importantly, no cytotoxicity was observed when cells were treated with a non-specific Isotype ADC at either time point **(Figures 37A and 37B)**, confirming that the observed effects were FGFR4-dependent. These results also support the stability of the ADCs in the extracellular

environment and indicate that MMAE is triggered specifically upon internalization into FGFR4-expressing cells, thereby limiting off-target toxicity. Treatment with MMAE resulted in cytotoxicity across all cell types at both time points **(Figures 37A and 37B)**, further validating the antigen-specific mechanism of action of the ADCs. As with the ADCs, MMAE-induced cytotoxicity was more pronounced after prolonged exposure, with mortality rates of almost 100% in MDA-MB-231 and MDA-MB-453 cells **(Figures 37B)**.

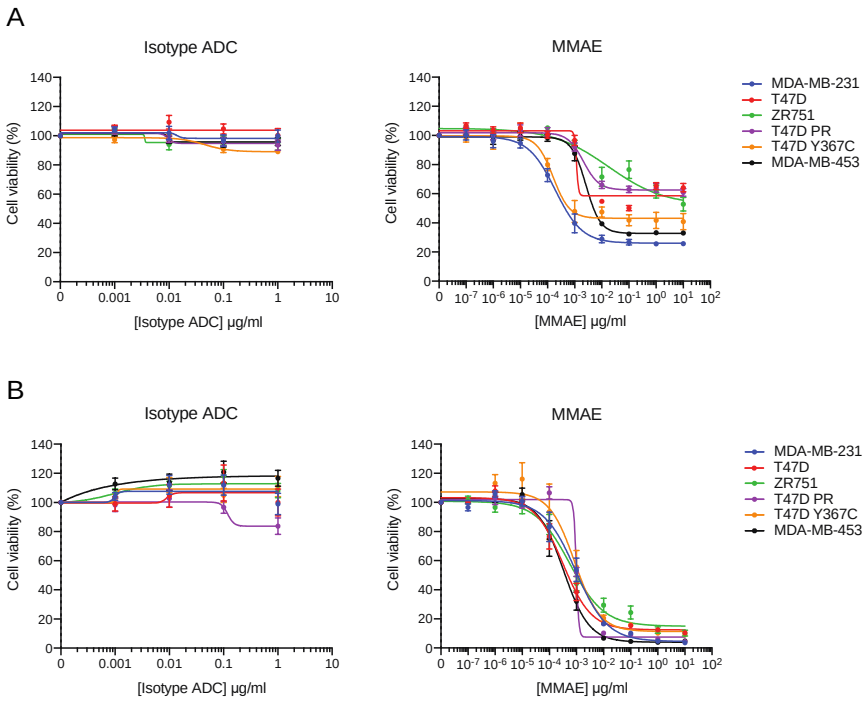

Figure 37. Assessment of the cytotoxic properties of non-specific control ADCs and MMAE. Cells were treated with increasing doses of Isotype ADC or MMAE for (A) 72 h or (B) 144 h. Shown are representative graphs of cell viability readouts determined by Cell Titer AQueous. Data was normalized to untreated cells and three independent experiments were performed. Mean values ± SEM are shown.

To further confirm the long-term specificity and potency of the ADC-2 construct, a clonogenic assay was performed. FGFR4-high cells treated with ADC-2 over an extended period (~17 days) displayed a marked reduction in colony formation **(Figure 38A and 38B)**. To assess target specificity, the cell viability at the highest dose (1 µg/ml) was compared between FGFR4-negative/low and FGFR4-high cell lines **(Figure 38C)**. FGFR4-high cells exhibited a significantly lower survival fraction relative to FGFR4-negative/low cells ($p = 0.004$), highlighting the selective toxicity of ADC-2 toward FGFR4-expressing populations.

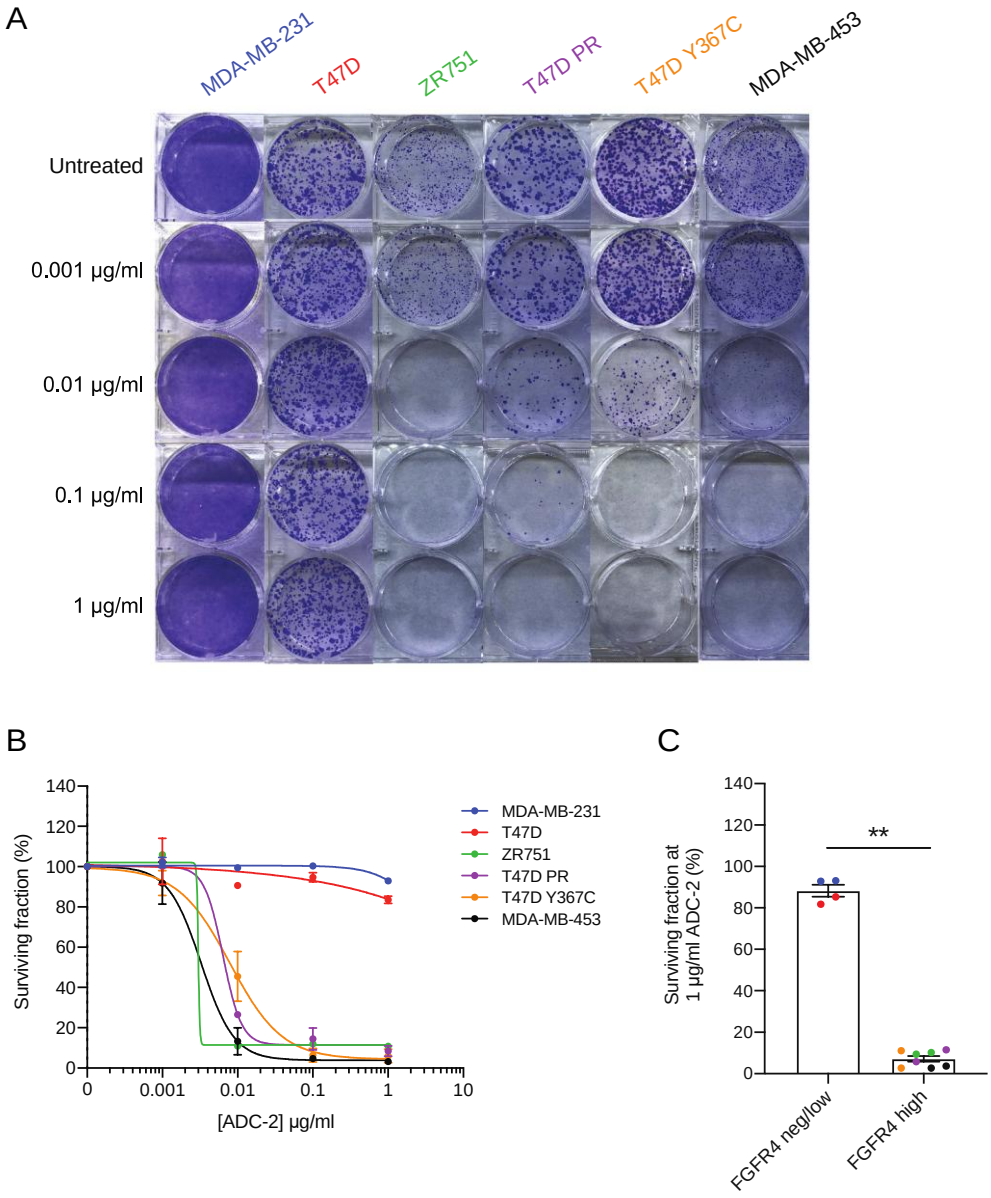

Figure 38. Assessment of the clonogenic ability of breast cancer cell lines after prolonged ADC-2 treatment. Cells were treated with increasing doses of ADC-2 every 3 days until untreated cells reached confluency. (A) Crystal violet staining of cells after ADC-2 treatment. (B) Representative graph of cell viability readouts after crystal violet staining of cells. Data was normalized to untreated cells. Three experimental and two biological replicates were performed for each condition. Mean values ± SEM are shown. (C) Bar plot showing cell viability of FGFR4-negative/low vs FGFR4-high cells after treatment with 1 µg/ml ADC-2. FGFR4-high cells exhibited significantly reduced survival (p = 0.004). Three experimental and two biological replicates were performed for each condition. Mean values ± SEM are shown.

Based on its favorable cytotoxic profile, target specificity, and PK properties (detailed in the Methods section 3.2 (Antibodies and antibody-drug conjugates)), ADC-2 was selected as the lead ADC candidate for further development.

3.6 Bystander killing effect of ADC-2

The bystander effect of an ADC refers to the phenomenon by which cytotoxic agents, released from targeted cancer cells, diffuse through cellular membranes into the surrounding microenvironment inducing cell death in neighboring cells regardless of their antigen expression **(Figure 39)** (273).

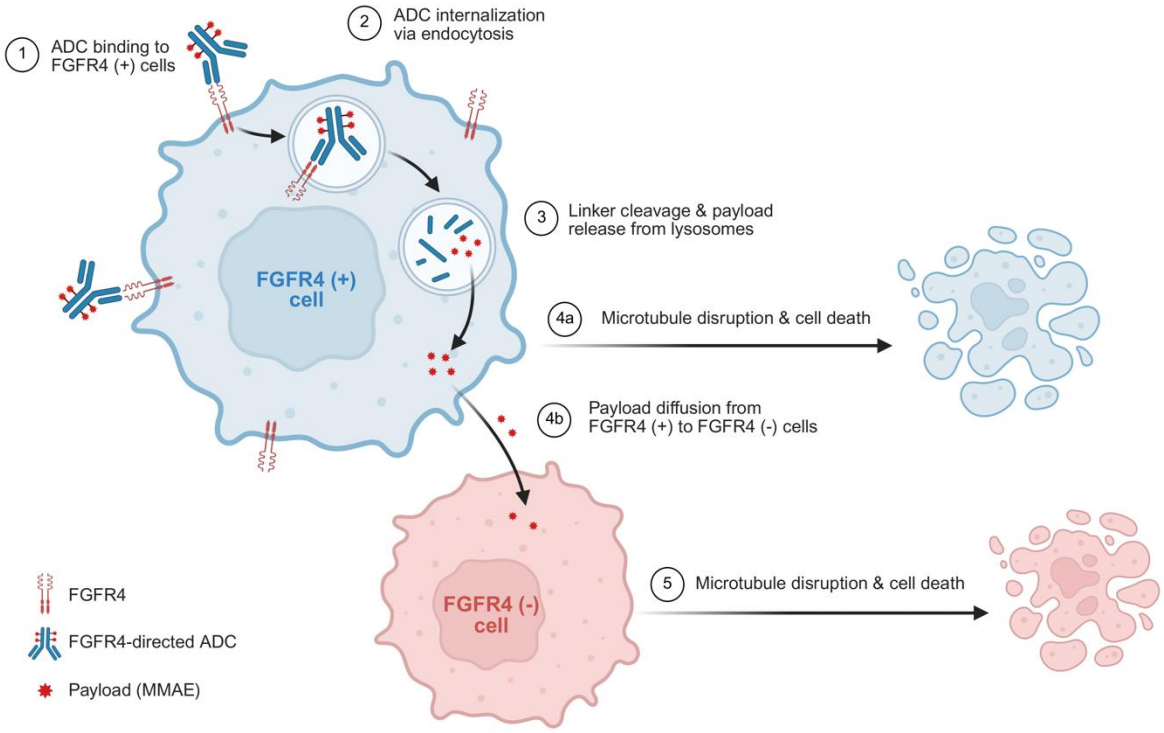

Figure 39. Schematic representation of the bystander killing effect mediated by an FGFR4-directed MMAE-based ADC from FGFR4 (+) to FGFR4 (-) cells. (1) The FGFR4-directed MMAE-based ADC binds specifically to FGFR4 (+) cells and (2) is internalized via endocytosis. (3) Upon trafficking to the lysosomal compartment, the linker is cleaved, releasing the cytotoxic payload. (4a) The payload induces microtubule disruption, leading to cell death in FGFR4 (+) cells. (4b) In parallel, the released payload can diffuse into neighboring FGFR4 (-) cells, exerting cytotoxic effects. This phenomenon is referred to as the bystander effect. Illustration created in BioRender.com

This effect is particularly relevant in tumors exhibiting intratumoral heterogeneity, as not all cells may express the target antigen and could therefore evade direct targeting (273). To investigate this possibility, we assessed FGFR4 expression by IHC in breast tumor samples from the CDK clinical cohort. Among all tumors analyzed, notable variation in staining across different regions, indicative of intratumoral heterogeneity, was observed in 1.8% of cases (4 out of 228; **Figure 40)**. Although such heterogeneity was relatively rare, its presence may have important implications for targeted therapies, particularly those involving ADCs with cleavable linkers and membrane-permeable payloads.

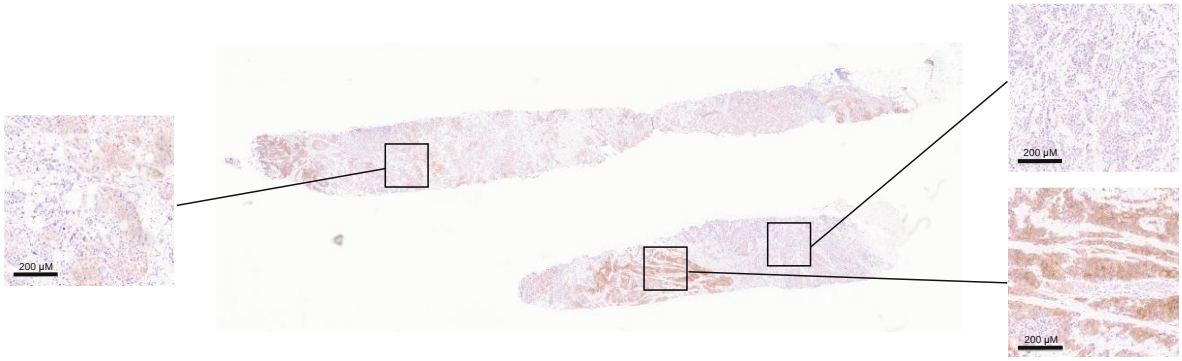

Figure 40. Representative image of a tumor sample with intratumoral heterogeneity of FGFR4 expression. FGFR4 IHC analysis in a tumor from the CDK clinical cohort. Overall FGFR4 H-Score: 150.

To assess the bystander killing effect of ADC-2, we treated FGFR4-negative MDA-MB-231 cells expressing RFP (MDA-MB-231-RFP+) co-cultured with FGFR4-high MDA-MB-453 cells. First, the cytotoxic effect of ADC-2, Isotype-ADC-2, and MMAE was evaluated in monocultures following 96- or 120-h treatments **(Figure 41)**. A concentration of 0.3 µg/ml of ADC-2 and Isotype-ADC-2 was chosen for the co-culture assay, as it resulted in approximately 80% cell death in MDA-MB-453 cells while having no impact on MDA-MB-231-RFP+ cells.

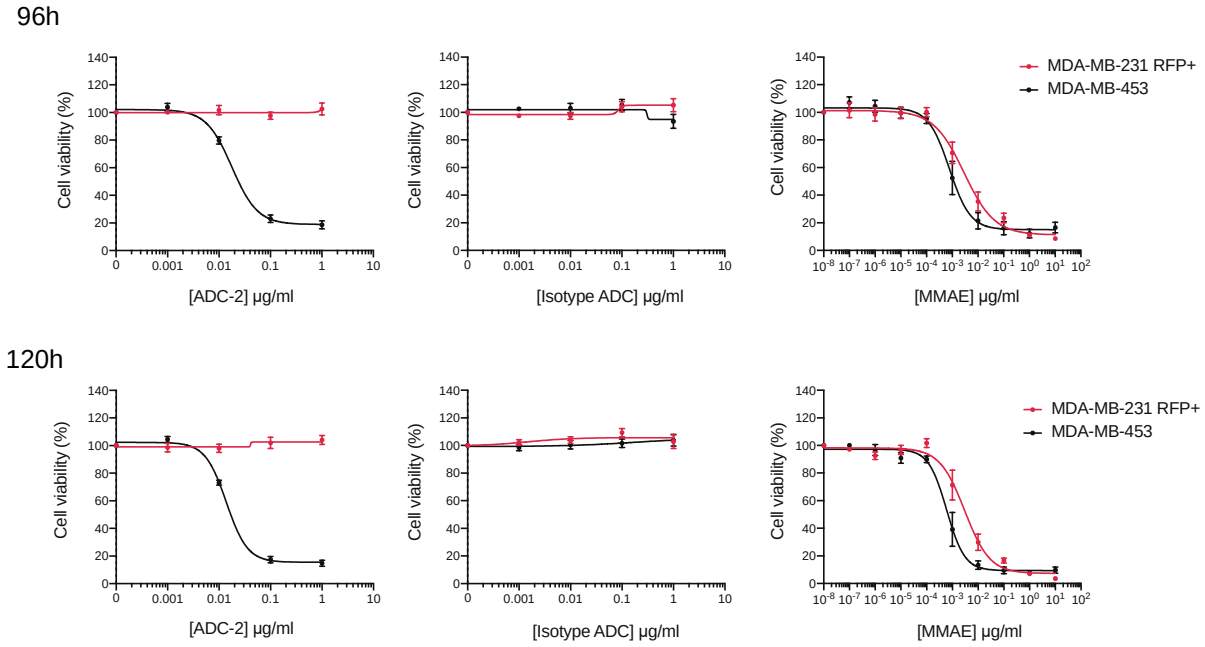

Figure 41. Cytotoxicity of ADC-2, isotype control ADC, and MMAE in MDA-MB-231-RFP+ and MDA-MB-453 monocultures. Cells were treated with increasing doses of ADC-2, isotype control ADC, or MMAE for 144h. Shown are representative graphs of cell viability readouts determined by Cell Titer AQueous. Data was normalized to untreated cells and three independent experiments were performed. Mean values ± SEM are shown.

MDA-MB-231-RFP+ and MDA-MB-453 cells were co-cultured at ratios of 1:20 or 1:5 and treated with ADC-2, Isotype-ADC-2, or MMAE for 96 or 120h, respectively. As expected, ADC-2 significantly reduced the survival of MDA-MB-453 cells in both monoculture and co-culture conditions and in both experimental settings. Notably, ADC-2 had no effect on MDA-MB-231-RFP+ cells when cultured alone but significantly decreased their survival when co-cultured with MDA-MB-453 cells at both ratios, indicating a bystander effect. This effect was more pronounced in the 1:20 ratio co-cultures, where four times more FGFR4-high cells per FGFR4-negative cell were seeded compared to the 1:5 ratio. Nonetheless, the bystander effect exerted in the co-cultured cells was statistically significant in both experimental settings ($p < 0.0001$). In contrast, the Isotype-ADC-2 control showed no cytotoxic activity in either monoculture or co-culture, while MMAE induced cell death in both conditions ($p < 0.0001$), independent of FGFR4 expression and experimental setting **(Figure 42)**.

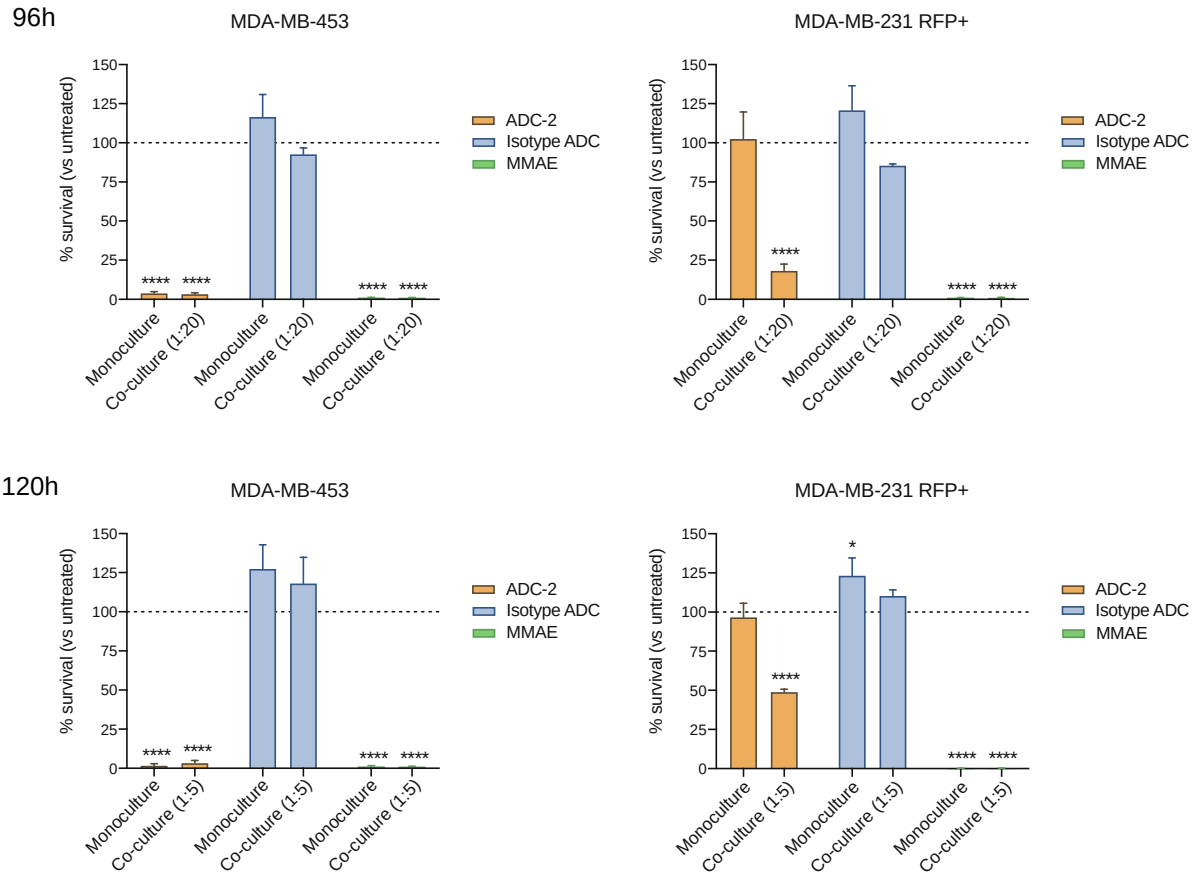

Figure 42. Bystander killing effect of ADC-2 in a co-culture model of breast cancer cell lines. MDA-MB-231-RFP+ and MDA-MB-453 cells were co-cultured (1:20 or 1:5 ratios) and treated with ADC-2, Isotype-ADC-2, or MMAE for 96 or 120 h. The number of RFP+ events was established by cytometry. Data were normalized to the corresponding untreated cells, which were set to 100% and are represented by a dashed line in the graphs to facilitate visual comparison. Three independent experiments were performed and mean values ± SEM are shown. Statistical analyses were performed using two-way ANOVA, comparing each treatment condition to the corresponding untreated control. * $p < 0.05$ and **** $p < 0.0001$.

3.7 Effects of Ab-2, ADC-2 and MMAE on gene expression in breast cancer cells

Changes in gene expression were analyzed following treatment with the naked Ab-2, the FGFR4-directed ADC-2, and the payload MMAE. As shown in **Figure 43**, treatment with Ab-2 did not result in any detectable changes in gene expression, consistent with its lack of cytotoxic activity in our panel of cell lines **(Figure 32)**. In contrast, treatment with ADC-2 or MMAE induced distinct transcriptional responses depending on FGFR4 status. Across all cell lines, MMAE consistently led to a significant reduction in proliferation-related genes and/or the Proliferation Score. ADC-2 elicited similar effects, but only in FGFR4-high cell lines, highlighting both the specificity of the ADC and the contribution of the MMAE payload to its activity **(Figure 43)**.

In FGFR4-high T47D PR and T47D Y367C cells, both ADC-2 and MMAE significantly downregulated Luminal B and Basal-like PAM50 signatures, as well as the Proliferation Score, while upregulating HER2-enriched, Luminal A, and Normal-like signatures (FDR < 5%). An increase in FGFR4 expression was observed following treatment with either ADC-2 or MMAE at both the mRNA and protein levels **(Figures 43 and 44)**. However, this upregulation was transient, as shown in **Figure 46**, and likely reflects an acute cellular response to cytotoxic stress and/or early compensatory signaling mechanisms.

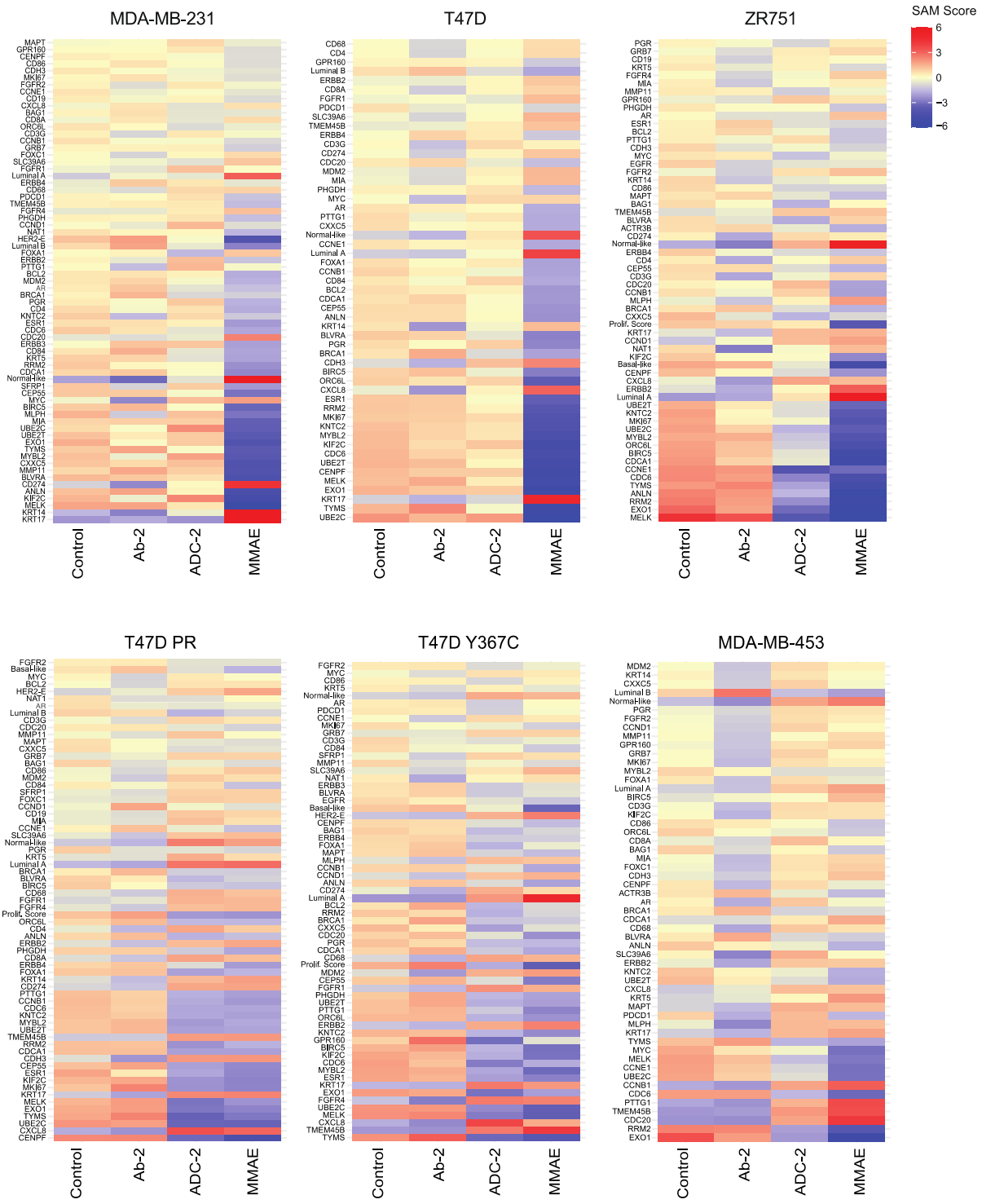

Figure 43. Changes in gene expression after treatment with ADC-2 and MMAE in breast cancer cell lines. Heatmap of a multiclass SAM representing the PAM50 molecular subtypes, Proliferation Score and genes that are differentially expressed (FDR < 5%) in cells treated with 10 μg/ml Ab-2, 0.1 μg/ml ADC-2, or 0.01 μg/ml MMAE for 72 h. Three independent mRNA extractions per condition were performed.

Besides increased FGFR4 expression in T47D PR and T47D Y367C cells, western blotting also showed that both ADC-2 and MMAE induce cell cycle arrest in these FGFR4-high cells, evidenced by a pronounced reduction in p-Rb. In contrast, this effect was only observed in FGFR4-negative and FGFR4-low cells following MMAE treatment **(Figure 44)**, further supporting the specificity of ADC-2 and its role in regulating the cell cycle.

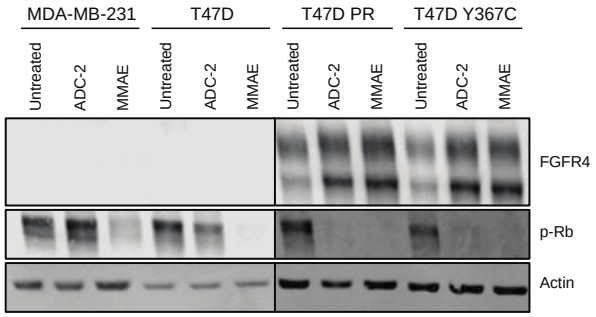

Figure 44. Changes in protein expression after treatment with ADC-2 and MMAE in breast cancer cell lines. FGFR4 and p-Rb expression after treatment with 0.1 μg/ml ADC-2 or 0.01 μg/ml MMAE for 72h. Actin was used as a loading control.

3.8 Generation and characterization of an ADC-2-resistant cell line

Next, we developed a new T47D PR ADC-2-resistant (ADC-2-R) cell line by culturing T47D PR cells with increasing doses of ADC-2 in combination with 500 nM palbociclib over eight months **(Figure 45A)**. Compared to T47D PR cells, T47D PR ADC-2-R cells exhibited reduced FGFR4 expression at both the mRNA **(Figure 45B)** and protein **(Figure 45C)** levels. IHC analysis of cell pellets confirmed decreased FGFR4 in both the membrane and cytoplasm, with H-Scores of 155 (membrane), 120 (cytoplasm), and 145 (total) in the resistant line **(Figure 45D)**. While the reduction in FGFR4 was substantial and consistent across measurement methods, FGFR4 levels in T47D PR ADC-2-R did not fully revert to the low levels characteristic of the parental T47D line **(Figures 45B-D)**, indicating only a partial shift toward the FGFR4-low phenotype.

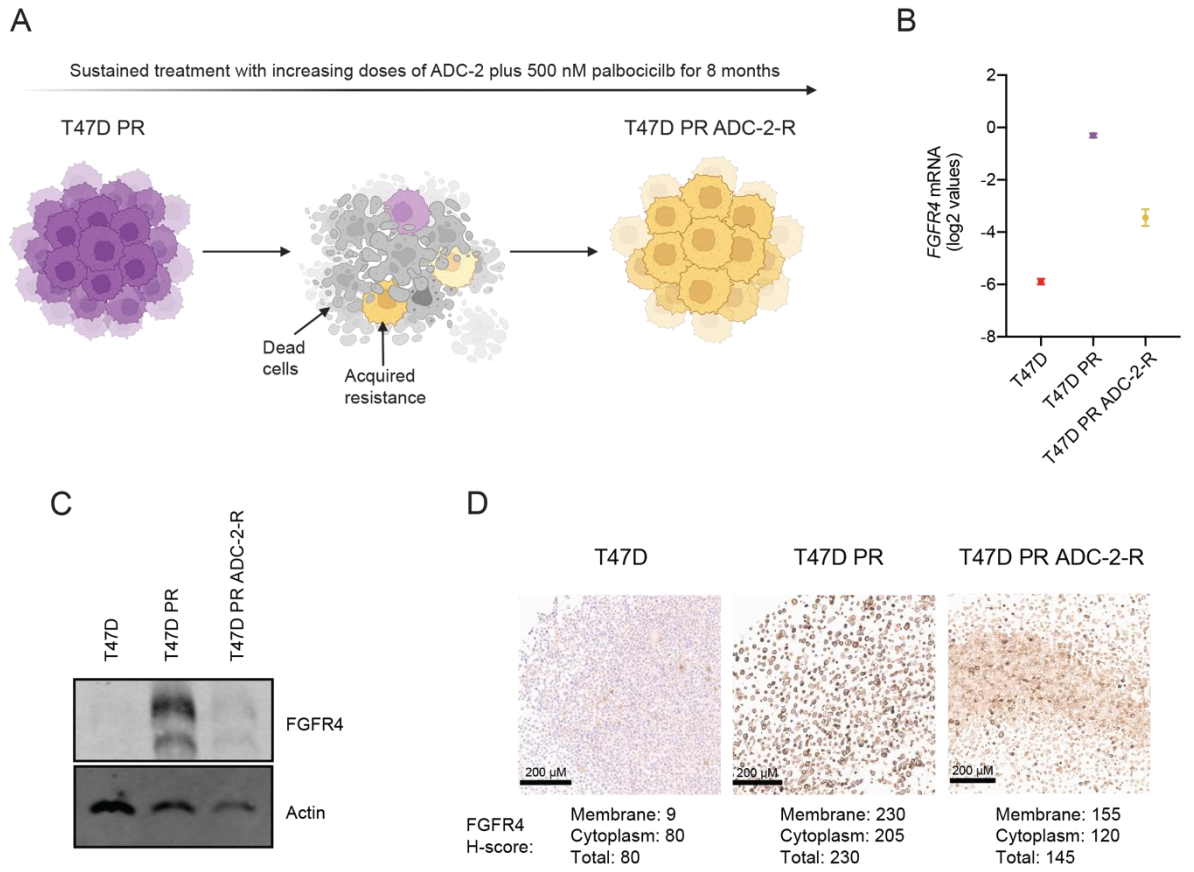

Figure 45. Generation and characterization of the T47D PR ADC-2-R cell line. (A) Schematic illustrating the process of generating T47D PR ADC-2-R cells. Created in BioRender.com (B) *FGFR4* mRNA expression across cell lines. At least three independent mRNA extractions per cell line were performed. Mean values ± SEM are shown. (C) FGFR4 protein expression. Actin was used as a loading control. (D) FGFR4 IHC staining from cellular pellets. Shown are the H-Scores for membrane, cytoplasm, and total FGFR4 stainings.

To further explore the durability of the transcriptional responses observed after ADC-2 treatment **(Figure 43)** and their potential role in acquired resistance, we examined gene expression changes in ADC-2-resistant cells.

T47D, T47D PR, and T47D PR ADC-2-R cells were treated with ADC-2 or MMAE for 72 h, and changes in PAM50 intrinsic subtypes and *FGFR4* expression were evaluated. Notably, untreated T47D PR ADC-2-R cells exhibited a shift toward a more Basal-like and Luminal B phenotype, characterized by increased proliferation and reduced expression of the Luminal A and Normal-like signatures **(Figure 46)**. Treatment with ADC-2 or MMAE led to small changes in the PAM50 subtypes, with a more pronounced shift observed following MMAE treatment.

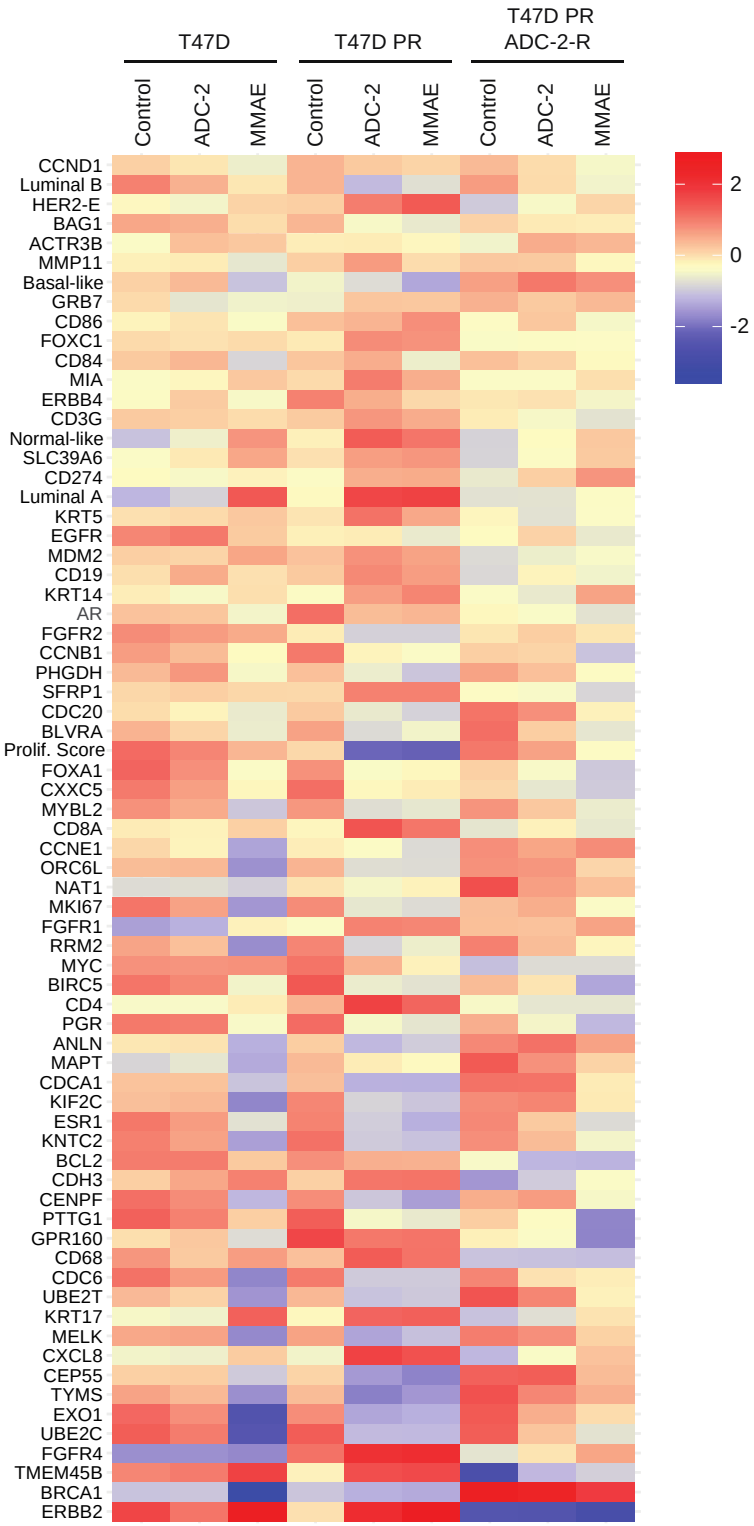

Figure 46. PAM50 subtypes and FGFR4 expression changes in T47D, T47D PR, and T47D PR ADC-2-R cells following drug treatment. Heatmap of a multiclass SAM representing the PAM50 molecular subtypes, Proliferation Score and genes that are differentially expressed (FDR < 5%) in cells treated with 0.1 μg/ml ADC-2 or 0.01 μg/ml MMAE for 72 h. Three independent mRNA extractions per condition were performed.

Compared to T47D PR cells, T47D PR ADC-2-R cells showed a decrease in the HER2-enriched subtype and reduced *FGFR4* expression. Upon treatment with ADC-2 or MMAE, both the HER2-enriched signature and *FGFR4* expression increased, particularly in response to MMAE **(Figure 46)**. These changes resembled the early transcriptional responses observed in FGFR4-high T47D PR and T47D Y367C cells after 72 h of treatment **(Figures 43 and 46)**. While the transcriptional changes observed after 72 h of ADC-2 or MMAE treatment in FGFR4-high cells appear to be transient and likely reflect short-term adaptative responses, the alterations seen in T47D PR ADC-2-R cells persisted for over 6 months, indicating a more stable and potentially acquired phenotype.

The cytotoxic effect of ADC-2 and MMAE was assessed in T47D PR ADC-2-R cells. After 144 h of treatment with ADC-2, T47D PR ADC-2-R cells showed a 4.2-fold increase in their IC50 compared to T47D PR cells (0.092 vs 0.022 µg/ml). Such differences were not observed when treating cells with MMAE, as all cell lines, including FGFR4-low T47D, showed a similar cytotoxic response **(Figure 47A)**. These results were further confirmed by treating the cells with Ab-2-DXd-ADC, another FGFR4-directed ADC consisting of the Ab-2 linked to DXd with a DAR of 8, as well as with DXd alone **(Figure 47B)**. T47D PR ADC-2-R treated with Ab-2-DXd-ADC showed no effect, even when treated with the highest doses.

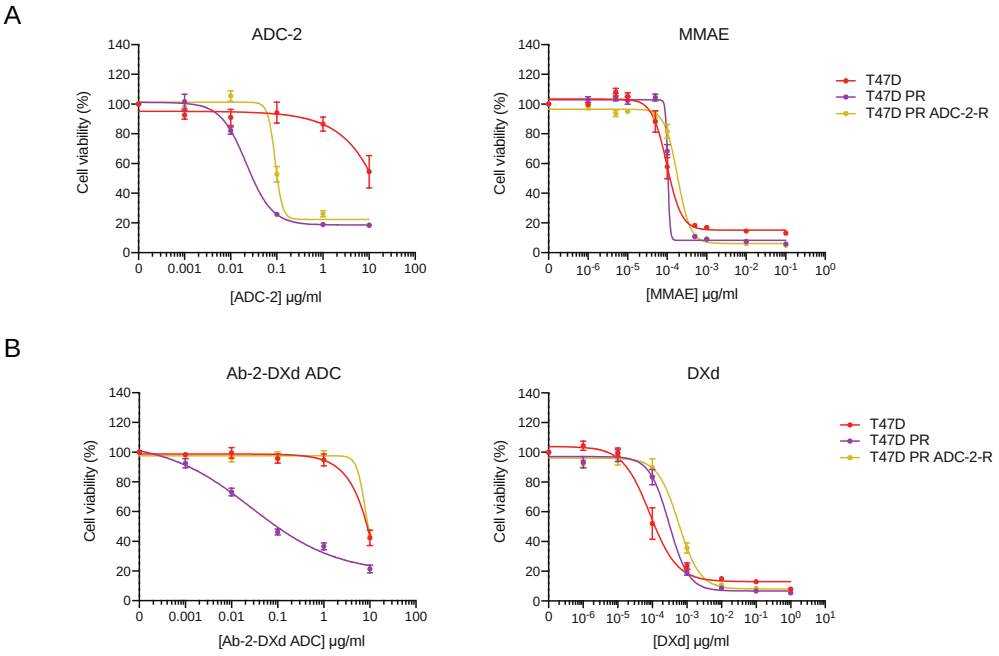

Figure 47. Assessment of the cytotoxic properties of ADC-2, MMAE, Ab-2-DXd-ADC, and DXd in T47D PR ADC-2-R cells. T47D, T47D PR, and T47D PR ADC-2-R cells were treated with increasing doses of (A) ADC-2, MMAE, (B) Ab-2-DXd-ADC, and DXd for 144 h. Shown are representative graphs of cell viability readouts determined by Cell Titer AQueous. Data was normalized to untreated cells and three independent experiments were performed. Mean values ± SEM are shown.

Overall, these findings demonstrate that, in our *in vitro* model, resistance to ADC-2 is associated with reduced FGFR4 expression and a shift toward a more aggressive intrinsic subtype profile. Importantly, the retained sensitivity to MMAE suggests that alternative targeting strategies could remain effective in overcoming ADC-2 resistance within this system. While these results provide valuable mechanistic insights, we emphasize that they reflect a behavior in a controlled *in vitro* context. As such, they should not be directly extrapolated to predict clinical resistance mechanisms or ADC efficacy in patients.

3.9 Validation of anti-FGFR4 therapies *in vivo* using breast cancer CDX models

To validate our *in vitro* findings, two breast cancer CDX mouse models were used. All *in vivo* experiments were conducted in collaboration with the Growth Control and Cancer Metastasis Research Group, led by Roger Gomis at the Institut de Recerca Biomèdica (IRB) in Barcelona.

Cells were injected to mice, and tumors were allowed to grow in the presence of supplemented estrogens. Upon reaching a measurable size (~75 mm^3), mice were randomized and treated with vehicle, an Isotypic-ADC and FGFR4-directed ADC-2 (2 or 5 mg/kg) once a week 4 times and subsequently followed (**Figure 48**).

Figure 48. Schematic representation of the generation of the two CDX models and the experimental approach. ZR751 and T47D cells were subcutaneously injected into BALB/c nude mice to establish CDX models. When tumors reached approximately 75 mm^3, mice were treated weekly for four weeks with vehicle (grey), isotypic-ADC 2 mg/kg (blue), isotypic-ADC 5 mg/kg (green), FGFR4-directed ADC-2 2 mg/kg (red), or FGFR4-directed ADC-2 5 mg/kg (pink).

No differences in terms of mouse weight were observed across treatment groups, indicating good tolerability (**Figure 49).** An average weight loss of approximately 10% was recorded in all studies, which remains within the acceptable threnshold (<20%) for preclinical models.

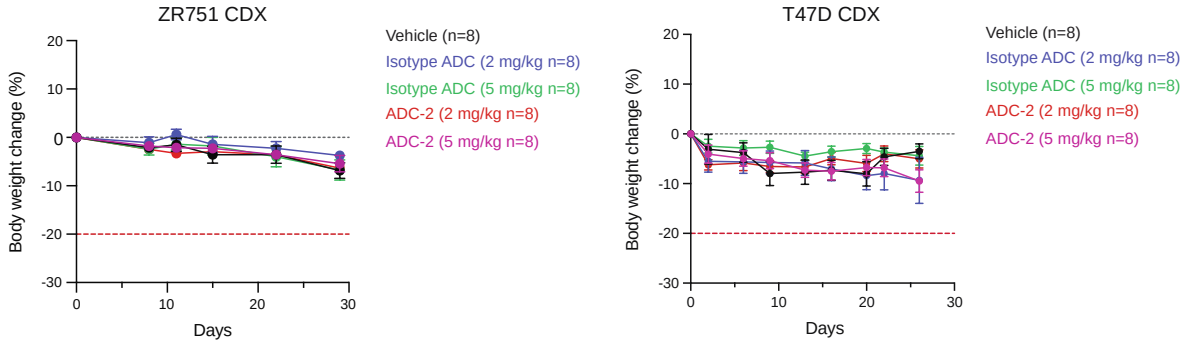

Figure 49. Average body weight change in mice following treatment across *in vivo* studies.

In FGFR4-high ZR751 xenograft models, subtle or no effect was observed when mice were treated with vehicle or isotype ADC and tumors developed regardless of treatment. In contrast, systemic treatment with ADC-2 significantly reduced tumor volume at both doses compared to the vehicle ($p < 0.0001$), with the 5 mg/kg dose showing a more pronounced effect than 2 mg/kg ($p = 0.0003$), leading to complete tumor regression by day 29 **(Figure 50A)**.

After harvesting tumors, we analyzed PAM50 gene expression of ZR751 xenograft models using the nCounter platform and confirmed a change from HER2-enriched subtype to Luminal subtypes only after treatment with the FGFR4-ADC. This change in PAM50 subtype was associated with significant expression of 59 genes, including reduced expression of *FGFR4* and proliferation genes and an increase in the expression of luminal-related genes in tumors treated with the FGFR4-ADC **(Figure 50B)**.

A second *in vivo* experiment was conducted using FGFR4-low T47D xenograft models. ADC-2 at 5 mg/kg elicited a modest yet statistically significant reduction in tumor growth ($p = 0.009$), while the 2 mg/kg dose was ineffective ($p = 0.267$) **(Figure 50C)**. The isotype control ADC had no effect on tumor growth at either dose ($p = 0.123$ and $p = 0.134$ at 2 or 5 mg/kg, respectively). In this model, only 2 genes were differentially expressed across treatment conditions **(Figure 50D)**.

These findings collectively demonstrate that ADC-2's anti-tumor efficacy is highly dependent on FGFR4 expression and is dose-responsive *in vivo*. While ADC-2 retains some activity in FGFR4-low tumors at higher doses, its therapeutic potential is markedly enhanced in FGFR4-

high models **(Figures 50A and 50C)**. Notably, in tumors expressing high FGFR4, ADC-2 treatment induces a shift towards less aggressive tumor phenotypes, characterized by reductions in proliferative and aggressive subtypes and increased representation of Luminal A and Normal-like signatures **(Figures 50B)**.

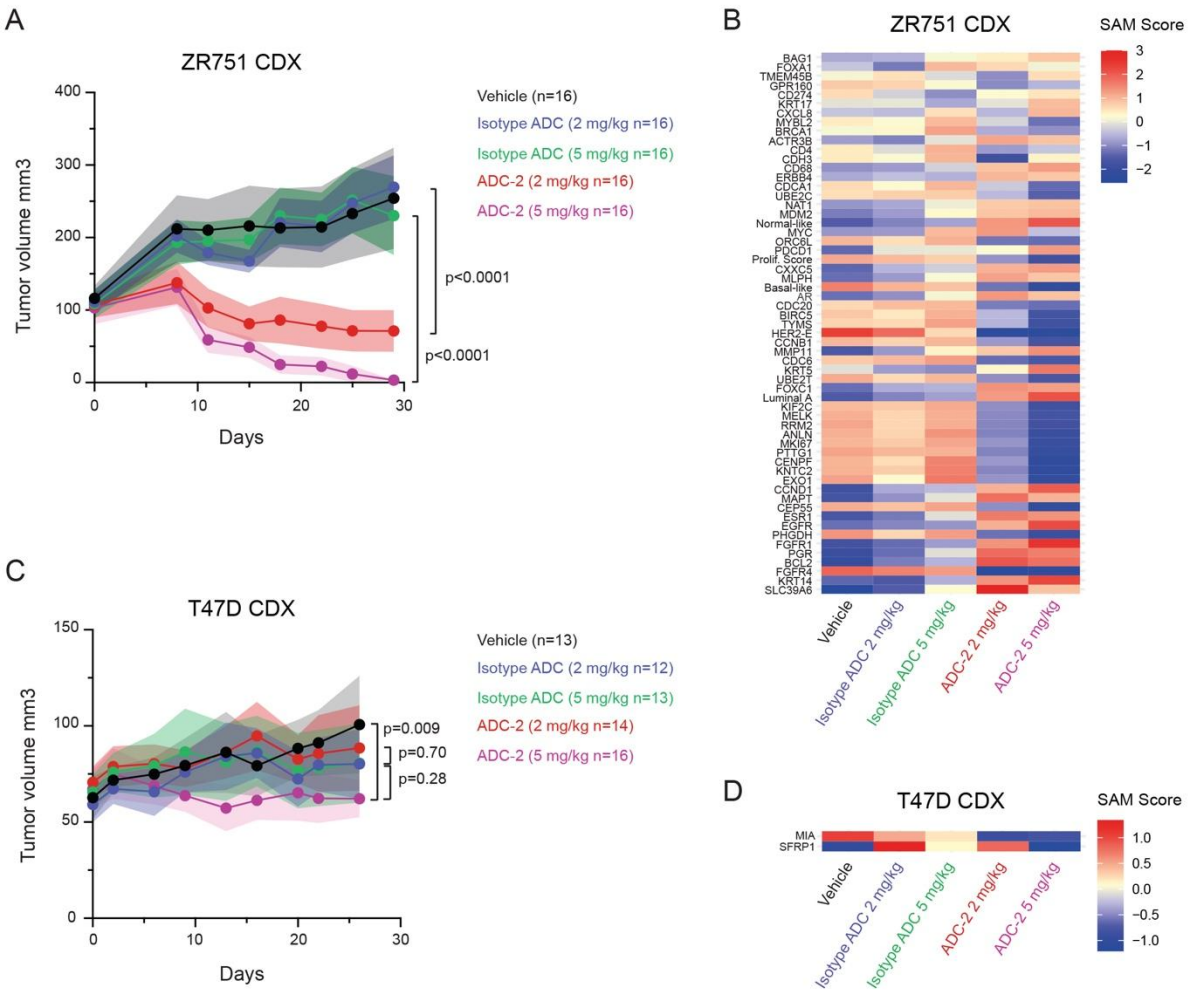

Figure 50. Therapeutic efficacy and transcriptional effects of ADC-2 *in vivo*. (A) Tumor growth curves of ZR751 xenografts after treatment. Statistical analyses were performed using the Mann-Whitney U test. (B) Heatmap of a multiclass SAM representing the PAM50 molecular subtypes, Proliferation Score and genes that are differentially expressed (FDR < 5%) upon treatment in ZR751 xenografts. (C) Tumor growth curves of T47D xenografts after treatment. Statistical analyses were performed using the Mann-Whitney U test. (D) Heatmap of a multiclass SAM representing the PAM50 molecular subtypes, Proliferation Score and genes that are differentially expressed (FDR < 5%) upon treatment in T47D xenografts.

Overall, in the second part of this thesis, we have confirmed that FGFR4 is a driver of resistance to CDK4/6 inhibitors and is associated with poorer prognosis in HR+/HER2-/HER2-enriched breast cancer. Importantly, we have demonstrated that direct targeting of FGFR4 using an ADC represents a strong therapeutic strategy in breast cancer *in vitro* and a potential therapeutic strategy for patients with breast cancer who have progressed following standard of care treatments.

DISCUSSION

In recent years, three CDK4/6 inhibitors (i.e., palbociclib, ribociclib, abemaciclib) have been approved for the treatment of patients with metastatic HR+/HER2- breast cancer in combination with endocrine therapy (103–113). Although these inhibitors are generally considered to provide a similar class effect, they differ in their chemical structure, pharmacological properties, and dosing regimens (138,142). Currently, no specific biomarkers are available to guide the selection of the first-line CDK4/6 inhibitor (274). Furthermore, resistance to CDK4/6 inhibitors represents a major clinical challenge, limiting the long-term efficacy of these therapies in HR+ breast cancer. While many patients initially benefit from these agents in combination with endocrine therapy, most eventually experience disease progression. A deeper understanding of the mechanisms underlying resistance is critical to guide next-line treatment strategies and improve patient outcomes. Efforts are already underway to characterize the genomic landscape associated with CDK4/6 inhibitor resistance (275), but further research is needed to identify reliable predictive biomarkers and develop strategies to overcome or prevent resistance.

In this thesis, we investigated mechanisms of response and resistance to CDK4/6 inhibition and evaluated a novel therapeutic strategy targeting resistant disease in HR+/HER2- breast cancer. First, we compared the molecular effects of palbociclib and ribociclib using *in vitro* models and clinical samples from two neoadjuvant phase II trials. Second, we studied the association of *FGFR4* expression with the HER2-enriched PAM50 subtype and its impact on clinical outcomes in metastatic tumors. Third, we explored different means of targeting FGFR4 in preclinical models. Notably, findings from Chapters 2 and 3 have supported the advancement of an ADC into a phase I first-in-human clinical trial in Spain, with expansion planned in Europe during the phase II.

In the following discussion, we reflect on the rationale, limitations, and implications of our findings within the broader context of CDK4/6-targeted therapy and resistance.

1. Palbociclib and ribociclib induce comparable molecular changes, modulated by dose, combination with fulvestrant, and timing

While the first-line trials with ribociclib and palbociclib demonstrated identical primary endpoint PFS results, recent data have revealed differences in OS, with palbociclib failing to show a significant OS benefit (276). The reasons for this discrepancy, whether due to differences in the inhibitor type, trial design, patient population, or other factors, remain unclear. Importantly, the PAM50 molecular subtypes have been shown to be prognostic in patients treated with CDK4/6 inhibitors (178,180,181). Accumulated evidence suggests that ribociclib, when combined with endocrine therapy, may be more effective than palbociclib in patients with advanced HR+/HER2-/HER2-enriched breast cancer. Retrospective analyses of the MONALEESA-2,-3, and -7 trials (180) revealed that patients with HER2-enriched tumors who received ribociclib alongside endocrine therapy exhibited improved PFS and OS, while those treated with palbociclib in the PALOMA-2 trial (178) did not show such benefits. However, this retrospective analysis of PALOMA-2 was not powered to assess the effect across PAM50 subtypes. The recent results of the phase III PATINA trial have shown that adding palbociclib to anti-HER2 therapy and endocrine threapy provides a significant PFS benefit in patients with HR+/HER2+ metastatic breast cancer, supporting the use of CDK4/6 inhibitors in this setting (277). However, the PATRICIA trial, which specifically investigated the role of palbociclib in combination with anti-HER2 therapy, suggested that the observed benefit is restricted to tumors of the luminal subtype, with HER2-enriched tumors showing limited or no benefit (181). These findings underscore the importance of molecular subtyping for optimal patient stratification to identify the patients most likely to benefit from CDK4/6 inhibiton.

The hypothesis that ribociclib might be more effective in HER2-enriched breast cancer is yet to be formally tested in a head-to-head trial. The SOLTI-2101 HARMONIA prospective phase III trial (NCT05207709) (187) was designed to evaluate whether ribociclib combined with endocrine therapy is superior to palbociclib combined with endocrine therapy in prolonging PFS in this patient subset. However, given the consistent OS advantage observed with ribociclib over palbociclib, recruitment did not progress as anticipated and has now been closed. Samples from enrolled patients will still be analyzed, although the trial will not be able to formally test its primary hypothesis. In this thesis, we conducted *in vitro* and transcriptomic

analyses to compare the effects of palbociclib and ribociclib on breast cancer cell lines and patient tumor samples.

In order to better understand the molecular effects of palbociclib and ribociclib, we analyzed both cell lines and clinical samples treated with CDK4/6 inhibitors. Our main observations in breast cancer cell lines were that palbociclib and ribociclib had identical dose-dependent proliferation inhibition and that in CDK4/6 inhibitor-sensitive cell lines, both inhibitors reduced the levels of p-Rb (marker of cell cycle inhibition (137)) and Lamin-B1 (marker of senescence (278–280)) in a similar manner, where treatment duration played a part but changes mostly relied on the administered doses.

Importantly, gene expression analyses revealed that palbociclib and ribociclib significantly increased the Luminal A and Normal-like signatures and decreased the Luminal B, Basal-like, and Proliferation signatures with both doses. However, the HER2-enriched signature was only significantly reduced in cells treated with 500 nM of CDK4/6 inhibitors +/− fulvestrant. Interestingly, treatment with fulvestrant alone significantly increased the HER2-enriched signature, but the addition of 500 nM palbociclib or ribociclib was still capable of significantly decreasing its levels. Assessment of individual gene expression suggested that in lower doses palbociclib might be more potent CDK4/6 inhibitor than ribociclib, and that co-treatment with fulvestrant further enhances these changes in gene expression.

In patient tumor samples from the CORALLEEN and NeoPalAna phase II studies, a similar change in PAM50 biology was observed with both drugs, namely an increase in Luminal A and Normal-like signatures and a decrease in Luminal B and Proliferation signatures after 2 weeks of treatment and at surgery. At 2 weeks of treatment, the HER2-enriched signature was significantly decreased in both studies. However, the decrease in the HER2-enriched signature was only observed in surgical samples of patients treated with ribociclib, but not palbociclib. Interestingly, in patients from NeoPalAna who underwent surgery at 8 days from the last dose of palbociclib or before, a reduction of the HER2-enriched signature was observed, although it was not of statistical significance possibly due to sample size. This result is consistent with the results of the NeoPalAna trial, where a Ki-67 rebound at surgery following palbociclib was observed in patients where palbociclib treatment was finalized more than 8 days before surgery, while this washout was suppressed if patients received a cycle 5 of palbociclib (179).

If palbociclib was given until surgery, the effect could be as good as the effect of ribociclib. However, sample size in NeoPalAna was much smaller compared to CORALLEEN and this represents a limitation on the interpretation of the results.

Our study acknowledges several other limitations. Firstly, our analysis was limited to early-stage breast cancer tumor samples, as obtaining paired biopsies in a metastatic setting is challenging. This may restrict the applicability of our findings to more advanced disease stages. Secondly, while most of these samples were not HER2-enriched, we attempted to mitigate this by analyzing each PAM50 intrinsic subtype score as a continuous variable, since these scores are strictly related to the biological information provided by the PAM50 genes characterizing each breast cancer intrinsic subtype (58). Nonetheless, we acknowledge this may not fully capture the complexities of HER2-enriched biology. Thirdly, there is an acknowledged gap in our understanding of the actual concentration of palbociclib and ribociclib that reaches the tumor in patients, which may differ from the prescribed doses and preclinical models, adding a layer of uncertainty to the direct translatability of our results to clinical practice. Fourthly, the specificity of the CORALLEEN trial to patients with PAM50 Luminal B disease narrows the breadth of our findings, potentially limiting their generalizability to other breast cancer subtypes. Lastly, our study did not include abemaciclib, which has been proposed to target additional CDKs in addition to CDK4/6 (281,282). These limitations highlight the need for further research in order to fully understand the implications of CDK4/6 inhibitors in varying contexts of breast cancer treatment.

In conclusion, our results show that biological responses to palbociclib and ribociclib are primarily dose-dependent and influenced by the addition of fulvestrant. Our findings suggest that while both CDK4/6 inhibitors effectively modulate key biological pathways in HR+/HER2- breast cancer, nuances in their impact, particularly on the HER2-enriched signature, warrant further investigation. Analyses of available patient samples from the SOLTI-2101 HARMONIA trial (187) may still provide valuable insights into the distinct biological effects of these agents in HER2-enriched breast cancer.

2. FGFR4 drives resistance to CDK4/6 inhibition in HR+/HER2- breast cancer

The development of resistance to CDK4/6 inhibitors in HR+/HER2- metastatic breast cancer remains a major clinical challenge, limiting the long-term efficacy of current standard of care treatments. The PAM50 HER2-enriched intrinsic subtype has been associated with poor clinical outcomes (179,180,182,219,283), and our group and others have identified FGFR4 as a driver of the HER2-enriched subtype in HER2-negative tumors (170,218,219). Additionally, aberrant FGFR4 signaling has been linked to poor clinical outcomes and therapeutic resistance in HR+ breast cancer (218–220).

Here, we analyzed real-world data from a clinical cohort of 275 patients with HR+/HER2- metastatic breast cancer treated with endocrine therapy and CDK4/6 inhibitors. The dataset includes 253 baseline tumor samples and 59 post-progression samples, 37 of which are paired baseline-PD samples from the same patients. Consistent with previously reported findings (65,170–173), our data demonstrate that tumors can evolve after progressing to CDK4/6 inhibitors in combination with endocrine therapy, often resulting in changes to their intrinsic subtype. Subtype switching was frequent: 64.9% of paired samples showed a shift in PAM50 subtype, most commonly toward HER2-enriched. Accordingly, the proportion of HER2-enriched tumors increased from 14.6% at baseline to 45.8% at progression. Importantly, patients with HER2-enriched tumors at baseline had significantly shorter PFS and OS, underscoring the poor prognosis associated with this phenotype.

We found that a substantial proportion of tumors progressing on CDK4/6 inhibitors exhibited elevated FGFR4 expression at both mRNA and protein levels. Notably, the proportion of samples with FGFR4 H-Scores above 50 doubled at progression compared to baseline. Additionally, we observed that FGFR4 H-Scores determined by IHC showed a moderately strong correlation with mRNA levels derived from transcriptomic analyses (Pearson $r = 0.66$, $p < 0.001$), highlighting the consistency between protein and gene expression data. Furthermore, high FGFR4 mRNA expression at baseline was significantly associated with shorter PFS and OS, underscoring its potential as a prognostic biomarker.

Although our study did not directly assess downstream signaling, prior preclinical studies have shown that FGFR4 can activate mitogenic pathways such as RAS/MAPK, PI3K/AKT, and STAT3, which may contribute to treatment resistance by sustaining cell proliferation and survival (218,250). Our findings support the idea that FGFR4 overexpression might contribute to treatment resistance to CDK4/6 inhibitors in a subset of HR+/HER2- tumors.

Similarly, while we did not investigate the underlying causes of *FGFR4* overexpression, recent findings have suggested that elevated *FGFR4* expression in HER2-enriched tumors is associated with an epigenetic mechanism involving hypomethylation of CpG shores in the *FGFR4* promoter (219). Our observation of increased FGFR4 expression at progression is compatible with this model, although further epigenetic profiling would be required to confirm this in our cohort. Hohmann et al. also reported that these CpG regions are typically hypermethylated in normal breast tissue. Here, we performed IHC staining on a panel of healthy tissues and found that FGFR4 expression was undetectable, suggesting that FGFR4-targeted therapies could be both effective and well tolerated.

Overall, our findings support and extend prior evidence indicating that FGFR4 is a key driver of the HER2-enriched phenotype in HR+/HER2- tumors (170,218,219) and that HER2-enriched tumors derive significantly less benefit from CDK4/6 inhibitors combined with endocrine therapy compared to the Luminal A and B PAM50 subtypes, exhibiting the lowest PFS and OS probability (179,180,182,219,283).

From a translational perspective, our results identify FGFR4 as a clinically relevant driver of resistance to CDK4/6 inhibitors and endocrine therapy in HR+/HER2- metastatic breast cancer, associated with intrinsic subtype switching and poor clinical outcomes. While additional mechanistic studies are warranted, our findings strengthen the rationale for therapeutic strategies targeting FGFR4 in this context.

3. FGFR4 as a therapeutic target in HR+/HER2- breast cancer

FGFR4 is an RTK that plays a key role in regulating cell proliferation, differentiation, and survival. Imbalances in FGFR signaling have been shown to play oncogenic roles in many cancers (224). In breast cancer, *FGFR4* overexpression and hotspot mutations have been reported in endocrine therapy-resistant metastatic ER+ lobular carcinoma (240), and recent findings suggest that *FGFR4* expression may be epigenetically upregulated in HR+/HER2-/HER2-enriched tumors (219).

FGFR4 is structurally and functionally distinct from other members of the FGFR family, with a unique kinase domain that may confer a unique role when compared to other FGFRs (225). Selective FGFR4 inhibitors are currently under development, with promising activity demonstrated in preclinical models of HCC (243) and early clinical responses observed in patients with advanced HCC (244). High expression and mutations of *FGFR4* have also been identified as a driver of metastasis in rhabdomyosarcomas (252), where FGFR4 is being explored as a target for CAR-T cell therapy (253). Additionally, an ADC against FGFR4 is also under development for rhabdomyosarcoma and HCC (254), further supporting the therapeutic relevance of FGFR4. In breast cancer, an *in silico* analysis that identified FGFR4 as a potential cell surface target for CAR-T cell therapy and ADC development was performed in our group (255).

3.1 Limited efficacy of FGFR4 kinase inhibition in breast cancer

To evaluate the pharmacological potential of FGFR4 inhibition in breast cancer, we tested the selective FGFR4 inhibitor INCB062079 in twelve breast cancer cell lines with varying levels of *FGFR4* mRNA expression. Surprisingly, only one cell line, MDA-MB-453, which harbors the intrinsic *FGFR4* Y367C mutation, showed sensitivity to INCB062079, with a measurable cytotoxic response. Significant changes in gene expression following treatment were also restricted to this cell line.

Interestingly, the T47D Y367C line, which was engineered to express the same activating mutation, did not respond to the inhibitor. This suggests that having the *FGFR4* Y367C

mutation alone is not enough to make cells sensitive to FGFR4 kinase inhibition. Other factors, such as how much the cells depend on FGFR4 signaling or whether compensatory pathways are activated, may affect their sensitivity to the inhibitor.

Overall, these findings indicate limited efficacy of FGFR4 kinase inhibition in this context. Therefore, further evaluation of INCB062079 was not pursued in this study.

3.2 Development and preclinical evaluation of FGFR4-directed ADCs

Over the past decade, ADCs have emerged as powerful anti-cancer therapies. In HR+/HER2- metastatic breast cancer, three ADCs have demonstrated significant clinical efficacy: SG (155), Dato-DXd (157), and T-DXd (160,161). Nevertheless, disease progression remains inevitable, underscoring the need for new targets, payloads, and combination strategies to improve patient outcomes.

Recent data highlight key limitations of current ADCs, particularly those carrying TOP1-based paylaods. Evidence suggests the emergence of cross-resistance within this class. In a study by Abelman et al., recurrent TOP1 mutations were identified in approximately 13% of patients with metastatic breast cancer who progressed on TOP1-based ADC therapy, compared to <1% in non-ADC-treated patients or in public datasets such as TCGA. These mutations were associated with markedly reduced benefit from sequential ADC treatment, with median treatment durations of 52 days on a second ADC compared with 455 days on the first (169).

Real-world outcomes further support these observations. Tarantino et al. reported consistently poor outcomes in patients treated after progression on T-DXd, with median PFS of 4.6 months in HER2-positive, 3.4 months in HR+/HER2-negative, and 2.8 months in TNBC (284) Patients receiving SG after T-DXd experienced particularly poor outcomes, suggesting potential cross-resistance between agents. Based on these findings, the authors propose that patients with HR+/HER2-negative metastatic breast cancer may benefit more from conventional chemotherapies than from another TOP1-based ADC, although SG was still the most frequently administered therapy following T-DXd in their cohort. Tarantino et al. further

note that smaller retrospective studies have supported a median PFS of only 2-3 months after sequential treatment with a second TOP1-based ADC, supporting their observations.

These findings have important implications for the design of next-generation ADCs for HR+/HER2- metastatic breast tumors. The limited sequential efficacy of TOP1 inhibitor-based ADCs indicates that alternative strategies are required, including the development of ADCs with novel payload classes.

FGFR4 is a tumor surface antigen with increased expression in tumors progressing on CDK4/6 inhibitors and has not been previously exploited in breast cancer. Linking an anti-FGFR4 antibody to a non-TOP1 payload may avoid cross-resistance and provide a new opportunity for effective sequential therapy.

In breast cancer, several monoclonal antibodies have been approved, such as the anti-HER2 antibodies trastuzumab and pertuzumab, both of which have shown significant improvements in PFS and OS in patients with HER2+ breast cancer (285–287). However, to date, no FGFR4-directed antibodies have been clinically tested or approved. In other cancer types, several FGFR4-directed monoclonal antibodies have demonstrated promising preclinical activity. LD1 is an FGFR4 neutralizing antibody that inhibits downstream signaling, colony formation, and cell proliferation in malignant cells, while also significantly suppressing tumor growth in *in vivo* models of liver cancer (288). Similarly, U3-1784, a fully humanized, high-affinity antibody that competes with FGFs for FGFR4 binding, has demonstrated antitumor activity in FGF19-overxpressing liver tumors (289). In rhabdomyosarcoma, monoclonal antibody 3A11, developed from hybridoma lines generated in mice immunized with the human FGFR4 extracellular domain, has shown strong FGFR4 specificity and is currently being explored for therapeutic use (257).

These results highlight the potential of FGFR4 as a therapeutic target, supported by recent data on existing ADCs that underscore the limitations of current strategies.

3.2.1 Characterization of anti-FGFR4 antibodies for targeted delivery

Building on the existing evidence, we evaluated the binding, internalization, and cytotoxic properties of three anti-FGFR4 monoclonal antibodies (i.e., Ab-1 (260), Ab-2 (261), Ab-3 (262))

across six breast cancer cell lines with varying FGFR4 expression (categorized as FGFR4-high, FGFR4-low, FGFR4-negative). All three antibodies demonstrated FGFR4-specific binding and internalization, confirming their selectivity and supporting their potential for further therapeutic development.

In our study, none of the selected anti-FGFR4 antibodies induced direct cytotoxicity in any breast cancer cell line, regardless of FGFR4 expression. This lack of intrinsic cytotoxic activity suggests that the antibodies alone do not have therapeutic efficacy in this context. However, when combined with anti-human secondary antibodies conjugated to cytotoxic payloads, a strong cytotoxic response was observed in FGFR4-high cells. This finding indicates that while the antibodies themselves are biologically inert in terms of direct cytotoxicity *in vitro*, they can serve as highly specific delivery vehicles for cytotoxic agents, highlighting their potential as components of an ADC. Their selective internalization into FGFR4-high cells further supports their use in targeted therapies for tumors with FGFR4 overexpression, particularly in the context of CDK4/6 inhibitor-resistant HR+/HER2- breast cancer.

3.2.2 Design and optimization of FGFR4-targeted ADCs

Based on these observations, we proceeded to design and develop three FGFR4-directed ADCs using the Fc-silent variant of the Ab-2 antibody as the carrier due to its high specificity as well as its efficient internalization, its optimal PK properties, and off-patent status. It was conjugated to MMAE, a highly potent tubulin inhibitor that blocks microtubule polymerization, leading to cell cycle arrest and apoptosis. It is effective at low doses and has membrane permeability and can therefore exert a bystander effect (271–273). Although MMAE has demonstrated strong efficacy in other solid tumors, and MMAE-based ADCs are currently being evaluated in clincal trials for breast cancer (NCT05904964), it has not yet been widely approved or established in breast cancer treatment (290,291).

In breast cancer treatment, most approved ADCs use TOP1 inhibitors as their cytotoxic payloads (168). Resistance to payloads often arises from structural alterations in their molecular targets, such as mutations in TOP1 (292–294), modifications in the microtubule/tubulin complex, or dysregulated cyclins (293,294). Additionally, factors such as impaired ADC internalization or lysosomal function, increased expression of drug-efflux

pumps, overactivation of survival signaling pathways, and alterations in apoptotic regulation can further reduce tumor sensitivity to ADC therapies (293,294). Given these resistance mechanisms, diversifying both the target antigen and payload presents a promising strategy to enhance ADC effectiveness and overcome therapeutic resistance (168).

MMAE is typically conjugated to antibodies via cleavable linker, allowing for precise drug release inside cancer cells as well as the possibility of exerting a bystander effect (271,272). Here, the microtubule inhibitor was conjugated through a VC-PAB linker (patent US7829531B2, expired). Two average DARs were evaluated: DAR4, which is the standard marketed MMAE-ADCs (149), and DAR8. ADC conjugation strategies included random lysine conjugation (for ADC-2) and cysteine conjugation (for ADC-1 and ADC-3).

3.3 Functional validation, resistance mechanisms and translational potential of ADC-2

3.3.1 *In vitro* and *in vivo* evaluation of ADC-2

After ensuring that the cytotoxicity of the three ADCs was FGFR4-specific and studying their PK and specificity properties, ADC-2 was chosen as the lead ADC for further development. While it's true that all three constructs exhibited FGFR4 binding and acceptable plasma stability, cysteine conjugates showed increased non-specific binding and rapid *in vivo* clearance, while the lysine-conjugated ADC had superior *in vivo* PK properties.

The bystander effect of ADC-2 was confirmed *in vitro*. As research on ADCs has progressed, the ability of certain payloads to induce a bystander effect has been recognized for its potential to enhance the therapeutic impact, particularly in the context of variable target expression (273). MMAE, due to its membrane permeability, can diffuse from targeted cells into neighboring cells following intracellular release, potentially expanding the therapeutic impact of the ADC beyond FGFR4-expressing cells. While not all tumors exhibit FGFR4 heterogeneity, variable expression can occur. In such scenarios, a bystander-capable payload may help eliminate low-antigen-expressing cells that would otherwise evade treatment.

The *in vivo* validation of ADC-2 using breast cancer CDX models provided strong evidence supporting the efficacy and specificity of the ADC. By using two breast cancer cell lines with varying FGFR4 expression levels (i.e., ZR751 (FGFR4-high) and T47D (FGFR4-low)), we were able to interrogate how FGFR4 expression modulates ADC-2 responsiveness *in vivo*. The results from the ZR751 CDX model highlight a clear therapeutic benefit, with ADC-2 eliciting robust tumor suppression in a dose-dependent manner. Notably, ADC-2 at both 2 mg/kg and 5 mg/kg doses significantly reduced tumor volume, with the higher dose resulting in complete tumor regression. In contrast, the isotype control ADC had no significant impact on tumor growth, reinforcing the specificity of ADC-2's action through FGFR4 targeting. The observed tumor regression with the 5 mg/kg dose emphasizes the importance of optimizing dosing regimens for achieving maximal therapeutic outcomes. Interestingly, no major differences in efficacy were observed between the 2 mg/kg and 5 mg/kg doses in terms of molecular subtype shifts.

The results in the T47D CDX model further underscore the importance of target expression as a determinant of ADC efficacy. The smaller therapeutic impact in FGFR4-low tumors confirm that ADC-2's antitumor activity is tightly coupled to FGFR4-mediated internalization and payload delivery. However, given the intratumoral heterogeneity that can exist in tumors, we wonder if ADC-2 might still exert effects through a bystander mechanism. This possibility remains to be addressed, but could expand the therapeutic scope of ADC-2 beyond strictly FGFR4-high tumors.

3.3.2 Molecular response to ADC-2 and PAM50 signature shifts

Our findings also provide key insights into the molecular response of breast cancer cells to Ab-2, MMAE, and ADC-2 treatment. Gene expression analyses revealed that in FGFR4-high cells, both ADC-2 and MMAE induced significant changes, shifting PAM50 subtype signatures and reducing proliferation scores. In contrast, FGFR4-low and FGFR4-negative cells only responded to MMAE, underscoring the specificity of this ADC towards FGFR4-expressing cells. Treatment with the naked antibody Ab-2 alone also failed to induce changes in gene expression. These results further validate ADC-2's targeted mechanism of action and its capacity to modulate breast cancer cell phenotypes in an FGFR4-dependent manner.

A particularly interesting finding was the increase in FGFR4 expression following treatment with ADC-2 or MMAE in two FGFR4-high cell lines, T47D PR and T47D Y367C, suggesting a potential adaptive response to treatment. However, we hypothesize that this increase reflects the selection of more resistant cells that persist in the wells at the time of mRNA extraction. Consequently, this observation probably does not accurately reflect the overall cell population response or have significant biological implications. Similarly, the observed shifts in molecular subtypes, including increased HER2-enriched, Luminal A, and Normal-like signatures, and decrease Luminal B and Basal-like signatures, were assessed at 72 h post-treatment and are likely transient, without necessarily indicating long-term therapeutic effects.

3.3.3 Mechanisms of acquired resistance to ADC-2

To better distinguish between transient adaptative responses and durable resistance mechanisms, we developed and characterized ADC-2-resistant (ADC-2-R) cells. These cells offer a more accurate representation of the long-term cellular response to treatment *in vitro*. Compared to parental T47D PR cells, T47D PR ADC-2-R cells exhibited a significant reduction in FGFR4 expression at both the mRNA and protein levels, along with decreased membrane FGFR4 density. This loss of *FGFR4* expression was associated with a shift towards a more Basal-like and Luminal B phenotype, accompanied by increased proliferation, suggesting an adaptive mechanism through which cancer cells evade ADC-2-mediated cytotoxicity.

Interestingly, T47D PR ADC-2-R cells retained sensitivity to MMAE, with IC50 values comparable to those observed in both T47D PR and parental T47D cells. This finding further confirms that resistance to ADC-2 is primarily driven by the loss of FGFR4 expression rather than by resistance to the cytotoxic payload itself. The preserved activity of MMAE in FGFR4-low cells highlights the potential of future alternative therapeutic strategies using this payload.

This was further supported by our evaluation of Ab-2-DXd-ADC, an FGFR4-directed ADC conjugated to a TOP1 inhibitor. As expected, Ab-2-DXd-ADC exhibited cytotoxic activity only in FGFR4-high T47D PR cells, whereas treatment with unconjugated DXd resulted in strong cytotoxicity in all three cell lines. Despite demonstrating potent antitumor effects *in vivo*,

TOP1-based ADCs often show limited *in vitro* activity due to their reliance on high receptor expression threshold, which explains the absence of cytotoxic activity in T47D PR ADC-2-R cells. As a result, IC50 values obtained from *in vitro* experiments cannot be directly compared across the two assessed ADCs. Differences in mechanisms of action, receptor dependency, and exposure times must be considered when interpreting such results. Within this context, the Ab-2-DXd-ADC experiment serves primarily as a validation of the receptor-expression-dependent nature of ADC efficacy, rather than a direct quantitative comparison between the two ADCs.

3.4 Clinical implications and future directions

These findings support a biomarker-driven approach to patient selection. Stratifying patients based on FGFR4 expression will likely be crucial in order to maximize response to ADC-2. The observed shifts toward less aggressive tumor subtypes following ADC-2 treatment provide promising evidence of its potential to not only inhibit tumor growth but also alter the tumor's nature to a more favorable, less proliferative state. Future studies should explore the mechanisms underlying these phenotype shifts and evaluate the long-term outcomes of ADC-2 treatment.

Although our study provides strong evidence supporting the role of FGFR4 in mediating resistance and its potential as a therapeutic target, several questions remain unanswered. For instance, while we show that FGFR4 expression is elevated in resistant tumors, the upstream regulatory mechanisms controlling FGFR4 expression have not been elucidated. Future studies should further investigate whether genetic, epigenetic, or microenvironmental factors contribute to *FGFR4* overexpression. Moreover, work is needed to dissect the downstream signaling pathways of FGFR4, which could identify additional therapeutic targets and refine combination strategies. In addition, evaluating the intrapatient heterogeneity of FGFR4 expression across different metastatic sites and testing the ADC in immune-competent preclinical models will be critical to further assess the clinical utility of targeting FGFR4.

In conclusion, our study identifies FGFR4 overexpression and the HER2-enriched phenotype as key contributors to resistance against CDK4/6 inhibitors combined with endocrine therapy

in HR+/HER2- metastatic breast cancer. We demonstrate that targeting FGFR4 with a novel MMAE-based ADC, known as ADC-2, offers a promising therapeutic strategy for patients who develop such resistance. By leveraging an alternative payload and a highly specific target, our strategy could address the limitations of current therapies and improve outcomes for patients with resistant breast cancer. Importantly, these findings have supported the development of a novel FGFR4-targeted ADC, named ONA-255, which will be evaluated in a Phase I first-in-human clinical trial starting in Q4 2025.

CONCLUSIONS

1. Palbociclib and ribociclib induce largely comparable, dose-dependent molecular changes in HR+/HER2- breast cancer *in vitro*, influenced by co-treatment with fulvestrant and treatment timing.

2. Both CDK4/6 inhibitors elicit similar shifts in intrinsic subtypes *in vitro* and in early-stage patient tumor samples.

3. In surgical clinical samples, ribociclib sustains these molecular changes more consistently, particularly in the HER2-enriched subtype.

4. The SOLTI-2101 HARMONIA trial will explore which CDK4/6 inhibitor is more active in patients with HR+/HER2-/HER2-enriched advanced breast cancer.

5. Tumors progressing on CDK4/6 inhibitors and endocrine therapy show intrinsic subtype shifts, with an increased proportion of HER2-enriched tumors at progression.

6. FGFR4 expression is significantly elevated in tumors after progression, strongly correlating with the HER2-enriched subtype and poorer survival outcomes.

7. FGFR4 is a driver of resistance to CDK4/6 inhibitors in HR+/HER2- metastatic breast cancer.

8. FGFR4 is absent in normal tissues, making it a promising and potentially well-tolerated therapeutic target.

9. Selective FGFR4 kinase inhibition shows limited efficacy in breast cancer models, indicating the need for alternative therapeutic approaches.

10. The novel FGFR4-directed ADC-2 exhibits potent and selective antitumor activity in FGFR4-high breast cancer models both *in vitro* and *in vivo*.

11. ADC-2 treatment shifts molecular subtypes toward less aggressive phenotypes and reduces tumor proliferation both *in vitro* and *in vivo*.

REFERENCES

1. Bray F, Laversanne M, Sung H, Ferlay J, Siegel RL, Soerjomataram I, et al. Global cancer statistics 2022: GLOBOCAN estimates of incidence and mortality worldwide for 36 cancers in 185 countries. CA Cancer J Clin. 2024;74(3):229–63.
2. Sociedad Española de Oncología Médica. Las cifras del cáncer en España 2025 [Internet]. Madrid: SEOM; 2025 [cited 2025 Jul 29]. Available from: https://www.seom.org
3. Noone AM, Howlader N, Krapcho M, Miller D, Brest A, Yu M, et al. Surveillance, Epidemiology, and End Results Program [Internet]. Cancer Statistics Review, 2015-2021. Bethesda: National Cancer Institute; 2021 [cited 2025 Jul 29]. Available from: https://seer.cancer.gov/statfacts/html/breast.html
4. PDQ Adult Treatment Editorial Board. Breast Cancer Treatment (PDQ) [Internet]. Bethesda: National Cancer Institute; [cited 2025 Jul 29]. Available from: https://www.cancer.gov/types/breast/hp/breast-treatment-pdq
5. Cardoso F, Tjan-Heijnen V, Božović-Spasojević I, Vaz Batista M. Breast Cancer Essentials for Clinicians. 2nd ed. Lugano: ESMO Press; 2024.
6. Sessa C, Balmaña J, Bober SL, Cardoso MJ, Colombo N, Curigliano G, et al. Risk reduction and screening of cancer in hereditary breast-ovarian cancer syndromes: ESMO Clinical Practice Guideline. Ann Oncol. 2023;34(1):33–47.
7. Goodwin PJ, Phillips KA, West DW, Ennis M, Hopper JL, John EM, et al. Breast cancer prognosis in BRCA1 and BRCA2 mutation carriers: An international prospective breast cancer family registry population-based cohort study. J Clin Oncol. 2012;30(1):19–26.
8. Mavaddat N, Barrowdale D, Andrulis IL, Domchek SM, Eccles D, Nevanlinna H, et al. Pathology of breast and ovarian cancers among BRCA1 and BRCA2 mutation carriers: Results from the consortium of investigators of modifiers of BRCA1/2 (CIMBA). Cancer Epidemiol Biomarkers Prev. 2012;21(1):134–47.
9. Ritte R, Lukanova A, Tjønneland A, Olsen A, Overvad K, Mesrine S, et al. Height, age at menarche and risk of hormone receptor-positive and -negative breast cancer: A cohort study. Int J Cancer. 2013;132(11):2619–29.

10. Hamajima N, Hirose K, Tajima K, Rohan T, Friedenreich CM, Calle EE, et al. Menarche, menopause, and breast cancer risk: Individual participant meta-analysis, including 118 964 women with breast cancer from 117 epidemiological studies. Lancet Oncol. 2012;13(11):1141–51.
11. IARC Monographs on the Evaluation of Carcinogenic Risks to Humans: Combined Estrogen-Progestogen Contraceptives and Combined Estrogen-Progestogen Menopausal Therapy [Internet]. Vol. 91. Lyon, France: International Agency for Research on Cancer (IARC); 2007 [cited 2025 Jul 29]. Available from: https://publications.iarc.who.int/Book-And-Report-Series/Iarc-Monographs-On-The-Identification-Of-Carcinogenic-Hazards-To-Humans/Combined-Estrogen--Progestogen-Contraceptives-And-Combined-Estrogen-Progestogen-Menopausal-Therapy-2007
12. Wolin KY, Carson K, Colditz GA. Obesity and Cancer. Oncologist. 2010;15(6):556–65.
13. Razzaghi H, Troester MA, Gierach GL, Olshan AF, Yankaskas BC, Millikan RC. Mammographic density and breast cancer risk in White and African American Women. Breast Cancer Res Treat. 2012;135(2):571–80.
14. Kotsopoulos J, Chen WY, Gates MA, Tworoger SS, Hankinson SE, Rosner BA. Risk factors for ductal and lobular breast cancer: Results from the nurses' health study. Breast Cancer Res. 2010;12(6):1–11.
15. Goldacre MJ, Abisgold JD, Yeates DGR, Vessey MP. Benign breast disease and subsequent breast cancer: English record linkage studies. J Public Health (Oxf). 2010;32(4):565–71.
16. Kabat GC, Jones JG, Olson N, Negassa A, Duggan C, Ginsberg M, et al. A multi-center prospective cohort study of benign breast disease and risk of subsequent breast cancer. Cancer Causes Control. 2010;21(6):821–8.
17. Worsham MJ, Raju U, Lu M, Kapke A, Bottrell A, Cheng J, et al. Risk factors for breast cancer from benign breast disease in a diverse population. Breast Cancer Res Treat. 2009;118(1):1–7.
18. Travis LB, Hill DA, Dores GM, Gospodarowicz M, van Leeuwen FE, Holowaty E, et al. Breast Cancer Following Radiotherapy and Chemotherapy Among Young Women With Hodgkin Disease. JAMA. 2003;290(4):465–75.
19. Hanahan D, Weinberg RA. The Hallmarks of Cancer. Cell. 2000;100(1):57–70.

20. Hanahan D, Weinberg RA. Hallmarks of cancer: The next generation. Cell. 2011;144(5):646–74.
21. Hanahan D. Hallmarks of Cancer: New Dimensions. Cancer Discov. 2022;12(1):31–46.
22. Cooper GM. The Cell: A Molecular Approach [Internet]. 2nd ed. Sunderland (MA): Sinauer Associates; 2000 [cited 2025 Jul 29]. Available from: https://www.ncbi.nlm.nih.gov/books/NBK9839
23. Rivenbark AG, O'Connor SM, Coleman WB. Molecular and cellular heterogeneity in breast cancer: Challenges for personalized medicine. Am J Pathol. 2013;183(4):1113–24.
24. Polyak K. Breast cancer: Origins and evolution. J Clin Invest. 2007;117(11):3155–63.
25. Wen HY, Brogi E. Lobular Carcinoma In Situ. Surg Pathol Clin. 2018;11(1):123–45.
26. American Joint Committee on Cancer Staging and End Results Reporting. Manual for Staging of Cancer. 1st ed. Chicago: American Joint Committee on Cancer; 1977.
27. Amin MB, Greene FL, Edge SB, Compton CC, Gershenwald JE, Brookland RK, et al. The Eighth Edition AJCC Cancer Staging Manual: Continuing to build a bridge from a population-based to a more "personalized" approach to cancer staging. CA Cancer J Clin. 2017;67(2):93–9.
28. Hortobagyi GN, Edge SB, Giuliano A. New and Important Changes in the TNM Staging System for Breast Cancer. Am Soc Clin Oncol Educ Book. 2018;38:457–67.
29. Rakha EA, Reis-Filho JS, Baehner F, Dabbs DJ, Decker T, Eusebi V, et al. Breast cancer prognostic classification in the molecular era: the role of histological grade. Breast Cancer Res. 2010;12:207.
30. Allison KH, Hammond MEH, Dowsett M, Mckernin SE, Carey LA, Fitzgibbons PL, et al. Estrogen and Progesterone Receptor Testing in Breast Cancer: ASCO/CAP Guideline Update. J Clin Oncol. 2020;38(12):1346–66.
31. Wolff AC, Somerfield MR, Dowsett M, Hammond MEH, Hayes DF, Mcshane LM, et al. Human Epidermal Growth Factor Receptor 2 Testing in Breast Cancer: ASCO-College of American Pathologists Guideline Update. J Clin Oncol. 2023;41(22):3867–72.
32. Chen Z, Jia H, Zhang H, Chen L, Zhao P, Zhao J, et al. Is HER2 ultra-low breast cancer different from HER2 null or HER2 low breast cancer? A study of 1363 patients. Breast Cancer Res Treat. 2023;202(2):313–23.

33. Mehta S, Iyengar A, Barman H, Rangarajan N, Woo MSA, Sredni ST, et al. Prevalence of “HER2 ultra-low” among patients with advanced breast cancer with historical IHC0 status. J Clin Oncol. 2024;42(16 Suppl):e13156.
34. Schettini F, Chic N, Brasó-Maristany F, Paré L, Pascual T, Conte B, et al. Clinical, pathological, and PAM50 gene expression features of HER2-low breast cancer. NPJ Breast Cancer. 2021;7(1):1–13.
35. Anderson WF, Chatterjee N, Hill D. The impact of estrogen receptor status in the Surveillance, Epidemiology, and End Results database. Breast Cancer Res Treat. 2002;76:27–36.
36. Loibl S, André F, Bachelot T, Barrios CH, Bergh J, Burstein HJ, et al. Early breast cancer: ESMO Clinical Practice Guideline for diagnosis, treatment and follow-up. Ann Oncol. 2024;35(2):159–82.
37. Johnston SRD, Harbeck N, Hegg R, Toi M, Martin M, Min Shao Z, et al. Abemaciclib Combined With Endocrine Therapy for the Adjuvant Treatment of HR+, HER2-, Node-Positive, High-Risk, Early Breast Cancer (monarchE). J Clin Oncol. 2020;38(34):3987–98.
38. Giordano SH, Franzoi MAB, Temin S, Anders CK, Chandarlapaty S, Crews JR, et al. Systemic Therapy for Advanced Human Epidermal Growth Factor Receptor 2-Positive Breast Cancer: ASCO Guideline Update. J Clin Oncol. 2022;40(23):2612–35.
39. Anders C, Carey LA, Carey L. Understanding and Treating Triple-Negative Breast Cancer. Oncology. 2008;22(11):1233–43.
40. Robson M, Im SA, Senkus E, Xu B, Domchek SM, Masuda N, et al. Olaparib for Metastatic Breast Cancer in Patients with a Germline BRCA Mutation. N Engl J Med. 2017;377(6):523–33.
41. Litton JK, Rugo HS, Ettl J, Hurvitz SA, Gonçalves A, Lee KH, et al. Talazoparib in Patients with Advanced Breast Cancer and a Germline BRCA Mutation. N Engl J Med. 2018;379(8):753–63.
42. Cortes J, Rugo HS, Cescon DW, Im SA, Yusof MM, Gallardo C, et al. Pembrolizumab plus Chemotherapy in Advanced Triple-Negative Breast Cancer. N Engl J Med. 2022;387(3):217–26.
43. Schmid P, Adams S, Rugo HS, Schneeweiss A, Barrios CH, Iwata H, et al. Atezolizumab and Nab-Paclitaxel in Advanced Triple-Negative Breast Cancer. N Engl J Med. 2018;379(22):2108–21.

44. Loi S, Sirtaine N, Piette F, Salgado R, Viale G, Van Eenoo F, et al. Prognostic and predictive value of tumor-infiltrating lymphocytes in a phase III randomized adjuvant breast cancer trial in node-positive breast cancer comparing the addition of docetaxel to doxorubicin with doxorubicin-based chemotherapy: BIG 02-98. J Clin Oncol. 2013;31(7):860–7.

45. Adams S, Gray RJ, Demaria S, Goldstein L, Perez EA, Shulman LN, et al. Prognostic value of tumor-infiltrating lymphocytes in triple-negative breast cancers from two phase III randomized adjuvant breast cancer trials: ECOG 2197 and ECOG 1199. J Clin Oncol. 2014;32(27):2959–66.

46. Salgado R, Denkert C, Demaria S, Sirtaine N, Klauschen F, Pruneri G, et al. The evaluation of tumor-infiltrating lymphocytes (TILS) in breast cancer: Recommendations by an International TILS Working Group 2014. Ann Oncol. 2015;26(2):259–71.

47. Denkert C, von Minckwitz G, Darb-Esfahani S, Lederer B, Heppner BI, Weber KE, et al. Tumour-infiltrating lymphocytes and prognosis in different subtypes of breast cancer: a pooled analysis of 3771 patients treated with neoadjuvant therapy. Lancet Oncol. 2018;19:40–50.

48. Savas P, Salgado R, Denkert C, Sotiriou C, Darcy PK, Smyth MJ, et al. Clinical relevance of host immunity in breast cancer: From TILs to the clinic. Nat Rev Clin Oncol. 2016;13:228–41.

49. Lee HJ, Kim JY, Park IA, Song IH, Yu JH, Ahn JH, et al. Prognostic significance of tumor-infiltrating lymphocytes and the tertiary lymphoid structures in HER2-positive breast cancer treated with adjuvant trastuzumab. Am J Clin Pathol. 2015;144(2):278–88.

50. Salgado R, Denkert C, Campbell C, Savas P, Nuciforo P, Aura C, et al. Tumor-infiltrating lymphocytes and associations with pathological complete response and event-free survival in HER2-positive early-stage breast cancer treated with lapatinib and trastuzumab: A secondary analysis of the NeoALTTO trial. JAMA Oncol. 2015;1(4):448–55.

51. Loi S, Michiels S, Salgado R, Sirtaine N, Jose V, Fumagalli D, et al. Tumor infiltrating lymphocytes are prognostic in triple negative breast cancer and predictive for trastuzumab benefit in early breast cancer: Results from the FinHER trial. Ann Oncol. 2014;25(8):1544–50.

52. Perez EA, Thompson EA, Ballman K V., Anderson SK, Asmann YW, Kalari KR, et al. Genomic analysis reveals that immune function genes are strongly linked to clinical outcome in the North Central Cancer Treatment Group N9831 adjuvant trastuzumab trial. J Clin Oncol. 2015;33(7):701–8.
53. Criscitiello C, Vingiani A, Maisonneuve P, Viale G, Curigliano G. Tumor-infiltrating lymphocytes (TILs) in ER+/HER2− breast cancer. Breast Cancer Res Treat. 2020;183(2):347–54.
54. Prat A, Perou CM. Deconstructing the molecular portraits of breast cancer. Mol Oncol. 2011;5(1):5–23.
55. Sørlie T, Perou CM, Tibshirani R, Aas T, Geisler S, Johnsen H, et al. Gene expression patterns of breast carcinomas distinguish tumor subclasses with clinical implications. Proc Natl Acad Sci. 2001;98(19):10869–74.
56. Perou CM, Sørlie T, Eisen MB, van de Rijn M, Jeffrey SS, Rees CA, et al. Molecular portraits of human breast tumours. Nature. 2000;406.
57. Schettini F, Brasó-Maristany F, Kuderer NM, Prat A. A perspective on the development and lack of interchangeability of the breast cancer intrinsic subtypes. NPJ Breast Cancer. 2022;8(85):1–4.
58. Parker JS, Mullins M, Cheung MCU, Leung S, Voduc D, Vickery T, et al. Supervised risk predictor of breast cancer based on intrinsic subtypes. J Clin Oncol. 2009;27(8):1160–7.
59. Carey LA, Perou CM, Livasy CA, Dressler LG, Cowan D, Conway K, et al. Race, Breast Cancer Subtypes, and Survival in the Carolina Breast Cancer Study. JAMA. 2006;295(21):2492–502.
60. Prat A, Fan C, Fernández A, Hoadley KA, Martinello R, Vidal M, et al. Response and survival of breast cancer intrinsic subtypes following multi-agent neoadjuvant chemotherapy. BMC Med. 2015;13(303):1–11.
61. Llombart-Cussac A, Cortés J, Paré L, Galván P, Bermejo B, Martínez N, et al. HER2-enriched subtype as a predictor of pathological complete response following trastuzumab and lapatinib without chemotherapy in early-stage HER2-positive breast cancer (PAMELA): an open-label, single-group, multicentre, phase 2 trial. Lancet Oncol. 2017;18(4):545–54.

62. Prat A, Cheang MCU, Galván P, Nuciforo P, Paré L, Adamo B, et al. Prognostic Value of Intrinsic Subtypes in Hormone Receptor-Positive Metastatic Breast Cancer Treated With Letrozole With or Without Lapatinib. JAMA Oncol. 2016;2(10):1287–94.
63. Prat A, Pineda E, Adamo B, Galván P, Fernández A, Gaba L, et al. Clinical implications of the intrinsic molecular subtypes of breast cancer. Breast. 2015;24:S26–35.
64. The Cancer Genome Atlas Network. Comprehensive molecular portraits of human breast tumours. Nature. 2012;490(7418):61–70.
65. Cejalvo JM, Pascual T, Fernández-Martínez A, Brasó-Maristany F, Gomis RR, Perou CM, et al. Clinical implications of the non-luminal intrinsic subtypes in hormone receptor-positive breast cancer. Cancer Treat Rev. 2018;67:63–70.
66. Prat A, Cheang MCU, Martín M, Parker JS, Carrasco E, Caballero R, et al. Prognostic significance of progesterone receptor-positive tumor cells within immunohistochemically defined luminal A breast cancer. J Clin Oncol. 2013;31(2):203–9.
67. Kanu N, Cerone MA, Goh G, Zalmas LP, Bartkova J, Dietzen M, et al. DNA replication stress mediates APOBEC3 family mutagenesis in breast cancer. Genome Biol. 2016;17(185):1–15.
68. Prat A, Adamo B, Cheang MCU, Anders CK, Carey LA, Perou CM. Molecular Characterization of Basal-Like and Non-Basal-Like Triple-Negative Breast Cancer. Oncologist. 2013;18(2):123–33.
69. Vidal M, Peg V, Galván P, Tres A, Cortés J, Ramón y Cajal S, et al. Gene expression-based classifications of fibroadenomas and phyllodes tumours of the breast. Mol Oncol. 2015;9(6):1081–90.
70. Koboldt DC, Fulton RS, McLellan MD, Schmidt H, Kalicki-Veizer J, McMichael JF, et al. Comprehensive molecular portraits of human breast tumours. Nature. 2012;490:61–70.
71. Prat A, Parker JS, Karginova O, Fan C, Livasy C, Herschkowitz JI, et al. Phenotypic and molecular characterization of the claudin-low intrinsic subtype of breast cancer. Breast Cancer Res. 2010;12(5):1–18.
72. Cejalvo Andújar JM. Uncovering the molecular and cellular mechanisms of metastatic dormancy in luminal breast cancer: PhD Thesis [Internet]. Barcelona: University of

Barcelona; 2019 [cited 2025 Jul 29]. Available from: https://diposit.ub.edu/dspace/bitstream/2445/152318/1/JMCA_PhD_THESIS.pdf

73. Gupta GP, Massagué J. Cancer Metastasis: Building a Framework. Cell. 2006;127(4):679–95.
74. Chaffer CL, Weinberg RA. A Perspective on Cancer Cell Metastasis. Science (1979). 2011;331:1559–64.
75. Chiang AC, Massagué J. Molecular Basis of Metastasis. N Engl J Med. 2008;359(26):2814–23.
76. Seltzer S, Corrigan M, O'Reilly S. The clinicomolecular landscape of de novo versus relapsed stage IV metastatic breast cancer. Exp Mol Pathol. 2020;114(104404):1–11.
77. Brasó-Maristany F, Paré L, Chic N, Martínez-Sáez O, Pascual T, Mallafré-Larrosa M, et al. Gene expression profiles of breast cancer metastasis according to organ site. Mol Oncol. 2022;16:69–87.
78. Kennecke H, Yerushalmi R, Woods R, Cheang MCU, Voduc D, Speers CH, et al. Metastatic behavior of breast cancer subtypes. J Clin Oncol. 2010;28(20):3271–7.
79. Weil RJ, Palmieri DC, Bronder JL, Stark AM, Steeg PS. Breast Cancer Metastasis to the Central Nervous System. Am J Pathol. 2005;167(4):913–20.
80. Kotecki N, Lefranc F, Devriendt D, Awada A. Therapy of breast cancer brain metastases: challenges, emerging treatments and perspectives. Ther Adv Med Oncol. 2018;10:1–10.
81. Dent R, Hanna WM, Trudeau M, Rawlinson E, Sun P, Narod SA. Pattern of metastatic spread in triple-negative breast cancer. Breast Cancer Res Treat. 2009;115(2):423–8.
82. Weinberg RA. The biology of cancer. 2nd ed. Bochicchio A, Zayatz E, Mickey RK, editors. New York: Garland Science; 2014.
83. Riggio AI, Varley KE, Welm AL. The lingering mysteries of metastatic recurrence in breast cancer. Br J Cancer. 2021;124:13–26.
84. Valastyan S, Weinberg RA. Tumor metastasis: Molecular insights and evolving paradigms. Cell. 2011;147(2):275–92.
85. Luzzi KJ, MacDonald IC, Schmidt EE, Kerkvliet N, Morris VL, Chambers AF, et al. Multistep Nature of Metastatic Inefficiency: Dormancy of Solitary Cells after Successful Extravasation and Limited Survival of Early Micrometastases. Am J Pathol. 1998;153(3):865–73.

86. Kessenbrock K, Plaks V, Werb Z. Matrix Metalloproteinases: Regulators of the Tumor Microenvironment. Cell. 2010;141(1):52–67.
87. Condeelis J, Segall JE. Intravital imaging of cell movement in tumours. Nat Rev Cancer. 2003;3(12):921–30.
88. Thiery JP, Sleeman JP. Complex networks orchestrate epithelial-mesenchymal transitions. Nat Rev Mol Cell Biol. 2006;7:131–42.
89. Yang J, Antin P, Berx G, Blanpain C, Brabletz T, Bronner M, et al. Guidelines and definitions for research on epithelial-mesenchymal transition. Nat Rev Mol Cell Biol. 2020;21:341–52.
90. Janda E, Nevolo M, Lehmann K, Downward J, Beug H, Grieco M. Raf plus TGFB-dependent EMT is initiated by endocytosis and lysosomal degradation of E-cadherin. Oncogene. 2006;25(54):7117–30.
91. Frixen UH, Behrens J, Sachs M, Eberle G, Voss B, Warda A, et al. E-Cadherin-mediated Cell-Cell Adhesion Prevents Invasiveness of Human Carcinoma Cells. J Cell Biol. 1991;113(1):173–85.
92. Batlle E, Sancho E, Francí C, Domínguez D, Monfar M, Baulida J, et al. The transcription factor Snail is a repressor of E-cadherin gene expression in epithelial tumour cells. Nat Cell Biol. 2000;2:84–9.
93. Yang J, Mani SA, Donaher JL, Ramaswamy S, Itzykson RA, Come C, et al. Twist, a Master Regulator of Morphogenesis, Plays an Essential Role in Tumor Metastasis. Cell. 2004;117:927–39.
94. Fontana R, Mestre-Farrera A, Yang J. Update on Epithelial-Mesenchymal Plasticity in Cancer Progression. Annu Rev Pathol. 2024;19:133–56.
95. Friedl P, Wolf K. Tumour-cell invasion and migration: Diversity and escape mechanisms. Nat Rev Cancer. 2003;3(5):362–74.
96. Guo W, Giancotti FG. Integrin signalling during tumour progression. Nat Rev Mol Cell Biol. 2004;5(10):816–26.
97. Joyce JA, Pollard JW. Microenvironmental regulation of metastasis. Nat Rev Cancer. 2009;9(4):239–52.
98. Nieswandt B, Hafner M, Echtenacher B, Männel DN. Lysis of Tumor Cells by Natural Killer Cells in Mice Is Impeded by Platelets. Cancer Res. 1999;59:1295–300.

99. Chambers AF, Groom AC, MacDonald IC. Dissemination and growth of cancer cells in metastatic sites. Nat Rev Cancer. 2002;2(8):563–72.

100. Wong CW, Song C, Grimes MM, Fu W, Dewhirst MW, Muschel RJ, et al. Short Communication Intravascular Location of Breast Cancer Cells after Spontaneous Metastasis to the Lung. Am J Pathol. 2002;161:749–53.

101. Early Breast Cancer Trialists' Collaborative Group (EBCTCG). Effects of chemotherapy and hormonal therapy for early breast cancer on recurrence and 15-year survival: An overview of the randomised trials. Lancet. 2005;365(9472):1687–717.

102. Finn RS, Crown JP, Lang I, Boer K, Bondarenko IM, Kulyk SO, et al. The cyclin-dependent kinase 4/6 inhibitor palbociclib in combination with letrozole versus letrozole alone as first-line treatment of oestrogen receptor-positive, HER2-negative, advanced breast cancer (PALOMA-1/TRIO-18): A randomised phase 2 study. Lancet Oncol. 2015;16(1):25–35.

103. Finn RS, Martin M, Rugo HS, Jones S, Im SA, Gelmon K, et al. Palbociclib and Letrozole in Advanced Breast Cancer. N Engl J Med. 2016;375(20):1925–36.

104. Cristofanilli M, Turner NC, Bondarenko I, Ro J, Im SA, Masuda N, et al. Fulvestrant plus palbociclib versus fulvestrant plus placebo for treatment of hormone-receptor-positive, HER2-negative metastatic breast cancer that progressed on previous endocrine therapy (PALOMA-3): final analysis of the multicentre, double-blind, phase 3 randomised controlled trial. Lancet Oncol. 2016;17(4):425–39.

105. Turner NC, Slamon DJ, Ro J, Bondarenko I, Im SA, Masuda N, et al. Overall Survival with Palbociclib and Fulvestrant in Advanced Breast Cancer. New England Journal of Medicine. 2018;379(20):1926–36.

106. Hortobagyi GN, Stemmer SM, Burris HA, Yap YS, Sonke GS, Paluch-Shimon S, et al. Updated results from MONALEESA-2, a phase III trial of first-line ribociclib plus letrozole versus placebo plus letrozole in hormone receptor-positive, HER2-negative advanced breast cancer. Annals of Oncology. 2018;29(7):1541–7.

107. Slamon DJ, Neven P, Chia S, Fasching PA, De Laurentiis M, Im SA, et al. Phase III Randomized Study of Ribociclib and Fulvestrant in Hormone Receptor-Positive, Human Epidermal Growth Factor Receptor 2-Negative Advanced Breast Cancer: MONALEESA-3. J Clin Oncol. 2018;36(24):2465–72.

108. Im SA, Lu YS, Bardia A, Harbeck N, Colleoni M, Franke F, et al. Overall Survival with Ribociclib plus Endocrine Therapy in Breast Cancer. N Engl J Med. 2019;381(4):307–16.
109. Tripathy D, Im SA, Colleoni M, Franke F, Bardia A, Harbeck N, et al. Ribociclib plus endocrine therapy for premenopausal women with hormone-receptor-positive, advanced breast cancer (MONALEESA-7): a randomised phase 3 trial. Lancet Oncol. 2018;19(7):904–15.
110. Sledge GW, Toi M, Neven P, Sohn J, Inoue K, Pivot X, et al. MONARCH 2: Abemaciclib in combination with fulvestrant in women with HR+/HER2-advanced breast cancer who had progressed while receiving endocrine therapy. Journal of Clinical Oncology. 2017;35(25):2875–84.
111. Sledge GW, Toi M, Neven P, Sohn J, Inoue K, Pivot X, et al. The Effect of Abemaciclib Plus Fulvestrant on Overall Survival in Hormone Receptor-Positive, ERBB2-Negative Breast Cancer That Progressed on Endocrine Therapy - MONARCH 2: A Randomized Clinical Trial. JAMA Oncol. 2020;6(1):116–24.
112. Goetz MP, Toi M, Campone M, Trédan O, Bourayou N, Sohn J, et al. MONARCH 3: Abemaciclib as initial therapy for advanced breast cancer. Journal of Clinical Oncology. 2017;35(32):3638–46.
113. Johnston S, Martin M, Di Leo A, Im SA, Awada A, Forrester T, et al. MONARCH 3 final PFS: a randomized study of abemaciclib as initial therapy for advanced breast cancer. NPJ Breast Cancer. 2019;5:1–8.
114. Slamon DJ, Neven P, Chia S, Fasching PA, De Laurentiis M, Im SA, et al. Overall Survival with Ribociclib plus Fulvestrant in Advanced Breast Cancer. New England Journal of Medicine. 2020;382(6):514–24.
115. Hortobagyi GN, Stemmer SM, Burris HA, Yap YS, Sonke GS, Hart L, et al. Overall Survival with Ribociclib plus Letrozole in Advanced Breast Cancer. N Engl J Med. 2022;386(10):942–50.
116. Goetz MP, Toi M, Huober J, Sohn J, Trédan O, Park IH, et al. Abemaciclib plus a nonsteroidal aromatase inhibitor as initial therapy for HR+, HER2− advanced breast cancer: final overall survival results of MONARCH 3. Annals of Oncology. 2024;35(8):718–27.

117. Patel HK, Bihani T. Selective estrogen receptor modulators (SERMs) and selective estrogen receptor degraders (SERDs) in cancer treatment. Pharmacol Ther. 2018;186:1–24.
118. Aggelis V, Johnston SRD. Advances in Endocrine-Based Therapies for Estrogen Receptor-Positive Metastatic Breast Cancer. Drugs. 2019;79(17):1849–66.
119. Cole M, Jones C, Todd I. A new anti-oestrogenic agent in late breast cancer. An early clinical appraisal of IC146474. Br J Cancer. 1971;25:270–5.
120. Osborne CK, Wakeling A, Nicholson RI. Fulvestrant: An oestrogen receptor antagonist with a novel mechanism of action. Br J Cancer. 2004;90(1 Suppl):S2–6.
121. Bidard FC, Kaklamani VG, Neven P, Streich G, Montero AJ, Forget F, et al. Elacestrant (oral selective estrogen receptor degrader) Versus Standard Endocrine Therapy for Estrogen Receptor-Positive, Human Epidermal Growth Factor Receptor 2-Negative Advanced Breast Cancer: Results From the Randomized Phase III EMERALD Trial. J Clin Oncol. 2022;40(28):3246–56.
122. Walker GA, Xenophontos M, Chen LC, Cheung KL. Long-term efficacy and safety of exemestane in the treatment of breast cancer. Patient Prefer Adherence. 2013;7:245–58.
123. Dowsett M, Cuzick J, Ingle J, Coates A, Forbes J, Bliss J, et al. Meta-analysis of breast cancer outcomes in adjuvant trials of aromatase inhibitors versus tamoxifen. J Clin Oncol. 2010;28(3):509–18.
124. Mauri D, Pavlidis N, Polyzos NP, Ioannidis JPA. Survival with aromatase inhibitors and inactivators versus standard hormonal therapy in advanced breast cancer: Meta-analysis. J Natl Cancer Inst. 2006;98(18):1285–91.
125. Everest HM, Hislop JN, Harding T, Uney JB, Flynn A, Millar RP, et al. Signaling and Antiproliferative Effects Mediated by GnRH Receptors After Expression in Breast Cancer Cells Using Recombinant Adenovirus. Endocrinology. 2001;142(11):4663–72.
126. Huerta-Reyes M, Maya-Núñez G, Pérez-Solis MA, López-Muñoz E, Guillén N, Olivo-Marin JC, et al. Treatment of Breast Cancer With Gonadotropin-Releasing Hormone Analogs. Front Oncol. 2019;9(943):1–17.
127. Cardoso F, Senkus E, Curigliano G, Aapro MS, André F, Barrios CH, et al. 5th ESO-ESMO international consensus guidelines for advanced breast cancer (ABC 5). 2020;31(12):1623–49.

128. Gao JJ, Cheng J, Bloomquist E, Sanchez J, Wedam SB, Singh H, et al. CDK4/6 inhibitor treatment for patients with hormone receptor-positive, HER2-negative, advanced or metastatic breast cancer: a US Food and Drug Administration pooled analysis. Lancet Oncol. 2020;21:250–60.
129. Dickler MN, Tolaney SM, Rugo HS, Cortes J, Dieras V, Patt D, et al. MONARCH 1, a phase II study of abemaciclib, a CDK4 and CDK6 inhibitor, as a single agent, n patients with refractory HR+/HER2- metastatic breast cancer. Clinical Cancer Research. 2017;23(17):5218–24.
130. Cao L, Chen F, Yang X, Xu W, Xie J, Yu L. Phylogenetic analysis of CDK and cyclin proteins in premetazoan lineages. BMC Evol Biol. 2014;14(10):1–16.
131. Ding L, Cao J, Lin W, Chen H, Xiong X, Ao H, et al. The roles of cyclin-dependent kinases in cell-cycle progression and therapeutic strategies in human breast cancer. Int J Mol Sci. 2020;21(1960):1–28.
132. Malumbres M, Barbacid M. Mammalian cyclin-dependent kinases. Trends Biochem Sci. 2005;30(11):630–41.
133. Matsushime H, Quelle DE, Shurtleff SA, Shibuya M, Sherr CJ, Kato JY. D-Type Cyclin-Dependent Kinase Activity in Mammalian Cells. Mol Cell Biol. 1994;14(3):2066–76.
134. Sherr CJ. D-type cyclins. Trends Biochem Sci. 1995;20(5):187–90.
135. Pernas S, Tolaney SM, Winer EP, Goel S. CDK4/6 inhibition in breast cancer: current practice and future directions. Ther Adv Med Oncol. 2018;10:1–15.
136. Watts CKW, Sweeney KJE, Warlters A, Musgrove EA, Sutherland RL. Antiestrogen regulation of cell cycle progression and cyclin D1 gene expression in MCF-7 human breast cancer cells. Breast Cancer Res Treat. 1994;31(1):95–105.
137. Asghar U, Witkiewicz AK, Turner NC, Knudsen ES. The history and future of targeting cyclin-dependent kinases in cancer therapy. Nat Rev Drug Discov. 2015;14(2):130–46.
138. George MA, Qureshi S, Omene C, Toppmeyer DL, Ganesan S. Clinical and Pharmacologic Differences of CDK4/6 Inhibitors in Breast Cancer. Front Oncol. 2021;11(693104).
139. Braal CL, Jongbloed EM, Wilting SM, Mathijssen RHJ, Koolen SLW, Jager A. Inhibiting CDK4/6 in Breast Cancer with Palbociclib, Ribociclib, and Abemaciclib: Similarities and Differences. Drugs. 2021;81:317–31.

140. Dean JL, Thangavel C, McClendon AK, Reed CA, Knudsen ES. Therapeutic CDK4/6 inhibition in breast cancer: Key mechanisms of response and failure. Oncogene. 2010;29:4018–32.
141. Marra A, Curigliano G. Are all cyclin-dependent kinases 4/6 inhibitors created equal? NPJ Breast Cancer. 2019;5(27):1–9.
142. Schettini F, De Santo I, Rea CG, De Placido P, Formisano L, Giuliano M, et al. CDK 4/6 inhibitors as single agent in advanced solid tumors. Front Oncol. 2018;8(608):1–12.
143. Chen P, Lee N V, Hu W, Xu M, Ferre RA, Lam H, et al. Spectrum and degree of CDK drug interactions predicts clinical performance. Mol Cancer Ther. 2016;15(10):2273–81.
144. Tolaney SM, Sahebjam S, Le Rhun E, Bachelot T, Kabos P, Awada A, et al. A phase II study of abemaciclib in patients with brain metastases secondary to hormone receptor-positive breast cancer. Clin Cancer Res. 2020;26(20):5310–9.
145. André F, Ciruelos E, Rubovszky G, Campone M, Loibl S, Rugo HS, et al. Alpelisib for PIK3CA-Mutated, Hormone Receptor-Positive Advanced Breast Cancer. N Engl J Med. 2019;380(20):1929–40.
146. Turner NC, Oliveira M, Howell SJ, Dalenc F, Cortes J, Gomez Moreno HL, et al. Capivasertib in Hormone Receptor–Positive Advanced Breast Cancer. N Engl J Med. 2023;388(22):2058–70.
147. Baselga J, Campone M, Piccart M, Burris HA, Rugo HS, Sahmoud T, et al. Everolimus in Postmenopausal Hormone-Receptor–Positive Advanced Breast Cancer. N Engl J Med. 2012;366(6):520–9.
148. Birrer MJ, Moore KN, Betella I, Bates RC. Antibody-Drug Conjugate-Based Therapeutics: State of the Science. J Natl Cancer Inst. 2019;111(6):538–49.
149. Grairi M, Le Borgne M. Antibody–drug conjugates: prospects for the next generation. Drug Discov Today. 2024;29(12):1–11.
150. Goldenberg DM, Stein R, Sharkey RM. The emergence of trophoblast cell-surface antigen 2 (TROP-2) as a novel cancer target. Oncotarget. 2018;9(48):28989–9006.
151. Mathijssen RHJ, van Alphen RJ, Verweij J, Loos WJ, Nooter K, Stoter G, et al. Clinical Pharmacokinetics and Metabolism of Irinotecan (CPT-11). Clin Cancer Res. 2001;7:2182–94.

152. Vidula N, Yau C, Rugo HS. Trop2 gene expression (Trop2e) in primary breast cancer (BC): Correlations with clinical and tumor characteristics. J Clin Oncol. 2017;35(15 Suppl):1075.
153. Ambrogi F, Fornili M, Boracchi P, Trerotola M, Relli V, Simeone P, et al. Trop-2 is a determinant of breast cancer survival. PLoS One. 2014;9(5):e96993.
154. Bardia A, Tolaney SM, Punie K, Loirat D, Oliveira M, Kalinsky K, et al. Biomarker analyses in the phase III ASCENT study of sacituzumab govitecan versus chemotherapy in patients with metastatic triple-negative breast cancer. Ann Oncol. 2021;32(9):1148–56.
155. Rugo HS, Bardia A, Marmé F, Cortes J, Schmid P, Loirat D, et al. Sacituzumab Govitecan in Hormone Receptor-Positive/Human Epidermal Growth Factor Receptor 2-Negative Metastatic Breast Cancer. J Clin Oncol. 2022;40(29):3365–76.
156. Bardia A, Krop IE, Kogawa T, Juric D, Tolcher AW, Hamilton EP, et al. Datopotamab Deruxtecan in Advanced or Metastatic HR+/HER2- and Triple-Negative Breast Cancer: Results from the Phase I TROPION-PanTumor01 Study. J Clin Oncol. 2024;42(19):2281–94.
157. Bardia A, Jhaveri K, Im SA, Pernas S, De Laurentiis M, Wang S, et al. Datopotamab Deruxtecan Versus Chemotherapy in Previously Treated Inoperable/Metastatic Hormone Receptor–Positive Human Epidermal Growth Factor Receptor 2–Negative Breast Cancer: Primary Results From TROPION-Breast01. J Clin Oncol. 2024;43(3):285–96.
158. Barroso-Sousa R, Tolaney SM. Clinical Development of New Antibody–Drug Conjugates in Breast Cancer: To Infinity and Beyond. BioDrugs. 2021;35:159–74.
159. Nakada T, Sugihara K, Jikoh T, Abe Y, Agatsuma T. The Latest Research and Development into the Antibody-Drug Conjugate, [fam-] Trastuzumab Deruxtecan (DS-8201a), for HER2 Cancer Therapy. Chem Pharm Bull (Tokyo). 2019;67(3):173–85.
160. Modi S, Jacot W, Yamashita T, Sohn J, Vidal M, Tokunaga E, et al. Trastuzumab Deruxtecan in Previously Treated HER2-Low Advanced Breast Cancer. N Engl J Med. 2022;387(1):9–20.
161. Bardia A, Hu X, Dent R, Yonemori K, Barrios CH, O'Shaughnessy JA, et al. Trastuzumab Deruxtecan after Endocrine Therapy in Metastatic Breast Cancer. N Engl J Med. 2024;391(22):2110–22.

162. Pistilli B, Pierotti L, Lacroix-Triki M, Vicier C, Frenel JS, D'Hondt V, et al. Efficacy, safety and biomarker analysis of ICARUS-BREAST01: A phase II study of patritumab deruxtecan (HER3-DXd) in patients (pts) with HR+/HER2- advanced breast cancer (ABC). Ann Oncol. 2024;35(2 Suppl):S357.
163. Tolaney SM, D'Amico P, Jia L, Hirshfield KM, Cardoso F. Phase III, randomized, open-label TroFuse-010 Study of sacituzumab tirumotecan (sac-TMT) alone and with pembrolizumab vs treatment of physician's choice chemotherapy (TPC) in patients with HR+/HER2- unresectable locally advanced or metastatic breast cancer. Ann Oncol. 2024;35(2 Suppl):S402.
164. Schmid P, Wysocki PJ, Ma CX, Park YH, Fernandes R, Lord S, et al. SKB264 (MK-2870) in previously treated hormone receptor-positive (HR+)/ HER2-negative metastatic breast cancer (mBC): Results from a phase I/II, single-arm, basket trial. Ann Oncol. 2023;34(2 Suppl):S337.
165. Banerji U, van Herpen CML, Saura C, Thistlethwaite F, Lord S, Moreno V, et al. Trastuzumab duocarmazine in locally advanced and metastatic solid tumours and HER2-expressing breast cancer: a phase 1 dose-escalation and dose-expansion study. Lancet Oncol. 2019;20(8):1124–35.
166. Jiang Z, Sun T, Wang X, Liu Q, Yan M, Tong Z, et al. A multiple center, open-label, single-arm, phase II clinical trial of MRG002, an HER2-targeted antibody-drug conjugate, in patients with HER2-low expressing advanced or metastatic breast cancer. J Clin Oncol. 2022;40(16 Suppl):1102.
167. Qu F, Li W, Yi Y. Efficacy and safety of the recombinant humanized anti-HER2 monoclonal antibody-MMAE conjugate RC48-ADC in patients with HER2-positive and HER2-low expressing, locally advanced or metastatic breast cancer: A single-arm phase II study. Ann Oncol. 2023;34(2 Suppl):S348.
168. Grinda T, Rassy E, Pistilli B. Antibody–Drug Conjugate Revolution in Breast Cancer: The Road Ahead. Curr Treat Options Oncol. 2023;24(5):442–65.
169. Abelman RO, Wu B, Barnes H, Medford A, Norden B, Putur A, et al. TOP1 Mutations and Cross-Resistance to Antibody–Drug Conjugates in Patients with Metastatic Breast Cancer. Clinical Cancer Research. 2025;31(10):1966–74.

170. Cejalvo JM, De Dueñas EM, Galván P, García-Recio S, Gasión OB, Paré L, et al. Intrinsic subtypes and gene expression profiles in primary and metastatic breast cancer. Cancer Res. 2017;77(9):2213–21.
171. Aftimos P, Oliveira M, Irrthum A, Fumagalli D, Sotiriou C, Gal-Yam EN, et al. Genomic and transcriptomic analyses of breast cancer primaries and matched metastases in AURORA, the breast international group (BIG) molecular screening initiative. Cancer Discov. 2021;11:2796–811.
172. Falato C, Schettini F, Pascual T, Brasó-Maristany F, Prat A. Clinical implications of the intrinsic molecular subtypes in hormone receptor-positive and HER2-negative metastatic breast cancer. Cancer Treat Rev. 2023 Jan;112(102496):1–15.
173. Jørgensen CLT, Larsson AM, Forsare C, Aaltonen K, Jansson S, Bradshaw R, et al. PAM50 intrinsic subtype profiles in primary and metastatic breast cancer show a significant shift toward more aggressive subtypes with prognostic implications. Cancers (Basel). 2021;13(1592):1–18.
174. Denkert C, Rachakonda S, Karn T, Weber K, Martin M, Marmé F, et al. Dynamics of molecular heterogeneity in high-risk luminal breast cancer—From intrinsic to adaptive subtyping. Cancer Cell. 2025;43(2):232–47.
175. Johnston S, Pippen J, Pivot X, Lichinitser M, Sadeghi S, Dieras V, et al. Lapatinib combined with letrozole versus letrozole and placebo as first-line therapy for postmenopausal hormone receptor-positive metastatic breast cancer. J Clin Oncol. 2009;27(33):5538–46.
176. Ciruelos E, Saura C, Gonzalez-Farré X, Salvador Bofill FJ, Vidal M, Blancas I, et al. SOLTI-1718 NEREA Trial: Neratinib in hormone receptor (HR)-positive/HER2-negative HER2-enriched (HER2-E) advanced breast cancer (BC). Cancer Res. 2024;84(9 Suppl):P030507.
177. Prat A, Brase JC, Cheng Y, Nuciforo P, Paré L, Pascual T, et al. Everolimus plus Exemestane for Hormone Receptor-Positive Advanced Breast Cancer: A PAM50 Intrinsic Subtype Analysis of BOLERO-2. Oncologist. 2019;24:893–900.
178. Finn RS, Liu Y, Zhu Z, Martin M, Rugo HS, Dieras V, et al. Biomarker analyses of response to cyclin-dependent kinase 4/6 inhibition and endocrine therapy in women with treatment-naïve metastatic breast cancer. Clin Cancer Res. 2020;26(1):110–21.

179. Ma CX, Gao F, Luo J, Northfelt DW, Goetz M, Forero A, et al. NeoPalAna: Neoadjuvant palbociclib, a cyclin-dependent kinase 4/6 inhibitor, and anastrozole for clinical stage 2 or 3 estrogen receptor-positive breast cancer. Clin Cancer Res. 2017;23(15):4055–65.
180. Prat A, Chaudhury A, Solovieff N, Pare L, Martinez D, Chic N, et al. Correlative Biomarker Analysis of Intrinsic Subtypes and Efficacy Across the MONALEESA Phase III Studies. J Clin Oncol. 2021;39(13):148–1467.
181. Ciruelos E, Villagrasa P, Pascual T, Oliveira M, Pernas S, Paré L, et al. Palbociclib and trastuzumab in HER2-positive advanced breast cancer: Results from the phase II SOLTI-1303 PATRICIA trial. Clin Cancer Res. 2020;26(22):5820–9.
182. Prat A, Solovieff N, André F, O'Shaughnessy J, Cameron DA, Janni W, et al. Intrinsic Subtype and Overall Survival of Patients with Advanced HR+/HER2- Breast Cancer Treated with Ribociclib and ET: Correlative Analysis of MONALEESA-2, -3, -7. Clin Cancer Res. 2024;30(4):793–802.
183. Schäffler H, Mergel F, Pfister K, Lukac S, Fink A, Veselinovic K, et al. The Clinical Relevance of the NATALEE Study: Application of the NATALEE Criteria to a Real-World Cohort from Two Large German Breast Cancer Centers. Int J Mol Sci. 2023;24(22):16366.
184. Slamon DJ, Fasching PA, Hurvitz S, Chia S, Crown J, Martín M, et al. Rationale and trial design of NATALEE: a Phase III trial of adjuvant ribociclib + endocrine therapy versus endocrine therapy alone in patients with HR+/HER2− early breast cancer. Ther Adv Med Oncol. 2023;15:1–16.
185. Loibl S, Marmé F, Martin M, Untch M, Bonnefoi H, Kim SB, et al. Palbociclib for residual high-risk invasive HR-positive and HER2-negative early breast cancer-the penelope-B trial. J Clin Oncol. 2021;39(14):1518–30.
186. Gnant M, Dueck AC, Frantal S, Martin M, Burstein HJ, Greil ; Richard, et al. Adjuvant Palbociclib for Early Breast Cancer: The PALLAS Trial Results (ABCSG-42/AFT-05/BIG-14-03). J Clin Oncol. 2021;40(3):282–93.
187. Pascual T, Stover DG, Thuerigen A, Sanchez-Bayona R, Perou CM, Ciruelos EM, et al. Ribociclib (RIB) vs. palbociclib (PAL) in patients (pts) with hormone receptor-positive/HER2-negative/HER2-enriched (HR+/HER2-/HER2-E) advanced breast cancer (ABC): A head-to-head phase III study-HARMONIA SOLTI-2101/AFT-58. J Clin Oncol. 2023;41(16 Suppl):1125.

188. Schettini F, Martínez-Sáez O, Falato C, De Santo I, Conte B, Garcia-Fructuoso I, et al. Prognostic value of intrinsic subtypes in hormone-receptor-positive metastatic breast cancer: systematic review and meta-analysis. ESMO Open. 2023;8(3):1–10.
189. Prat A, Pascual T, Muñoz M, Hernando C, Vazquez S, Blanch S, et al. TATEN TRIAL (SOLTI-1716) Targeting non-Luminal disease by PAM50 with pembrolizumab + paclitaxel in Hormone Receptor-positive/HER2-negative (HR+/HER2-) metastatic breast cancer (MBC): interim analysis. Cancer Res. 2023;83(5 Suppl):P30602.
190. Pandey K, An HJ, Kim SK, Lee SA, Kim S, Lim SM, et al. Molecular mechanisms of resistance to CDK4/6 inhibitors in breast cancer: A review. Int J Cancer. 2019;145:1179–88.
191. Condorelli R, Spring L, O'Shaughnessy J, Lacroix L, Bailleux C, Scott V, et al. Polyclonal RB1 mutations and acquired resistance to CDK 4/6 inhibitors in patients with metastatic breast cancer. Ann Oncol. 2018;29:640–5.
192. Herrera-Abreu MT, Palafox M, Asghar U, Rivas MA, Cutts RJ, Garcia-Murillas I, et al. Early adaptation and acquired resistance to CDK4/6 inhibition in estrogen receptor-positive breast cancer. Cancer Res. 2016;76(8):2301–13.
193. Malorni L, Piazza S, Ciani Y, Guarducci C, Bonechi M, Biagioni C, et al. A gene expression signature of retinoblastoma loss-of-function is a predictive biomarker of resistance to palbociclib in breast cancer cell lines and is prognostic in patients with ER positive early breast cancer. Oncotarget. 2016;7(42):68012–22.
194. Guarducci C, Bonechi M, Benelli M, Biagioni C, Boccalini G, Romagnoli D, et al. Cyclin E1 and Rb modulation as common events at time of resistance to palbociclib in hormone receptor-positive breast cancer. NPJ Breast Cancer. 2018;4(38):1–10.
195. Romagosa C, Simonetti S, López-Vicente L, Mazo A, Lleonart ME, Castellvi J, et al. p16Ink4a overexpression in cancer: A tumor suppressor gene associated with senescence and high-grade tumors. Oncogene. 2011;30:2087–97.
196. Dean JL, McClendon AK, Hickey TE, Butler LM, Tilley WD, Witkiewicz AK, et al. Therapeutic response to CDK4/6 inhibition in breast cancer defined by ex vivo analyses of human tumors. Cell Cycle. 2012;11(14):2756–61.
197. Olanich ME, Sun W, Hewitt SM, Abdullaev Z, Pack SD, Barr FG. CDK4 amplification reduces sensitivity to CDK4/6 inhibition in fusion-positive rhabdomyosarcoma. Clin Cancer Res. 2016;21(21):4947–59.

198. Yang C, Li Z, Bhatt T, Dickler M, Giri D, Scaltriti M, et al. Acquired CDK6 amplification promotes breast cancer resistance to CDK4/6 inhibitors and loss of ER signaling and dependence. Oncogene. 2017;36:2255–64.
199. Guarducci C, Nardone A, Feiglin A, Migliaccio I, Malorni L, Bonechi M, et al. Inhibition of CDK7 overcomes resistance to CDK4/6 inhibitors in hormone receptor positive breast cancer cells. Cancer Res. 2019;79(4 Suppl):PD712.
200. Turner NC, Liu Y, Zhu Z, Loi S, Colleoni M, Loibl S, et al. Cyclin E1 expression and palbociclib efficacy in previously treated hormone receptor-positive metastatic breast cancer. J Clin Oncol. 2019;37(14):1169–78.
201. Chandarlapaty S, Razavi P. Cyclin e mRNA: Assessing cyclin-dependent kinase (CDK) activation state to elucidate breast cancer resistance to CDK4/6 Inhibitors. J Clin Oncol. 2019;37(14):1148–50.
202. Brooks AN, Kilgour E, Smith PD. Molecular pathways: Fibroblast growth factor signaling: A new therapeutic opportunity in cancer. Clin Cancer Res. 2012;18(7):1855–62.
203. Mao P, Cohen O, Kowalski KJ, Kusiel JG, Buendia-Buendia JE, Cuoco MS, et al. Acquired FGFR and FGF alterations confer resistance to Estrogen Receptor (ER) targeted therapy in ER+ metastatic breast cancer. Clin Cancer Res. 2020;26:5974–89.
204. Formisano L, Lu Y, Servetto A, Hanker AB, Jansen VM, Bauer JA, et al. Aberrant FGFR signaling mediates resistance to CDK4/6 inhibitors in ER+ breast cancer. Nat Commun. 2019;10(1373).
205. Sobhani N, Fassl A, Mondani G, Generali D, Otto T. Targeting aberrant FGFR signaling to overcome CDK4/6 inhibitor resistance in breast cancer. Cells. 2021;10(293):1–14.
206. Jansen VM, Bhola NE, Bauer JA, Formisano L, Lee KM, Hutchinson KE, et al. Kinome-wide RNA interference screen reveals a role for PDK1 in acquired resistance to CDK4/6 inhibition in ER-positive breast cancer. Cancer Res. 2017;77(9):2488–99.
207. Iida M, Nakamura M, Tokuda E, Niwa T, Ishida T, Hayashi SI. CDK6 might be a key factor for efficacy of CDK4/6 inhibitor and the hormone sensitivity following acquired resistance. Cancer Res. 2018;78(4 Suppl):P60402.
208. O'Brien T, Xiao Y, Ong C, Daemen A, Friedman L. Identification of preclinical mechanisms driving acquired resistance to selective ERa degraders (SERDs), CDK4/6 inhibitors, or to combinations of both agents. Cancer Res. 2017;77(4 Suppl):P30424.

209. Iida M, Toyosawa D, Nakamura M, Tsuboi K, Tokuda E, Niwa T, et al. Decreased ER dependency after acquired resistance to CDK4/6 inhibitors. Breast Cancer. 2020;27:963–72.
210. Michaloglou C, Crafter C, Siersbaek R, Delpuech O, Curwen JO, Carnevalli LS, et al. Combined inhibition of mTOR and CDK4/6 is required for optimal blockade of E2F function and long-term growth inhibition in estrogen receptor-positive breast cancer. Mol Cancer Ther. 2018;17(5):908–20.
211. Vora SR, Juric D, Kim N, Mino-Kenudson M, Huynh T, Costa C, et al. CDK 4/6 Inhibitors Sensitize PIK3CA Mutant Breast Cancer to PI3K Inhibitors. Cancer Cell. 2014;26(1):136–49.
212. Scheiblecker L, Kollmann K, Sexl V. CDK4/6 and MAPK-crosstalk as opportunity for cancer treatment. Pharmaceuticals. 2020;13(418):1–26.
213. De Blander H, Morel AP, Senaratne AP, Ouzounova M, Puisieux A, Frisch SM. Cellular Plasticity: A Route to Senescence Exit and Tumorigenesis. Cancers (Basel). 2021;13(4561):1–17.
214. He S, Sharpless NE. Senescence in Health and Disease. Cell. 2017;169(6):1000–11.
215. Wang B, Kohli J, Demaria M. Senescent Cells in Cancer Therapy: Friends or Foes? Trends Cancer. 2020;6(10):838–57.
216. Faget D V., Ren Q, Stewart SA. Unmasking senescence: context-dependent effects of SASP in cancer. Nat Rev Cancer. 2019;19:439–53.
217. Prat A, Carey LA, Adamo B, Vidal M, Tabernero J, Cortés J, et al. Molecular features and survival outcomes of the intrinsic subtypes within HER2-positive breast cancer. J Natl Cancer Inst. 2014;106(8).
218. Garcia-Recio S, Thennavan A, East MP, Parker JS, Cejalvo JM, Garay JP, et al. FGFR4 regulates tumor subtype differentiation in luminal breast cancer and metastatic disease. J Clin Invest. 2020;130(9):4871–87.
219. Hohmann L, Sigurjonsdottir K, Campos AB, Nacer DF, Veerla S, Rosengren F, et al. Genomic characterization of the HER2-enriched intrinsic molecular subtype in primary ER-positive HER2-negative breast cancer. Nat Commun. 2025;16(2208):1–17.
220. Ding K, Chen L, Levine KM, Sikora MJ, Tasdemir N, Dabbs D, et al. FGFR4 in endocrine resistance: overexpression and estrogen regulation without direct causative role. Breast Cancer Res Treat. 2025;211:501–15.

221. De Moerlooze L, Spencer-Dene B, Revest JM, Hajihosseini M, Rosewell I, Dickson C. An important role for the IIIb isoform of fibroblast growth factor receptor 2 (FGFR2) in mesenchymal-epithelial signalling during mouse organogenesis. Development. 2000;127:483–92.
222. Yamaguchi TP, Harpal K, Henkemeyer M, Rossant J. fgfr-1 is required for embryonic growth and mesodermal patterning during mouse gastrulation. Genes Dev. 1994;8:3032–44.
223. El Agha E, Kosanovic D, Schermuly RT, Bellusci S. Role of fibroblast growth factors in organ regeneration and repair. Semin Cell Dev Biol. 2016;53:76–84.
224. Turner N, Grose R. Fibroblast growth factor signalling: From development to cancer. Nat Rev Cancer. 2010;10:116–29.
225. Beenken A, Mohammadi M. The FGF family: biology, pathophysiology and therapy. Nat Rev Drug Discov. 2009;8(3):235–53.
226. Mohammadi M, Olsen SK, Ibrahimi OA. Structural basis for fibroblast growth factor receptor activation. Cytokine Growth Factor Rev. 2005;16:107–37.
227. Kurosu H, Choi M, Ogawa Y, Dickson AS, Goetz R, Eliseenkova A V, et al. Tissue-specific Expression of βKlotho and Fibroblast Growth Factor (FGF) Receptor Isoforms Determines Metabolic Activity of FGF19 and FGF21. J Biol Chem. 2007;282(37):26687–95.
228. Eswarakumar VP, Lax I, Schlessinger J. Cellular signaling by fibroblast growth factor receptors. Cytokine Growth Factor Rev. 2005;16:139–49.
229. Thien CBF, Langdon WY. CBL: Many adaptations to regulate tyrosine kinases. Nat Rev Mol Cell Biol. 2001;2:294–305.
230. Fürthauer M, Lin W, Ang SL, Thisse B, Thisse C. Sef is a feedback-induced antagonist of Ras/MAPK-mediated FGF signalling. Nat Cell Biol. 2002;4(2):170–4.
231. Casci T, Vinó J, Freeman M. Sprouty, an Intracellular Inhibitor of Ras Signaling. Cell. 1999;96:655–65.
232. Zhao Y, Zhang ZY. The Mechanism of Dephosphorylation of Extracellular Signal-regulated Kinase 2 by Mitogen-activated Protein Kinase Phosphatase 3. J Biol Chem. 2001;276(34):32382–91.
233. Kostrzewa M, Muller U. Genomic structure and complete sequence of the human FGFR4 gene. Mamm Genome. 1998;9:131–5.

234. Levine KM, Ding K, Chen L, Oesterreich S. FGFR4: A promising therapeutic target for breast cancer and other solid tumors. Pharmacol Ther. 2020;214(107590):1–13.
235. Thisse B, Thisse C. Functions and regulations of fibroblast growth factor signaling during embryonic development. Dev Biol. 2005;287:390–402.
236. Holt JA, Luo G, Billin AN, Bisi J, McNeill YY, Kozarsky KF, et al. Definition of a novel growth factor-dependent signal cascade for the suppression of bile acid biosynthesis. Genes Dev. 2003;17:1581–91.
237. Yu C, Wang F, Kan M, Jin C, Jones RB, Weinstein M, et al. Elevated cholesterol metabolism and bile acid synthesis in mice lacking membrane tyrosine kinase receptor FGFR4. J Biol Chem. 2000;275(20):15482–9.
238. Zhao P, Caretti G, Mitchell S, Mckeehan WL, Boskey AL, Pachman LM, et al. Fgfr4 is required for effective muscle regeneration in vivo: Delineation of a MyoD-Tead2-Fgfr4 transcriptional pathway. J Biol Chem. 2006;281(1):429–38.
239. Helsten T, Elkin S, Arthur E, Tomson BN, Carter J, Kurzrock R. The FGFR landscape in cancer: Analysis of 4,853 tumors by next-generation sequencing. Clin Cancer Res. 2016;22(1):259–67.
240. Levine KM, Priedigkeit N, Basudan A, Tasdemir N, Sikora MJ, Sokol ES, et al. FGFR4 overexpression and hotspot mutations in metastatic ER+ breast cancer are enriched in the lobular subtype. NPJ Breast Cancer. 2019;5(1).
241. Wei W, You Z, Sun S, Wang Y, Zhang X, Pang D, et al. Prognostic implications of fibroblast growth factor receptor 4 polymorphisms in primary breast cancer. Mol Carcinog. 2018;57:988–96.
242. Ziegler M, Khoury N, Hommerich LM, Adler H, Loges S. Functional Characterization of Variants of Unknown Significance of Fibroblast Growth Factor Receptors 1-4 and Comparison With AI Model–Based Prediction. JCO Precis Oncol. 2025;9(e2400847):1–16.
243. Hagel M, Miduturu C, Sheets M, Rubin N, Weng W, Stransky N, et al. First selective small molecule inhibitor of FGFR4 for the treatment of hepatocellular carcinomas with an activated FGFR4 signaling pathway. Cancer Discov. 2015;5(4):424–37.
244. Kim RD, Sarker D, Meyer T, Yau T, Macarulla T, Park JW, et al. First-in-human phase I study of fisogatinib (BLU-554) validates aberrant FGF19 signaling as a driver event in hepatocellular carcinoma. Cancer Discov. 2019;9:1696–707.

245. Ruggeri B, Stubbs M, Yang Y, Juvekar A, Lu L, Condon S, et al. The novel FGFR4-selective inhibitor INCB062079 is efficacious in models of hepatocellular carcinoma harboring FGF19 amplification. Cancer Res. 2017;77(13 Suppl):1234.
246. Liu P, Lu L, Bowman K, Stubbs MC, Wu L, DiMatteo D, et al. Selective inhibition of FGFR4 by INCB062079 is efficacious in models of FGF19- and FGFR4-dependent cancers. Cancer Res. 2017;77(13 Suppl):2100.
247. Harding JJ, Jungels C, Machiels JP, Smith DC, Walker C, Ji T, et al. First-in-Human Study of INCB062079, a Fibroblast Growth Factor Receptor 4 Inhibitor, in Patients with Advanced Solid Tumors. Target Oncol. 2023;18:181–93.
248. Joshi JJ, Coffey H, Corcoran E, Tsai J, Huang CL, Ichikawa K, et al. H3B-6527 Is a potent and selective inhibitor of FGFR4 in FGF19-Driven hepatocellular carcinoma. Cancer Res. 2017;77(24):6999–7013.
249. Macarulla T, Moreno V, Chen LT, Sawyer MB, Goyal L, Muñoz Martín AJ. Phase I study of H3B-6527 in hepatocellular carcinoma (HCC) or intrahepatic cholangiocarcinoma (ICC). J Clin Oncol. 2021;39(15 Suppl):4090.
250. Weiss A, Adler F, Buhles A, Stamm C, Fairhurst RA, Kiffe M, et al. FGF401, A First-In-Class Highly Selective and Potent FGFR4 Inhibitor for the Treatment of FGF19-Driven Hepatocellular Cancer. Mol Cancer Ther. 2019;18(12):2194–206.
251. Chan SL, Schuler M, Kang YK, Yen CJ, Edeline J, Choo SP, et al. A first-in-human phase 1/2 study of FGF401 and combination of FGF401 with spartalizumab in patients with hepatocellular carcinoma or biomarker-selected solid tumors. J Exp Clin Cancer Res. 2022;41(189):1–19.
252. Taylor VI JG, Cheuk AT, Tsang PS, Chung JY, Song YK, Desai K, et al. Identification of FGFR4-activating mutations in human rhabdomyosarcomas that promote metastasis in xenotransplanted models. J Clin Invest. 2009;119(11):3395–407.
253. Xiao W, Xu L, Wang J, Yu K, Xu B, Que Y, et al. FGFR4-specific CAR-T cells with inducible caspase-9 suicide gene as an approach to treat rhabdomyosarcoma. Cancer Gene Ther. 2024;31:1571–84.
254. Cheuk A, Shivaprasad N, Skarzynski M, Baskar S, Azorsa P, Khan J. Anti-FGFR4 antibody drug conjugate for immune therapy of rhabdomyosarcoma and hepatocellular carcinoma. Cancer Res. 2018;78(13 Suppl):5618.

255. Schettini F, Barbao P, Brasó-Maristany F, Galván P, Martínez D, Paré L, et al. Identification of cell surface targets for CAR-T cell therapies and antibody–drug conjugates in breast cancer. ESMO Open. 2021;6(3):1–12.
256. Prat A, Saura C, Pascual T, Hernando C, Muñoz M, Paré L, et al. Ribociclib plus letrozole versus chemotherapy for postmenopausal women with hormone receptor-positive, HER2-negative, luminal B breast cancer (CORALLEEN): an open-label, multicentre, randomised, phase 2 trial. Lancet Oncol. 2020 Jan;21:33–43.
257. Tian M, Wei JS, Shivaprasad N, Highfill SL, Gryder BE, Milewski D, et al. Preclinical development of a chimeric antigen receptor T cell therapy targeting FGFR4 in rhabdomyosarcoma. Cell Rep Med. 2023;4(10):1–14.
258. Fitzgibbons PL, Connolly JL. Template for Reporting Results of Biomarker Testing of Specimens from Patients with Carcinoma of the Breast [Internet]. 2023. Available from: www.cap.org/cancerprotocols
259. Brasó-Maristany F, Griguolo G, Pascual T, Paré L, Nuciforo P, Llombart-Cussac A, et al. Phenotypic changes of HER2-positive breast cancer during and after dual HER2 blockade. Nat Commun. 2020;11(385):1–11.
260. Gallinari P, Paolini C, Filocamo G, Brunetti M, Lahm A, Grunert HF, et al. WO 2019/034427 A1. 2019.
261. Dennis M, Desnoyers L, French D. WO 2012/138975 A1. 2012.
262. Reimar A, Keisuke F, Tanja L, Johannes B, Ichiro W, Shinko H, et al. WO 2016/023894 A1. 2016.
263. Wilkinson I, Anderson S, Fry J, Julien LA, Neville D, Qureshi O, et al. Fc-engineered antibodies with immune effector functions completely abolished. PLoS One. 2021;16(12):1–26.
264. Raybould MIJ, Marks C, Krawczyk K, Taddese B, Nowak J, Lewis AP, et al. Five computational developability guidelines for therapeutic antibody profiling. Proc Natl Acad Sci U S A. 2019;116(10):4025–30.
265. Freund A, Laberge RM, Demaria M, Campisi J. Lamin B1 loss is a senescence-associated biomarker. Mol Biol Cell. 2012;23(11):2066–75.
266. Shimi T, Butin-Israeli V, Adam SA, Hamanaka RB, Goldman AE, Lucas CA, et al. The role of nuclear lamin B1 in cell proliferation and senescence. Genes Dev. 2011;25(24):2579–93.

267. Dimri GP, Lee X, Basile G, Acosta M, Scott G, Roskelley C, et al. A biomarker that identifies senescent human cells in culture and in aging skin in vivo. Proc Natl Acad Sci U S A. 1995;92(20):9363–7.
268. Lorman-Carbó N, Martínez-Sáez O, Fernandez-Martinez A, Galván P, Chic N, Garcia-Fructuoso I, et al. Comparative biological activity of palbociclib and ribociclib in hormone receptor-positive breast cancer. Sci Rep. 2024;14(16030):1–10.
269. Roidl A, Foo P, Wong W, Mann C, Bechtold S, Berger HJ, et al. The FGFR4 Y367C mutant is a dominant oncogene in MDA-MB453 breast cancer cells. Oncogene. 2010;29:1543–52.
270. Doronina SO, Toki BE, Torgov MY, Mendelsohn BA, Cerveny CG, Chace DF, et al. Development of potent monoclonal antibody auristatin conjugates for cancer therapy. Nat Biotechnol. 2003;21(7):778–941.
271. Li F, Emmerton KK, Jonas M, Zhang X, Miyamoto JB, Setter JR, et al. Intracellular released payload influences potency and bystander-killing effects of antibody-drug conjugates in preclinical models. Cancer Res. 2016;76(9):2710–9.
272. Doronina SO, Mendelsohn BA, Bovee TD, Cerveny CG, Alley SC, Meyer DL, et al. Enhanced activity of monomethylauristatin F through monoclonal antibody delivery: Effects of linker technology on efficacy and toxicity. Bioconjug Chem. 2006;17(1):114–24.
273. Giugliano F, Corti C, Tarantino P, Michelini F, Curigliano G. Bystander effect of antibody–drug conjugates: fact or fiction? Curr Oncol Rep. 2022;24:809–17.
274. Grinshpun A, Tolaney SM, Burstein HJ, Jeselsohn R, Mayer EL. The dilemma of selecting a first line CDK4/6 inhibitor for hormone receptor-positive/HER2-negative metastatic breast cancer. NPJ Breast Cancer. 2023;9(15):1–4.
275. Michaels E, Wander SA. POLARIS and Emerging Translational Efforts to Interrogate the Genomic Landscape of CDK4/6 Inhibitor Resistance. JCO Precis Oncol. 2025;(9).
276. Finn RS, Rugo HS, Dieras VC, Harbeck N, Im SA, Gelmon KA, et al. Overall survival (OS) with first-line palbociclib plus letrozole (PAL+LET) versus placebo plus letrozole (PBO+LET) in women with estrogen receptor–positive/human epidermal growth factor receptor 2–negative advanced breast cancer (ER+/HER2− ABC): Analyses from PALOMA-2. J Clin Oncol. 2022;40(17 Suppl):1003.

277. Metzger O, Mandrekar S, Demichele A, Gianni L, Gligorov J, Lim E, et al. AFT-38 PATINA: A randomized, open label, phase III trial to evaluate the efficacy and safety of palbociclib + anti-HER2 + endocrine therapy vs anti-HER2 therapy + endocrine therapy after induction treatment for hormone receptor-positive (HR+)/HER2-positive metastatic breast cancer. San Antonio, TX; 2024 Dec.
278. Saleh T, Alhesa A, El-Sadoni M, Shahin NA, Alsharaiah E, Shboul S Al, et al. The Expression of the Senescence-Associated Biomarker Lamin B1 in Human Breast Cancer. Diagnostics. 2022;12(3):1–14.
279. Matias I, Diniz LP, Damico IV, Araujo APB, Neves L da S, Vargas G, et al. Loss of lamin-B1 and defective nuclear morphology are hallmarks of astrocyte senescence in vitro and in the aging human hippocampus. Aging Cell. 2022;21(e13521):1–18.
280. Wang AS, Ong PF, Chojnowski A, Clavel C, Dreesen O. Loss of lamin B1 is a biomarker to quantify cellular senescence in photoaged skin. Sci Rep. 2017;7(15678):1–8.
281. Wells CI, Vasta JD, Corona CR, Wilkinson J, Zimprich CA, Ingold MR, et al. Quantifying CDK inhibitor selectivity in live cells. Nat Commun. 2020;11(2743):1–11.
282. Hafner M, Mills CE, Subramanian K, Chen C, Chung M, Boswell SA, et al. Multiomics Profiling Establishes the Polypharmacology of FDA-Approved CDK4/6 Inhibitors and the Potential for Differential Clinical Activity. Cell Chem Biol. 2019;26(8):1067-1080.e8.
283. Finn R, Liu Y, Martin M, Rugo H, Dieras V, Im SA, et al. Comprehensive gene expression biomarker analysis of CDK 4/6 and endocrine pathways from the PALOMA-2 study. Cancer Res. 2018;78(4 Suppl):P20910.
284. Tarantino P, Lee D, Foldi J, Soulos PR, Gross CP, O'Meara T, et al. Outcomes of subsequent treatment regimens after trastuzumab deruxtecan in patients with metastatic breast cancer. JNCI. 2025;
285. Slamon DJ, Leyland-Jones B, Shak S, Fuchs H, Paton V, Bajamonde A, et al. Use of chemotherapy plus a monoclonal antibody against HER2 for metastatic breast cancer that overexpresses HER2. N Engl J Med. 2001;344(11):783–92.
286. Swain SM, Kim SB, Cortés J, Ro J, Semiglazov V, Campone M, et al. Pertuzumab, trastuzumab, and docetaxel for HER2-positive metastatic breast cancer (CLEOPATRA study): Overall survival results from a randomised, double-blind, placebo-controlled, phase 3 study. Lancet Oncol. 2013;14(6):461–71.

287. Swain SM, Baselga J, Kim SB, Ro J, Semiglazov V, Campone M, et al. Pertuzumab, Trastuzumab, and Docetaxel in HER2-Positive Metastatic Breast Cancer. N Engl J Med. 2015;372(8):724–34.
288. French DM, Lin BC, Wang M, Adams C, Shek T, Hötzel K, et al. Targeting FGFR4 inhibits hepatocellular carcinoma in preclinical mouse models. PLoS One. 2012;7(5):1–12.
289. Bartz R, Fukuchi K, Ohtsuka T, Lange T, Gruner K, Watanabe I, et al. Preclinical Development of U3-1784, a Novel FGFR4 Antibody against Cancer, and Avoidance of Its On-target Toxicity. Mol Cancer Ther. 2019;18(10):1832–43.
290. Fu Z, Li S, Han S, Shi C, Zhang Y. Antibody drug conjugate: the “biological missile” for targeted cancer therapy. Signal Transduct Target Ther. 2022;7(1):1–25.
291. Chen H, Lin Z, Arnst KE, Miller DD, Li W. Tubulin inhibitor-based antibody-drug conjugates for cancer therapy. Molecules. 2017;22(8):1–28.
292. Abelman RO, Wu B, Barnes H, Medford A, Norden B, Putur A, et al. TOP1 Mutations and Cross-Resistance to Antibody-Drug Conjugates in Patients with Metastatic Breast Cancer. Clin Cancer Res. 2025;31(10):1966–74.
293. Chen YF, Xu Y ying, Shao ZM, Yu K Da. Resistance to antibody-drug conjugates in breast cancer: mechanisms and solutions. Cancer Commun. 2023;43(3):297–337.
294. Khoury R, Saleh K, Khalife N, Saleh M, Chahine C, Ibrahim R, et al. Mechanisms of Resistance to Antibody-Drug Conjugates. Int J Mol Sci. 2023;24(11):1–21.

ANNEX

scientific reports

Check for updates

OPEN

Comparative biological activity of palbociclib and ribociclib in hormone receptor-positive breast cancer

Natàlia Lorman-Carbó[1,6], Olga Martínez-Sáez[1,2], Aranzazu Fernandez-Martinez[3,4], Patricia Galván[1], Nuria Chic[1,5], Isabel Garcia-Fructuoso[1,2], Adela Rodríguez[1,2], Raquel Gómez-Bravo[1,2], Francesco Schettini[1,2,6], Paula Blasco[1], Oleguer Castillo[1], Blanca González-Farré[1,7], Barbara Adamo[1,2], Maria Vidal[1,2,8,9], Montserrat Muñoz[1,2,8], Charles M. Perou[3,4], Marcos Malumbres[10,11], Joaquín Gavilá[8,12], Tomás Pascual[1,2,8], Aleix Prat[1,2,6,9,13] & Fara Brasó-Maristany[1,13]✉

This study examines the biological effects of palbociclib and ribociclib in hormone receptor-positive breast cancer, pivotal to the HARMONIA prospective phase III clinical trial. We explore the downstream impacts of these CDK4/6 inhibitors, focusing on cell lines and patient-derived tumor samples. We treated HR+ breast cancer cell lines (T47D, MCF7, and BT474) with palbociclib or ribociclib (100 nM or 500 nM), alone or combined with fulvestrant (1 nM), over periods of 24, 72, or 144 h. Our assessments included PAM50 gene expression, RB1 phosphorylation, Lamin-B1 protein levels, and senescence-associated β-galactosidase activity. We further analyzed PAM50 gene signatures from the CORALLEEN and NeoPalAna phase II trials. Both CDK4/6 inhibitors similarly inhibited proliferation across the cell lines. At 100 nM, both drugs partially reduced p-RB1, with further decreases at 500 nM over 144 h. Treatment led to reduced Lamin-B1 expression and increased senescence-associated β-galactosidase activity. Both drugs enhanced Luminal A and reduced Luminal B and proliferation signatures at both doses. However, the HER2-enriched signature significantly diminished only at the higher dose of 500 nM. Corresponding changes were observed in tumor samples from the CORALLEEN and NeoPalAna studies. At 2 weeks of treatment, both drugs significantly reduced the HER2-enriched signature, but at surgery, this reduction was consistent only with ribociclib. Our findings suggest that while both CDK4/6 inhibitors effectively modulate key biological pathways in HR+/HER2- breast cancer, nuances in their impact, particularly on the HER2-enriched signature, are dose-dependent, influenced by the addition of fulvestrant and warrant further investigation.

The addition of cyclin-dependent kinase 4/6 (CDK4/6) inhibitors to endocrine therapy in the treatment of patients with advanced hormone receptor-positive and HER2-negative (HR+/HER2-) breast cancer has significantly improved survival outcomes becoming the first-line standard of care therapy in this group of patients[1–11]. However, not all patients benefit to the same extent and efforts to identify biomarkers of sensitivity and resistance are ongoing.

[1]Translational Genomics and Targeted Therapies in Solid Tumors, August Pi I Sunyer Biomedical Research Institute (IDIBAPS), Carrer de Casanova, 143, 08036 Barcelona, Spain. [2]Medical Oncology Department, Hospital Clinic of Barcelona, Barcelona, Spain. [3]Lineberger Comprehensive Cancer Center, University of North Carolina, Chapel Hill, NC, USA. [4]Department of Genetics, University of North Carolina, Chapel Hill, NC, USA. [5]Division of Research, Peter MacCallum Cancer Centre, Melbourne, Australia. [6]Present address: University of Barcelona, Barcelona, Spain. [7]Pathology Department, Hospital Clinic of Barcelona, Barcelona, Spain. [8]SOLTI Cooperative Group, Barcelona, Spain. [9]Institute of Oncology-Hospital Quirónsalud, Barcelona, Spain. [10]Cancer Cell Cycle Group, Vall d'Hebron Institute of Oncology (VHIO), Vall d'Hebron Barcelona Hospital Campus, Barcelona, Spain. [11]ICREA, Barcelona, Spain. [12]Department of Medical Oncology, Instituto Valenciano de Oncología, Valencia, Spain. [13]Reveal Genomics, S.L, Barcelona, Spain. ✉email: fbraso@recerca.clinic.cat

HR+/HER2- breast cancer can be classified into four main molecular subtypes using gene expression profiling (PAM50) (i.e., Luminal A, Luminal B, HER2-enriched, and Basal-like)[12]. Of note, 5%–20% of HR+/HER2- tumors do not fall into the Luminal A or B subtypes but rather fall into the HER2-enriched phenotype[13,14]. Moreover, a higher proportion of the HER2-enriched subtype is detected in metastases compared to primary HR+/HER2- tumors, while the proportion of the Luminal A subtype is lower in metastases and the proportion of Luminal B and Basal-like subtypes is similar in metastases and primary tumors[15].

The ability of the molecular subtypes to predict benefit from CDK4/6 inhibitors in breast cancer has been evaluated in samples from the PALOMA-2[16], the NeoPalAna[17], and the MONALEESA-2,-3, and -7[18] studies. A retrospective analysis of the PALOMA-2 trial, which randomized patients with HR+/HER2− advanced breast cancer to letrozole +/− palbociclib, analyzed the molecular subtype of 455 tumors. Whilst Luminal A (50%) and Luminal B (30%) subtypes benefited from the addition of palbociclib to letrozole, the HER2-enriched (18.7%) and Basal-like (0.5%) subtypes were associated with worse progression-free survival (PFS) in both treatment arms compared to the Luminal A group[16]. In the NeoPalAna study, which evaluated the effects of palbociclib plus anastrazole in patients with primary breast cancer, PAM50 subtype was determined in 32 tumors at baseline. Of note, two tumors with non-luminal subtypes were identified, both of which were resistant to palbociclib[17]. Additionally, the SOLTI-1303 PATRICIA study of palbociclib and trastuzumab in HR+/HER2 + advanced breast cancer showed that the Luminal A and B subtypes benefited substantially from palbociclib, while the HER2-enriched group had very small absolute benefit[19]. In contrast, a retrospective pooled analysis of the MONALEESA-2, -3, and -7 pivotal trials with ribociclib and endocrine therapy evaluated the PAM50 subtype of 1,160 tumor samples. Except for Basal-like tumors (2.6%), all other intrinsic subtypes showed a consistent PFS and overall survival (OS) benefit from the combination of endocrine therapy and ribociclib over endocrine therapy alone, with the HER2-enriched subtype (12.7%) exhibiting the highest relative and absolute benefit[18,20].

In retinoblastoma (RB1)-competent cells, CDK4/6 inhibitors trigger cell cycle arrest by reducing the phosphorylation of downstream RB1 tumor suppressor protein and can also induce cellular senescence. Palbociclib and ribociclib are CDK4/6 inhibitors of similar structure that selectively bind to the ATP-binding pocket of CDK4 (palbociclib IC50 = 9–11 nM, ribociclib IC50 = 10 nM) and CDK6 (palbociclib IC50 = 15 nM, ribociclib IC50 = 39 nM)[21,22]. One could argue that despite both being CDK4/6 inhibitors their slightly different chemical structures[23,24], mechanisms of action[25] and pharmacokinetics[24–26] might lead to dissimilarities in efficacy. On the other hand, in clinical practice palbociclib is given at a lower dose than ribociclib (125 mg daily vs 600 mg daily, respectively)[27], which could indicate a dose-dependent efficacy of CDK4/6 inhibitors in this biologically aggressive subtype. These differences may have relevant clinical implications as ribociclib, but not palbociclib, has shown clinical benefit in other clinical scenarios such as high-risk early breast cancer[28–31].

Here, we assess the biological changes that occur upon CDK4/6 inhibition in breast cancer cell lines and clinical samples of patients who participated in two neoadjuvant phase II studies of ribociclib or palbociclib in combination with endocrine therapy.

Results

Phenotypic changes in breast *cancer* cell lines during CDK4/6 inhibition

The biological changes that occur during CDK4/6 inhibition were assessed in T47D (HR+/HER2-/HER2-enriched), MCF7 (HR+/HER2-/Luminal B), and BT474 (HR+/HER2+ /HER2-enriched) breast cancer cell lines. Despite being HER2+ , the inclusion of the BT474 cell line to our study could be of relevance since it belongs to the HER2-enriched subtype by PAM50, and palbociclib has been shown to be less efficient in HR+/HER2+/HER2-enriched breast cancer[19]. Moreover, it has been shown that, except for the amplification and RNA/protein overexpression of *ERBB2* in HER2+ tumors, very minor biological differences exist at DNA, RNA, and protein levels between HER2+/HER2-enriched and HER2-/HER2-enriched tumors[32].

First, we analyzed the proliferation inhibitory effect of palbociclib and ribociclib +/− fulvestrant against all three cell lines and found that both CDK4/6 inhibitors had very similar effects (Fig. 1A, Supplementary Fig. 1A). In T47D and MCF7 cells, the combination of CDK4/6 inhibitors plus fulvestrant was superior than palbociclib or ribociclib alone, while in BT474 no significant differences were observed between the combination of CDK4/6 inhibitors with fulvestrant and palbociclib or ribociclib alone (Supplementary Fig. 2A).

RB1-competent T47D and MCF7 cell lines were treated with two different doses of palbociclib or ribociclib (i.e., 100 or 500 nM) for different periods of time (i.e., 24, 72, or 144 h) in order to assess changes in the phosphorylation of RB1 (p-RB1). In T47D and MCF7 cells treatment with 100 nM CDK4/6 inhibitors partially reduced p-RB1 with a further decrease in cells treated with 500 nM palbociclib or ribociclib regardless of treatment duration (Fig. 1B). Total *RB1* mRNA expression did not change after CDK4/6 inhibition (Supplementary Fig. 3). The cytotoxic effect of palbociclib and ribociclib was also assessed in the *RB1*-mutated MDA-MB-468 cell line to ensure that no off-target effects were given with the chosen doses (i.e., 100 or 500 nM) (Supplementary Fig. 2B).

Next, the effect on cellular senescence was assessed upon treatment with CDK4/6 inhibitors by determining protein expression levels of Lamin-B1, a structural component of the nucleus whose loss has been associated with senescence[33,34]. In T47D and MCF7 cells, CDK4/6 inhibitors decreased the expression of Lamin-B1 in a time and dose-dependent manner, with the lowest expression levels corresponding to those treated with 500 nM palbociclib or ribociclib for 144 h (Fig. 1B). Additionally, we assessed the senescence-associated β-galactosidase (SA-β-gal) activity. Both palbociclib and ribociclib (100 or 500 nM) increased β-galactosidase staining in T47D and MCF7 cell lines after 72 or 144 h treatments compared to non-treated controls indicating induction of senescence[35] (Fig. 1C). Although no significant differences were observed between treatment conditions, a dose- and time-related tendency was noticeable, with the highest β-galactosidase staining levels corresponding to cells treated with 500 nM CDK4/6 inhibitors for 144 h. Similar changes were observed in cells treated with palbociclib or ribociclib for all treatment conditions (Fig. 1C).

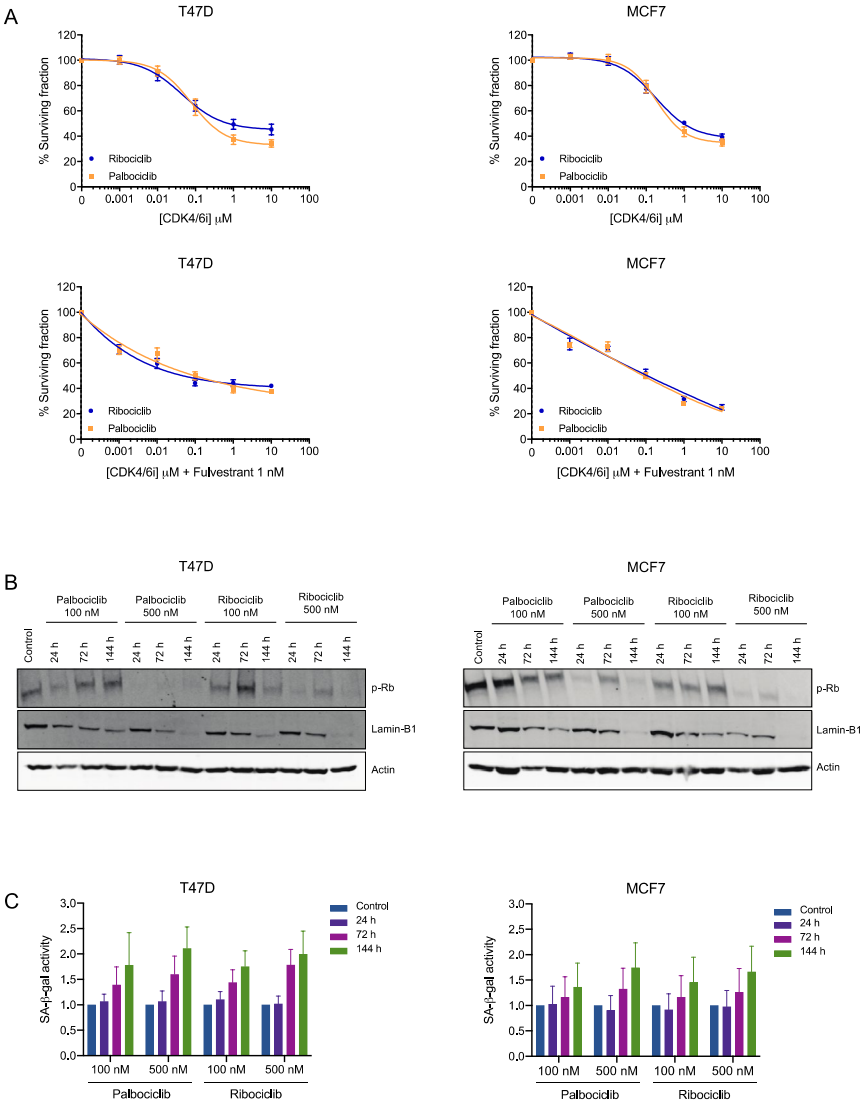

Figure 1. Biological changes during CDK4/6 inhibition in vitro. **(A)** T47D and MCF7 cells were treated with increasing doses of palbociclib or ribociclib +/− fulvestrant (1 nM) for 72 h. Shown are representative graphs of cell viability redouts determined by Hoechst 33342. Data was normalised to untreated cells and three independent experiments were performed. Mean values ± SEM are shown. **(B)** T47D and MCF7 cells were treated with palbociclib or ribociclib (100 or 500 nM) for 24, 72 or 144 h and expression of p-RB1 and Lamin-B1 was assessed by western blot. Actin was used as a loading control. **(C)** T47D and MCF7 cells were treated with palbociclib or ribociclib (100 or 500 nM) for 24, 72 or 144 h and SA-β-gal activity was determined by flow cytometry. Data was normalised to untreated cells and three independent experiments were performed. Mean values ± SEM are shown.

As for the RB1-competent BT474 cell line, a reduction of p-RB1 was also observed upon 24 or 72 h treatments with CDK4/6 inhibitors (100 or 500 nM), although p-RB1 levels were reestablished 144 h from treatment (Supplementary Fig. 1B). Lower levels of β-galactosidase activity were detected generally and the highest activity was detected after 72 h treatments with either CDK4/6 inhibitor, followed by a decrease in cellular senescence 144 h from treatments (Supplementary Fig. 1C). These observations indicate that the BT474 cell line may harbor an intrinsic resistance to CDK4/6 inhibition +/− fulvestrant compared to the T47D and MCF7 cell lines.

Effects of CDK4/6 inhibition on gene expression in breast *cancer* cell lines

Gene expression profiling was performed in untreated cells and upon treatment in order to identify changes in the PAM50 biology induced by CDK4/6 inhibitors in T47D, MCF7, and BT474 cell lines treated with different doses of palbociclib and ribociclib (100 or 500 nM) +/− fulvestrant (1 nM). The expression of the 50 genes of the PAM50 intrinsic subtype predictor and 6 signatures (Basal-like, HER2-enriched, Luminal A, Luminal B, Normal-like, and the 11-gene proliferation score) were explored at both treatment conditions. Paired t-tests and multiclass SAM showed that both CDK4/6 inhibitors (100 or 500 nM) +/− fulvestrant (1 nM) significantly increased (FDR < 5%) the Luminal A and Normal-like signatures and significantly decreased (FDR < 5%) the

Basal-like and proliferation signatures (Fig. 2A, Supplementary Fig. 4). Interestingly, the HER2-enriched signature was only significantly reduced when the CDK4/6 inhibitors were given at 500 nM either alone (palbociclib $p = 0.045$, ribociclib $p = 0.041$) or in combination with fulvestrant (palbociclib $p = 0.002$, ribociclib $p = 0.012$), while no significant changes were observed with 100 nM CDK4/6 inhibitor monotherapy (palbociclib $p = 0.275$, ribociclib $p = 0.596$) or in combination with fulvestrant (palbociclib $p = 0.466$, ribociclib $p = 0.613$) (Fig. 2A,B). Treatment with fulvestrant alone significantly increased the HER2-enriched signature ($p < 0.001$) (Fig. 2A,B).

Next, we assessed individual gene expression across treatments using multiclass SAM. Forty-three (64.2%) genes were differentially expressed across treatment groups (FDR < 5%). Notably, both inhibitors, especially at 500 nM, led to a lower expression of proliferative genes (e.g.: *CDC20*, *UBE2C*, *KNTC2*, *MKI67*, *BIRC5*, *CDCA1*, *PTTG1*, *CEP55*, *TYMS*, and *RRM2*). Interestingly, in lower doses of CDK4/6 inhibitors (100 nM) the combination of fulvestrant and palbociclib had a stronger inhibitory effect over cell proliferation than the combination of fulvestrant and ribociclib. Additionally, we performed a paired SAM analysis to check the differences between 500 nM of palbociclib vs 500 nM ribociclib with or without fulvestrant. A proportion of 19.4% and 25.3% of genes were differentially expressed after treatment with 500 nM of palbociclib vs 500 nM ribociclib with or without fulvestrant, respectively (Supplementary Table 1). Interestingly, a higher expression of the HER2-enriched genes

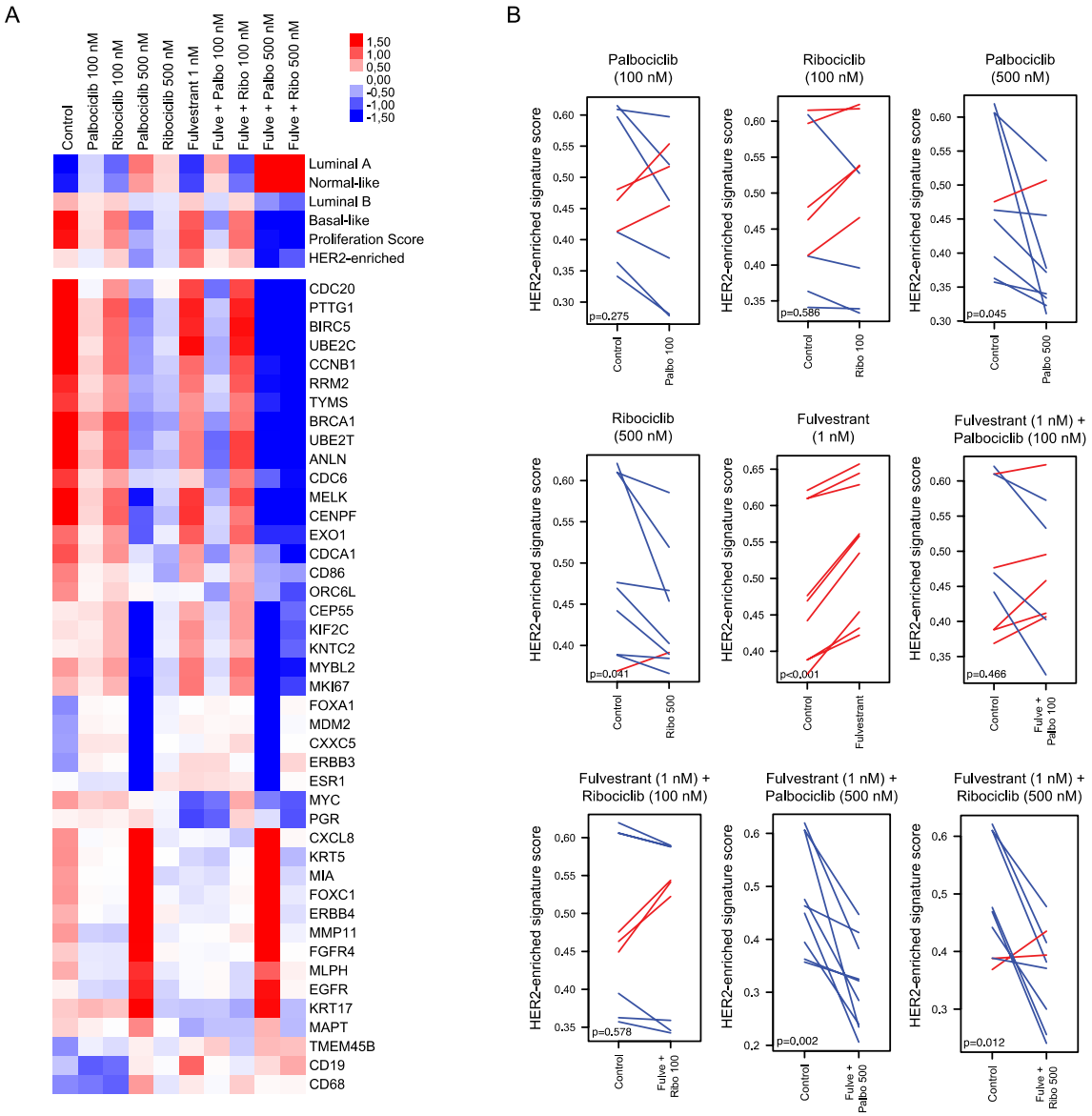

Figure 2. Changes in the HER2-enriched signature upon treatment with CDK4/6 inhibitors +/− fulvestrant in vitro. **(A)** Heatmap of a multiclass SAM representing the PAM50 molecular subtypes, proliferation score and genes that are differentially expressed (FDR < 5%) in T47D, MCF7, and BT474 cells treated with CDK4/6 inhibitors (100 or 500 nM) +/− fulvestrant (1 nM). Three independent mRNA extractions per cell line were performed. **(B)** Paired samples t-test analyses showing changes in the HER2-enriched signature following treatment of T47D, MCF7, and BT474 cells with CDK4/6 inhibitors (100 or 500 nM) +/− fulvestrant (1 nM). Three independent mRNA extractions and gene expression analyses were performed for each cell line.

FGFR4 and *TMEM45B* was observed in cells treated with 500 nM palbociclib compared to those treated with 500 nM ribociclib with and without fulvestrant (Fig. 2A).

Early in vivo biological changes during CDK4/6 inhibitor in tumor samples from CORALLEEN and NeoPalAna phase II studies

To identify molecular changes induced by CDK4/6 inhibitors, we performed gene expression analyses in baseline, day 15, and surgery tumor samples of patients treated with ribociclib plus letrozole in the CORALLEEN trial (Fig. 3A) as well as in baseline, day 15, and surgery samples of patients treated with palbociclib plus anastrazole in the NeoPalAna trial (Fig. 3B).

First, we assessed early changes in 49 paired baseline and day 15 tumor samples from the CORALLEEN trial (Fig. 3C) and 23 paired baseline and day 15 tumor samples from the NeoPalAna trial (Fig. 3D). Treatment with ribociclib and endocrine therapy led to a significant increase in Luminal A ($p < 0.001$) and Normal-like ($p < 0.001$) signatures and a significant decrease in Basal-like ($p < 0.001$), HER2-enriched ($p < 0.001$), Luminal B ($p < 0.001$) and proliferation ($p < 0.001$) signatures (Fig. 3C). Similarly, treatment with palbociclib plus endocrine therapy led to a significant increase in Luminal A ($p < 0.001$) and Normal-like ($p < 0.001$) signatures and a significant decrease in HER2-enriched ($p < 0.001$), Luminal B ($p < 0.001$) and proliferation ($p < 0.001$) signatures (Fig. 3D).

Biological changes after CDK4/6 inhibitor in tumor samples from CORALLEEN and NeoPalAna phase II studies

Next, we assessed changes in 49 paired baseline and surgery tumor samples from the CORALLEEN (Fig. 3E) and 16 paired baseline and surgery tumor samples from the NeoPalAna (Fig. 3F).

Treatment with ribociclib and endocrine therapy led to a significant increase in Luminal A ($p < 0.001$) and Normal-like ($p < 0.001$) signatures and a significant decrease in HER2-enriched ($p < 0.001$), Luminal B ($p < 0.001$), and proliferation ($p < 0.001$) signatures (Fig. 3E). Treatment with palbociclib plus endocrine therapy led to a significant increase in the Normal-like ($p = 0.012$) signature and a significant decrease in the Luminal B ($p = 0.021$) and proliferation signature ($p = 0.018$) (Fig. 3F). Importantly, the HER2-enriched signature did not decrease in surgical samples of patients treated with palbociclib ($p = 0.194$), although a difference in sample size could explain this result (Figs. 3F).

In CORALLEEN, the median number of days between the last dose of ribociclib and surgery was 13.1 days (range: 1–78)[36], whereas in NeoPalAna the median number of days between the last dose of palbociclib and surgery was 29 days (range: 8–49), except for 8 patients who received additional 10–12 days of palbociclib immediately before surgery[17]. In patients from CORALLEEN, the HER2-enriched signature was significantly decreased in patients who underwent surgery at 8 days from the last dose of ribociclib or before ($p < 0.001$), as well as in those who underwent surgery after > 8 days from the last dose of ribociclib ($p < 0.001$) (Fig. 3G). In 4 patients from NeoPalAna who underwent surgery at 8 days from the last dose of palbociclib or before, a tendency of reduction in the HER2-enriched signature was also observed. However, in patients who underwent surgery after > 8 days from the last dose of palbociclib, the HER2-enriched signature increased in 50% of the cases (Fig. 3H).

Discussion

In the last few years, three CDK4/6 inhibitors (i.e., palbociclib, ribociclib, abemaciclib) have been approved for the treatment of patients with metastatic HR+/HER2- breast cancer in combination with endocrine therapy[1–11]. While the three inhibitors are theoretically considered to provide a similar class effect, they have some chemical and pharmacological differences and are given at different doses[22,25]. Currently, no specific biomarkers are used to select the first-line CDK4/6 inhibitor[37]. On one side, the first-line trials using the CDK4/6 inhibitors ribociclib and palbociclib, despite demonstrating identical primary endpoint PFS results, have recently reported different OS results, with palbociclib not showing an OS benefit[38]. It is unknown if this is due to differences in the type of inhibitor, trial, patient population, or other features.

On the other side, it has been demonstrated that the PAM50 molecular subtypes are prognostic in patients treated with CDK4/6 inhibitors[16,18,19] and accumulated evidence suggests that the combination of endocrine therapy with palbociclib might be less effective than combination with ribociclib in patients with advanced HR+/HER2- and HER2-enriched breast cancer. Indeed, retrospective analyses on samples of the MONALEESA-2,-3, and -7[18] trials showed that patients that harbored HER2-enriched tumors exhibited a PFS and OS benefit from the combination of endocrine therapy and ribociclib, whereas those treated with endocrine therapy and palbociclib in the PALOMA-2[16] did not benefit from the combination, even though the retrospective analysis of PALOMA-2 was not powered to study the effect across PAM50 subtypes. Nevertheless, this hypothesis has not been formally tested head-to-head, and the SOLTI-2101 HARMONIA[39] prospective phase III trial (NCT05207709) is currently evaluating if the combination of ribociclib with endocrine therapy is superior to the combination with palbociclib in prolonging PFS in this particular subset of patients.

In order to better understand the molecular effects of palbociclib and ribociclib, we analyzed both cell lines and clinical samples treated with CDK4/6 inhibitors. Our main observations in breast cancer cell lines were that palbociclib and ribociclib had identical dose-dependent proliferation inhibition and that in CDK4/6 inhibitor-sensitive cell lines, both inhibitors reduced the levels of p-RB1 (marker of cell cycle inhibition[21]) and Lamin-B1 (marker of senescence[40–42]) in a similar manner, where treatment duration played a part but changes mostly relied on the administered doses.

Importantly, gene expression analyses revealed that palbociclib and ribociclib significantly increased the Luminal A and Normal-like signatures and decreased the Luminal B, Basal-like, and proliferation signatures with both doses. However, the HER2-enriched signature was only significantly reduced in cells treated with 500 nM

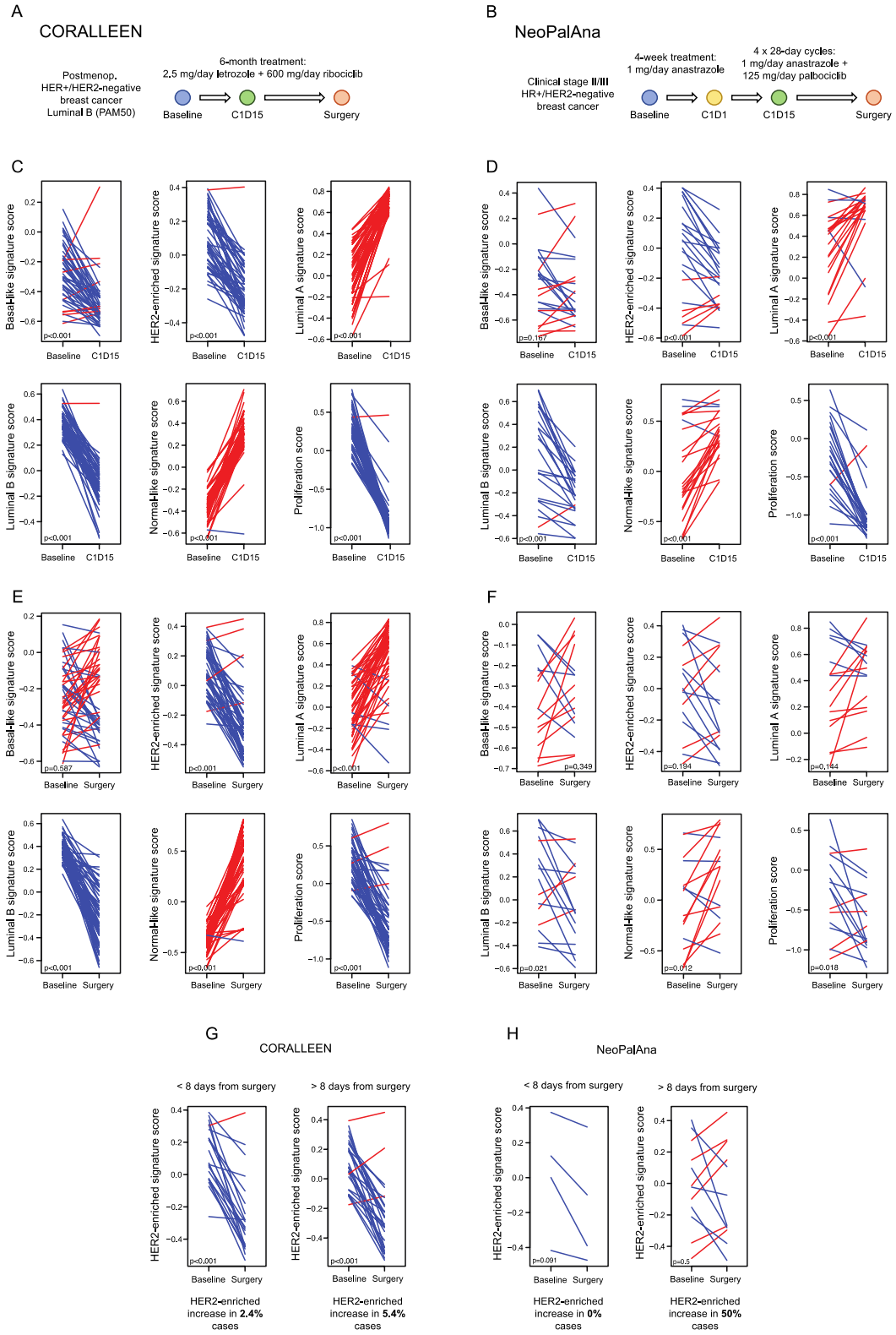

Figure 3. Changes in the PAM50 signatures in the CORALLEEN and NeoPalAna studies. Schematic summaries of the samples analyzed from **(A)** the CORALLEEN trial design and **(B)** the NeoPalAna trial design. **(C)** Paired samples t-test analyses showing changes in the PAM50 signatures at cycle 1 day 15 (C1D15) in tumor samples from CORALLEEN and **(D)** NeoPalAna phase II studies. **(E)** Changes in the PAM50 signatures at surgery in tumor samples from CORALLEEN and **(F)** NeoPalAna. **(G)** Changes in the HER2-enriched signature in tumor samples from CORALLEEN and **(H)** NeoPalAna from patients who underwent surgery ≤ 8 or > 8 days from the last dose of CDK4/6 inhibitors + endocrine therapy.

of CDK4/6 inhibitors +/− fulvestrant. Interestingly, treatment with fulvestrant alone significantly increased the HER2-enriched signature, but the addition of 500 nM palbociclib or ribociclib was still capable of significantly decreasing its levels. Assessment of individual gene expression suggested that in lower doses palbociclib might be more potent CDK4/6 inhibitor than ribociclib, and that co-treatment with fulvestrant further enhances these changes in gene expression.

In patient tumor samples from the CORALLEEN and NeoPalAna phase II studies a similar change in PAM50 biology was observed with both drugs namely an increase in Luminal A and Normal-like signatures and a decrease in Luminal B and proliferation signatures after 2 weeks of treatment and at surgery. At 2 weeks of treatment the HER2-enriched signature was significantly decreased in both studies. However, the decrease in the HER2-enriched signature was only observed in surgical samples of patients treated with ribociclib, but not palbociclib. Interestingly, in patients from NeoPalAna who underwent surgery at 8 days from the last dose of palbociclib or before, a reduction of the HER2-enriched signature was observed, although it was not of statistical significance possibly due to sample size. This result is consistent with the results of the NeoPalAna trial, where a Ki67 rebound at surgery following palbociclib was observed in patients where palbociclib treatment was finalized > 8 days before surgery, while this washout was suppressed if patients received a cycle 5 of palbociclib[17]. If palbociclib was given until surgery, the effect could be as good as the effect of ribociclib. However, sample size in NeoPalAna was much smaller compared to CORALLEEN and this represents a limitation on the interpretation of the results.

Our study acknowledges several other limitations. Firstly, our analysis was limited to early-stage breast cancer tumor samples, as obtaining paired biopsies in a metastatic setting is challenging. This may restrict the applicability of our findings to more advanced disease stages. Secondly, while most of these samples were not HER2-enriched, we attempted to mitigate this by analyzing each PAM50 intrinsic subtype score as a continuous variable, since these scores are strictly related to the biological information provided by the PAM50 genes characterizing each breast cancer intrinsic subtype[43]. Nonetheless, we acknowledge this may not fully capture the complexities of HER2-enriched biology. Thirdly, there is an acknowledged gap in our understanding of the actual concentration of palbociclib and ribociclib that reaches the tumor in patients, which may differ from the prescribed doses and preclinical models, adding a layer of uncertainty to the direct translatability of our results to clinical practice. Fourthly, the specificity of the CORALLEEN trial to patients with PAM50 Luminal B disease narrows the breadth of our findings, potentially limiting their generalizability to other breast cancer subtypes. Lastly, our study did not include abemaciclib, which has been proposed to target additional CDKs in addition to CDK4/6[44,45]. These limitations highlight the need for further research in order to fully understand the implications of CDK4/6 inhibitors in varying contexts of breast cancer treatment.

In conclusion, our results show that biological responses to palbociclib and ribociclib are primarily dose-dependent and influenced by the addition of fulvestrant. Our findings suggest that while both CDK4/6 inhibitors effectively modulate key biological pathways in HR+/HER2- breast cancer, nuances in their impact, particularly on the HER2-enriched signature, warrant further investigation. The ongoing SOLTI-2101 HARMONIA trial[39] will ultimately test which CDK4/6 inhibitor is best for continued response and survival benefit in patients with HER2-enriched breast cancer.

Methods

Cell lines and drugs

MCF7, T47D, BT474, and MDA-MB-468 cell lines were obtained from the American Type Culture Collection (ATCC, Manassas, VA, USA) and cultured in Dulbecco's Modified Eagle Medium (DMEM)/nutrient mixture F-12 supplemented with 10% v/v heat-inactivated fetal bovine serum (FBS) (Gibco; Thermo Fisher Scientific Inc., Waltham, MA, USA), 1% GlutaMAX (Gibco; Thermo Fisher Scientific Inc.), and 1% Penicillin/Streptomycin (Sigma-Aldrich, Saint Louis, MO, USA) in a 37 °C, 5% CO_2 humidified incubator. Cells were detached from flasks by incubation with 0.25% Trypsin–EDTA (1X) (Gibco; Thermo Fisher Scientific Inc.). Palbociclib, ribociclib, and fulvestrant were purchased from Selleckchem (Houston, TX, USA).

Clinical samples

The SOLTI-1402 CORALLEEN phase II study (NCT03248427) randomized 106 postmenopausal women with stage I–IIIA HR+/HER2- breast cancer and Luminal B by PAM50 with histologically confirmed, operable primary tumour size of at least 2 cm in diameter as measured by magnetic resonance imaging (MRI). Patients were randomly assigned (1:1) to receive either six 28-days cycles of ribociclib (oral 600 mg once daily for 3 weeks on, 1 week off) plus daily letrozole (oral 2.5 mg/day) or four cycles of doxorubicin (intravenous 60 mg/m^2) and cyclophosphamide (intravenous 600 mg/m^2) every 21 days followed by weekly paclitaxel (intravenous 80 mg/m^2) for 12 weeks[36]. Here, we analyzed formalin-fixed, paraffin-embedded (FFPE) tumor samples of the ribociclib plus letrozole arm, including 49 paired baseline versus cycle 1 day 15 (C1D15) samples and 49 paired baseline versus surgery samples.

Additionally, gene expression data of the NeoPalAna phase II trial (NCT01723774), which treated 50 patients with HR+/HER2- early breast cancer with anastrazole (1 mg daily) for 4 weeks, followed by four 28-day cycles of palbociclib (125 mg daily) plus anastrazole (1 mg daily)[17], was downloaded from the Gene Expression Omnibus (GSE93204). We analyzed 23 paired baseline versus C1D15 samples and 16 paired baseline versus surgery samples.

Ethics approval and consent to participate

This study was approved by the Ethics Committee at Hospital Clinic of Barcelona (HCB.2022.0086) and all methods were carried out in accordance with relevant guidelines and regulations. This study involves the use of tissue

samples of patients that have received treatment with CDK4/6 inhibitors within the context of the CORALLEEN trial. These samples are stored in the biorepository of the Translational genomics and targeted therapies in solid tumors group at IDIBAPS as long as patients sign the specific informed consent of the collection.

RNA extraction

RNA of tumor samples from the CORALLEEN study was extracted using the High Pure FFPET RNA isolation kit (Roche, Indianapolis, IN, USA) following manufacturer's protocol. At least 1–5 10 µm FFPE slides were used for each tumor specimen and macrodissection was performed to avoid contamination with normal breast tissue if needed. MCF7, T47D, and BT474 cells were seeded in a 6-well plate at 150,000 cells per well and after overnight incubation medium was replaced with two different dose levels of palbociclib or ribociclib (i.e., 100 nM or 500 nM) +/− fulvestrant (1 nM) for 72 h (h). mRNA was extracted using QIAGEN's RNeasy extraction kit (QIAGEN, Hilden, Germany) following manufacturer's instructions.

Gene expression analysis

The nCounter platform (NanoString Technologies, Seattle, WA, USA) analyzed RNA samples from tumor samples and cell lines. A minimum of 100 ng of total RNA was used to measure the expression of 50 genes of the PAM50 intrinsic subtype predictor assay and 5 housekeeping genes (*ACTB, MRPL19, PSMC4, RPLP0* and *SF3A1*). Expression counts were then normalized and the PAM50 signature scores (Basal-like, HER2-enriched, Luminal A and B, Normal-like) and the proliferation signature score were calculated using customized R scripts[43]. PAM50 molecular subtypes were calculated in the publicly available gene expression data from the NeoPalAna including 23 baseline samples, 23 week-2 samples and 16 surgery samples.

In vitro cell growth assay

MCF7, T47D, BT474, and MDA-MB-468 cells were seeded in triplicate at 5,000 cells per well in 96-well plates. Following overnight incubation, cells were treated with five 1:10 serial dilutions of palbociclib or ribociclib starting at 10 µM. Cell viability was assessed after 72 h with Hoechst 33342 staining solution (Invitrogen, Thermo Fisher Scientific Inc.) and quantified using SynergyHT microplate reader and Windows based Gen5 software.

Western blotting

MCF7, T47D, and BT474 cells were seeded in 6-well plates at 150,000 cells per well and after overnight incubation medium was replaced with palbociclib or ribociclib (100 or 500 nM). After 24, 72, or 144 h, cell lysates were obtained using radioimmunoprecipitation (RIPA) lysis and extraction buffer (Thermo Fisher Scientific Inc.) supplemented with protease inhibitors: 5 mM sodium fluoride, 1 mg/ml aprotinin, 1 mM phenylmethylsulfonyl fluoride, 1 mM sodium orthovanadate, 1 mM benzamidine, 1 mM leupeptin, and 1 mM dithiothreitol. Total protein extracts were quantified using the DC Protein Assay (BioRad Laboratories, Hercules, CA, USA) and 50 µg of proteins were separated in reducing conditions (2.5% β-mercaptoethanol) by SDS–PAGE and transferred to nitrocellulose membranes (BioRad Laboratories) for further processing, following standard western blotting procedures. The primary antibodies used in this study were phospho-RB1 (Ser807/811) (D20B12) and Lamin-B1 (D9V6H) from Cell Signaling Technologies (Danvers, MA, USA) and anti-actin (A2066) from Sigma-Aldrich. The secondary fluorescent antibody used was the IRDye 800CW Donkey anti-Rabbit IgG (LI-COR Biosciences, Lincoln, NE, USA). Fluorescent signal was acquired by the Odyssey Imaging System (LI-COR Biosciences).

Senescence-associated β-galactosidase activity

MCF7, T47D, and BT474 cells were seeded in 24-well plates at 35,000 cells per well and after overnight incubation medium was replaced with palbociclib or ribociclib (100 or 500 nM). Following 24, 72, or 144 h treatments, senescence dye from the Senescence Assay Kit (Abcam, Cambridge, UK) was added to wells. Cells were incubated for 1–2 h in a 37 °C, 5% CO_2 humidified incubator and the mean fluorescence was analysed by flow cytometry for the detection of β-galactosidase activity. Propidium iodide (Invitrogen, Thermo Fisher Scientific Inc.) was used as a viability marker. Untreated controls were added, as well as unstained controls for the evaluation of potential auto-fluorescence.

Statistical analysis

Changes in gene expression and PAM50 signatures upon CDK4/6 inhibition were determined by paired t-tests and paired and multiclass significant analysis of microarray (SAM) with a false discovery rate (FDR) < 5%. These analyses were performed using R software. All statistical tests were two sided and the statistical significance level was set to $p < 0.05$. For in vitro cell growth, determination of half maximal inhibitory concentrations (IC50s), and senescence assays, GraphPad Prism was used for statistics.

Data availability

Investigators interested in data access and collaboration should contact the corresponding author. Access can be obtained for academic use only under a data transfer agreement and upon Ethics Committee approval.

Received: 6 March 2024; Accepted: 8 July 2024
Published online: 11 July 2024

References

1. Cristofanilli, M. *et al.* Fulvestrant plus palbociclib versus fulvestrant plus placebo for treatment of hormone-receptor-positive, HER2-negative metastatic breast cancer that progressed on previous endocrine therapy (PALOMA-3): Final analysis of the multicentre, double-blind, phas. *Lancet Oncol.* **17**(4), 425–439 (2016).
2. Finn, R. S. *et al.* Palbociclib and letrozole in advanced breast cancer. *N. Engl. J. Med.* **375**(20), 1925–1936 (2016).
3. Turner, N. C. *et al.* Overall survival with palbociclib and fulvestrant in advanced breast cancer. *N. Engl. J. Med.* **379**(20), 1926–1936 (2018).
4. Hortobagyi, G. N. *et al.* Updated results from MONALEESA-2, a phase III trial of first-line ribociclib plus letrozole versus placebo plus letrozole in hormone receptor-positive, HER2-negative advanced breast cancer. *Ann Oncol.* **29**(7), 1541–1547 (2018).
5. Im, S.-A. *et al.* Overall survival with ribociclib plus endocrine therapy in breast cancer. *N. Engl. J. Med.* **381**(4), 307–316 (2019).
6. Slamon, D. J. *et al.* Phase III randomized study of ribociclib and fulvestrant in hormone receptor-positive, human epidermal growth factor receptor 2-negative advanced breast cancer: MONALEESA-3. *J. Clin. Oncol.* **36**(24), 2465–2472 (2018).
7. Tripathy, D. *et al.* Ribociclib plus endocrine therapy for premenopausal women with hormone-receptor-positive, advanced breast cancer (MONALEESA-7): A randomised phase 3 trial. *Lancet Oncol.* **19**(7), 904–915 (2018).
8. Goetz, M. P. *et al.* MONARCH 3: Abemaciclib as initial therapy for advanced breast cancer. *J. Clin. Oncol.* **35**(32), 3638–3646 (2017).
9. Johnston, S. *et al.* MONARCH 3 final PFS: A randomized study of abemaciclib as initial therapy for advanced breast cancer. *NPJ Breast Cancer.* **5**(1), 1–8 (2019).
10. Sledge, G. W. *et al.* MONARCH 2: Abemaciclib in combination with fulvestrant in women with HR+/HER2-advanced breast cancer who had progressed while receiving endocrine therapy. *J. Clin. Oncol.* **35**(25), 2875–2884 (2017).
11. Sledge, G. W. *et al.* The effect of abemaciclib plus fulvestrant on overall survival in hormone receptor-positive, ERBB2-negative breast cancer that progressed on endocrine therapy—MONARCH 2: A randomized clinical trial. *JAMA Oncol.* **6**(1), 116–124 (2020).
12. Schettini, F., Brasó-Maristany, F., Kuderer, N. M. & Prat, A. A perspective on the development and lack of interchangeability of the breast cancer intrinsic subtypes. *NPJ Breast Cancer.* https://doi.org/10.1038/s41523-022-00451-9 (2022).
13. Cejalvo, J. M. *et al.* Clinical implications of the non-luminal intrinsic subtypes in hormone receptor-positive breast cancer. *Cancer Treat. Rev.* **67**, 63–70 (2018).
14. Aftimos, P. *et al.* Genomic and transcriptomic analyses of breast cancer primaries and matched metastases in Aurora, the breast international group (Big) molecular screening initiative. *Cancer Discov.* **11**, 2796–2811 (2021).
15. Falato, C., Schettini, F., Pascual, T., Brasó-Maristany, F. & Prat, A. Clinical implications of the intrinsic molecular subtypes in hormone receptor-positive and HER2-negative metastatic breast cancer. *Cancer Treat. Rev.* **112**, 102496 (2023).
16. Finn, R. S. *et al.* Biomarker analyses of response to cyclin-dependent kinase 4/6 inhibition and endocrine therapy in women with treatment-naïve metastatic breast cancer. *Clin. Cancer Res.* **26**(1), 110–121 (2020).
17. Ma, C. X. *et al.* NeoPalAna: Neoadjuvant palbociclib, a cyclin-dependent kinase 4/6 inhibitor, and anastrozole for clinical stage 2 or 3 estrogen receptor–positive breast cancer. *Clin. Cancer Res.* **23**(15), 4055–4065 (2017).
18. Prat, A. *et al.* Correlative biomarker analysis of intrinsic subtypes and efficacy across the MONALEESA phase III studies. *J. Clin. Oncol.* **39**(13), 148–1467 (2021).
19. Ciruelos, E. *et al.* Palbociclib and trastuzumab in HER2-positive advanced breast cancer: Results from the Phase II SOLTI-1303 PATRICIA Trial. *Clin. Cancer Res.* https://doi.org/10.1158/1078-0432.ccr-20-0844 (2020).
20. Prat, A. *et al.* Intrinsic subtype and overall survival of patients with advanced HR+/HER2− breast cancer treated with ribociclib and ET: Correlative analysis of MONALEESA-2, -3, -7. *Clin. Cancer Res.* https://doi.org/10.1158/1078-0432.ccr-23-0561 (2023).
21. Asghar, U., Witkiewicz, A. K., Turner, N. C. & Knudsen, E. S. The history and future of targeting cyclin-dependent kinases in cancer therapy. *Nat. Rev. Drug Discov.* **14**(2), 130–146 (2015).
22. Schettini, F. *et al.* CDK 4/6 inhibitors as single agent in advanced solid tumors. *Front Oncol.* **8**, 608 (2018).
23. Sabt, A. *et al.* Discovery of 3,6-disubstituted pyridazines as a novel class of anticancer agents targeting cyclin-dependent kinase 2: Synthesis, biological evaluation and in silico insights. *J. Enzyme Inhib. Med. Chem.* **35**(1), 1616–1630 (2020).
24. Marra, A. & Curigliano, G. Are all cyclin-dependent kinases 4/6 inhibitors created equal?. *NPJ Breast Cancer.* **5**(1), 1–9 (2019).
25. George, M. A., Qureshi, S., Omene, C., Toppmeyer, D. L. & Ganesan, S. Clinical and pharmacologic differences of CDK4/6 inhibitors in breast cancer. *Front Oncol.* **11**, 693104 (2021).
26. Braal, C. L. *et al.* Inhibiting CDK4/6 in breast cancer with palbociclib, ribociclib, and abemaciclib: Similarities and differences. *Drugs.* **81**(3), 317–331 (2021).
27. Kwapisz, D. Cyclin-dependent kinase 4/6 inhibitors in breast cancer: palbociclib, ribociclib, and abemaciclib. *Breast Cancer Res. Treat.* **166**(1), 41–54 (2017).
28. Schäffler, H. *et al.* The clinical relevance of the NATALEE study: Application of the NATALEE criteria to a real-world cohort from two large German breast cancer centers. *Int. J. Mol. Sci.* **24**(22), 1–12 (2023).
29. Slamon, D. J., Fasching, P. A., Hurvitz, S., Chia, S. & Hortobagyi, G. N. Rationale and trial design of NATALEE: A Phase III trial of adjuvant ribociclib + endocrine therapy versus endocrine therapy alone in patients with HR+/HER2- early breat cancer. *Ther. Adv. Med. Oncol.* **15**, 1–16 (2023).
30. Loibl, S. *et al.* Palbociclib for residual high-risk invasive HR-positive and HER2-negative early breast cancer-the penelope-B trial. *J. Clin. Oncol.* **39**(14), 1518–1530 (2021).
31. Gnant, M. *et al.* Adjuvant palbociclib for early breast cancer: The PALLAS trial results (ABCSG-42/AFT-05/BIG-14-03). *J. Clin. Oncol.* **40**(3), 282–293 (2021).
32. Prat, A. *et al.* Molecular features and survival outcomes of the intrinsic subtypes within HER2-positive breast cancer. *J. Natl. Cancer Inst.* **106**(8), 1–8 (2014).
33. Freund, A., Laberge, R. M., Demaria, M. & Campisi, J. Lamin B1 loss is a senescence-associated biomarker. *Mol. Biol. Cell.* **23**(11), 2066–2075 (2012).
34. Shimi, T. *et al.* The role of nuclear lamin B1 in cell proliferation and senescence. *Genes Dev.* **25**(24), 2579–2593 (2011).
35. Dimri, G. P. *et al.* A biomarker that identifies senescent human cells in culture and in aging skin in vivo. *Proc. Natl. Acad. Sci. USA.* **92**(20), 9363–9367 (1995).
36. Prat, A. *et al.* Ribociclib plus letrozole versus chemotherapy for postmenopausal women with hormone receptor-positive, HER2-negative, luminal B breast cancer (CORALLEEN): An open-label, multicentre, randomised, phase 2 trial. *Lancet Oncol.* **21**(1), 33–43 (2020).
37. Grinshpun, A., Tolaney, S. M., Burstein, H. J., Jeselsohn, R. & Mayer, E. L. The dilemma of selecting a first line CDK4/6 inhibitor for hormone receptor-positive/HER2-negative metastatic breast cancer. *NPJ Breast Cancer.* **9**(1), 1–4 (2023).
38. Finn, R. S., Rugo, H. S., Dieras, V. C., Harbeck, N., Im, S.-A., Gelmon, K. A., et al. Overall survival (OS) with first-line palbociclib plus letrozole (PAL+LET) versus placebo plus letrozole (PBO+LET) in women with estrogen receptor–positive/human epidermal growth factor receptor 2–negative advanced breast cancer (ER+/HER2− ABC): Analyses. 2022;**40**(17_suppl):LBA1003. https://doi.org/10.1200/JCO20224017_supplLBA1003
39. Pascual, T., Stover, D. G., Thuerigen, A., Sanchez-Bayona, R., Perou, C. M., Ciruelos, E. M., et al. Ribociclib (RIB) vs. palbociclib (PAL) in patients (pts) with hormone receptor-positive/HER2-negative/HER2-enriched (HR+/HER2-/HER2-E) advanced breast

cancer (ABC): A head-to-head phase III study—HARMONIA SOLTI-2101/AFT-58. 2023;**41**(16_suppl): TPS1125. https://doi.org/10.1200/JCO20234116_supplTPS1125.
40. Saleh, T. *et al.* The expression of the senescence-associated biomarker Lamin B1 in human breast cancer. *Diagnostics.* **12**, 609 (2022).
41. Matias, I. *et al.* Loss of lamin-B1 and defective nuclear morphology are hallmarks of astrocyte senescence in vitro and in the aging human hippocampus. *Aging Cell.* **21**, e13521 (2021).
42. Wang, A. S., Ong, P. F., Choj, A. & Clavel, C. Loss of lamin B1 is a biomarker to quantify cellular senescence in photoaged skin. *Sci. Rep.* **7**, 15678 (2017).
43. Parker, J. S. *et al.* Supervised risk predictor of breast cancer based on intrinsic subtypes. *J. Clin. Oncol.* **27**(8), 1160–1167 (2009).
44. Wells, C. I. *et al.* Quantifying CDK inhibitor selectivity in live cells. *Nat. Commun.* **11**, 1–11 (2020).
45. Hafner, M. *et al. Clin. Activity.* **26**(8), 1067–1080 (2019).

Acknowledgements

A.P. received funding from Fundació La Marató TV3 201935-30, Fundación CRIS contra el cáncer PR_EX_2021-14, Agència de Gestó d'Ajuts Universitaris i de Recerca 2021 SGR 01156, Fundación Fero BECA ONCOXXI21, Instituto de Salud Carlos III PI22/01017, Asociación Cáncer de Mama Metastásico IV Premios M. Chiara Giorgetti, Breast Cancer Research Foundation BCRF-22-198 and BCRF-23-198, and RESCUER, funded by European Union's Horizon 2020 Research and Innovation Programme under Grant Agreement No. 847912. F.B-M. received funding from Fundación científica AECC Ayudas Investigador AECC 2021 (INVES21943BRAS). N.C. is supported by Fundación SEOM, Becas FSEOM para Formación en Investigación en Centros de Referencia en el Extranjero 2021.

Author contributions

The authors confirm contribution to the paper as follows: study conception and design: F.B-M., A.P; data collection: N.L-C, P.G., P.B., O.C., O.G-M., A.F-M., N.C., I.G-F., A.R., R.G-B., B.A., M.V., M.M., F.S., T.P., C.M.P., J.G.; analysis and interpretation of results: N.L-C, F.B-M., A.P., O.G-M., A.F-M., N.C., F.S., T.P., M.M; draft manuscript preparation: F.B-M., A.P., N.L-C. All authors reviewed the results and approved the final version of the manuscript.

Competing interests

A.P. reports advisory and consulting fees from Roche, Pfizer, Novartis, Amgen, BMS, Puma, Oncolytics Biotech, MSD, Guardan Health, Peptomyc and Lilly, lecture fees from Roche, Pfizer, Novartis, Amgen, BMS, Nanostring Technologies and Daiichi Sankyo, institutional financial interests from Boehringer, Novartis, Roche, Nanostring, Sysmex Europa GmbH, Medica Scientia inno. Research, SL, Celgene, Astellas and Pfizer; stockholder and consultant of Reveal Genomics, SL; patents filed PCT/EP2016/080056, PCT/EP2022/086493, PCT/EP2023/060810, EP23382703 and EP23383369. F.B-M. has patents filed: PCT/EP2022/086493, PCT/EP2023/060810, EP23382703 and EP23383369 and part-time employment with Reveal Genomics, SL. J.G. reports scientific advisory board fees from Novartis, Pfizer and Lilly, consultancy training fees from Roche, Novartis and MSD, honoraria fees from Roche, Novartis and Pfizer. I.G-F. reports financing of courses and talks from Novartis. The remaining authors declare no competing interests.

Additional information

Supplementary Information The online version contains supplementary material available at https://doi.org/10.1038/s41598-024-67126-2.

Correspondence and requests for materials should be addressed to F.B.-M.